Chemical reactions in turbulence : numerical studies through direct numerical simulations

Wenwei Wu

Shanghai Jiao Tong University
Université du Littoral Côte d'Opale

Chemical Reactions in Turbulence: Numerical Studies Through Direct Numerical Simulations

by

Wenwei Wu

A thesis submitted in partial satisfaction of the requirements for the degree
of Doctor in Sciences of the Earth Universe, Space, specialty Earth, Fluid envelops
at Shanghai Jiao Tong University and Université du Littoral Côte d'Opale
Laboratory of Oceanology and Geosciences, Ecole doctorale Sciences Technologies Santé

Jury:
Ivana Vinkovic, Reviewer and President of the Jury
Lipo Wang, Thesis Advisor
Francois G. Schmitt, Thesis Advisor
Enrico Calzavarini, Thesis Advisor
Sergio Chibbaro, Reviewer
David Hung, Reviewer
Yongxiang Huang, Member
Chien-Pin Chen, Member

Shanghai
February 25th, 2021

上海交通大学交大密西根学院

Université du Littoral Côte d'Opale

湍流中的化学反应：通过直接数值模拟的数值研究

吴文伟

上海交通大学与 Université du Littoral Côte d'Opale 博士学位论文

地球科学、流体力学专业

委员会成员：

Ivana Vinkovic（主席）

王利坡

Francois G. Schmitt

Enrico Calzavarini

Sergio Chibbaro

孔令逊

黄永祥

陈谦斌

上海

2021 年 **2** 月 **25** 日

Abstract

The present work focuses on the statistical properties of reactive scalars undergoing reversible chemical reactions in incompressible turbulence. Theoretical analysis about the statistical properties of scalars at different order of moments were carried out based on appropriately proposed approximations and models. The theoretically derived results were then compared with numerical results obtained by direct numerical simulation (DNS). In the direct numerical simulation, the spatial derivatives were mainly approximated by using a pseudo-spectral method, since the turbulent velocity and scalar fields are generally of periodic boundary conditions. For the special configurations in which the boundary condition is not periodic, a finite difference method with fine schemes was used to approximate the spatial derivatives. The numerical time integration was implemented by a third order Runge-Kutta scheme.

In statistically steady homogeneous isotropic turbulence, the chemical species retained close to a dynamical equilibrium state sustained by random large-scale reactant sources. A competition exists between the chemical reaction that tends to dump reactant concentration fluctuations and enhance their correlation intensity and the turbulent mixing that on the contrary increases fluctuations and remove relative correlations. A unique control parameter, the Damköhler number (Da_θ) that can be constructed from the scalar Taylor micro-scale, the reactant diffusivity and the reaction rate, was found to characterize the functional dependence of fluctuations and correlations. Such a dependence was validated in a variety of conditions, i.e., at changing the reaction order, the Reynolds and the Schmidt numbers. The larger is the Damköhler number, the more depleted are the scalar fluctuations as compared to the fluctuations of a passive scalar field in the same conditions, and the more intense are the correlations. A saturation in this behaviour was observed beyond $Da_\theta \simeq \mathcal{O}(10)$. We provide an analytical prediction for this phenomenon which is in excellent agreement with the direct numerical simulation results.

In the non-homogeneous anisotropic turbulence: the turbulent Kolmogorov flow (TKF), it was found that the mean velocity profile has the same form with the forcing. The only non-zero shear stress term is proportional to the cosine function, and the normal stress components all involve a square cosine expression. The normal stresses are never equal, showing that as expected the turbulence is anisotropic. It was also shown that a quadratic nonlinear constitutive equation can be proposed for this flow, involving a linear term and two nonlinear terms in the form of traceless and symmetric tensors. For about half of the flow domain, the linear term is dominating. Whereas for the vanishing mean velocity gradient regions, only one non-linear term remains non-zero and becomes constant. The reversible reactions discussed in the homogeneous isotropic case were also studied with the background flow as the TKF. The theoretical predictions about the dependence of the fluctuations and the correlations of the reactive scalars on the Da_θ in homogeneous isotropic flow are found to work also for the TKF case. It indicates that, in the quasi-equilibrium state, the dependence of the statistical properties of reactive scalars on the scalar diffusion and reaction rate is weakly influenced by the background velocity field.

By adopting Dirichlet boundary conditions for the scalars, a combustor like configuration was also proposed. In such a configuration, the reacting system is strongly deviated from the chemical equilibrium. The entire flow consists of two buffer layers and a bulk region, in which the scalar mean gradient is maintained by the boundary conditions to provide non-negligible source of the chemical reaction. A theoretical model based on the PDF of the passive scalar can satisfactorily predict the mean and fluctuation of reactants, if the associated Damköhler

number (Da_1) is sufficiently large. The correlation coefficient between the scalar quantities are determined by two counteracting effects, the turbulent mixing and the chemical kinetics. Under the non-equilibrium condition with strong chemical sources, the chemical kinetics also plays important roles in determining the scalar energy spectra. For large Da_1, the spatial distribution of the forward reaction and net reaction assume stripe like structures, making the scalar field more intermittent. Consistently, large Da_1 will shift the scalar energy from the small wave number range to the large wave number range, which is different from the quasi-equilibrium case.

All the works carried out in this thesis are devoted to the numerical and theoretical explorations about reactive scalars in incompressible turbulence of different configurations. Our findings also suggest new ideas for future studies, which are discussed in the conclusions.

摘要

本工作着重于不可压缩湍流中涉及可逆反应的反应标量的统计特性研究。基于合理的假设和模型，对关于标量不同阶矩的统计特性进行了理论分析。并且，理论推导结果与直接数值模拟（DNS）结果进行了比对。因为研究所涉及的湍流速度与标量场的边界条件一般是周期性的，所以在直接数值模拟中，空间导数主要是通过伪谱法近似。对于一些边界条件不是周期性的特殊构造，空间导数由高精度有限差分法进行近似。数值上，时间推进采用三阶龙格-库塔格式。

在统计稳态均匀各向同性湍流中，由于大尺度随机源项的作用，反应物被约束在一个动态平衡之中。在此状态下，化学反应倾向于减小反应物的脉动并加强反应物之间的相关性。相反，湍流混合过程会促进反应物的脉动并减小反应物之间的相关性。结合标量的泰勒尺度、反应物扩散系数和反应速率，我们提出了一个关键控制系数：达姆科勒数 Da_e 用于定量描述反应物的脉动和相关性。相应定量关系在我们的工作所涉及的所有反应阶数、雷诺数和施密特数条件下都得到了证实。Da_e 越大，反应物的脉动相比于相同条件下非反应物标量的脉动就越小，同时反应物之间的相关性越强。相应趋势在 Da_e 接近于 10 的时候达到饱和。对此现象，我们做出理论预测并与直接数值模拟结果取得很好的一致。

在非均匀各向异性湍流：Kolmogorov 湍流中，我们发现平均速度与扰动力的形式一致。剪切应力项中只有一项非零，并成余弦形式；法向应力项都成余弦的平方的形式。各个法向应力项相互之间均不相等，体现了湍流的各向异性。此外，我们验证了关于 Kolmogorov 湍流的一种涉及一个线性项和两个非线性项的零迹对称张量形式的二次非线性本构方程。在大约一半的计算域中，线性项是主导项。然而在速度梯度接近于零的区域，只有一个非线性项不为零并以常数项的形式存在。均匀各向同性湍流中所讨论过的化学反应也在以 Kolmogorov 湍流为背景流体的情况下进行研究。均匀各向同性条件下理论推导所得到的关于反应标量脉动值和相关性与 Da_e 的定量关系在 Kolmogorov 湍流中也得到验证。这说明在近化学反应平衡态下，反应标量的统计特性与标量扩散过程以及反应速率的关系几乎不受背景流场的影响。

通过对标量给定狄利克雷边界条件，我们提出了一个类似燃烧器的结构。在该结构中，整个反应系统明显偏离化学反应平衡态。流场由两个缓冲区和一个主区组成。在主区中，标量的平均梯度由边界条件所维持，产生足够强的化学反应源项。我们提出了一个基于非反应物标量的概率密度函数预测反应物标量平均值和脉动值的理论分析模型，并在正向反应速率足够大的情况下得到验证。反应物之间的相关系数由湍流混合过程和化学机制所决定。在非化学平衡状态并且反应源项足够强的情况下，化学机制对标量的脉动能谱起关键作用。当正向反应速率足够大，正向反应速率和总反应速率的空间分布成条纹状，使得反应物场更具间越性。与之一致的是，正向反应速率足够大情况下，小波长范围的标量的脉动能量会被转移到大波长范围。该结果与近化学平衡态的结果十分不同。

本论文所做的所有工作都致力于关于不同构造下不可压缩湍流中化学反应的数值和理论探索。我们的工作同时对未来的相关工作提出了新的想法，具体详见结论部分。

Résumé

Dans cette thèse, les propriétés statistiques des scalaires réactifs subissant des réactions chimiques réversibles en turbulence incompressible ont été étudiées au moyen de simulations numériques directes et d'analyses théoriques. Les cas étudiés incluent les réactions proches et fortement déviées des états d'équilibre chimique, en écoulement turbulent homogène et isotrope, et inhomogène anisotrope. Des analyses théoriques des propriétés statistiques des scalaires pour différents ordres de moments ont été effectuées sur la base d'approximations et de modèles. Les résultats théoriques ont ensuite été comparés aux résultats numériques obtenus par simulations numériques directes.

Introduction

La turbulence, domaine complexe mais scientifiquement important, existe dans de nombreuses situations, telles que les écoulements dans les moteurs automobiles, les réacteurs chimiques, les écoulements environnementaux, y compris les océanographiques et météorologiques. Une caractéristique essentielle des écoulements turbulents est que le champ de vitesse du fluide varie de manière significative et irrégulière à la fois en position et en temps. En conséquence, les vitesses sont apparemment aléatoires et chaotiques. Cependant, du point de vue statistique, certaines propriétés intrinsèques et universelles de la turbulence peuvent être trouvées, par exemple la loi -5/3

décrivant le processus de cascade d'énergie régissant les tourbillons de turbulence. Dans la turbulence, il y a également des scalaires advectés. Certains sont appelés scalaires passifs car ils n'apportent pas de rétroaction sur l'écoulement (généralement incompressible). Certains sont appelés scalaires réactifs car ils impliquent une réaction en plus du transport par l'écoulement. L'objectif principal de cette thèse est d'étudier les propriétés statistiques de scalaires réactifs en turbulence incompressible, possédant une réaction sans influencer l'écoulement. Dans le monde réel, des exemples de scalaire réactif dans une turbulence incompressible peuvent être les concentrations de réactifs chimiques (sels nutritifs) ou le phytoplancton dans l'océan.

Simulations numériques directes

Les équations aux dérivées partielles à résoudre numériquement dans cette thèse sont les équations de Navier-Stokes pour la vitesse et les équations de advection-diffusion pour les scalaires non réactifs, ajoutés à des temres de réaction pour les scalaires réactifs. Les simulations numériques directes ont été mises en œuvre en résolvant ces équations aux dérivées partielles, dans différentes configurations, en utilisant la méthode pseudo-spectrale ou la méthode des différences finies. Lorsque les quantités ont des conditions aux limites périodiques, la méthode pseudo-spectrale est préférée en raison de sa grande précision dans l'approximation des dérivées

spatiales. Les méthodes pseudo-spectrales utilisées ici ont adopté les séries de Fourier comme fonctions orthogonales. Pour éviter l'erreur de crénelage due à la convolution des modes à grand nombre d'ondes introduite par le terme non linéaire, la technique de désaliasing lisse a été utilisée. Pour les configurations dans lesquelles les conditions aux limites des scalaires ne sont pas périodiques, une méthode aux différences finies avec des schémas d'ordre élevé (schéma de huitième ordre à pas spatial vers l'amont et schéma de centre du dixième ordre pour approximer respectivement les dérivées spatiales du premier et du second ordre) a été utilisée. L'intégration temporelle numérique a été implémentée de manière explicite par un schéma Runge-Kutta du troisième ordre. Les analyses statistiques des grandeurs d'intérêt ont été mises en œuvre dans un état stationnaire statistique, qui a été maintenu par forçage numérique pour la vitesse et les scalaires. Dans la configuration anisotrope, le forçage des scalaires se faisait via un gradient moyen, tandis que dans la configuration isotrope, la vitesse et les fluctuations scalaires sont soutenues par un forçage portant sur l'ensemble des nombres d'onde.

Résultats et discussion

Nous avons d'abord étudié le cas des réactions chimiques réversibles en turbulence homogène et isotrope. La réaction fait intervenir trois réactifs R_1, R_2 et P, dont les fluctuations ont été maintenues par un forçage à grande

échelle avec une amplitude constante et une phase aléatoire, subissant une réaction réversible. En outre, un scalaire passif non réactif T est également considéré pour comparaison. Le système réactionnel se trouve dans un état de quasi-équilibre chimique, qui est maintenu par la compétition entre la réversibilité de la réaction, qui impose un équilibre chimique global à l'état statistiquement stationnaire, et la variabilité du forçage scalaire, qui introduit une stochasticité dans les champs scalaires. L'amplitude du forçage scalaire a été contrainte pour générer de petites fluctuations scalaires par rapport à la quantité moyenne globale de scalaire (~10% de la quantité moyenne), sinon la quantité scalaire totale pourrait être négative, ce qui n'a aucun sens pour la concentration de réactif. Dans ce cas, la vitesse de réaction nette globale était faible dans l'état d'équilibre dynamique, et donc trop faible pour modifier les lois d’échelle et la distribution statistique des scalaires. En conséquence, les scalaires réactifs ont montré la même loi d’échelle (spectre d’énergie en Fourier) que celui du scalaire non réactif. Les fluctuations des scalaires réactifs et non réactifs normalisés par leurs écarts types obéissaient à des distributions gaussiennes. A partir des spectres de cohérence entre scalaires réactifs, il a été trouvé que les coefficients de corrélation entre scalaires réactifs sont indépendants du nombre d'onde (échelle de longueur). Un tel résultat suggère que le coefficient de corrélation entre deux scalaires réactifs est le même que celui entre leurs gradients.

L'effet de la réaction sur les propriétés statistiques des scalaires a été principalement mis en évidence dans les corrélations et l'amplitude des fluctuations, sur lesquelles nous avons réalisé non seulement des simulations numériques mais aussi des approches théoriques. Pour les analyses de modélisation des coefficients de corrélation des scalaires réactifs, quatre conditions ou hypothèses préalables sont nécessaires: 1. l'état stationnaire statistique; 2. la linéarisation des termes de la réaction, qui est viable à condition que les fluctuations des scalaires soient faibles par rapport aux quantités moyennes; 3. le fait que le coefficient de corrélation entre deux scalaires réactifs est le même que celui entre leurs gradients; 4. l'hypothèse que le forçage d'un scalaire ne peut pas être fortement corrélé avec celui d'un autre scalaire, ce qui est garanti par l'implémentation du forçage temporel aux scalaires. Puis dans le cadre de cette modélisation, à partir des équations gouvernant les scalaires réactifs, des dérivations mathématiques ont été effectuées pour obtenir des équations approchées sur les covariances et les auto-variances des scalaires réactifs, ce qui a finalement conduit à des expressions analytiques montrant que les coefficients de corrélation des scalaires réactifs sont des fonctions d'un paramètre de contrôle unique: le nombre de Damköhler (Da_θ). Da_θ est construit comme le rapport entre l'échelle de temps de diffusion scalaire à travers un domaine de la taille de la micro-échelle scalaire de Taylor (λ_θ^2/D) et l'échelle de temps de réaction chimique (τ_r). De plus, Da_θ s'est avéré être

une combinaison des paramètres importants caractérisant le mouvement turbulent et la diffusion scalaire, y compris le nombre de Reynold basé sur Taylor (Re_λ), le nombre de Schmidt (Sc), le nombre de Damköhler traditionnel (Da) et l'échelle de Taylor pour les scalaires. (λ_θ). Les prédictions théoriques sur les coefficients de corrélation montrent qu'avec un petit Da_θ (réaction faible), les scalaires réactifs sont faiblement corrélés avec des coefficients de corrélation négligeables. Au fur et à mesure que Da_θ augmente (réaction plus forte), les scalaires réactifs deviennent progressivement soit positifs soit négatifs en corrélation avec les coefficients de corrélation évoluant asymptotiquement vers certaines constantes. Les transitions entre zéro et les quantités saturées des coefficients de corrélation se produisent toujours lorsque Da_θ est à peu près dans la plage de [0,1,10]. En ce qui concerne l'amplitude de la fluctuation scalaire, bien que la réaction montre un effet global sur le dumping des fluctuations scalaires, nous pouvons supposer que l'apport d'énergie aux scalaires réactifs pour lesquels l'ordre de la réaction est de 1 (en R_1 et P) est à peu près le même qu'avec l'apport d'énergie au scalaire non réactif. Avec cette hypothèse supplémentaire, la modélisation peut être étendue aux fluctuations des scalaires réactifs normalisés par la fluctuation du scalaire non réactif, qui se sont également avérés être des fonctions du paramètre de contrôle de Da_θ. Les fluctuations normalisées des scalaires réactifs étaient théoriquement comme étant 1 lorsque Da_θ est petit (réaction

faible), indiquant que les scalaires réactifs sont des mêmes fluctuations avec le scalaire non réactif subissant le même environnement turbulent et le même forçage externe. Lorsque Da_θ augmente (réaction plus forte) jusqu'à des valeurs de l'ordre de 0.1, les fluctuations normalisées commencent à diminuer. Les tendances à la baisse cessent lorsque Da_θ atteint environ 10, les fluctuations normalisées saturant à certaines constantes. Les transitions se sont avérées se produire à peu près dans la même plage de Da_θ que celle des coefficients de corrélation. Selon la définition de Da_θ, la compétition entre les processus chimiques et le mélange turbulent est essentielle pour déterminer les fluctuations de concentration des réactifs et leur intensité de corrélation. Plus précisément, les processus chimiques ont tendance à réduire les fluctuations de concentration des réactifs et à améliorer leur intensité de corrélation. Alors qu'au contraire, le mélange turbulent augmente les fluctuations et supprime les corrélations relatives. Nos analyses de modélisation théorique ont été fortement validées par les simulations numériques, car les dépendances fonctionnelles des fluctuations et les corrélations des grandeurs scalaires caractérisées par Da_θ sont bien confirmées par les résultats DNS dans la gamme complète des conditions explorées avec un ordre de réaction variable (2 à 4), le nombre de Reynolds basé sur Taylor (20 à 150) et le nombre de Schmidt (0.1 à 4).

Le rôle clé de Da_θ implique également l'importance de la micro-échelle

scalaire de Taylor λ_θ dans le mélange des espèces chimiques. Tout d'abord, il a été remarqué que λ_θ ne varie pas significativement pour les différents champs scalaires R_1, R_2, P et le champ scalaire passif de référence T. De plus, nos résultats numériques ont montré que λ_θ est à peu près inversement proportionnel à la racine carrée du nombre de Schmidt, surtout sous la condition d'un grand nombre de Reynolds. Une telle relation implique que Da_θ peut être considéré comme le rapport de la plus grande échelle de temps de l'écoulement turbulent (grand temps de rotation des tourbillons) à l'échelle de temps typique associée au processus chimique (τ_r). Une telle idée a été témoignée dans une série de simulations où les champs scalaires sont advectés par l'écoulement turbulent spatialement filtré, ne conservant que de grands tourbillons. Il a été constaté que la micro-échelle de Taylor scalaire λ_θ et les coefficients de corrélation des scalaires réactifs dans les champs de vitesse de seulement quelques modes les plus grands sont les mêmes que ceux convectés par tout le flux. Cette dernière observation peut être d'un intérêt pratique pour l'estimation des régimes atteints par les réactions biogéochimiques à petite échelle dans l'océan. Par exemple, si l'on considère un champ réactif comme la concentration locale de phytoplancton dans l'océan. Les échelles de temps utilisées pour construire le nombre de Da_θ sont: le grand temps typique de rotation des tourbillons de l'écoulement turbulent tridimensionnel, qui est normalement de l'ordre de plusieurs heures, et le temps de croissance typique de la population,

c'est-à-dire du ordre d'un jour. Cela conduit à une valeur de Da_θ <1, ce qui signifie qu'à de petites échelles, plus précisément à des échelles où le flux océanique peut être approché comme un écoulement turbulent tridimensionnel avec une cascade d'énergie directe, la concentration de phytoplancton peut être considérée en toute sécurité comme un champ scalaire passif.

Dans le cas isotrope homogène, l'analyse théorique des propriétés statistiques des scalaires réactifs a été faiblement affectée par les propriétés à petite échelle de l'écoulement turbulent. Cela nous a incité à considérer la turbulence anisotrope non homogène, telle que l'écoulement turbulent de Kolmogorov (TKF). L'écoulement de Kolmogorov (KF) est un exemple d'écoulement de canal turbulent sans frontières, qui est statistiquement non homogène dans une direction et anisotrope. Généralement, le système KF correspond aux équations de Navier-Stokes étudiées dans un domaine périodique, à pression constante, et forcées par un forçage sinusoïdal. Au-dessus d'un nombre de Reynolds critique, l'écoulement devient turbulent et nous le désignons par écoulement turbulent de Kolmogorov (TKF).

Tout d'abord, nous avons acquis une compréhension plus approfondie du TKF forcé dans la direction x par une force sinusoïdale dépendant de la coordonnée z. On a constaté que le profil moyen de la composante de vitesse alignée sur le forçage a la même forme, avec un amortissement d'un facteur κ, par rapport à la valeur de vitesse moyenne calculée à partir du

terme de forçage. On a trouvé que la valeur de κ était comparable à celle rapportée dans les travaux existants et qu'elle augmentait faiblement avec le nombre de Reynolds, indiquant une possible saturation asymptotique à très grand Re. Le seul terme de contrainte de cisaillement non nul est la covariance entre les composantes de vitesse le long des directions x et z. Plus important encore, cette contrainte de cisaillement non nulle est proportionnelle à l'intégrale de la composante de vitesse moyenne le long de la direction z, qui est une fonction cosinus. Un tel résultat numérique a validé la convergence de la simulation, puisqu'il peut être théoriquement obtenu en faisant la moyenne de la composante x des équations de Navier-Stokes. Les composantes de contrainte normales impliquent toutes des fonctions cosinus carrées. Ces derniers ne sont jamais égaux, montrant que, comme prévu, la turbulence est anisotrope. En additionnant les trois contraintes normales, on obtient une expression en cosinus carré de l'énergie cinétique, dont les coefficients étaient en bon accord avec les valeurs rapportées par les travaux déjà publiés.

Ensuite, nous avons également étudié les fermetures pour l'écoulement turbulent de Kolmogorov, qui proposent des équations constitutives entre le tenseur de contrainte anisotrope et le tenseur de vitesse de déformation moyenne. Premièrement, selon l’hypothèse de viscosité turbulente de Boussinesq, un modèle de fermeture linéaire, qui suggère une relation linéaire entre les deux tenseurs. Un tel modèle linéaire suggère que

l'alignement entre les deux tenseurs est de 1. Les résultats numériques ont montré que l'alignement est supérieur à 0,9 pour environ 46% du volume, où le gradient moyen de vitesse est grand. Cela indique que pour environ la moitié du volume avec un fort gradient de vitesse moyenne, la relation linéaire entre les tenseurs de déformation et de contrainte est approximativement valide. Il a également été montré qu'une équation constitutive non linéaire quadratique peut être proposée pour ce flux, impliquant un terme linéaire et deux termes non linéaires sous forme de tenseurs sans trace et symétriques. Pour environ la moitié du domaine d'écoulement, le terme linéaire domine. Alors que pour les régions de gradient de vitesse moyenne de fuite, un seul terme non linéaire reste non nul et devient constant. Par conséquent, un coefficient de viscosité efficace peut en effet être estimé pour TKF, mais contrairement à ce qui a été dit précédemment, globalement tous les termes linéaires et non linéaires sont nécessaires pour la fermeture complète.

Après l’analyse du champ de vitesse dans le TKF, les réactions réversibles discutées pour le cas isotrope homogène ont également été introduites pour étendre notre analyse théorique sur les propriétés statistiques des scalaires réactifs turbulents à la turbulence non homogène et anisotrope, par exemple la TKF. Ici, nous n'avons considéré qu'une réaction du second ordre avec un nombre de Schmidt égal à 1. En tant que grandeur clé dans la définition de Da_θ, le carré de l'échelle micrométrique

scalaire de Taylor λ_θ s'est avéré être une fonction cosinus carrée de la position z. Cependant, ils n'ont pas de grandes fluctuations, correspondant à moins de 10% de la valeur moyenne. Ainsi, λ_θ peut grossièrement être considéré comme constant dans TKF. Pour les fluctuations normalisées et les coefficients de corrélation des scalaires réactifs, qui sont les principaux sujets des prédictions théoriques proposées dans le cas isotrope homogène précédent, nos résultats numériques ont montré qu'ils sont faiblement influencés par la position en TKF. Plus important encore, les dépendances des fluctuations normalisées et des coefficients de corrélation des scalaires réactifs sur le Da_θ, théoriquement dérivés dans le flux isotrope homogène, pourraient également être validées par les résultats numériques dans le cas TKF actuel. Ceci indique que, dans l'état de quasi-équilibre, les dépendances des propriétés statistiques des scalaires réactifs sur la diffusion scalaire et la vitesse de réaction sont faiblement influencées par le champ de vitesse sous-jacent.

Pour les réactions irréversibles en turbulence isotrope homogène, la linéarisation du terme de réaction est valable car les fluctuations des scalaires réactifs sont faibles par rapport aux quantités moyennes à l'état de quasi-équilibre. Cependant, un système réactif fortement dévié de l'état d'équilibre global et avec des fluctuations relativement plus importantes des scalaires réactifs peut être plus significatif sur le plan pratique. Par

exemple dans l'océan, les fluctuations affichées par les populations planctoniques peuvent atteindre des valeurs comparables à celles de la densité moyenne de population. De plus, les scalaires réactifs avec des fluctuations plus importantes sont plus intéressants physiquement, car l'écoulement réactif possède une non-linéarité plus forte, ce qui est une caractéristique principale des écoulements turbulents. Pour ces raisons, il sera intéressant d'explorer différentes configurations d'écoulement où de fortes sources chimiques pourraient produire des écarts prononcés par rapport à l'état d'équilibre global. Ainsi, une configuration semblable à une chambre de combustion de scalaires réactifs, dans laquelle les champs scalaires possèdent des conditions aux limites de Dirichlet dans une direction, a été explorée. Dans une telle configuration, l'écoulement global se compose de deux couches tampons générées par une technique numérique et d'une région centrale de mélange entre les deux. Les fluctuations des scalaires sont maintenues par un gradient moyen intrinsèque imposé par les conditions aux limites, au lieu d'un forçage isotrope comme adopté auparavant. En conséquence, le système réactif est supposé être fortement dévié de l'état d'équilibre chimique. Les propriétés statistiques et d'échelle des scalaires réactifs dans un système de réaction réversible du second ordre avec un nombre de Schmidt de 1 ont été étudiées, en comparaison avec un scalaire passif non réactif.

Dans ce cas, il existe deux nombres de Damköhler: Da_1 et Da_2 pour les

réactions directe et inverse respectivement. Nous avons maintenu Da_2 comme une constante et avons fait varier le rapport $\Gamma = Da_1/Da_2$ de 1 à 100. Les amplitudes des taux de réaction directe et inverse ont d'abord été examinées. On a trouvé que l'amplitude de la vitesse de réaction directe pouvait être significativement plus grande que celle de la vitesse de réaction inverse, en particulier lorsque Γ est grand. Ceci indique que le système réactif dans une telle configuration était en effet fortement dévié de l'état d'équilibre chimique. Pour une meilleure compréhension de cette configuration nouvellement développée composée de deux couches tampons et d'une région de mélange, les moments du scalaire passif ont été explorés à la fois numériquement et théoriquement. Sous la condition d'état stationnaire statistique et en utilisant l'hypothèse de longueur de mélange, l'expression analytique du profil moyen du scalaire passif peut être dérivée de l'équation d'advection-diffusion. Ces analyses théoriques suggèrent que le transport scalaire à la fois dans les couches tampons et dans la région centrale de mélange peut être considéré comme des diffusions scalaires turbulentes avec différentes diffusivités turbulentes. Surtout, les prévisions théoriques étaient en excellent accord avec les résultats numériques.

Avec un Γ grand, la fonction de densité de probabilité (PDF) de la vitesse de réaction nette (R_{net}) culmine pour la valeur $R_{net} = 0$ et devient asymétrique et plus étendue pour les grandes valeurs de R_{net}. Alors que lorsque Γ est proche de 1, la PDF culmine à une valeur modérée de R_{net}.

Une telle différence doit être causée par le mécanisme chimique, ce qui peut être vu plus clairement à partir de la distribution spatiale des vitesses de réaction. Les visualisations des taux de réaction ont montré que, pour les petits Γ, les régions avec une réaction directe élevée sont distribuées sur des valeurs étendues. Alors que pour Γ grand, les distributions spatiales de la réaction directe et de la réaction total se distribuent selon des structures en forme de bande, ce qui rend le champ scalaire plus intermittent par rapport au scalaire passif de référence. L'intermittence peut également être étudiée via les spectres d'énergie scalaire bidimensionnels. À partir des spectres d'énergie des scalaires réactifs normalisés par les spectres d'énergie du scalaire passif, il a été constaté qu'un Γ plus élevé fait passer plus d'énergie scalaire de grandes échelles de longueur à de petites échelles, indiquant que les réactions chimiques plus fortes ont tendance à concentrer la quantité scalaire locale et à renforcer l'intermittence scalaire.

Les coefficients de corrélation entre les scalaires réactifs ont été déterminés par deux effets antagonistes, le mélange turbulent et la cinétique chimique. Fait intéressant, les réactifs R_1 et R_2 se sont révélés plus positivement corrélés avec un Γ plus grand, bien qu'ils soient censés se consommer plus rapidement. Ce résultat peut s'expliquer par le fait que les PDF de R_1 et R_2 étaient de plus en plus positivement biaisés avec l'augmentation de Γ dans la configuration actuelle. De plus, les spectres de cohérence des scalaires réactifs étaient fortement dépendants du nombre

d'onde, en nette distinction avec le cas de quasi-équilibre. En particulier, la corrélation entre les scalaires réactifs construits avec une forte réaction provient principalement de la contribution à petite échelle.

A l'instar des analyses faites dans le cas homogène et isotrope, des prédictions théoriques sur les moments des scalaires réactifs (r.m.s des fluctuations et les grandeurs moyennes) ont également été réalisées ici. Une condition préalable nécessaire est que le PDF du scalaire passif (T) soit connu. Essentiellement, les analyses de modélisation actuelles se concentrent sur le lien entre le scalaire réactif et le scalaire passif, par lequel les moments des scalaires réactifs peuvent être calculés à partir du PDF connu du scalaire passif. Pour le cas de Γ infiniment grand (réaction directe extrêmement forte), les réactifs R_1 et R_2 ne peuvent pas coexister. Dans cette condition, des relations définies entre les scalaires réactifs et le scalaire passif peuvent être obtenues. Alors que pour le cas de Γ fini, nous avons dû proposer une hypothèse que le produit de R_1 et R_2 (R_1R_2) a localement une limite supérieure, qui est une constante divisée par Γ. De plus, la PDF conditionnelle de R_1R_2 sur le scalaire passif doit être modélisée. Ici, celle-ci a été initialement considérée comme étant uniformément distribuée. Ainsi, les prédictions théoriques sur les fluctuations moyennes et les quantités moyennes des scalaires réactifs pourraient être obtenues en faisant l'intégrale du scalaire réactif dans l'espace d'échantillonnage statistique du scalaire passif. Lorsque nous

avons validé les résultats de la modélisation avec des simulations numériques, il a été constaté que les prédictions théoriques pouvaient correspondre aux résultats numériques lorsque Γ est significativement grand. Les modèles devraient être encore améliorés pour comprendre les situations avec un Γ plus petit.

Contributions scientifiques

Les contributions scientifiques de cette thèse peuvent être résumées comme suit: (1) le sujet de cette thèse, qui est une combinaison de réaction et de scalaire passif dans des écoulements turbulents, est nouveau; (2) nous avons développé une configuration pour la simulation numérique de la réaction turbulente, dans laquelle la positivité et la forte fluctuation des scalaires réactifs sont assurées; (3) dans l'étude sur les réactions en turbulence isotrope homogène, nous avons introduit un paramètre clé (Da_θ) caractérisant la compétition entre diffusion scalaire et réaction, et montré son rôle important dans la détermination des fluctuations et corrélations du scalaire réactif; (4) dans l'étude sur les réactions chimiques soutenues par les conditions aux limites de Dirichlet, nous avons proposé une modélisation établissant un lien entre les moments du scalaire réactif et le PDF du scalaire non réactif.

Travaux futurs

Par rapport aux études sur la combustion turbulente et les scalaires passifs en turbulence, relativement peu de travaux ont été consacrés à la réaction en turbulence incompressible, en particulier les réactions réversibles. Un problème inévitable concernant les réactions réversibles est l'équilibre chimique. Les propriétés statistiques des scalaires réactifs peuvent être extrêmement différentes dans un système réactif proche et fortement dévié de l'état d'équilibre chimique. Pour le cas avec état de quasi-équilibre discuté dans cette thèse, les fluctuations des scalaires doivent être contraintes à environ 10% des quantités moyennes pour assurer la positivité des concentrations. Cependant, un tel phénomène n'a pas de bon sens pratique pour des problèmes de turbulence typiques. Dans l'océan réel, les fluctuations affichées par les populations phytoplanctoniques peuvent atteindre des valeurs comparables à celles de la densité moyenne de population, car il existe des régions où la densité est très faible et des situations où une énorme accumulation peut être observée. Des solutions simples peuvent être d'imposer des concentrations négatives numériques à zéro ou d'exprimer les quantités de concentration sous la forme de fonctions de puissance. Cependant, ces opérations introduisent trop d'interférences arbitraires dans le problème. Il est donc important de proposer des configurations assurant le quasi-équilibre chimique, la positivité des scalaires réactifs et non de petites fluctuations scalaires, de préférence sans trop d'interférences artificielles ou du moins seulement

avec des corrections physiquement raisonnables des quantités de concentration.

Une façon simple d'amplifier les fluctuations consiste à faire passer le système dans un état de non-équilibre. Une autre raison pour laquelle l'état de non-équilibre est intéressant est que le terme de réaction peut être plus important. Une opération proposée dans cette thèse consiste à introduire des conditions aux limites de Dirichlet pour les scalaires réactifs. Cependant, une telle configuration brise l'isotropie des scalaires. Une réflexion plus approfondie sur une configuration conservant l'isotropie des champs scalaires et possédant en même temps une source de réaction non négligeable par rapport à la convection ou à la diffusion peut être intéressante. De plus, il est également intéressant d'étudier les réactions irréversibles, dans lesquelles le terme de réaction peut être non négligeable car l'équilibre chimique n'est pas impliqué.

Sur la base du domaine cubique isotrope homogène étudié dans un premier temps dans cette thèse, une configuration anisotrope avec des conditions aux limites de Dirichlet et des couches tampons pour les scalaires a été développée et discutée. Les champs scalaires réactifs dans cette dernière configuration sont beaucoup plus complexes, car la non-linéarité induite par la source de réaction est bien présente et active. Ainsi, les analyses de modélisation sur les propriétés statistiques des scalaires réactifs sont beaucoup plus difficiles. Une telle configuration est d'un grand

potentiel pour une exploration plus profonde et plus large au-delà de l'analyse théorique menée jusqu'à présent dans cette thèse. Dans les présents travaux, les prédictions théoriques sur les profils moyens et les fluctuations des scalaires réactifs pourraient correspondre aux tests numériques uniquement pour les cas avec une réaction directe infiniment grande ou beaucoup plus grande que la réaction inverse. De plus, les prédictions théoriques actuelles sur les profils moyens et les fluctuations des scalaires réactifs nécessitent la condition préalable que le PDF du scalaire passif subissant la même convection et diffusion soit connu. Dans les travaux futurs sur une telle configuration, un objectif important peut être l'amélioration de la modélisation pour une gamme d'applications plus large et la proposition d'expressions plus compactes sur les moments des scalaires réactifs. Une autre direction peut être la modification des hypothèses actuelles, qui fonctionnent mal pour le cas de réaction directe faible. Ou tout nouveau cadre théorique basé directement sur les équations gouvernantes des scalaires réactifs peut également être envisagé.

En outre, une analyse plus approfondie et plus complète des autres propriétés statistiques des scalaires réactifs, par exemple les coefficients de corrélation, peut également être les sujets intéressants pour les travaux futurs sur cette configuration.

Concernant le cas d'écoulement de Kolmogorov étudié dans cette thèse, dans les travaux futurs, nous proposons également d'explorer différentes

formes de forçage pour mieux comprendre les expressions des différents moments du champ de vitesse. Il reste également à comprendre à partir d'arguments analytiques pourquoi la viscosité turbulente est une constante indépendante de la position dans un tel écoulement, contrairement à ce que l'on trouve dans un écoulement similaire mais différent tel qu'un écoulement en canal ou des écoulements en couche limite. De plus, les modèles de fermeture du scalaire passif dans le « Kolmogorov flow » peuvent également être examinés, et l'extension aux scalaires réactifs sera plus intéressante.

Les lois d'échelle des scalaires turbulents a toujours été d'un grand intérêt depuis le cadre théorique de Kolmogorov-Obukhov-Corrsin. La réaction, en particulier la réaction rapide, est censée introduire une structure « de falaise » (« ramp-cliff ») dans les champs scalaires, et ainsi favoriser l'intermittence. Pour examiner cette idée et l'explorer plus avant, la comparaison des statistiques pertinentes, telles que les fonctions de structure et les spectres d'énergie, entre les scalaires passifs et réactifs peut être utile. Etant donné que le terme de réaction est généralement non linéaire, la convolution des champs scalaires existants peut se refléter dans les nombres d'onde élevés. Ainsi, pour une simulation numérique directe convaincante sur les problèmes turbulents concernant la réaction, la demande en ressource de calcul est plus élevée, car la résolution spatiale numérique doit être plus fine que celle requise par le scalaire passif.

En un mot, cette thèse a mené des études de base et préliminaires sur les scalaires réactifs en turbulence incompressible, par des simulations numériques directes et des analyses théoriques. Les nouvelles découvertes accompagnent toujours de nouveaux problèmes. En complément ou en développement des travaux réalisés dans cette thèse, de nombreuses questions intéressantes attendent encore des investigations complémentaires dans les travaux futurs.

Contents

List of Figures

List of Tables

Chapter 0

Presentation of the thesis

0.1 Curriculum Vitae

I am studying in the framework of a Sino-France cotutella PhD degrees between Shanghai Jiao Tong University (China) and Université du Littoral Côte d'Opale (France), funded by the Shanghai Jiao Tong University and the Région Hauts de France.

0.1.1 PhD Thesis:

Research topic: Chemical reactions in turbulence: numerical studies through a direct numerical simulation.
Cotutella: between SJTU (China) and ULCO (France).
Advisers:
Lipo Wang, associate professor, UM-SJTU Joint Institute, Shanghai JiaoTong University 200240, Shanghai, China,
Francois G. Schmitt, senior researcher, CNRS, Laboratory of Oceanology and Geosciences, UMR LOG 8187, Wimereux, France,
Enrico Calzavarini, assistant professor, Univ. Lille, Unité de Mécanique de Lille, UML EA 7512, F 59000, Lille, France.
Dates of periods in each institution:
April 2017 - May 2019 Shanghai,
June 2019 - November 2020 Wimereux-Lille. This was the original plan but due to the covid-19 crisis, I went back to China in April 2020 and I could not come back to France due to the closing of borders.

0.1.2 Education:

2009.09-2013.06: School of Science, University of Mining and Technology, Bachelor of Science (GPA: 85.2/100).

2013.09-2016.06: Institute of Plasma Physics, Chinese Academy of Sciences, Master Degree, Plasma Physics (GPA: 83.6/100).

2017.04-now: University of Michigan - Shanghai Jiao Tong University Joint Institute, Shanghai Jiao Tong University, Power Engineering and Engineering Thermophysics.

2017.09-now: Laboratory of Oceanology and Geosciences, cotutella PhD.

0.1.3 Participation to summer schools and conferences:

[1] Wu, W.. CNRS Summer School, "Active transport in the Ocean: Turbulence, Chemistry & Biology", Wimereux, France, 2-6 July 2018. (no presentation).

[2] Wu, W., L. Wang, E. Calzavarini, and F. G. Schmitt. The Fourth Xiamen Symposium on Marine Environmental Sciences, "Direct numerical simulation of chemical reactions in homogeneous isotropic turbulence", Xiamen, P. R. China, 6-9 January 2019. (Poster).

[3] Wu, W., L. Wang, E. Calzavarini, and F. G. Schmitt. European Geosciences Union General Assembly 2019, "Numerical study of second-order chemical reaction in homogeneous isotropic turbulence", Vienna, Austria, 7-12 April 2019. (Poster).

[4] Wu, W., L. Wang, E. Calzavarini, F. G. Schmitt, and M. Gauding. The 17th European Turbulence Conference, "Reactive species in turbulence", Turino, Italy, 3-6 September 2019. (Oral).

[5] Wu, W., L. Wang, E. Calzavarini, and F. G. Schmitt. La 2ème Journée Scientifique de la Mécanique des Fluides Lilloise, "Reactive scalars near to chemical equilibrium in incompressible turbulence", Lille, France, 21 November 2019. (Oral).

0.1.4 Papers published and in preparation:

Wu, W., E. Calzavarini, F. G. Schmitt, and L. Wang (2020). Fluctuations and correlations of reactive scalars near chemical equilibrium in incompressible turbulence. *Physical Review Fluids 5*, 084608. doi:10.1103/PhysRevFluids.5.084608

Wu, W., F. G. Schmitt, E. Calzavarini, and L. Wang. A quadratic constitutive equation for the turbulent Kolmogorov flow. To be sumbitted.

Wu, W., L. Wang, E. Calzavarini, F. G. Schmitt. Reactive scalars in incompressible turbulence with strongly non-equilibrium chemistry. To be sumbitted.

0.2 Objectives of the thesis

In this thesis, direct numerical simulations are implemented to numerically study reversible chemical reactions in incompressible turbulence. The main focus is on the fundamental properties of reactive scalar mixing, in comparison with a passive scalar, under a statistically stationary state. The flow statistics, from global to scale-dependent features, are studied in details and theoretically modelled.

The objectives of this thesis are the following:

- Obtain numerically statistical laws characterizing the fluctuations of reactive quantities for second order reaction or higher orders;
- Estimate the scaling properties of the reactive and passive scalars, using Fourier power spectra and structure functions for the intermittent properties;
- Perform a parametric study by varying e.g. the reaction order or the Damkholer number and study their effects in a statistical sense;
- Check different configurations to try to obtain the universal laws.

0.3 Organization of the thesis

The rest of this thesis is organized as follows. Chapter 1 introduces some basic concepts and classical theories about the incompressible turbulence and passive scalar fields convected. Chapter 2 presents some fundamentals and models about the chemical reaction, and it reviews the literature discussing the dynamics of reactive scalars in incompressible turbulence. Chapter 3 introduces some basic ideas of the numerical methods in computational fluid mechincs, in particular the pseudo-spectral and the finite difference approaches. It also discusses how they were implemented in this thesis. The subsequent chapters are about the original works of this thesis. Chapter 4 focuses on the reaction processes in homogeneous isotropic turbulence. In Chapter 5, an anisotropic and non-homogeneous turbulent flow: the turbulent Kolmogorov flow is discussed by testing an original turbulence closure model and by investigating chemical reactions in such flow. As a development of the homogeneous isotropic case, a configuration with Dirichlet boundary conditions for scalars is introduced and investigated in

Chapter 6. This configuration has the advantage of producing strongly out of equilibrium chemical reactions. Finally, in Chapter 7, a summary of the thesis and some ideas about the future works are identified.

Chapter 1

Introduction

Turbulence, scientifically important and challenging, exists widely in various situations, such as flows in automotive engines, chemical reactors, environmental flows including oceanographical and meteorological flows. It can be observed from the clouds on the sky, a turbulent jet ejected by an aircraft generating wakes, plumes spiraling up and spreading, or the whirls on the sea surface visualized from a satellite. An essential feature of turbulent flows is that the fluid velocity field varies significantly and irregularly in both position and time. Thus they are seemingly random and chaotic (Pope, 2000). From the statistical point of view, physicists have been focusing on finding some intrinsic and universal properties of turbulence, although turbulent motions can be of different configurations, different boundary conditions, and generated by various types of forcing (such as string to a cup of water). In turbulence studies, turbulent flows are considered to be composed of eddies of different sizes, which can span a very large range of scales. For example, the largest eddies in the ocean are of the order of kilometers or even larger, but the smallest eddies are invisible to human eyes. Typically, the external forcing is exerted at the large scales. Because of the energy cascade, the turbulent kinetic energy flows hierarchically towards the smaller scales till the smallest end where the kinetic energy is dissipated to heat. According to a picture originally proposed by Kolmogorov (1941a,b), at the scales much smaller than the domain or forcing scale but larger than the smallest eddies, the information of boundary or forcing from largest scale is lost, and the effect of dissipation is negligible. Thus universality is believed to exist in the properties of turbulent motions of these scales because they are fully determined by the inertial interaction between eddies. This range of scales is called inertial range and it is the main focus of most of fundamental studies in turbulence theories.

This chapter is an introduction about some fundamentals concerning incompressible turbulence and non-reactive scalars transported in it. It is organized as follows. In section 1.1, the mathematical description of the

turbulent motion, Navier-Stokes equations, is first introduced. Then the idea of energy cascade in turbulent and the classical K41 theory quantifying the scaling behaviors in turbulent flow are introduced. Section 1.2 is about passive scalars in incompressible turbulence, focusing on the governing equations, statistical properties, scaling behaviors and intermittency of passive scalar. In next chapter, Chapter 2, the fundamentals about the reactive scalars in turbulence, which is the main topic of this thesis, are presented.

1.1 Turbulent flow

1.1.1 Navier-Stokes equations

Lagrangian and Eulerian description

To derive the equations fully describing the motion of turbulent flows, the clarification of the framework under which the motion of fluids is described is needed. There are two ways to describe fluid motion. One is the Lagrangian description, in which fluid particles are followed as they move through the flow field. The other is the Eulerian description, in which the properties of the flow field are monitored using a fixed reference frame. In fact, most studies about fluids mechanics are based on the Eulerian description, because the global properties of the flow field or the properties at specific region are of physicists' interests, instead of any particular fluid particles. However, the understanding of the Lagrangian description is also necessary because the derivation of the momentum equation about fluid motion is exactly the application of Newton's second law to the fluid particles.

The Lagrangian description is based on tracing the motion of fluid particles. The position of a fluid particle is the function of current time t, the reference time t_0 and the position of this particle at the reference time $\mathbf{r}_0$: $\mathbf{r}(t;\mathbf{r}_0,t_0)$. And the velocity of this particle is the temporal derivative of $\mathbf{r}(t;\mathbf{r}_0,t_0)$: $\mathbf{u} = d\mathbf{r}(t;\mathbf{r}_0,t_0)/dt$. In such a track-dependent description, a property of the fluid field F is described as function of the position and time: $F = F[\mathbf{r}(t;\mathbf{r}_0,t_0),t]$.

The Eulerian description focuses on properties of flow field at the locations of interest, in which the fluid particles are not discriminated. A property of the fluid field F is the function of position and time: $F = F(\mathbf{x},t)$.

$F[\mathbf{r}(t;\mathbf{r}_0,t_0),t]$ and $F(\mathbf{x},t)$ are two descriptions of one quantity. When $\mathbf{r} = \mathbf{x}$,

$$F[\mathbf{r}(t;\mathbf{r}_0,t_0),t] = F(\mathbf{x},t). \tag{1.1}$$

By taking the temporal derivative of Eq. (1.1), it yields

$$\begin{aligned}\frac{d}{dt}F[\mathbf{r}(t;\mathbf{r}_0,t_0),t] &= \frac{\partial F}{\partial r_1}\frac{dr_1}{dt}+\frac{\partial F}{\partial r_2}\frac{dr_2}{dt}+\frac{\partial F}{\partial r_3}\frac{dr_3}{dt}+\frac{\partial F}{\partial t}\\ &= \frac{\partial F}{\partial x_1}u_1+\frac{\partial F}{\partial x_2}u_2+\frac{\partial F}{\partial x_3}u_3+\frac{\partial F}{\partial t}=(\mathbf{u}\cdot\nabla)F+\frac{\partial F}{\partial t}=\frac{D}{Dt}F(\mathbf{x},t).\end{aligned} \tag{1.2}$$

Eq. (1.2) builds the connection between Lagrangian and Eulerian description of fluids, in which $\frac{D}{Dt}$ is called material derivative.

Continuum approximation and Reynolds' transport theorem

A fluid is composed of a huge number of fluid molecules. From the chemical or atomically physical point of view, the properties of these molecules may be taken into consideration. However, in fluid mechanics, the fluids are studied by considering a control volume much larger than the fluid molecule, and averaging the behavior of the fluid molecules inside. For example, the pressure of the flow field instead of the collision among fluid molecules is considered. These control volumes are microscopically infinitely large but macroscopically infinitely small. They are valid only when the length scale of physical interest is much larger than the mean free path of fluid molecules, which means the fluid is of continuous distribution. This is one of the fundamental hypotheses in fluid mechanics, called continuum approximation. The continuum approximation is valid when the Knudsen number $Kn = \iota/\mathcal{L}$ is much smaller than unity, where ι is the mean free path of the molecules and $\mathcal{L}$ is the length scale of interest. Generally, $Kn \ll 1$ is satisfied in the nature, except in very few cases, for example in the quasi-vacuum environment or at the thinner reaches of the tenuous gases.

Using the concepts of continuum and control volume, the governing equations of flow motions can be derived by considering the conservation laws of mass, momentum or energy. The physical laws applied to an control volume are always in Lagrangian description. As aforementioned, the operation of material derivative ($\frac{D}{Dt}$) is needed, and it is necessary to transform such operations into the volume integrals of Eulerian description. The theorem for this transformation is called Reynolds' transport theorem. Let $V(t)$ be a control volume of arbitrary shape and $F(t)$ be a quantity of interest as functions of time t. The Reynolds' transport theorem states

$$\frac{D}{Dt}\int\limits_{V(t)} F(t)dV = \int\limits_{S(t)} F(t)\mathbf{u}\cdot\mathbf{dS} + \int\limits_{V(t)}\frac{\partial F}{\partial t}dV. \tag{1.3}$$

The Reynolds' transport theorem can be mathematically derived by considering the definition of derivative from the perspective of limit (Kundu et al., 2012; Currie, 2002). The right hand side of Eq. (1.3) are in Eulerian

description and the left hand side ia applicable to refer to specific physical law.

Mass conservation and momentum conservation

By considering the mass conservation and the momentum conservation of fluid motion, the continuity equation and the equation of momentum conservation are readily obtained (Kundu et al., 2012; Currie, 2002):

$$\frac{1}{\rho}\frac{D\rho}{Dt} + \nabla \cdot \mathbf{u} = 0, \tag{1.4}$$

$$\rho(\frac{\partial \mathbf{u}}{\partial t} + (\mathbf{u} \cdot \nabla)\mathbf{u}) = \rho\mathbf{f} + \nabla(\tau_{ij}), \tag{1.5}$$

where ρ is number density of fluid particles, $\mathbf{f}$ is the acceleration by the net body force and τ_{ij} is the stress tensor. Mathematically, Eq. (1.4) is derived by considering the F in Eq. (1.3) as ρ, and Eq. (1.5) is derived by considering the F as $\rho\mathbf{u}$ and using Newton's second law.

The set of equations of Eq. (1.4) and Eq. (1.5) has more unknowns than the number of equations. In order to produce a solvable system, a constitutive equation about the stress tensor τ_{ij} (for newtonian fluid) is needed:

$$\tau_{ij} = -p\delta_{ij} + 2\mu(S_{ij} - \frac{1}{3}(\nabla \cdot \mathbf{u})\delta_{ij}) + \mu_v(\nabla \cdot \mathbf{u})\delta_{ij}, \tag{1.6}$$

where p is the pressure; μ is the coefficient of dynamic viscosity; μ_v is the coefficient of bulk viscosity, which can be considered as 0 by Stokes assumption (Kundu et al., 2012); δ_{ij} is Kronecker delta tensor, whose component is 1 when $i = j$ and 0 when $i \neq j$; $S_{ij} = \frac{1}{2}(\frac{u_i}{x_j} + \frac{u_j}{x_i})$ is the strain rate tensor. Substituting Eq. (1.6) into Eq. (1.5) produces the Navier-Stokes Equations:

$$\rho(\frac{\partial \mathbf{u}}{\partial t} + (\mathbf{u} \cdot \nabla)\mathbf{u}) = \rho\mathbf{f} - \nabla p + \mu\triangle\mathbf{u} + (\mu_v + \frac{1}{3}\mu)\nabla \cdot \mathbf{u}. \tag{1.7}$$

In this thesis, only the incompressible turbulent flows are considered, which are of constant density. For incompressible fluids, Eq. (1.4) and Eq. (1.7) are simplified to:

$$\nabla \cdot \mathbf{u} = 0, \tag{1.8}$$

and

$$\frac{\partial \mathbf{u}}{\partial t} + (\mathbf{u} \cdot \nabla)\mathbf{u} = -\nabla p/\rho + \nu\triangle\mathbf{u} + \mathbf{f}, \tag{1.9}$$

where $\nu = \mu/\rho$ is the coefficient of the kinematic viscosity.

Eq. (1.9) can be made dimensionless by choosing characteristic length scale L and characteristic velocity amplitude U as reference scales. This leads to the following dimensionless Navier-Stokes Equations for incompressible fluids:

$$\frac{\partial \mathbf{u}}{\partial t} + (\mathbf{u} \cdot \nabla)\mathbf{u} = Re^{-1} \triangle \mathbf{u} - \nabla p + \mathbf{f}, \tag{1.10}$$

where

$$Re = \frac{UL}{\nu} \tag{1.11}$$

is the Reynolds number. Turbulent flow is characterized by large Reynolds number, and the flow with small Reynolds number is called laminar flow. When $Re = LU/\nu \gg 1$, the non-linear convection term $((\mathbf{u} \cdot \nabla)\mathbf{u})$ is dominant, and the inertial force of the fluid motion is much stronger than the viscous force which is to slow down the fluid motion. Thus the flow is chaotic and unstable. More importantly, the flow with large Re is of most interest of physicists, because the flow motion is of a large span of length scales. Then the inertial range of length scales, which are between the largest scales and the smallest scales and believed to contain some universal properties, is more distinguishable.

Vortex stretching

The turbulent motion can be considered as a collection of numerous eddies. Thus an important feature of turbulence is the rotational motion (Pope, 2000). By taking the curl of Eq. (1.10) without external body forcing, it yields

$$\frac{D\omega}{Dt} = Re^{-1} \triangle \omega + \omega \cdot \nabla \mathbf{u}, \tag{1.12}$$

where $\omega = \nabla \times \mathbf{u}$ is called as the vector of vorticity, which is twice of the rotation rate of the fluid. In the circumstance of large Re, the viscous term $Re^{-1} \triangle \omega$ can be neglected.

Considering an infinitesimally small material line $\mathbf{l} = \delta \mathbf{x}$, it evolves as

$$\frac{D\mathbf{l}}{Dt} = \mathbf{l} \cdot \nabla \mathbf{u}, \tag{1.13}$$

which is exactly the same as Eq. (1.12) without the viscous term. Thus the vorticity component in the direction, along which the fluid material line element is stretched by the velocity gradient, tends to increase. In other word, the vector of the vorticity tends to align with the principle direction of the mean stain rate. Such a phenomenon is called as vortex stretching. It is very important in turbulent motion because it is the process about how the eddies extract energy from the mean shear flow. It is noteworthy that the process of vortex

stretching exists not only in two dimensional turbulence since the angular momentum of eddy is concerned. This indicates the three dimensional and two dimensional turbulence are fundamentally different.

1.1.2 Energy cascade

In about 500 years ago, the turbulent flow was recognized to be composed by eddies of different sizes, e.g. the drawing by Leonardo da Vinci of the flowing water out of a ditch, as shown in figure 1.1.

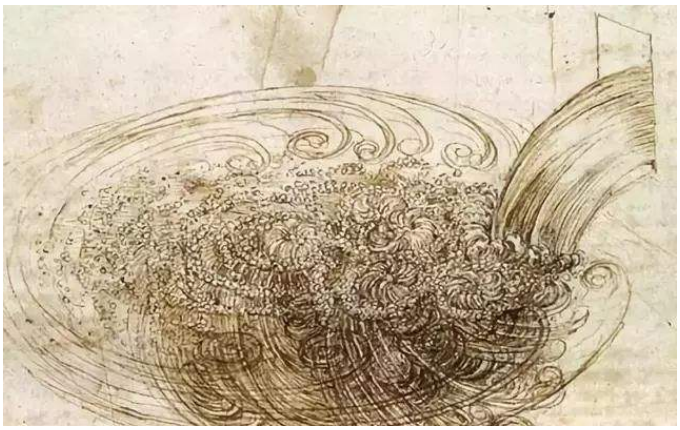

Figure 1.1: Drawing of turbulence by Leonardo da Vinci (15th century).

The energy from outside of the turbulent flow is injected, by external forces or boundary conditions, into the flow at the large scales. The flow motion at these scales are of largest Reynolds number, and most unstable. As a result, they eventually will break up into smaller and smaller eddies. Such a process stops when the eddies of small enough scales are reached, in which the viscosity is important. The breaking-up of eddies is accompanied with the transfer of energy, which will eventually be dissipated into heat by viscosity. This whole process is called turbulent cascade. An illustration about this process is given in figure 1.2. The concept of energy cascade in turbulence was first introduced by Richardson (1922) with a famous verse:

> Big whirls have little whirls
> that feed on their velocity,
> And little whirls have lesser whirls
> and so on to viscosity.

In Navier-Stokes equations (Eq. (1.10)), the convection term $((\mathbf{u}\cdot\nabla)\mathbf{u})$ is responsible for transferring the energy to smaller scales and the dissipation term $(Re^{-1}\triangle\mathbf{u})$ is responsible for dissipating the energy into heat at the smallest scales. In order to have stationary turbulence, energy have to be added at the large scales to maintain the motion of eddies, otherwise the entire kinetic energy will gradually vanish, through the cascade process.

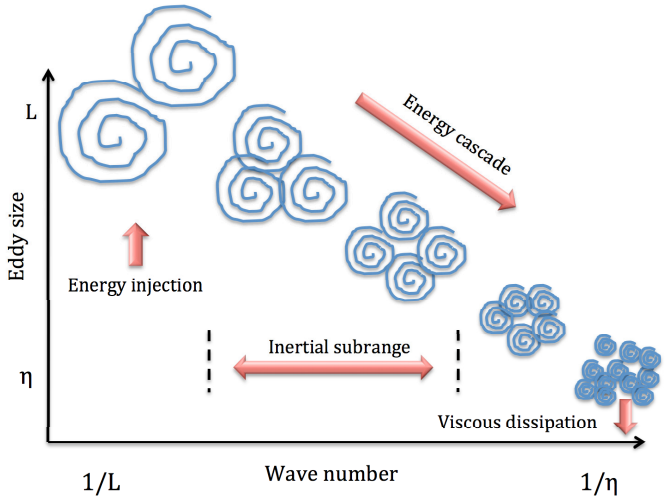

Figure 1.2: Illustration of turbulent cascade (Ardeshiri, 2016). L is the length scale of domain and η is the smallest length scale, kolmogorov microscale. Energy is injected from outside of the flow at the largest scales. Then the largest eddies break up into eddies of smaller and smaller size and energy is meanwhile transferred. This process continues until the smallest eddies and the energy is dissipated by viscosity.

1.1.3 Kolmogorov's 1941 theory

In general, the N-S equations can not be solved analytically. However based on the N-S equations, physicists have obtained some theories describing the fundamentals of turbulent motions, such as those proposed by Richardson (1922), Taylor (1935) and Kolmogorov (1941b,a). A milestone in the studies of turbulence is the Kolmogorov theory in 1941 (Kolmogorov, 1941a,b), which is the first quantitative description to the energy cascade process in turbulence. The Kolmogorov's 1941 (K41) theory is based on the following assumpotions:

> **Kolmogorov's hypothesis of local isotropy.** At sufficiently high Reynolds number, the small-scale turbulent motions of the scale ($l \ll L$) are statistically isotropic.
>
> **Kolmogorov's first similarity hypothesis.** In every turbulent flow at sufficiently high Reynolds number, the statistics of the small-scale turbulent motions of the scale ($l \ll L$) have a universal form that is uniquely determined by ν and ϵ (energy dissipation rate, the average rate of dissipation of turbulent kinetic energy per unit mass).
>
> **Kolmogorov's second similarity hypothesis.** In every turbulent flow at sufficiently high Reynolds number, the statistics of the small-scale turbulent motions of the scale in the range ($\eta \ll l \ll L$) have a universal form that is uniquely determined by ϵ, independent of ν .

The hypothesis of local isotropy states that the turbulent motions of small scales are isotropic, although the forcing or boundary conditions at large scale are generally anisotropic. When the energy cascade reaches small

enough scales, the information of largest scales is lost and the isotropy is restored.

The first similarity hypothesis states that when the information of largest scales is lost, the statistical properties of turbulent flows are fully dependent on the viscosity ν and dissipation rate ϵ ($\langle \frac{\nu}{2}(\frac{\partial u_i}{\partial x_j} + \frac{\partial u_j}{\partial x_i})^2 \rangle$). Therefore, by dimensional analysis, the smallest scales (Kolmogorov scales) are estimated as:

$$\eta = \left(\frac{\nu^3}{\epsilon}\right)^{1/4}, \qquad u_\eta = (\nu\epsilon)^{1/4}, \qquad \tau_\eta = \frac{\eta}{u_\eta} = \left(\frac{\nu}{\epsilon}\right)^{1/2}, \tag{1.14}$$

where η, u_η and τ_η are the Kolmogorov length scale, Kolmogorov velocity scale and Kolmogorov time scale respectively. The Reynolds number at the Kolmogorov scale is $Re_\eta = (\eta u_\eta)/\nu = 1$.

The second similarity hypothesis is about the inertial range of scale, where the effect of energy dissipation is also negligible. Thus the dissipation rate ϵ, which is also the energy injection rate at largest scales and energy transfer rate at the intermediate scales because of energy conservation, is the only key parameter to determine the properties of flow motion.

The motion of the largest eddies is of the integral length scale L and characteristic velocity U. By dimensional analysis, L can be estimated as

$$L = \frac{U^3}{\epsilon}. \tag{1.15}$$

According to Eq. (1.11) and (1.14), the ratio of the largest scale to the smallest scale is

$$\frac{L}{\eta} = Re^{3/4}. \tag{1.16}$$

This explains why the flow motion with larger Reynolds number spans a larger range of scales.

Kolmogorov assumes that the flow is self-similar at the scale much smaller than the largest scales. An important consequence of this assumption is that there is a unique scaling exponent h in the scaling relation of the velocity difference $\delta u(l) = u(x+l) - u(x)$:

$$\delta u(\alpha l) = \alpha^h \delta u(l). \tag{1.17}$$

This scaling relation implies the scaling behavior of the structure functions

$$S^q(l) = \langle |\delta u|^q \rangle = \langle |u(x+l) - u(x)|^q \rangle \sim l^{\zeta(q)}, \tag{1.18}$$

where $\zeta(q)$ is the scaling exponent of qth order structure function.

By considering the famous Kármán-Howarth equation in terms of the structure function and neglecting the viscous term in the inertial range (Monin and Yaglom, 1975; Pope, 2000), the Kolmogorov 4/5th law can be obtained as

$$\langle (u(x+l) - u(x))^3 \rangle = -\frac{4}{5}\epsilon l. \tag{1.19}$$

This is an exact result about the scaling behavior of third order longitudinal structure function derived from the Navier-Stokes equations, indicating the scaling exponent of third order structure function is $\zeta(3) = 1$. K41 theory suggests that $\zeta(q)$ is linearly dependant on q, i.e. $\zeta(q) = q/3$.

However, the linear dependance between $\zeta(q)$ and q was later found incorrect, because of the internal intermittency. The phenomenon of the internal intermittency in turbulence was first found in the turbulent motion by Batchelor and Townsend (1949), when they revealed that the instantaneous energy dissipation rate could evolve to large value intermittently in their experiment. In order to take the internal intermittency into account, the refined similarity hypotheses were proposed by Kolmogorov (1962) and Obukhov (1962) for the velocity field. This hypothesis leads to a non-linear expression of $\zeta(q)$ as

$$\zeta(q) = \frac{q}{3} - \frac{\mu}{18}(q^2 - 3q), \tag{1.20}$$

where μ is a constant, called as intermittency exponent. Later, in the the multifractal framework (Yaglom, 1966; Mandelbrot, 1974; Frisch, 1995), which suggests that the energy cascade has multifractal statistics, the scaling exponent is estimated as

$$\zeta(q) = \frac{q}{3} - K(\frac{q}{3}), \tag{1.21}$$

where $K(\frac{q}{3})$ is model-dependant (for example β model (Frisch et al., 1978) or lognormal model (Obukhov, 1962; Kolmogorov, 1962)).

Although K41 theory was found questionable, for second order structure function, $\zeta(2) = 2/3$ is nevertheless a good estimation. In the work by Kolmogorov (1941b), the second order structure function was considered. And by dimensional analysis, it was derived that

$$S^2(l) = C'\epsilon^{2/3} l^{2/3}, \tag{1.22}$$

where C' is the Kolmogorov constant and believed to be universal. Such a result confirms the estimation of $\zeta(2) = 2/3$. The scaling law of the energy cascade can also be derived based on the results of structure functions.

Taking the advantage of Fourier Transform, for the eddies of length scale of l, $k = 2\pi/l$ is the corresponding wave number. To fully understand the energy cascade, the velocity $\mathbf{u}$ is decomposed into mean part and fluctuating part:

$$\mathbf{u} = \langle \mathbf{u} \rangle + \mathbf{u}'. \tag{1.23}$$

in which $\langle \cdot \rangle$ means the ensemble average, $\langle \mathbf{u} \rangle$ is the mean velocity, i.e. the motion of $\mathbf{0}$ wave number (largest scale), and $\mathbf{u}'$ is the sum of the velocity of other modes (smaller scales). An important feature of turbulent flow is that $\mathbf{u}'$ is comparable with or dominant over $\langle \mathbf{u} \rangle$. The tensor of autocovariance is

$$R_{ij}(\mathbf{r}) = \langle \mathbf{u}_i'(\mathbf{x}) \mathbf{u}_j'(\mathbf{x} + \mathbf{r}) \rangle. \tag{1.24}$$

Taking the Fourier transform of $R_{ij}(\mathbf{r})$ produces

$$\Phi_{ij}(\mathbf{k}) = \frac{1}{8\pi^3} \int R_{ij}(\mathbf{r}) e^{-i\mathbf{k}\cdot\mathbf{r}} d\mathbf{r}, \tag{1.25}$$

where $\mathbf{k}$ is the vector of wave number. Then the energy spectrum is defined in $\mathbf{k}$ space, as the integral of $\frac{1}{2}\Phi_{ii}$ in the sphere with radius of $|\mathbf{k}|$:

$$E(k) = \int \frac{1}{2} \Phi_{ii}(\mathbf{k}) \delta(k - |\mathbf{k}|) d\mathbf{k}, \tag{1.26}$$

where the repeating index of Φ_{ii} is Einstein summation convention, i.e. $\frac{1}{2}\Phi_{ii} = \frac{1}{2}(\Phi_{11} + \Phi_{22} + \Phi_{33})$ in three dimensional space.

The autocovariance R_{ij} has the same dimension with the second order structure function $S_2(l)$. Thus by dimensional analysis, a $-5/3$ scaling relation can be found in the energy spectrum (Obukhov, 1941):

$$E(k) = C\epsilon^{2/3} k^{-5/3}, \tag{1.27}$$

where C is a constant. This result is known as Kolomogorov-Obukhov's $-5/3$ law (Kolmogorov, 1941a,b; Obukhov, 1941), quantitatively describing the energy cascade in the inertial range.

1.2 Passive Scalars

The concentration of a substance or intensity of a property convected by a turbulent flow can exhibit a very complex structure, evolving broadly in both space and time. Such substances can be dye diluted in the water or smoke dispersing in air. The property can be the temperature of air flow when cooling a hot fin. The

turbulent convection of these substances are important in many circumstances, such as in the atmospheric studies, chemical and thermal engineering, and biological research. They are all one-dimensional quantities and share the same form of governing equation. Thus they are described as scalars (in comparison with vector such as velocity). Scalars in the turbulent environment are transported and dispersed by the turbulent eddies from largest to smallest scales, under the action of thermal or molecular diffusion as well. In many cases, the advected scalars have strong effects on the turbulent flow, i.e. the velocity field. For example, some considerable change in temperature can significantly change the fluid density. These scalars are called active scalars, which are beyond the consideration of this thesis. The passive scalars are undergoing dispersion and mixing processes mainly driven by the turbulent flow, but does not couple back on the flow dynamics, leading to negligible change in the property of background flow (Monin and Yaglom, 1975; Libby and Williams, 1976; Shraiman and Siggia, 2000; Warhaft, 2000; Mitrovic and Papavassiliou, 2004).

1.2.1 Advection-diffusion equation

Let θ be a passive scalar field, for example representing the molecular concentration of any species. By considering the F in Eq. (1.3) as the volumetric density ($\theta\rho$) and using the Fick's law of diffusion (Bergman et al., 2011), the advection-diffusion equation of passive scalar can be obtained. In incompressible fluid, it reads

$$\frac{\partial\theta}{\partial t} + (\mathbf{u}\cdot\nabla)\theta = D\triangle\theta + \dot{q}, \tag{1.28}$$

where θ is the passive scalar, D is the species diffusivity for species or thermal conductivity for temperature, $\dot{q}$ is the external source or sink. In the dimensionless from, the governing equation of passive scalar is

$$\frac{\partial\theta}{\partial t} + (\mathbf{u}\cdot\nabla)\theta = (Re\cdot Sc)^{-1}\triangle\theta + \dot{q}, \tag{1.29}$$

where $Sc = \nu/D$ is the Schmidt number.

Eq. (1.29) is in a form similar with Eq. (1.10). Thus physicists are interested in analogizing the properties of passive scalar to that of velocity, especially questing for the universality in the inertial range of scales and under the condition of large enough Reynolds (Re) and Peclét ($Pe = Re\cdot Sc$) numbers.

Moments of passive scalar

Similar with the Reynolds decomposition of velocity $\mathbf{u}$ (Eq. (1.23)), θ can be decomposed into mean part and fluctuating part:

$$\theta = \langle\theta\rangle + \theta'. \tag{1.30}$$

The $\langle\theta\rangle$ is the mean quantity of scalar, i.e. the amplitude of the $\mathbf{0}$ wave number mode (largest scale), and θ' is the sum of the rest modes (smaller scales). Then the scalar variance is defined as the mean square of the fluctuating part: $\langle\theta'^2\rangle$. The scalar variance describing the magnitude of the fluctuation of θ is also called as scalar energy, because it is an analogy of the kinematic energy for velocity $\langle(u_i'u_i'/2)\rangle$. Considering the ensemble average ($\langle\cdot\rangle$) of Eq. (1.28), it yields

$$\frac{\partial\langle\theta\rangle}{\partial t} + \nabla\cdot(\langle\mathbf{u}\rangle\langle\theta\rangle) = D\triangle\langle\theta\rangle - \nabla\cdot\langle\mathbf{u}'\theta'\rangle + \langle\dot{q}\rangle. \tag{1.31}$$

The covariance between passive scalar and velocity $\langle\mathbf{u}'\theta'\rangle$ at the right-hand-side of the Eq. (1.31) is the turbulent flux of passive scalar.

The passive scalar flux is generally unknown. Its determination belongs to the closure of turbulence. As an analogy with molecular motion and the introduction of the diffusivity constant, a simplifying assumption is sometimes used, which sates that the passive scalar flux is linked with the mean gradient, using a diffusivity tensor. This was proposed by Batchelor (1949), as

$$\langle\mathbf{u}'\theta'\rangle = -D_{T,ij}\nabla\langle\theta\rangle, \tag{1.32}$$

where $D_{T,ij}$ is the turbulent diffusivity tensor. A further simplification is to assume that this diffusivity tensor is diagonal (Monin and Yaglom, 1975). A last simplification is to assume that this tensor is proportional to the unit tensor, and thus depends on only one parameter D_T, providing a proportionality between vectors (Pope, 2000; Tennekes and Lumley, 1972):

$$\langle\mathbf{u}'\theta'\rangle = -D_T\nabla\langle\theta\rangle, \tag{1.33}$$

where D_T is the turbulent diffusivity of the passive scalar. This is called the mixing length hypothesis, which is useful for modelling purpose, but is not compatible with intermittency and long-range correlations in turbulent fluctuations. As mentioned in the book by Tennekes and Lumley (1972), the mixing length hypothesis is rather well satisfied only when the turbulent flow is mean gradient driven. But in other cases, such as buoyancy driven flow or homogeneous flow, the mixing length hypothesis is not valid.

The energy of the passive scalar is defined as the variance of the fluctuation $\langle\theta'^2\rangle$. In a canonical case where the mean gradient of passive scalar $\nabla\theta$ is constant and the external source is of zero mean $\langle\dot{q}\rangle = 0$, the governing equation of θ' can be derived from the Reynolds decomposition of Eq. (1.28), as

$$\frac{D\theta'}{Dt} = D\triangle\theta' + \dot{q}' - \mathbf{u}\cdot\nabla\langle\theta\rangle. \tag{1.34}$$

By multiplying Eq. (1.34) with θ' and taking ensemble average ($\langle\cdot\rangle$), it can be obtained that

$$\frac{1}{2}\frac{D\langle\theta'^2\rangle}{Dt} = -D\langle(\nabla\theta')^2\rangle + \langle\theta'\dot{q}'\rangle - \langle\mathbf{u}'\theta'\rangle\cdot\nabla\langle\theta\rangle. \tag{1.35}$$

The minus sign of the dissipation term $D\langle|\nabla\theta'^2|\rangle$ indicates it is responsible for the energy lose of the fluctuation of passive scalar. On the other hand, in addition to the energy injection from the external source, the fluctuation of passive scalar can also be sustained by the passive scalar mean gradient, whose energy injection power is proportional to the flux of passive scalar $\langle\mathbf{u}'\theta'\rangle$.

1.2.2 Obukhov-Corrsin theory

Similarily with Kolmogorov's and Obukhov's theories for the scaling properties of the velocity field, results for passive scalars can also be obtained.

The autocovariance of scalar is defined as

$$R_\theta(\mathbf{r}) = \langle\theta'(\mathbf{x})\theta'(\mathbf{x}+\mathbf{r})\rangle. \tag{1.36}$$

Taking the Fourier transform of $R_\theta(\mathbf{r})$ produces

$$\Phi_\theta(\mathbf{k}) = \frac{1}{8\pi^3}\int R_\theta(\mathbf{r})e^{-i\mathbf{k}\cdot\mathbf{r}}d\mathbf{r}. \tag{1.37}$$

Then the energy spectrum is defined in $\mathbf{k}$ space, as the integral of $\frac{1}{2}\Phi_\theta$ in the sphere with radius of $|\mathbf{k}|$:

$$E_\theta(k) = \int\frac{1}{2}\Phi_\theta(\mathbf{k})\delta(k-|\mathbf{k}|)d\mathbf{k}. \tag{1.38}$$

The global scalar variance is the integral of $E_\theta(k)$ all over the amplitude of wave numbers:

$$\langle\theta'^2\rangle = \int E_\theta(k)dk. \tag{1.39}$$

Here the the energy spectrum of the scalar $E_\theta(k)$ describes the fluctuation of θ at the length scale of $(2\pi/k)$.

Following Kolmogorov (1941b), Obukhov (1949) and Corrsin (1951) argued that, under the condition of high enough Re and Pe numbers, there is also an energy cascade process of passive scalars from large to small scales, at which the fields of passive scalars are locally isotropic. Together with the scaling of the velocity field, this forms the classical KOC (Kolmogorov-Obukhov-Corrsin) theoretical framework.

In real space, Obukhov and Corrsin's results (Obukhov, 1949; Corrsin, 1951), stated independently, are that the scaling relation second order structure function of a passive scalar follow:

$$S_\theta^2(l) = \langle|\delta\theta|^2\rangle = C'_\theta \epsilon^{-1/3}\epsilon_\theta l^{2/3}, \tag{1.40}$$

and in Fourier space:

$$E_\theta(k) = C_\theta \epsilon^{-1/3}\epsilon_\theta k^{-5/3}, \tag{1.41}$$

where C'_θ and C_θ are constants and ϵ_θ $(2D\langle\frac{\partial\theta}{\partial x_i}\frac{\partial\theta}{\partial x_i}\rangle)$ is the dissipation rate of scalar variance. The energy spectrum of scalar variance obeys a similar scaling law with the kinematic energy spectrum in the inertial range.

Effect of Schmidt number

An extension of Obukhov-Corrsin theory was done by Batchelor in 1959 (Batchelor, 1959; Batchelor et al., 1959). In the study about turbulent passive scalar field, the smallest length scale is characterized by the Batchelor scale η_B (Batchelor, 1959) which is different from the smallest length scale of velocity field (Kolmogorov scale η) with a factor of the square root of Schmidt number Sc (ν/D), as:

$$\eta_B = \frac{\eta}{Sc^{1/2}}. \tag{1.42}$$

When $Sc \sim 1$, the $-5/3$ law for passive scalar refers to the scaling behavior in the inertial range (between large scale L and η). For the case of very large Sc $(\eta \gg \eta_B)$, the length scales between L and η is referred as inertial-convective range, in which the $-5/3$ scaling law holds. Moreover, in this circumstance, the range of length scales even smaller than η but larger than η_B (called as the viscous-convective range) is also of interest, in which the energy of passive scalar variation scales as k^{-1} (Batchelor, 1959). For a passive scalar field with $Sc \ll 1$ $(\eta_B \gg \eta)$, the inertial range can be divided into inertial-convective range (between L and η_B) and inertial-diffusive range (between η_B and η). The $-5/3$ law holds in the inertial-convective range, while the

scaling coefficient in the inertial-diffusive range is $-17/3$ (Batchelor et al., 1959).

Numerical studies of the Obukhov-Corrsin theory

Soon after the use of computers, a lot of numerical studies based on the N-S equations and the convection-diffusion equation of passive scalar were implemented for examining the Obukhov-Corrsin theory (Sreenivasan, 1991; Sreenivasan and Antonia, 1997), whose prerequisite is high enough Re and Pe numbers. With the development of super computers, the numerical spatial resolution becomes finer and finer. Thus the direct numerical simulations about the passive scalar in turbulence with high Re and Pe numbers (the Kolmogorov scale is smaller and finer grid size is required to resolve it) is possible.

The $-5/3$ scaling behavior in the energy spectrum of the passive scalar variance is one main conclusion of the Obukhov-Corrsin theory. This have been well observed in some numerical studies (Warhaft, 2000; Yeung et al., 2005). In the past few decades, several numerical studies about the passive scalar spectrum were interested in the effect of Sc number. Some works focused on the cases of small Sc (Yeung et al., 2002; Yeung and Sreenivasan, 2014; Hill, 2017). In the work by Briard and Gomez (2015), the energy spectrum of passive scalar variance in isotropic turbulence, with $Re = 160$ and Pr between 10^{-6} and 1, was numerically studied*. For the case of $Pr = 1$, a $-5/3$ slope was found for the spectrum between $Pr^{3/4}k_\eta$ and k_η, where k_η is wave number corresponding to the Kolmogorov scale. With the decrease of Pr, a more detailed scaling behavior than that stated by Batchelor et al. (1959) was detected. The spectrum gradually evolves into a combination of a $-17/3$ slope between $Pr^{3/4}k_\eta$ and $\sqrt{Pr}k_\eta$ and a $-11/3$ slope between $\sqrt{Pr}k_\eta$ and k_η. Meanwhile, high Sc number, for which even better resolution is required to resolve the Batchelor scale ($\eta/Sc^{1/2}$), is also of high interest (Warhaft, 2000; Gotoh et al., 2015). In the work by Donzis et al. (2010), direct numerical simulation data was used to examine the spectrum of passive scalar fluctuation maintained by uniform mean gradient in forced stationary isotropic turbulence. The Sc number varies from 1/8 to 1024, and Taylor-scale Reynolds number (Re_λ) varies from 8 to 650 on the periodic domains of 64^3 to 4096^3 grid points. It was clearly observed that, for all Reynolds numbers, there was a general trend for the high wave number spectrum to flatten towards k^{-1} as Sc increases.

1.2.3 Probability density function, structure function and intermittency

The probability density function (PDF) of the passive scalar did not received attention as much as the energy spectrum until the 1980s, because the fluctuation of passive scalar normalized by its standard derivation had

*Pr means Prandtl number, which is equivalent to Sc when dealing with temperature as a passive scalar.

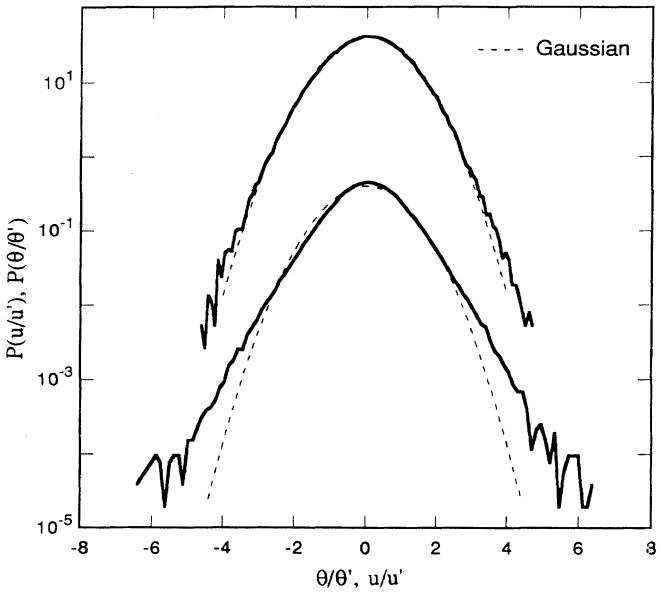

Figure 1.3: The probability density function of normalized velocity (upper curve) and temperature (lower curve) in a grid-generated turbulence (shown in the work of Jayesh and Warhaft (1991)). For legibility purpose, the upper curve has been shifted by 2 decades with respect to the lower one. Note that in the labels, the θ and u are the fluctuations and θ' and u' are the corresponding rms. The deviation of PDF from Gaussian curve for the scalar is larger than that of the velocity, because the intermittency of the scalar field is relatively stronger.

been assumed of Gaussian distribution in homogeneous turbulence, which was a satisfactory model. However, it was then found in experimental and theoretical studies that the PDF of the passive scalar has exponential tails (see figure 1.3). It indicates that the probability of the scalar to reach extremely high or low values is larger than what was believed before. Such a phenomenon is of practical interest, for example when the scalar is the concentration of a toxic chemical. The exponential tails in the profile of scalar PDF is a manifestation of the internal intermittency of passive scalars, associated with the sharp ramp-cliff structures in the small scale scalar field (Shraiman and Siggia, 2000; Warhaft, 2000). Figure 1.4 is a numerical result showing the intermittency in a passive scalar field, in which the large scale of plateau structures are separated by small scale cliff structures.

The most common measure of intermittency is the scaling exponents of the structure functions, hence not for the field itself, but for its increments. For passive scalars, similarily with Eq. (1.18), the KOC theory implies a scaling relation of the structure function of the passive scalar as

$$S_\theta^q(l) = \langle|\delta\theta|^q\rangle = \langle|\theta(x+l) - \theta(x)|^q\rangle \sim l^{\zeta_\theta(q)}, \tag{1.43}$$

where $\zeta_\theta(q)$ is the scaling exponent of qth order passive scalar structure function. Without intermittency, the

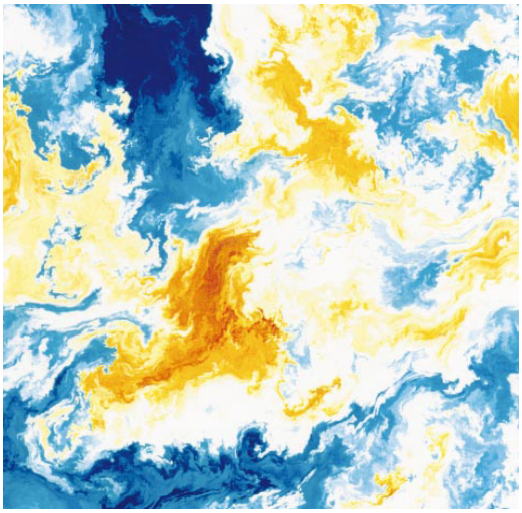

Figure 1.4: A visualization of a passive scalar field, by Chen and Kraichnan (1998).

scaling behaviors of passive scalar and velocity are supposed to be identical, as

$$\zeta(q) = \zeta_\theta(q) = q/3. \tag{1.44}$$

Taking the internal intermittency into consideration, similar with velocity (Kolmogorov, 1962; Obukhov, 1962), the refined similarity hypotheses for passive scalars were also proposed (Stolovitzky et al., 1995). Then it was soon confirmed that, with intermittency, the ζ-q and ζ_θ-q curves are nonlinear instead of straight lines (see figure 1.5).

With the help of super computers, more precise inspection of the intermittency is an interesting topic for the numerical simulations of passive scalar in high Reynolds number turbulent flow (Warhaft, 2000; Borgas et al., 2004; Yeung et al., 2005). Iyer et al. (2018) studied the intermittency of a passive scalar in three-dimensional turbulence at Taylor-scale Reynolds number of 650, using direct numerical simulations on a 4096^3 grid. The Schmidt number is unity. The passive scalar fluctuation was forced by a uniform mean gradient. The scaling exponents of structure function of order higher than about 12 was found to saturate to about 1.2. Interestingly, the fractal dimension of the steepest fronts, associated with very large scalar gradients, was found as about 1.8, which adds up with the saturation value of scaling exponent to be the number of spatial dimension 3. In the work by Gotoh and Watanabe (2015), direct numerical simulation with 4096^3 grid points was implemented for an isotropic steady turbulence with $Re_\lambda = 805$. Two passive scalars with $Sc = 0.72$ were studied: one (θ) is forced by a random source that is Gaussian and white in time, and the other (q) is forced by the mean uniform scalar gradient. The local scaling exponents of the two passive scalars: $\zeta^\theta_{n,0}(r)$ and $\zeta^q_{n,0}(r)$ as functions of separation distance r and order n were introduced. They were computed based on the zeroth (isotropic) terms

of the Legendre expansions of the structure function. Then the scaling exponents ζ_n^θ and ζ_n^q were determined as the slopes of the $\zeta_{n,0}^\theta(r) - r$ and $\zeta_{n,0}^q(r) - r$ curves (obtained by fitting with least-square method). Mostly importantly, ζ_n^θ and ζ_n^q were found to be very close to each other. Such a result revealed the universality in the scaling behavior of turbulent passive scalar. In figure 1.3, non-Gaussian tails are more clearly found in the PDF profiles of passive scalars compared with the PDF of velocity. Moreover, figure 1.5 shows the ζ_θ-q curve is more bending than the ζ-q curve, i.e. the structure function of the passive scalar is of more abnormal scaling behavior. Both these results suggest that the passive scalar field is more intermittent than the velocity.

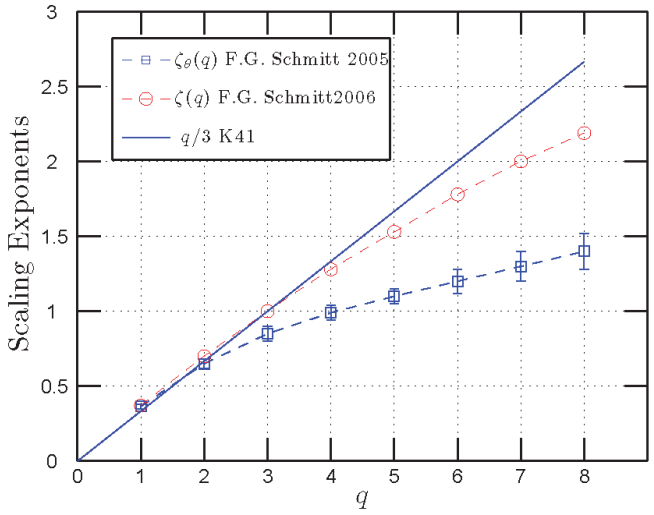

Figure 1.5: The scaling exponents ζ and ζ_θ from experiments by Schmitt (2005, 2006), compared with the theoretical predictions of K41 and KOC theories (Huang, 2009).

Chapter 2

Reactive scalars in incompressible turbulence

The problem of scalar transport and mixing becomes physically rich when reactions are taken into consideration, such as biological or chemical reactions. For example, in the marine system, many micro-biological species are under the influence of both the turbulent dynamics of their living fluid environment and the reactive interactions between the species, or species and nutrition distribution. Specifically, species interaction can be modeled as chemical or biological reactions, e.g. preys and predators or species and nutrition, involving chemical or biological quantities (such as the concentration of phytho- or zooplanktons) as reactive scalars. Different from the passive scalars, which are transported without reaction, reactive scalars are more complex because the reactions almost always make the system non-linear (Eq. (2.7)). Because of the motion of turbulent eddies in the ocean, the plankton and nutrition as reactants and products of reactions are efficiently mixed and redistributed. When transported in the turbulent flow, the turbulence is responsible for not only bringing reactants together so that reaction can occur within a finite time, but also for dispersing the products of reaction. These species and nutrients are at the bottom of the food chain in the marine world. Thus the dynamics of such system is important in a number of aspects, e.g. larval recruitment, fishing and environmental monitoring (Hill, 1976; Warhaft, 2000; Neufeld and Hernández-García, 2009).

From a fundamental point of view, such a reactive scalar mixing problem in incompressible turbulence is especially meaningful in the following senses. Firstly, the nonreactive passive scalar turbulence alone has been the subject of many studies (Monin and Yaglom, 1975; Libby and Williams, 1976; Mitrovic and Papavassiliou, 2004). When the chemical source is added, how scalars interact needs to be taken into consideration. Secondly,

reactive turbulence has been typically considered as the combustion case, with large variation of the fluid density and very fast reaction rates. There exist abundant literature on turbulence combustion (Peters, 2000; Pope, 2000; Poinsot, 2017; Zhao et al., 2018a; Zhang et al., 2020). Relatively, the theoretical knowledge of statistical laws, including scaling behavior, of the reactive scalars and the effects of chemical reaction on the passive scalar mixing in incompressible turbulence is still very sparse.

In this chapter the basic concepts, fundamental theories and some numerical studies about reactive scalars in incompressible turbulence are introduced. It is organized as follows. Section 2.1 introduces the basic chemical kinetics for formulating the reaction source terms in the governing equations of reactive scalars, and some chemical and biological models, which simplify the real reacting system from a theoretical point of view. In section 2.2, the statistical properties of reactive scalars, including the mean, variance and correlation are discussed based on the governing equations of reactive scalars. Last but not least, in section 2.3, a literature review about the analytical, numerical and experimental studies of turbulent reactive scalar is presented.

2.1 Chemical kinetics

2.1.1 General descriptions

The basic concepts about chemical kinetics (Law, 2006; Neufeld and Hernández-García, 2009) are introduced here, before being used in the fluid mechanics framework.

The general form of irreversible reaction between N species: M_1, M_2, ..., M_N is

$$\sum_{i=1}^{N} n_i' M_i \quad \xrightarrow{\gamma_1} \quad \sum_{i=1}^{N} n_i'' M_i, \tag{2.1}$$

where M_i can be a reactant or a product; γ_1 is the reaction rate coefficient; n_i' and n_i'' are the reaction order of M_i. The order of the reaction is $\sum_{i=1}^{N} n_i'$. Considering the mole concentration of M_i: θ_i, the rate of change of θ_i is

$$\omega_i = \frac{d\theta_i}{dt}. \tag{2.2}$$

For any two reacting species M_i and M_j, a species independent quantity ω can be introduced:

$$\omega = \frac{\omega_i}{n_i'' - n_i'} = \frac{\omega_j}{n_j'' - n_j'}. \tag{2.3}$$

Thus ω is defined as the reaction rate. The phenomenological law of chemical reaction states that ω is propor-

tional to the product of the concentrations of the reactants:

$$\omega = \gamma_1 \prod_{i=1}^{N} \theta_i^{n_i'}. \tag{2.4}$$

It is noteworthy that, according to Eq. (2.4), the dimension of the reaction rate coefficient γ_1 is not universal, but dependent on which reaction it refers to.

In reality, there is no absolutely irreversible reaction, every reaction of (2.1) is associated with the reverse reaction of it. The overall reaction is a reversible reaction:

$$\sum_{i=1}^{N} n_i' M_i \quad \underset{\gamma_2}{\overset{\gamma_1}{\rightleftharpoons}} \quad \sum_{i=1}^{N} n_i'' M_i, \tag{2.5}$$

where γ_2 is the reaction rate coefficient of backward reaction. The reaction rate of the backward reaction is defined similar with the forward reaction. Thus the net reaction is

$$\omega_{forward} - \omega_{backward} = \gamma_1 \prod_{i=1}^{N} \theta_i^{n_i'} - \gamma_2 \prod_{i=1}^{N} \theta_i^{n_i''}. \tag{2.6}$$

For specific species M_j, the net chemical source is

$$\omega_j = (n_j'' - n_j')(\gamma_1 \prod_{i=1}^{N} \theta_i^{n_i'} - \gamma_2 \prod_{i=1}^{N} \theta_i^{n_i''}). \tag{2.7}$$

After enough long time and without external supply of reactant, the reversible reaction will finally reach its chemical equilibrium state, at which both the forward and backward reactions are still ongoing but of the same rate, i.e. the net reaction rate is 0.

2.1.2 Models in chemical and biological systems

In a incompressible turbulence environment, such as in the ocean, various reactions exist. For example the decomposition of carbonic acid into H_2O and CO_2 and the process of photosynthesis. However, chemical reactions in reality are always highly multi-steps and of complex chemical dynamics. From a theoretical point of view, it is appreciated to propose some chemical models summarizing the main mechanism and behaviors in complex chemical reactions. More generally, some biological processes can also be modeled as reaction. For example, the cluster of plankton blooms where the reactants are various nutrients transported by the flow. Theoretically, the interaction between plankton and their nutrition can be considered as two reactants in one

reaction with one's number grows at the cost of the consumption of the other. In this section, some mathematical models about the chemical and biological process are reviewed (Neufeld and Hernández-García, 2009).

Chemical models

As an example of the chemical kinematics described in section 2.1, an elementary second order irreversible reaction is in the from of:

$$\mathrm{A} + \mathrm{B} \xrightarrow{\gamma} \mathrm{C}. \tag{2.8}$$

If we consider it as a 0-dimensional problem, the concentrations of A, B and C evolve according to

$$\frac{d\mathrm{A}}{dt} = \frac{d\mathrm{B}}{dt} = -\frac{d\mathrm{C}}{dt} = -\gamma \mathrm{AB}, \tag{2.9}$$

from which the difference between the concentration of A and B is found as invariant, because

$$\frac{d(\mathrm{A} - \mathrm{B})}{dt} = 0.$$

Thus we can define constant Q as

$$Q = \mathrm{A}(t) - \mathrm{B}(t) = \mathrm{A}(0) - \mathrm{B}(0),$$

which then produces the temporal ordinary partial equation of A as

$$\frac{d\mathrm{A}}{dt} = \gamma Q \mathrm{A} - \gamma \mathrm{A}^2. \tag{2.10}$$

Eq. (2.10) is an example of how a nonlinear term arise in a single chemical reaction.

In the reaction of (2.8), if the concentration of one reactant is hold as constant (for example the reactant of B), the equation about the temporal evolutions of A and C become

$$\frac{d\mathrm{A}}{dt} = -\frac{d\mathrm{C}}{dt} = -\gamma' \mathrm{A}, \tag{2.11}$$

where $\gamma' = \gamma \mathrm{B}$ can be taken as another reaction rate coefficient. Then the reaction is

$$\mathrm{A} \xrightarrow{\gamma'} \mathrm{C}, \tag{2.12}$$

which is an example of first order reaction. Consider the reverse of reaction (2.8):

$$\mathrm{C} \xrightarrow{\gamma} \mathrm{A} + \mathrm{B}. \tag{2.13}$$

Such a decomposition process is another example of first order reaction.

Imagine the concentration of C is the reaction (2.12) is also hold as constant. Then the reaction becomes

$$\mathrm{A} \xrightarrow{\gamma'} \emptyset. \tag{2.14}$$

Such a reaction corresponds to the decaying process of a chemical, generally in an exponential manner. The reverse of reaction (2.14) is

$$\emptyset \xrightarrow{\gamma'} \mathrm{A}, \tag{2.15}$$

which is called as zeroth reaction.

Biological models

When dealing with a single species, the evolution of the population can be modelled in the framework of birth-death-saturation model. For an individual species A, the model considering only birth and death states that the temporal evolution of A follows

$$\frac{d\mathrm{A}}{dt} = b\mathrm{A} - d\mathrm{A}. \tag{2.16}$$

Here the b and d are the growth rate and death rate respectively. The terms of bA and $-d$A indicate that this process consists of the combination of the reaction of $\mathrm{A} \xrightarrow{b} 2\mathrm{A}$ and $\mathrm{A} \xrightarrow{d} \emptyset$. In such case, it is easy to find that A evolves exponentially as $e^{(b-d)t}$. Thus if b is smaller than d, A will decay to infinitesimally small quickly. The case with b larger than d is of more interest, in which A can grow explosively. However this is unrealistic in biology. The problem lies in the modelling about the growth. The growth of a species replies on the supply from the environment, such as food and oxygen. Thus the growth subjects to the finiteness of the resources. The reaction $\mathrm{A} \xrightarrow{b} 2\mathrm{A}$ has to be replaced with $\mathrm{A} + \mathrm{B} \xrightarrow{b'} 2\mathrm{A}$, where B represents the food. The modified coefficient of reaction rate b' is function of A, as $b' = b(1 - \mathrm{A}/\mathrm{A}_{max})$, where A_{max} is the carrying capacity of the environment, also the saturation value of A. It means that A cannot grow without superior limit, but it will saturate when approaching A_{max}.

Another model for biological reaction is the prey-predator model, which can be used for studying the evolution of fish population due to fishing behavior. Let A and B represent the concentrations of prey and

predator. In addition to the aforementioned birth and death for both prey and predator, the number of preys is supposed to decrease with large number of predators, and the predators can flourish with plenty of preys. The behavior of preying is the key in the prey-predator model. Thus for the prey, it is assumed that the decrease in population is mostly due to being preyed, i.e. the natural death of prey is less important. Similarly, the increase of predator population is assumed as strongly dependant on the feeding and relatively weakly on proliferation. Therefore, the evolutions of A and B follow:

$$\frac{d\mathrm{A}}{dt} = (\gamma_1 - \gamma_2 \mathrm{B})\mathrm{A}, \qquad \frac{d\mathrm{B}}{dt} = (\gamma_2 \mathrm{A} - \gamma_3)\mathrm{B}. \tag{2.17}$$

And the corresponding reactions are

$$\mathrm{A} \xrightarrow{\gamma_1} 2\mathrm{A}, \qquad \mathrm{A} + \mathrm{B} \xrightarrow{\gamma_2} 2\mathrm{B}, \qquad \mathrm{B} \xrightarrow{\gamma_3} \emptyset. \tag{2.18}$$

Consequently, such a chemical scheme produces persistent chemical oscillations, in which A and B increase and decrease alternatively and periodically.

2.2 Advection-diffusion-reaction equation

The governing equation of a reactive scalar θ_j is the advection-diffusion equation of passive scalar (Eq. (1.28)) with the addition of the chemical source term ω_j:

$$\frac{\partial \theta_j}{\partial t} + (\mathbf{u} \cdot \nabla)\theta_j = D \triangle \theta_j + \omega_j + \dot{q}. \tag{2.19}$$

Let Θ_j (can be the global average of θ_j) be the characteristic quantity of θ_j. The characteristic time scale for the reaction is Θ_j/ω_j. Let us note τ_{mix} the characteristic time scale of scalar transport, which is generally dependant on the scalar convection and diffusion. The Damköhler number Da is defined as the ratio between the time scales of scalar transport and reaction, as:

$$Da = \frac{\tau_{mix}}{\Theta_j/\omega_j}. \tag{2.20}$$

Such a dimensionless parameter is a key parameter, quantifying the effect of reaction on the evolution of reactive scalar in comparison with the effect of turbulent convection-diffusion.

In the advection-diffusion-reaction equation (Eq. (2.19)), the reaction term ω_j is generally non-linear. As

a result, it is generally impossible to derive the analytical expression about the statistical properties of the reactive scalar (the mean quantity or the variance etc.), unless the reaction is simple and of low order, such as the first-order reaction (Corrsin, 1958). Consider θ as a reactive scalar undergoing first order reaction of

$$\theta \xrightarrow{\gamma} \emptyset. \tag{2.21}$$

in homogeneous isotropic turbulent flow. Then the evolution equation for $\theta(\mathbf{x}, t)$ reads

$$\frac{\partial \theta}{\partial t} + (\mathbf{u} \cdot \nabla)\theta = D\triangle\theta - \gamma\theta + \dot{q}. \tag{2.22}$$

By writing the left-hand-side of Eq. (2.22) in the form of material derivative and doing the ensemble average, it yields

$$\frac{D\langle\theta\rangle}{Dt} = D\triangle\langle\theta\rangle - \gamma\langle\theta\rangle + \langle\dot{q}\rangle. \tag{2.23}$$

The diffusion term $D\triangle\langle\theta\rangle$ is 0 because of the homogeneity. Thus if there is no external supply ($\dot{q} = 0$), the mean quantity $\langle\theta\rangle$ is supposed to decay exponentially.

Considering the variance of θ, by multiplying the equation of fluctuating scalar (obtained from (2.22)-(2.23)) and doing ensemble average, it yields

$$\frac{1}{2}\frac{D\langle\theta'^2\rangle}{Dt} = -D\langle|\nabla\theta|^2\rangle - \gamma\langle\frac{1}{2}\theta'^2\rangle + \langle\dot{q}'\theta'\rangle. \tag{2.24}$$

Similarly with Eq. (1.35), the fluctuations of reactive scalars in homogeneous isotropic turbulence are sustained by the external energy source $\langle\dot{q}'\theta'\rangle$, and dissipated by the dissipation term $-D\langle|\nabla\theta|^2\rangle$. In addition, the decrease of scalar fluctuation energy due to reaction is more rapid because the term of $-\gamma\langle\frac{1}{2}\theta'^2\rangle$ produces an exponential decay.

Consider a second order reaction in the most simple form :

$$\theta_1 + \theta_2 \xrightarrow{\gamma} \emptyset. \tag{2.25}$$

With isotropy and homogeneity, similar with Eq. (2.24), the evolution equations of the mean and variance of θ_1 are

$$\frac{D\langle\theta_1\rangle}{Dt} = D\triangle\langle\theta_1\rangle - \gamma\langle\theta_1\rangle\langle\theta_2\rangle - \gamma\langle\theta_1'\theta_2'\rangle + \langle\dot{q}_1\rangle \tag{2.26}$$

and

$$\frac{1}{2}\frac{D\langle\theta_1'^2\rangle}{Dt} = -D\langle|\nabla\theta_1|^2\rangle - \gamma\langle\theta_1'^2\theta_2'\rangle - \gamma\langle\theta_1'^2\rangle\langle\theta_2\rangle - \gamma\langle\theta_1'\theta_2'\rangle\langle\theta_1\rangle + \langle\dot{q}_1'\theta_1'\rangle. \tag{2.27}$$

Compared with first order reaction (Eq. (2.23) and (2.24)), the evolutions of the mean and variance of reactive scalars in the second reaction are much more complicated, because the non-linear reaction term involves the second and even third order covariance of the fluctuations of reactants. The covariance normalized by the product of the r.m.s of scalar fluctuations is the correlation coefficient between the reactive scalars:

$$r(\theta_1, \theta_2) = \frac{\langle\theta_1'\theta_2'\rangle}{\langle\theta_1'^2\rangle^{1/2}\langle\theta_2'^2\rangle^{1/2}}. \tag{2.28}$$

The correlation coefficient is a classical mathematical quantity characterizing how strong two zero-mean vari-

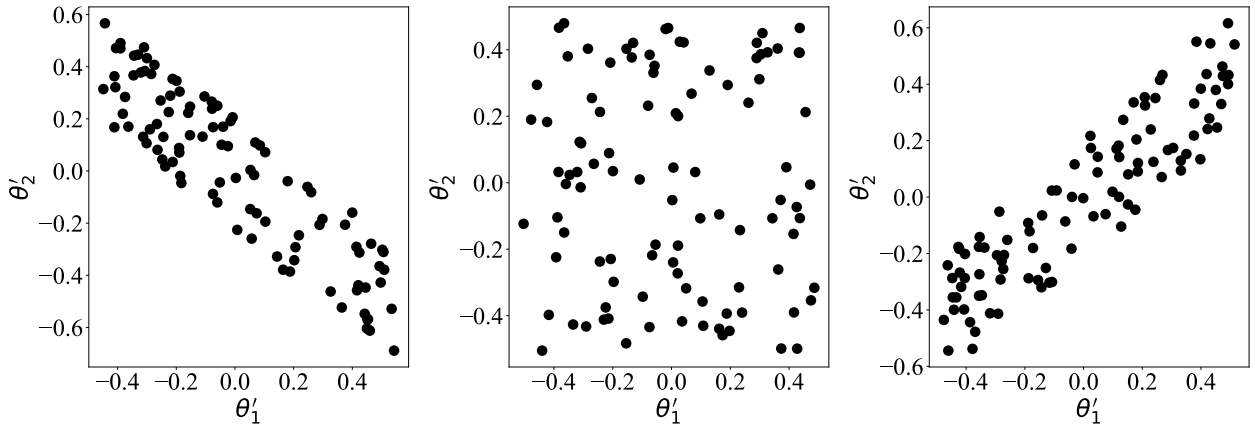

Figure 2.1: Scatter plots about the example θ_1'-θ_2' joint distribution in the case of (a) $r(\theta_1, \theta_2) = -0.9$; (b) $r(\theta_1, \theta_2) = 0$; and (c) $r(\theta_1, \theta_2) = 0.9$.

ables (θ_1' and θ_2') are correlated. According to Cauchy-Schwartz inequality, $r(\theta_1, \theta_2)$ can only evaluate in the range of

$$-1 \leq r(\theta_1, \theta_2) \leq 1. \tag{2.29}$$

$r(\theta_1, \theta_2) = 0$ means θ_1 and θ_2 are not correlated. For example, in figure 2.1(b), a distribution of θ_1' is independent with θ_2'. A positive $r(\theta_1, \theta_2)$ corresponds to the case of θ_1 and θ_2 being positively correlated, in which θ_1' is more likely to be the same sign with θ_2'. Figure 2.1(c) shows the joint distribution of θ_1' and θ_2' in the case of $r(\theta_1, \theta_2) = 0.9$, which means θ_1 and θ_2 are strongly correlated. Similarly, a negative $r(\theta_1, \theta_2)$ indicates that θ_1' is more likely to be the opposite sign with θ_2' (figure 2.1(a)). Extremely, when $r(\theta_1, \theta_2)$ is 1 or -1, θ_1 and θ_2 are perfectly positively or negatively correlated.

2.3 Interactions between turbulence and reactions

Taking advantage of computer science and the governing equations, there were some analytical and numerical studies aiming at better understanding and exploring the statistical properties of the reactive scalars in the interaction with incompressible turbulence. On the other hand, a well known example for the turbulent reactive scalars in the real world is the ocean. Thus some experimental studies carried out measurement of the statistical properties of reactive scalars in the ocean or aquatic environment. In this section, some of these studies are reviewed.

2.3.1 Analytical studies on reactive scalars

In fully developed turbulence, universal scaling relations are classically discussed in the framework of Kolmogorov-Obukhov phenomenology for the velocity field, as well as the Obukhov-Corrsin approach for passive scalars advected by the turbulent velocity. This now forms the classical KOC (Kolmogorov-Obukhov-Corrsin) theoretical framework for fluid turbulence with advected passive scalars (Warhaft, 2000). Chemical reactions have been considered quite early in such framework, for some specific cases. The earliest works on the statistical theory of turbulent chemical reactions were done by Corrsin (1958, 1961, 1964a), Pao (1964) and O'Brien (1966, 1971, 1975).

In the work by Corrsin (1958), the reactive scalar in first order reaction ($\Gamma \xrightarrow{C} \emptyset$) and homogeneous turbulence was considered. The equation of the global scalar variance (Eq. (2.24)), which indicates a exponential decay of scalar variance, was derived. Corrsin (1961) studied the mixing of a scalar contaminant undergoing a first-order chemical reaction in isotropic turbulence. Theoretically he deduced the energy spectrum of the reactive scalar in different wave number ranges. A $-5/3$ scaling relation was found for the reactive scalar in the inertial range (figure 2.2(a)). Later, Corrsin (1962) extended the problem to the first order reaction with product ($\Gamma \xrightarrow{C} \mathrm{P}$), and derived that the mean, variance and energy spectrum of P were similar with that of Γ, only with slight amendment. It is noteworthy that, in the process of deriving the variance of P, the covariance term between Γ and P was involved. Corrsin (1962) simply assumed that Γ and P are perfectly correlated. Then Corrsin (1964a) extended the theoretical analysis about the first order reaction to a second order reaction. A $-5/3$ scaling relation was also found in the inertial range of the energy spectrum (figure 2.2(b)). Moreover, the nonlinear reaction term causes some additional spectral transfer and more importantly a loss in the spectral energy.

In the work by Pao (1964), the theories about the evolution of mean and variance of reactive scalar in a first order reaction was developed into a general form, which theoretically quantifies the decaying process of

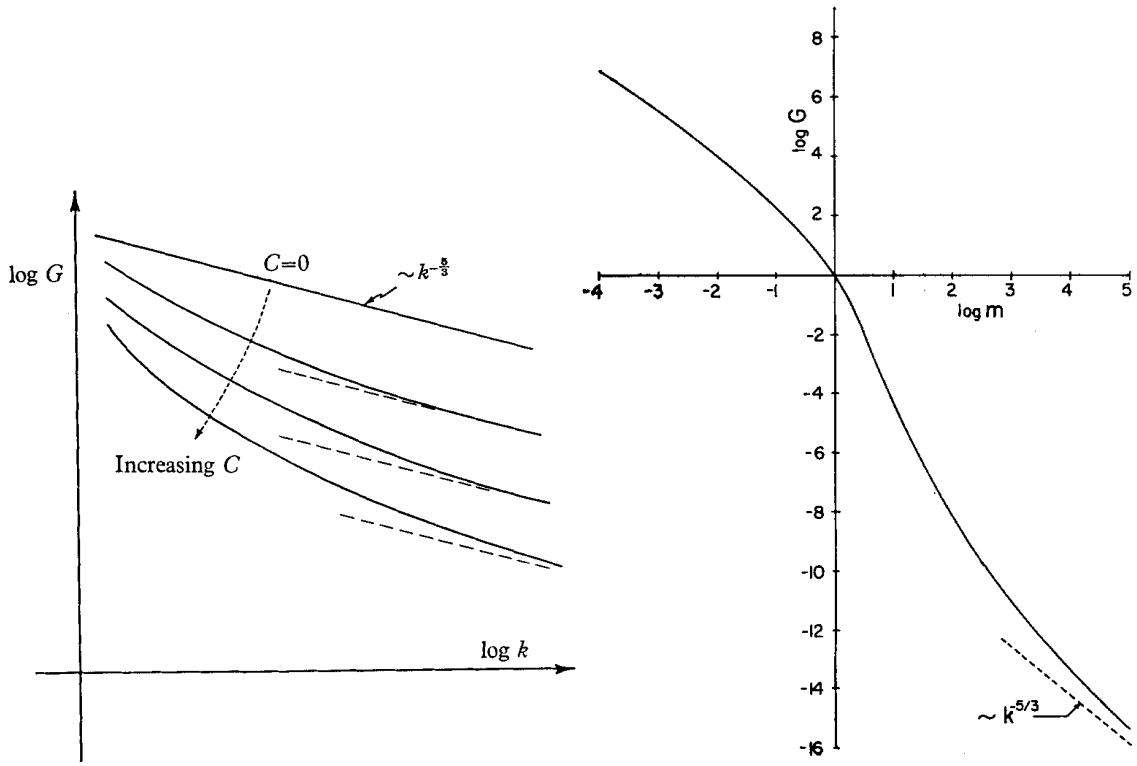

(a) (b)

Figure 2.2: (a) Figure 1 in Corrsin (1961): A quantitative sketch of the variance spectrum of reactive scalar undergoing a first order reaction. (b) Figure 1 in Corrsin (1964a): A quantitative sketch of the variance spectrum of reactive scalar undergoing a second order reaction. Here C is the coefficient of reaction rate; k or m is the wave number; G is the wave number dependant scalar variance.

reactants in various first order reaction, such as $A \to B$; $A \leftrightarrows B$; $A \to B$, $B \to C$; $A \to B \to C$. Moreover, an unified spectral transfer concept was proposed, which led to a general expression about the variance spectrum. Such a formulation generalizes the scaling behavior of first order reactive scalar at the range of large wave number (for both the cases of Sc number much smaller and larger than 1), which was the same with that of the passive scalar. O'Brien (1966) extended the theoretical analysis about the decaying moments of reactive scalars to a second order reaction with single reactant, where the reaction term for the reactant A is $-\gamma \mathrm{A}^2$, where γ is the reaction rate coefficient. The global variance of the reactive scalar was shown to decay asymptotically as $t^{-11/2}$. O'Brien (1971) further investigated a high order reaction with two reactants (A and B) and a rapid reaction rate. It was derived that, for the stoichiometric case (take A as example, same for B),

$$\lim_{t\to\infty} \langle \mathrm{A}'^2 \rangle \sim t^{-3/2}, \qquad \lim_{t\to\infty} \langle \mathrm{A} \rangle^2 \sim t^{-3/2}, \qquad \lim_{t\to\infty} \langle \mathrm{A}'^2 \rangle / \langle \mathrm{A} \rangle^2 = \pi - 1. \tag{2.30}$$

While for the non-stoichiometric case, the asymptotical decay of the covariance $\langle A'B' \rangle$ follows $t^{-9/4}e^{-\gamma t^{3/2}}$, where γ is the reaction rate coefficient.

2.3.2 Numerical studies on reactive scalars

The covariance between reactants and the development of the introduction of models for the covariance terms were important early topics of turbulent mixing analyses (Lamb and Shu, 1978; Heeb and Brodkey, 1990). Heeb and Brodkey (1990) did numerical simulations about the irreversible reactions during turbulent mixing, and compared with experimental results to examine 14 closure theories. For the two non-premixed reactants case, it was found (Toor, 1969) that the covariance is almost invariant for very slow and very rapid second-order reactions. In a direct numerical simulation about the influence of convective turbulence on chemical reactions in the atmospheric boundary layer by Molemaker and de Arellano (1998), two species A and B representing the reactants in second order irreversible reaction were introduced. The one-dimensional spectrum of covariance between the reactants (averaged in space and time and normalized) were plotted (figure 2.3), and a $-2/3$ scaling law was found. Chemical reaction introduces various complexities to the passive scalar

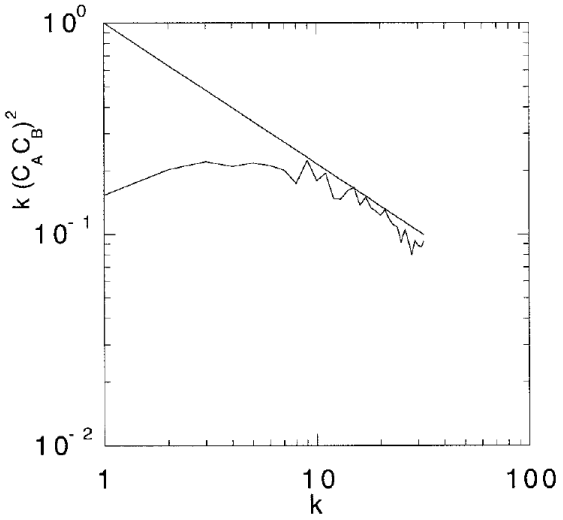

Figure 2.3: Figure 2(b) in Molemaker and de Arellano (1998): one-dimensional spectrum of the covariance between two chemical species (averaged in space and time and normalized).

problem, e.g. new characteristic time scale and the nonlinear source of the governing equation. Theoretically, the order of the chemical reaction determines the linearity of the scalar equation. For the purpose of validating a theory of turbulent diffusion of chemically reacting gaseous admixtures, Elperin et al. (1998) numerically studied the irreversible first-order reaction in homogeneous and isotropic incompressible turbulence to satisfy the assumptions used in analyses. The direct numerical simulation results demonstrated that turbulent transport

is strongly modified with chemical reactions or phase transitions, where the diffusion of the admixtures is strongly reduced when the Damköhler number is large. Moreover, Elperin et al. (2017) numerically studied a reactive premixed flow through a channel to simulate the highly nonlinear dependence of the reaction rate in a typical premixed flames. The modeled reaction rate depends only on the species concentration. The numerical results showed that the vortex tubes do not change across the reaction zone; meanwhile the calculated turbulent diffusion coefficients match well the theoretical predictions.

Among the existing results, the effects of chemical reaction on the turbulent mixing are also of particular interest (Hill, 1976). For instance, the second-order chemical reactions in a reactor (Mao and Toor, 1971), or series-parallel reactions ($A + B \rightarrow R$, $R + B \rightarrow S$) (Chakrabarti et al., 1995). Sykes et al. (1994) used Large Eddy Simulation (LES) to study the chemically reactive mixing of two species, in a system with one reactant injected into an uniformly mixed layer containing the other one. The segregation coefficient, defined as the covariance of the two reactants normalized by the product of their mean quantities, is the measure of the turbulent mixing. It was shown that the two reactants were significantly segregated when the reaction was fast. Komori et al. (1991) simulated two reactants of second-order irreversible reaction introduced through different parts of the bounding surface of turbulent flow. They developed a model with the Damköhler number based on the integral timescale to estimate the segregation parameter. Leonard and Hill (1988) studied the decaying reactive scalars undergoing a second-order irreversible reaction in homogeneous turbulence, with pseudospectral method and in up to 128^3 domains. Two interesting results were found. The first one is that the regions in the flow field where reaction rates are the highest are correlated with locations of high strain rates. The other one is that the chemical reaction rate constant does not appreciably affect the microscales of the dissipation of concentration fluctuations, which is supported by a closure theory. Numerical simulations about the decay moments of reactive scalars in irreversible reactions was also carried out, which are one main focus of early theoretical studies (Corrsin, 1958, 1964a; O'Brien, 1966). Neufeld et al. (2002) carried out a two-dimensional numerical simulation about the temporal evolution of the spatial distribution of reactive scalar in the advection of fluid field. The reactants were in elementary reactions in open or closed flows. The evolution of the reactive scalar field was found to be dependent on the Damköhler number. When the Damköhler number is small, the variance decays and the reactive scalar field is gradually of spatially homogeneous distribution. But when Damköhler number is large, the structure of filaments with strong perturbations soon grows in the reactive scalar field.

Following these early studies and numerical results, we developed in this thesis numerical simulations of reactive scalars, in different configurations, which are the topic of the different remaining chapters.

2.3.3 Turbulence and reactive scalars in biological oceanography

With ocean turbulence in mind, Lopez et al. (2001) numerically studied the nutrient-phytoplankton-zooplankton interactions in chaotic flows. The simulation results displayed a smooth-filamental transition in the concentration patterns. Hernandez-Garcia and Lopez (2004) studied the planktonic population living in an open and chaotic fluid flow, using a predator-prey model. This study showed that a strong chaotic flow is beneficial for sustaining plankton blooms by deforming the filament structures of the flow under the action of stretching and dilution. Grošelj et al. (2015) carried out a two dimensional numerical study about a cyclic competition between three biological species. The reacting system consists of $A + B \to A$, $A \to 2A$, $B + C \to B$, $B \to 2B$, $C + A \to C$, $C \to 2C$. The effect of reaction, in comparison with the turbulent convection-diffusion, on the evolution of the global statistical property of reactants was investigated. A transition from rotating spiral waves to collective oscillations as Damköhler number decreases from very large to very small was observed for the evolutions of the average densities of the species. The work by Powell and Okubo (1994) explored the effect the biological interaction on the variance spectrum of the plankton populations in the sea, using a predator-prey model. They concluded that there is no general result in this phenomenon, since the biological interaction may either flatten or steepen the spectrum, which is dependant on the process of diffusion.

The scaling behavior of reactive scalar is also of high interest. Some studies focus on possible applications in the field of chemical and biological oceanography, where the typical times of biogeochemical reactions may be large. Seuront et al. (1996, 1999) studied the intermittency of phytoplankton and temperature fields from ocean observations. It has been found that phytoplankton was nearly dynamically passive (similar to temperature) at small scales but biologically active at large scales. The phytoplankton statistics, considered via the proxy of fluorescence measurements, have found some scaling relations with -1.2 spectral slopes, interpreted as signature of biological activity (Seuront et al., 1996; Lovejoy et al., 2001; Derot et al., 2015). Such -1.2 slope was not always detected: Yamazaki et al. (2006) measured the microstructure of phytoplankton in fully developed oceanic turbulence by using LED (Light Emitting Diode) fluorescence probe. The spectra of both phytoplankton and velocity exhibited $-5/3$ slope in the inertial subrange.

An important aspect in understanding ocean turbulence is the species transport process, either in the interior or at the interface of the ocean. This issue is particularly acute for biogeochemical studies. For instance, the mixing process at the ocean and atmosphere interface drives the pelagic food because of the light available for photosynthesis at the surface. Till now, there is no unanimous agreement on the effects of turbulence on species transportation, including the feeding, growth and mortality rates of the species (Mackenzie, 2000). Under some conditions, the swimming marine species, together with high dissipation rates produced by the aggregations of

living organisms of different sizes, might generate intense turbulence comparable with those by the strong winds near the ocean surface (Kunze, 2019). In these studies, a major question was how efficient the mixing will be in the ocean. From the important multiscale feature in turbulence, it is reasonable to expect that the mixing efficiency hinges on length scales. Very small whorls introduced into a fluid will be quickly damped by friction, and thus will not mix the fluid. Probably, zooplankton schooling introduces larger scales and increases mixing efficiency (Dewar, 2009).

So far, there are no considerable number of studies devoted into the turbulence-reaction interaction concerning oceanology and biology. The main reasons are that such a topic is highly interdisciplinary and the conditions in the ocean are not controllable. Thus the problems are too complicated to have universal and unanimous conclusions. In the contrast, more studies about turbulent reactive scalar are interested in the numerical simulations of the canonical cases.

Chapter 3

Numerical implementation of direct numerical simulations

The partial differential equations in turbulence studies (Eqs. (1.9), (1.28), (2.19)) are generally not analytically solvable, i.e. the analytical expressions of the velocity and scalars as functions of continuous spatial and temporal variables ($\mathbf{x}$ and t) generally can not be derived from the governing equations. Alternatively, the numerical solutions expressed as functions of discrete variables can be used to describe the flow and scalar fields. These numerical solutions are obtained by solving the set of algebraic equations derived from the governing equations in the discrete domain. To have a detailed and reliable numerical solution, considerable computational time and storage for obtaining and recording the data are needed. Thus the numerical simulations of turbulence problems strongly rely on the availability of computers.

A lot of methods have been developed for the numerical simulations of the turbulence problems. Some numerical methods include models about the turbulent motions, for example the Smagorinsky model (Smagorinsky, 1963) and dynamic model (Germano et al., 1991; Lilly, 1992; Meneveau et al., 1996) in Large Eddy Simulation (LES), $k-\epsilon$ model (Jones and Launder, 1972) and $k-\omega$ model (Menter, 1994) in Reynolds-Averaged Navier-Stokes (RANS). The general idea of these models is to build the linkage between the small-scale quantities and the large-scale quantities based on the modeling of turbulent fluxes. Then the large-scale quantities are to be numerically solved, while the small-scale statistics are provided by the model. The benefit of using models in numerical simulations is lower computational cost, since the fineness of the spatial resolution is only required for resolving the large scale. However, the drawback is also evident. The models introduce some artificial hypotheses and simplifications to the problem, at the risk of reducing the accuracy and credibility of the results.

In contrast, the Direct Numerical Simulation (DNS) implements numerical simulation based directly on the governing equations without modeling assumptions. The spatial resolution of DNS is required to be fine enough to resolve the smallest scale (e.g. Kolmogorov scale for velocity (1.14) and Batchelor scale for scalar (1.42)). The results obtained by DNS are much more reliable than using models. Thus DNS is also called numerical experiment, as the preferred numerical method for examining theoretical analysis. However, The computational cost is high (Pope, 2000; Laizet and Lamballais, 2009; Koblitz et al., 2017), with a computational time roughly proportional to Re^3 (Davidson, 2004). The numerical simulations for this thesis are implemented as DNS.

3.1 Spatial discretization and approximation of derivatives

The discretization of the spatial domain is the first and very important step for numerical simulations of turbulent flows. It not only defines the framework in which the numerical solutions are expressed, but also allows the approximation of the spatial derivative with an algebraic expression of the discrete quantities. Essentially, the process of spatial discretization means to build a mesh of discrete grid points in the spatial domain. Such a mesh is supposed to be all over the positions of interest, orthogonal or at least near-orthogonal, and fine enough or specially refined to capture the physically interesting structures (Liseikin, 1999; Ferziger and Perić, 2001; Zikanov, 2010). The spatial discretization can be very complicated in irregular or nonuniform geometries, such as the wing flow or engine.

In this thesis, the canonical case of turbulence and reaction have been studied. The computational domain is a three dimensional cube. The spatial discretization is implemented by building uniformly structured discrete grids along the straight lines of Cartesian coordinate systems. The spatial coordinate vector $\mathbf{x}$ in the discrete domain is

$$\mathbf{x} = i\frac{L_x}{N_x}\mathbf{e}_x + j\frac{L_y}{N_y}\mathbf{e}_y + k\frac{L_z}{N_z}\mathbf{e}_z, \tag{3.1}$$

where L_x, L_y, L_z and N_x, N_y, N_z are the length of the domain and the number of discrete grids in each direction; i, j and k are integers ranging from 1 to N_x, N_y and N_z respectively. Because of the cubic computational domain, we have $N_x = N_y = N_z = N$ and $L_x = L_y = L_z = L$ in this thesis. Larger N provides better spatial resolution, but meanwhile increases the cost of computation.

3.1.1 Pseudo-spectral methods

As proposed in K41 theory (Kolmogorov, 1941a,b) and validated by numerous works (Sreenivasan, 1991; Sreenivasan and Antonia, 1997), for the turbulent flow at the scale much smaller than the geometric size of the domain,

the information of large scale or boundary conditions are lost. Thus in the studies focusing on the universal properties of turbulent motion, the boundary condition can be as simple as possible, generally periodic. In this circumstance, pseudo-spectral methods (Orszag, 1971; Eswaran and Pope, 1988b; Mansour and Wray, 1994; Sripakagorn et al., 2004; Hou and Li, 2007) are the preferred numerical approach, because of their high accuracy in approximating the spatial derivatives.

The general idea of pseudo-spectral methods

The idea of pseudo-spectral methods is similar with the method of separation of variables used for solving partial differential equations analytically. When the method of separation of variables is used for solving PDEs, the solutions are expressed as a series of infinite number of continuous eigenfunctions with coefficients. These eigenfunctions are linearly independent and orthogonal with each other, for example cos, sin, Bessel functions and Chebyshev polynomials (Zikanov, 2010; Moin, 2010). Then in the numerical simulation with pseudo-spectral methods, the solutions are expressed as a series of finite number of discrete eigenfunctions with coefficients, where the number of the eigenfunctions are generally equal or proportional to the number of discrete grids. For both methods, the final solutions are obtained by determining the coefficients of the eigenfunctions.

In the numerical simulation of turbulent motions in a periodic domain with a pseudo-spectral method, the eigenfunctions mostly used are the Fourier series (other functions such as Chebychev polynomials for bounded domain). Specifically for solving the Navier-Stokes equations (Eq. (1.9)) and the diffusion-convection equations of the scalars (Eq. (1.28) and (2.19)), the velocity and scalar in real space $\mathbf{u}(\mathbf{x},t)$ and $\theta(\mathbf{x},t)$ are represented in spectral space (also called Fourier space) by finite Fourier series:

$$\mathbf{u}(\mathbf{x},t)=\sum_{\mathbf{k}}\hat{\mathbf{u}}(\mathbf{k},t)e^{i\mathbf{k}\cdot\mathbf{x}},\qquad \theta(\mathbf{x},t)=\sum_{\mathbf{k}}\hat{\theta}(\mathbf{k},t)e^{i\mathbf{k}\cdot\mathbf{x}}. \tag{3.2}$$

The discrete wave number vector $\mathbf{k}$ is

$$\mathbf{k}=\frac{2\pi}{L}(i\mathbf{e}_{k_x}+j\mathbf{e}_{k_y}+k\mathbf{e}_{k_z}), \tag{3.3}$$

where i, j and k are integers ranging from $-\frac{N}{2}+1$ to $\frac{N}{2}$ (N is generally even integer). $\frac{N\pi}{L}$ represents the computational maximum resolved wave number in Fourier space. Actually, when non-linear term is concerned, for dealiasing, the maximum resolved wave number should be smaller (Hou and Li, 2007). $e^{i\mathbf{k}\cdot\mathbf{x}}$ is the discrete complex eigenfunction at the mode $\mathbf{k}$. $\hat{\mathbf{u}}(\mathbf{k},t)$ and $\hat{\theta}(\mathbf{k},t)$ are complex numbers, called the Fourier coefficients of velocity and scalar at the mode $\mathbf{k}$. The objective of pseudo-spectral methods is to determine the $\hat{\mathbf{u}}(\mathbf{k},t)$ and

$\hat{\theta}(\mathbf{k},t)$, which can then be transformed into real space quantities ($\mathbf{u}(\mathbf{x},t)$ and $\theta(\mathbf{x},t)$) via Eq. (3.2). Eq. (3.2) is called as the discrete Fourier inverse transform for obtaining real space quantities with Fourier space quantities. The reverse of Eq. (3.2) is called the discrete Fourier transform:

$$\hat{\mathbf{u}}(\mathbf{k},t) = \sum_{\mathbf{x}} \mathbf{u}(\mathbf{x},t) e^{-i\mathbf{k}\cdot\mathbf{x}}, \qquad \hat{\theta}(\mathbf{k},t) = \sum_{\mathbf{x}} \theta(\mathbf{x},t) e^{-i\mathbf{k}\cdot\mathbf{x}}, \tag{3.4}$$

where $\mathbf{x}$ goes over all the discrete grid points. It is very convenient to approximate the spatial derivatives by using Fourier series in a pseudo-spectral method, because the operation of spatial derivation in real space is a arithmetic operation of multiplication in Fourier space. For example from Eq. (3.2), it can be easily found that

$$\nabla \cdot \mathbf{u}(\mathbf{x},t) = \sum_{\mathbf{k}} i\mathbf{k} \cdot \hat{\mathbf{u}}(\mathbf{k},t) e^{i\mathbf{k}\cdot\mathbf{x}}, \qquad \frac{\partial \theta}{\partial x}(\mathbf{x},t) = \sum_{\mathbf{k}} i k_x \hat{\theta}(\mathbf{k},t) e^{i\mathbf{k}\cdot\mathbf{x}}. \tag{3.5}$$

It is noteworthy that the pseudo-spectral method is not called spectral method because not every term in the Navier-Stokes equations (Eq. (1.9)) and the diffusion-convection equations of the scalars (Eq. (1.28) and (2.19)) are computed in Fourier space (Orszag, 1971, 1972). In Fourier space, it is efficient and accurate in computing the real space derivatives but not the non-linear terms (convection term and probably also reaction term), which become convolutions. In a pseudo-spectral method, it is in real space that the non-linear terms are computed, whose Fourier coefficients are then obtained by Fourier transform. By computing the non-linear term in real space, the number of operations at each time step can be proportional to $Nlog(N)$, where N represents the number of discrete grids in real space and also the maximum resolved wave number in Fourier space, instead of N^2 by computing the convolution (Canuto et al., 1987).

Smooth dealiasing

In the discrete Fourier transform of non-linear terms, there are high wave number modes beyond the resolved range generated. These extra high wave number modes are called aliasing error. To maintain the numerical stability, dealiasing is needed to get rid of the aliasing error. Otherwise, as shown in figure 3.1, the aliasing error can lead to the abnormal peak of the energy spectrum at the resolved high wave number modes. Moreover, the numerical results at the the low wave number modes can be also distorted. The implementation of dealiasing leads to neglect some of the largest resolvable wave number components, generally performed for each numerical time step. The most commonly method is the 2/3 spherical truncation (Orszag, 1971), which means to enforce the Fourier coefficients of the modes with $|\mathbf{k}| > \frac{2}{3}\frac{N\pi}{L}$ as 0. In this thesis, the method of smooth dealiasing was used. Instead of the sudden cut-off, a filter of the high wave number modes with a relative smooth filtering

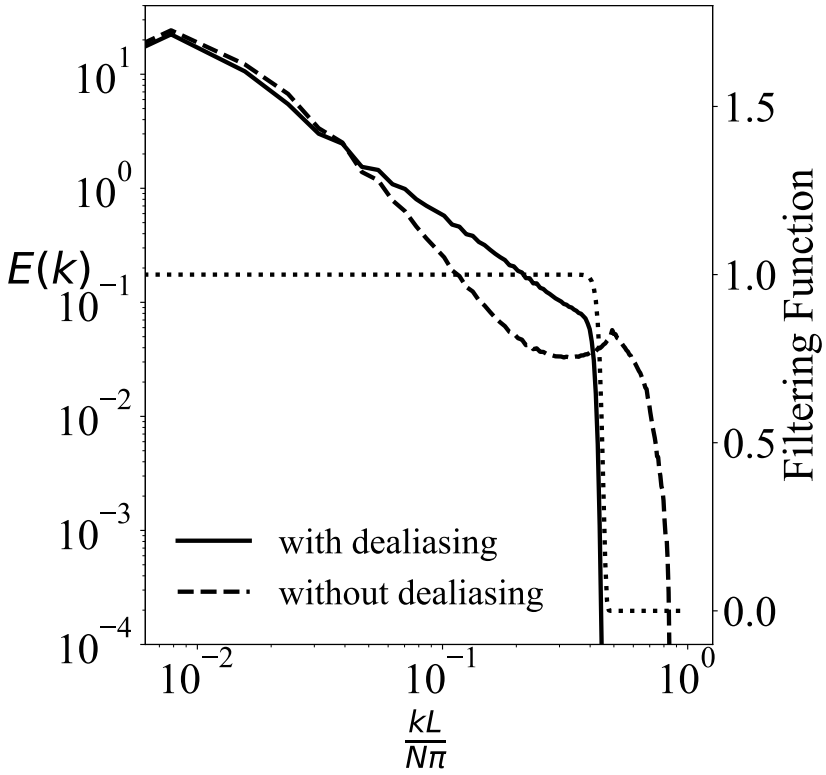

Figure 3.1: The comparison of the energy spectra of velocity numerically obtained by pseudo-spectral methods with and without dealiasing. $k = |\mathbf{k}|$ is the amplitude of wave number vector. The dotted curve is the filtering function of smooth dealiasing.

function is suggested in the smooth dealiasing. Numerically, at each time step, the $\hat{\mathbf{u}}(\mathbf{k}, t)$ and $\hat{\theta}(\mathbf{k}, t)$ are filtered by multiplying a real filtering coefficient $F(k)$, which is the function of wave number amplitude $k = |\mathbf{k}|$. Specifically:

$$F(k) = e^{-\alpha(\frac{kL}{N\pi})^{\beta}}, \tag{3.6}$$

where $\alpha = \beta = 36$ is generally suggested (the dotted curve in figure 3.1). Compared with the conventional 2/3 rule approach, the smooth dealiasing is capable to reduce numerical high frequency instabilities (Hou and Li, 2007).

The implementation of pseudo-spectral method in this thesis

In this thesis, the pseudo-spectral method is used for solving the Navier-Stokes equations (Eq. (1.9)), also the diffusion-convection equation of the scalars (Eq. (1.28) and (2.19)) when the scalar fields are of periodic

boundary conditions. Specifically, Eq. (1.9) and (2.19) are first rewritten as:

$$\frac{\partial \mathbf{u}}{\partial t} = \nu \triangle \mathbf{u} + L(\mathbf{u}), \qquad \frac{\partial \theta}{\partial t} = D \triangle \theta + L(\theta), \tag{3.7}$$
$$\text{with } L(\mathbf{u}) = -(\mathbf{u} \cdot \nabla)\mathbf{u} - \frac{\nabla p}{\rho} + \mathbf{f}, \qquad L(\theta) = -(\mathbf{u} \cdot \nabla)\theta + \omega + \dot{q}.$$

In Fourier space, Eq. (3.7) are expressed as

$$\frac{\partial \hat{\mathbf{u}}}{\partial t} = -\nu |\mathbf{k}|^2 \hat{\mathbf{u}} + \hat{L}(\hat{\mathbf{u}}), \qquad \frac{\partial \hat{\theta}}{\partial t} = -\nu |\mathbf{k}|^2 \hat{\theta} + \hat{L}(\hat{\theta}), \tag{3.8}$$

where $\hat{\mathbf{u}}$, $\hat{L}(\hat{\mathbf{u}})$, $\hat{\theta}$ and $\hat{L}(\hat{\theta})$ as the Fourier coefficients obtained from the discrete Fourier transform of $\mathbf{u}$, $L(\mathbf{u})$, θ and $L(\theta)$ respectively. The pressure term $-\nabla p/\rho$ in $L(\mathbf{u})$ is dealt with projection method (page 211 in (Pope, 2000)). Then new variables $\tilde{\mathbf{u}}$ and $\tilde{\theta}$ are defined as:

$$\tilde{\mathbf{u}} = \hat{\mathbf{u}} \cdot \exp(\nu |\mathbf{k}|^2 t), \qquad \tilde{\theta} = \hat{\theta} \cdot \exp(\nu |\mathbf{k}|^2 t), \tag{3.9}$$

which lead to

$$\frac{\partial \tilde{\mathbf{u}}}{\partial t} = (\frac{\partial \hat{\mathbf{u}}}{\partial t} + \nu |\mathbf{k}|^2 \hat{\mathbf{u}}) \exp(\nu |\mathbf{k}|^2 t), \qquad \frac{\partial \tilde{\theta}}{\partial t} = (\frac{\partial \hat{\theta}}{\partial t} + \nu |\mathbf{k}|^2 \hat{\theta}) \exp(\nu |\mathbf{k}|^2 t). \tag{3.10}$$

Thus the compact expressions about $\tilde{\mathbf{u}}$ and $\tilde{\theta}$ can be derived by substituting Eq. (3.9) into Eq. (3.8), as

$$\frac{\partial \tilde{\mathbf{u}}}{\partial t} = \hat{L}(\tilde{\mathbf{u}} \cdot \exp(-\nu |\mathbf{k}|^2 t)) \exp(\nu |\mathbf{k}|^2 t), \qquad \frac{\partial \tilde{\theta}}{\partial t} = \hat{L}(\tilde{\theta} \cdot \exp(-\nu |\mathbf{k}|^2 t)) \exp(\nu |\mathbf{k}|^2 t). \tag{3.11}$$

Eq. (3.11) are transient PDEs, which can be solved by performing discrete time marching strating from the initial conditions. More details about the time marching are presented in section 3.2.

3.1.2 Finite difference methods

In addition to the pseudo-spectral method, the finite difference method (Zhao et al., 2018a,b; Demosthenous et al., 2016) and finite volume method (Versteeg and Malalasekra, 2007) are also widely used in approximating the spatial derivatives. In this thesis, the cases with the scalar fields of Dirichlet boundary conditions, by which the scalar quantity at the boundary are prescribed, are also investigated. In such circumstance, the finite difference method was used for solving the scalar equations.

Some basic concepts about finite difference methods

As commonly used methods in the direct numerical simulation of turbulent motions (Kristoffersen and Andersson, 1993; Desjardins et al., 2008; Demosthenous et al., 2016), the general idea of the approximation of spatial derivative using finite difference method is originated from the definition of derivatives. In a two-dimensional continuous domain with x and y as coordinate variables, the derivative of a function $F(x, y)$ with respect to x is defined as

$$\frac{\partial F}{\partial x}(x, y) = \lim_{\Delta x \to 0} \frac{F(x + \Delta x, y) - F(x, y)}{\Delta x}. \tag{3.12}$$

It is very straightforward to show that in the discrete domain, the $\frac{\partial F}{\partial x}$ at the grid point of (i, j) can be approximated as

$$\frac{\partial F}{\partial x}\Big|_{i,j} \approx \frac{F_{i+1,j} - F_{i,j}}{\Delta x}, \tag{3.13}$$

where $\Delta x = x_{i+1} - x_i$ is the grid step. When the spatial resolution tends to be infinitely fine, i.e. Δx approaches 0, such an approximation approaches the exact derivative. The approximation of (3.13) is called first order forward scheme. It can also be derived by considering the Taylor series of $F(x, y)$ at the grid of (x_{i+1}, y_i) with respect to (x_i, y_i), which is

$$F_{i+1,j} = F_{i,j} + \frac{\partial F}{\partial x}\Big|_{i,j}\Delta x + \frac{\partial^2 F}{\partial x^2}\Big|_{i,j}\frac{(\Delta x)^2}{2} + \frac{\partial^3 F}{\partial x^3}\Big|_{i,j}\frac{(\Delta x)^3}{6} + \dots. \tag{3.14}$$

Then a precise expression of $\frac{\partial F}{\partial x}\big|_{i,j}$ is obtained as

$$\frac{\partial F}{\partial x}\Big|_{i,j} = \frac{F_{i+1,j} - F_{i,j}}{\Delta x} + \frac{\partial^2 F}{\partial x^2}\Big|_{i,j}\frac{\Delta x}{2} + \frac{\partial^3 F}{\partial x^3}\Big|_{i,j}\frac{(\Delta x)^2}{6} + \dots. \tag{3.15}$$

It is clearly seen that the approximation of (3.13) can be obtained by neglecting the polynomial terms with the order of $\mathcal{O}(\Delta x)$ and higher in (3.15). These neglected terms are called truncation error. The scheme of (3.13) is of first order accuracy because its truncation error is dominated by the first order polynomial.

Construction of finite difference schemes of high order of accuracy

One advantage of finite difference methods is the convenience in constructing difference schemes of high order of accuracy, which is necessary for capturing the intermittent structure, for example in turbulence or rapid reactions.

One most commonly used method for constructing a difference scheme of high order of accuracy is by considering the Taylor expansions at more grid points, i.e. taking the information from more grid points into

consideration. For example, to approximate $\frac{\partial F}{\partial x}\big|_{i,j}$, the Taylor expansion at the grid point of (x_{i-1}, y_j):

$$F_{i-1,j} = F_{i,j} - \frac{\partial F}{\partial x}\big|_{i,j}\Delta x + \frac{\partial^2 F}{\partial x^2}\big|_{i,j}\frac{(\Delta x)^2}{2} - \frac{\partial^3 F}{\partial x^3}\big|_{i,j}\frac{(\Delta x)^3}{6} + \ldots, \tag{3.16}$$

can also be considered.

By subtracting Eq. (3.14) by Eq. (3.16) and neglecting the polynomial terms with order higher than $\mathcal{O}(\Delta x^2)$, it yields

$$\frac{\partial F}{\partial x}\big|_{i,j} \approx \frac{F_{i+1,j} - F_{i-1,j}}{2\Delta x}. \tag{3.17}$$

The approximation by Eq. (3.17) is of second order accuracy, called second order center scheme.

Similarly, difference schemes with higher order of accuracy or for higher order derivatives can be constructed by considering more grid points. For example, the fourth order center scheme for $\frac{\partial F}{\partial x}\big|_{i,j}$ reads

$$\frac{\partial F}{\partial x}\big|_{i,j} \approx \frac{-F_{i+2,j} + 8F_{i+1,j} - 8F_{i-1,j} + F_{i-2,j}}{12\Delta x}, \tag{3.18}$$

the second order center scheme for $\frac{\partial^2 F}{\partial x^2}\big|_{i,j}$ reads

$$\frac{\partial^2 F}{\partial x^2}\big|_{i,j} \approx \frac{F_{i+1,j} - 2F_{i,j} + F_{i-1,j}}{\Delta x^2}, \tag{3.19}$$

and the second order center scheme for mixed derivative $\frac{\partial^2 F}{\partial x \partial y}\big|_{i,j}$ reads

$$\frac{\partial^2 F}{\partial x \partial y}\big|_{i,j} = \frac{1}{2\Delta x}\left(\frac{F_{i+1,j+1} - F_{i+1,j-1}}{2\Delta y} - \frac{F_{i-1,j+1} - F_{i-1,j-1}}{2\Delta y}\right) + \mathcal{O}((\Delta x)^2, (\Delta y)^2). \tag{3.20}$$

Boundary conditions

In finite difference method, for the grid points in the inner domain, the difference scheme discussed above can be directly applied to the governing equations to obtain the discrete algebraic equations. However, for the grids at the boundaries, special treatments are generally needed, because the boundary conditions are generally not periodic. Otherwise the boundary grids are essentially the same as those in the inner domain, like in pseudo-spectral methods.

There is one important requirement for the scheme used for the boundary grids, that is to have the order of accuracy not lower than that of the inner domain grids, because the accuracy of the entire numerical simulation is determined by the calculation on all the grid points. A big truncation in one grid will be propagated to other grids, and gradually to the entire domain. Thus a lower order of accuracy at the boundary will compromise

high orders of accuracy at other positions.

For a function $F(x)$ with $x \in [0, L]$, the discrete function and coordinate can be $F = [F_0, F_1, \ldots, F_N]$ and $x = [x_0, x_1, \ldots, x_N]$ with $x_0 = 0$ and $x_N = L$. A Dirichlet boundary condition such as $F(0) = \alpha$ can numerically be employed as $F_0 = \alpha$. For a Neumann boundary condition, which prescribes the gradient of the quantity at the boundary, an asymmetric scheme can be used. If it is a second order center scheme used in the inner domain, the numerical implementation of the Neumann boundary condition $\frac{\partial F}{\partial x}\big|_{0 \text{ or } L} = \beta$ at the grid of x_1 and x_N can be

$$\frac{-3F_0 + 4F_1 - F_2}{2\Delta x} = \beta \text{ and } \frac{3F_{N-2} - 4F_{N-1} + F_N}{2\Delta x} = \beta. \tag{3.21}$$

An important technique for implementing the boundary condition is using the ghost grids, i.e. defining the grids beyond the boundary, such as the grids of $x_{-2} = -2\Delta x$, $x_{-1} = -\Delta x$ and $x_{N+1} = L + \Delta x$, $x_{N+2} = L + 2\Delta x$. For example with the Dirichlet boundary of $F(0) = \alpha$, if the approximation of $\frac{\partial F}{\partial x}$ in the inner domain is implemented with the fourth order center scheme (Eq. (3.18)), we can have not only $F_0 = \alpha$ but also $F_{-1} = \alpha$ at the ghost grid. The benefit of doing this is that there is no special treatment needed in the approximation of $\frac{\partial F}{\partial x}\big|_1$, which requires the value of F_{-1} according to Eq. (3.18). With the Neumann boundary condition $\frac{\partial F}{\partial x}\big|_0 = \beta$, F_{-1} can be prescribed as $F_0 - \Delta x\beta$, which suggests a slope of the Neumann boundary condition value between the boundary grid and ghost grid.

The implementation of finite difference method in this thesis

In some configurations explored in this thesis, the scalar fields are of Dirichlet boundary conditions (Chapter 6), which requires a finite difference method for solving the scalar equations. In order to ensure the accurate approximation of the intermittent structures in the turbulent motion or fast reaction, very fine finite difference schemes are used. Specially, the first-order derivative is approximated by using eighth order upwind difference scheme, which is dependent on the local velocity. For example, at the grid point of (x_i, y_j, z_k), when $u_{x;i,j,k} > 0$, $\frac{\partial \theta}{\partial x}\big|_{i,j,k}$ is approximated as

$$\begin{aligned}\frac{\partial \theta}{\partial x}\Big|_{i,j,k} \approx & \frac{1}{280}\left(\frac{\theta_{i,j,k} - \theta_{i-5,j,k}}{\Delta x}\right) - \frac{1}{28}\left(\frac{\theta_{i,j,k} - \theta_{i-4,j,k}}{\Delta x}\right) + \frac{1}{6}\left(\frac{\theta_{i,j,k} - \theta_{i-3,j,k}}{\Delta x}\right) - \frac{1}{2}\left(\frac{\theta_{i,j,k} - \theta_{i-2,j,k}}{\Delta x}\right) \\ & + \frac{5}{4}\left(\frac{\theta_{i,j,k} - \theta_{i-1,j,k}}{\Delta x}\right) - \frac{1}{2}\left(\frac{\theta_{i,j,k} - \theta_{i+1,j,k}}{\Delta x}\right) + \frac{1}{14}\left(\frac{\theta_{i,j,k} - \theta_{i+2,j,k}}{\Delta x}\right) - \frac{1}{168}\left(\frac{\theta_{i,j,k} - \theta_{i+3,j,k}}{\Delta x}\right),\end{aligned}$$

and when $u_{x;i,j,k} < 0$, $\frac{\partial\theta}{\partial x}\big|_{i,j,k}$ is approximated as

$$\begin{aligned}\frac{\partial\theta}{\partial x}\big|_{i,j,k} \approx & \frac{1}{280}\left(\frac{\theta_{i+5,j,k}-\theta_{i,j,k}}{\Delta x}\right) - \frac{1}{28}\left(\frac{\theta_{i+4,j,k}-\theta_{i,j,k}}{\Delta x}\right) + \frac{1}{6}\left(\frac{\theta_{i+3,j,k}-\theta_{i,j,k}}{\Delta x}\right) - \frac{1}{2}\left(\frac{\theta_{i+2,j,k}-\theta_{i,j,k}}{\Delta x}\right) \\ & + \frac{5}{4}\left(\frac{\theta_{i+1,j,k}-\theta_{i,j,k}}{\Delta x}\right) - \frac{1}{2}\left(\frac{\theta_{i-1,j,k}-\theta_{i,j,k}}{\Delta x}\right) + \frac{1}{14}\left(\frac{\theta_{i-2,j,k}-\theta_{i,j,k}}{\Delta x}\right) - \frac{1}{168}\left(\frac{\theta_{i-3,j,k}-\theta_{i,j,k}}{\Delta x}\right).\end{aligned}$$

As to the second-order derivative $\frac{\partial^2\theta}{\partial x^2}\big|_{i,j,k}$, tenth order center difference scheme is used:

$$\begin{aligned}\frac{\partial^2\theta}{\partial x^2}\big|_{i,j,k} \approx & \frac{5}{3}\left(\frac{\theta_{i+1,j,k}-2\theta_{i,j,k}+\theta_{i-1,j,k}}{\Delta x^2}\right) - \frac{20}{21}\left(\frac{\theta_{i+2,j,k}-2\theta_{i,j,k}+\theta_{i-2,j,k}}{4\Delta x^2}\right) \\ & + \frac{5}{14}\left(\frac{\theta_{i+3,j,k}-2\theta_{i,j,k}+\theta_{i-3,j,k}}{9\Delta x^2}\right) - \frac{5}{63}\left(\frac{\theta_{i+4,j,k}-2\theta_{i,j,k}+\theta_{i-4,j,k}}{16\Delta x^2}\right) \\ & + \frac{1}{126}\left(\frac{\theta_{i+5,j,k}-2\theta_{i,j,k}+\theta_{i-5,j,k}}{25\Delta x^2}\right).\end{aligned}$$

The polynomial coefficients in the above schemes are determined by considering the Taylor expansions of the neighbor grids, by which 8th and 10th order of accuracy are ensured for the approximations of the first and second order derivative respectively.

The Dirichlet boundary conditions are employed by prescribing the scalar quantities at the boundary grids and using 4 extra ghost grids beyond the boundary. Thereby, the above schemes can be applied to both the grids on the boundaries and the inner domain.

3.2 Temporal discretization and time integration

For a time-dependent PDE, the temporal discretization is needed for approximating the time-derivative terms. The discretization of the temporal domain is generally implemented by discretizing the temporal coordinate t into a series of uniform time steps: $t^n = t_0 + n\Delta t$ with n as an integer rangeing from 0 to infinity. t_0 corresponds to the initial time, at which the quantities of the entire spatial domain are prescribed by the initial conditions. Then a specific marching scheme is applied to the governing equations for doing the numerical temporal integration, in which the known information of one time step (t^n) can be used to compute the unknown quantities at next time step (t^{n+1}).

3.2.1 Numerical marching schemes

Implicit and explicit schemes

In turbulent studies, the temporal derivative is generally linear and only of first order (Eq. (1.9) and (2.19)). Therefore, the PDE about of F (representing velocity components or scalar), which is a function of spatial and temporal coordinates ($\mathbf{x}$ and t), can be written in the form of

$$\frac{\partial F}{\partial t} = \mathfrak{L}(\mathbf{x}, F, \frac{\partial F}{\partial x}, \frac{\partial^2 F}{\partial x^2}, \cdots), \tag{3.22}$$

where $\mathfrak{L}$ includes every term of the PDE except the temporal derivative, like Eq. (3.11).

A simple way to approximate $\frac{\partial F}{\partial t}$ can be a scheme similar with Eq. (3.13). Moreover, after the spatial discretization of the spatial derivatives, the right hand side of Eq. (3.22) are approximated with algebraic expressions of the discrete F. Therefore, in a discrete form, Eq. (3.22) can be approximated as

$$\frac{F_i^{n+1} - F_i^n}{\Delta t} \approx \mathfrak{L}(\cdots, F_{i-1}^n, F_i^n, F_{i+1}^n, \cdots). \tag{3.23}$$

In Eq. (3.23), the quantities with superscript of n are of the time step of t^n, which are known; and the superscript of $n+1$ indicates the time step of t^{n+1}, which are unknown and to be computed. Thus Eq. (3.23) provides a straightforward scheme for numerical temporal integration, as

$$F_i^{n+1} \approx \mathfrak{L}(\cdots, F_{i-1}^n, F_i^n, F_{i+1}^n, \cdots)\Delta t + F_i^n. \tag{3.24}$$

Eq. (3.24) is one of the explicit schemes, which means the every unknown quantity at the time step of t^{n+1} can be explicitly expressed as function of quantities at the time step of t^n. In contrast, if the quantities used in the right hand side of Eq. (3.23) are all of the unknown time step, an implicit scheme can be derived, as

$$F_i^{n+1} - \mathfrak{L}(\cdots, F_{i-1}^{n+1}, F_i^{n+1}, F_{i+1}^{n+1}, \cdots)\Delta t \approx F_i^n. \tag{3.25}$$

With such a scheme, the numerical marching from t^n to t^{n+1} is generally implemented by considering Eq. (3.25) for all the spatial grid points simultaneously and doing the computation in the form of vector and matrix.

The explicit scheme is easier for implementation than the implicit scheme, however the implicit scheme is generally more stable (Magoulès, 2011), which allows a larger Δt. Sometimes, a compromise can be made between the explicit and implicit schemes, i.e. considering the discrete quantities at both the current and next

time steps in the approximation of spatial derivatives. For example Eq. (3.22) can be approximated as

$$\frac{F_i^{n+1} - F_i^n}{\Delta t} \approx \mathfrak{L}(\cdots, F_{i-2}^n, F_{i-1}^n, F_i^n, F_{i+1}^{n+1}, F_{i+2}^{n+1}, \cdots), \tag{3.26}$$

which provides a semi-implicit temporal marching scheme.

The third order Runge-Kutta scheme

The numerical temporal integration in this thesis is implemented by using third order Runge-Kutta scheme (Shu and Osher, 1988). For a canonical temporal differential equation

$$\frac{\partial F}{\partial t} = \mathfrak{L}(F), \tag{3.27}$$

the third order Runge-Kutta scheme reads

$$\begin{aligned} F^1 =& F^0 + \Delta t \cdot \mathfrak{L}(F^0), \\ F^2 =& \frac{3}{4}F^0 + \frac{1}{4}F^1 + \frac{1}{4}\Delta t \cdot \mathfrak{L}(F^1), \\ F^3 =& \frac{1}{3}F^0 + \frac{2}{3}F^2 + \frac{2}{3}\Delta t \cdot \mathfrak{L}(F^2). \end{aligned} \tag{3.28}$$

where F^3 are the unknown quantities at the time of $(t + \Delta t)$, and F^0 are the known quantities at the time t. Let us take the pseudo-spectral method as example (it is more straightforward in finite difference method). Applying (3.28) to Eq. (3.11), it yields the expressions of obtaining $\hat{\mathbf{u}}^3$ and $\hat{\theta}^3$ at the time of $t + \Delta t$ with $\hat{\mathbf{u}}^0$ and $\hat{\theta}^0$ at the time of t as

$$\begin{aligned} \hat{\mathbf{u}}^1 &= (\hat{\mathbf{u}}^0 + \Delta t \hat{L}(\hat{\mathbf{u}}^0)) \cdot \exp(-\nu|\mathbf{k}|^2 \Delta t), \\ \hat{\mathbf{u}}^2 &= \frac{3}{4}\hat{\mathbf{u}}^0 \cdot \exp(-\nu|\mathbf{k}|^2 \frac{\Delta t}{2}) + \frac{1}{4}\hat{\mathbf{u}}^1 \cdot \exp(\nu|\mathbf{k}|^2 \frac{\Delta t}{2}) + \frac{1}{4}\Delta t \hat{L}(\hat{\mathbf{u}}^1) \cdot \exp(\nu|\mathbf{k}|^2 \frac{\Delta t}{2}), \\ \hat{\mathbf{u}}^3 &= \frac{1}{3}\hat{\mathbf{u}}^0 \cdot \exp(-\nu|\mathbf{k}|^2 \Delta t) + \frac{2}{3}\hat{\mathbf{u}}^2 \cdot \exp(-\nu|\mathbf{k}|^2 \frac{\Delta t}{2}) + \frac{2}{3}\Delta t \hat{L}(\hat{\mathbf{u}}^2) \cdot \exp(-\nu|\mathbf{k}|^2 \frac{\Delta t}{2}), \end{aligned} \tag{3.29}$$

and

$$\begin{aligned}
\hat{\theta}^1 &= (\hat{\theta}^0 + \Delta t \hat{L}(\hat{\theta}^0)) \cdot \exp(-\nu|\mathbf{k}|^2 \Delta t), \\
\hat{\theta}^2 &= \frac{3}{4}\hat{\theta}^0 \cdot \exp(-\nu|\mathbf{k}|^2 \frac{\Delta t}{2}) + \frac{1}{4}\hat{\theta}^1 \cdot \exp(\nu|\mathbf{k}|^2 \frac{\Delta t}{2}) + \frac{1}{4}\Delta t \hat{L}(\hat{\theta}^1) \cdot \exp(\nu|\mathbf{k}|^2 \frac{\Delta t}{2}), \\
\hat{\theta}^3 &= \frac{1}{3}\hat{\theta}^0 \cdot \exp(-\nu|\mathbf{k}|^2 \Delta t) + \frac{2}{3}\hat{\theta}^2 \cdot \exp(-\nu|\mathbf{k}|^2 \frac{\Delta t}{2}) + \frac{2}{3}\Delta t \hat{L}(\hat{\theta}^2) \cdot \exp(-\nu|\mathbf{k}|^2 \frac{\Delta t}{2}).
\end{aligned} \tag{3.30}$$

3.2.2 Choice of the time step

Generally, a larger numerical time step Δt is favorable for the efficiency of numerical simulation, because fewer time steps of computation are required for the simulation to converge or reach a statistically stationary state. However, similarly with Δx, which needs to be smaller enough for a good resolution, the Δt also cannot be too large for the sake of numerical stability.

The stability of a numerical simulation mainly concerns the round-off error. After approximating the spatial and temporal derivatives with certain difference schemes, the continuous PDEs are transformed into some algebraic equations. These algebraic equations are solved by computers. Since the data stored in the computers are of finite digits, the final solutions we can get must be different from the exact solutions. Such difference are called the round-off error. Although the round-off error can be very small with advanced computers, if inappropriate numerical marching methods are chosen, the round-off error will be amplified at each numerical time step and finally lead to the divergence.

Therefore, the maximum Δt can be determined by considering the temporal evolution of the round-off errors. The two most widely used methods for the stability analysis are the Neumann method and the matrix method. The general idea of both methods are deriving the evolution equations of the round-off error (ϵ^n) based on the discrete governing equations and then expressing the increasing rate of the amplitude of the round-off error $\frac{|\epsilon^{n+1}|}{|\epsilon^n|}$ as function of Δx and Δt. Then under the constraint of $\frac{|\epsilon^{n+1}|}{|\epsilon^n|} \leqslant 1$, the maximum Δt as function of Δx can be obtained. More details can be referred to Zikanov (2010). It is noteworthy that the stability analysis provides the necessary but not sufficient condition for the numerical stability.

The Courant-Friedrichs-Lewy stability condition

When the time marching is implemented with explicit scheme, the value of time step is always crucial for the numerical stability. In a famous paper by Courant et al. (1928) (English translation as Courant et al. (1967)), the Courant-Friedrichs-Lewy (CFL) stability condition is proposed as the necessary condition for the stability of explicit time-stepping schemes. The CFL condition states that, for a discrete point in the temporal-spatial

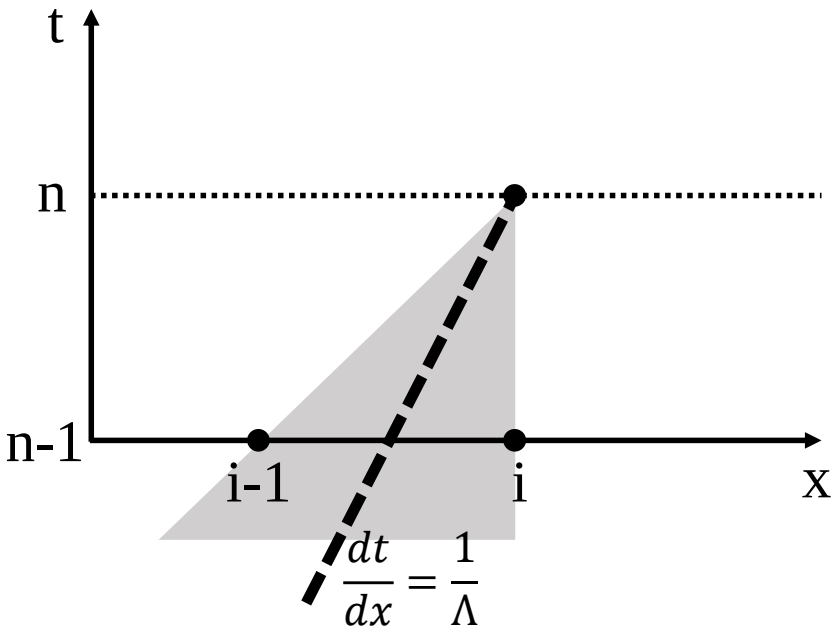

Figure 3.2: The illustration of the physical domain of dependence of Eq. (3.31) (thick dashed line) and the numerical domain of dependence (gray area).

space, its physical domain of dependence must be included in the numerical domain of dependence. A good example to explain the CFL condition is the one-dimensional linear convection equation:

$$\frac{\partial s}{\partial t} + \Lambda \frac{\partial s}{\partial x} = 0, \tag{3.31}$$

where $s = s(x,t)$ is any quantity as function of x and t; Λ is a positive constant, as the speed of propagation. The PDE of Eq. (3.31) has a general solution as:

$$s = F(x - \Lambda t), \tag{3.32}$$

where F is any function of $x - \Lambda t$. The solution of (3.32) indicates that $s(x,t)$ is in the form of wave propagation at the constant speed of Λ. Thus for the point of $(x_i,\ t^n)$, the physical domain of dependence is the straight line of the slope of $1/\Lambda$ and passing it, as shown in figure 3.2. Numerically, if Eq. (3.31) is discretized with the approximation of

$$\frac{\partial s}{\partial t}\Big|_i^n \approx \frac{s_i^{n+1} - s_i^n}{\Delta t}, \quad \frac{\partial s}{\partial x}\Big|_i^n \approx \frac{s_i^n - s_{i-1}^n}{\Delta x}, \tag{3.33}$$

the time marching is implemented as

$$s_i^{n+1} = -\Lambda \frac{\Delta t}{\Delta x}(s_i^n - s_{i-1}^n) + s_i^n. \tag{3.34}$$

The numerical result of s_i^{n+1} is dependent on s_i^n and s_{i-1}^n. Thus the numerical domain of dependence is the grey area shown in figure 3.2. In figure 3.2, the numerical domain of dependence includes the physical domain of dependence. Thus the scheme of (3.34) can be stable, although not surely. Otherwise, if the slope of $\Delta t/\Delta x$ is larger than $1/\Lambda$, the numerical scheme is unstable because it fails to capture the physical information in need. The Courant number (also called CFL number) (Le Veque, 1990; Blazek, 2005) is defined as

$$\Lambda \frac{\Delta t}{\Delta x}. \tag{3.35}$$

Quantitatively, CFL stability condition states that the CFL number should not be larger than unity.

The PDE of Eq. (3.31) is meaningful to the turbulence simulation because its spatial derivative term is in a similar form with the convection term of the N-S equation and the scalar equation (Eq. (1.9) and (1.28)), which is generally the dominant term. When the N-S equation or the scalar equation is solved with an explicit method, the CFL number can be defined as

$$|u|_{max} \frac{\Delta t}{\Delta x}, \tag{3.36}$$

where $|u|_{max}$ is the global maximum of the absolute value of single-component velocity.

3.3 Numerical forcing

The energy cascade of the kinematic energy and scalar fluctuation in the inertial length scale are of high interest in turbulence studies. The source of the fluctuation comes generally from the mean part of the quantity of interest in physical space or external input in spectral space. Thus in the numerical simulations about a turbulence in statistically stationary state, lots of techniques for numerical forcing were developed (Eswaran and Pope, 1988a,b; Moin and Mahesh, 1998; Overholt and Pope, 1998; Alvelius, 1999; Rao and de Bruyn Kops, 2011). Each forcing scheme has pros and cons.

The energy cascade concerns only the fluctuating part of velocity or scalar. Thus it is a natural choice to introduce the forcing from the mean part, for example by imposing a mean gradient (Sreenivasan, 1991; Gotoh and Watanabe, 2015; Gauding et al., 2017; Iyer et al., 2018). With the existence of a mean gradient, due to the vortex stretching as discussed in the sections of 1.1.1, the energy is extracted from the mean motions and transferred into the fluctuations of velocity by shear stress, i.e. turbulent diffusion. For the scalar, in the case of no external forcing and when the scalar is of constant mean gradient such as $\theta = \theta' + Gz$, the governing

equation of the variance of scalar (Eq. (1.35)) becomes

$$\frac{1}{2}\frac{D\langle\theta'^2\rangle}{Dt} = -D\langle(\nabla\theta')^2\rangle - G\langle u_z'\theta'\rangle. \tag{3.37}$$

The variance of scalar fluctuations can be sustained by a source proportional to the turbulent flux of scalar (covariance of scalar and velocity) (Tennekes and Lumley, 1972). However, the forcing by a mean gradient makes one particular direction different from the others, leading to the breakdown of the local isotropy (Sreenivasan, 1991; Biferale and Procaccia, 2005; Gotoh and Watanabe, 2015; Iyer et al., 2018).

Another widely used numerical forcing is the large scales forcing, which is generally isotropic. The idea of this type of forcing is to limit the artificial information at several largest scales, without significant interference to the universal properties in the inertial range of turbulent motions. Typically these numerical forcings are implemented in Fourier space, in which the length scales can be well-identified after the discrete Fourier transform.

To have a steady supply of turbulent energy, many works simply prescribed the energy spectrum at large scale modes, for example by freezing the amplitude of the velocity in a given range of wave numbers (Siggia and Patterson, 1978). The large scale motions were totally artificial. The desired spectrum in the prescribed range should be known in advance, otherwise there might be a big distortion to the problem being studied especially when the maximum wave number was not large enough. A modification can be allowing the free evolutions of individual modes in a range of scales while maintaining the average energy in this range as constant (Chasnov, 1991; Machiels, 1997). It allowed a more physically meaningful energy spectrum. However there was a discontinuity between forced and unforced modes, which might develop to be a large numerical error (Kerr, 1985; Sullivan et al., 1994). There are also some other works adopting the idea of prescribing the large scale quantities. For example Siggia (1981) tried to model the stain rate of large scales.

In order to avoid introducing too much artificial information, instead of prescribing the large scale quantities, some works adopted a deterministic forcing, which is a linear amplification of the existing large scale fields (Kerr, 1981; Vincent and Meneguzzi, 1991). The factor of amplification was generally dynamically determined for controlling the numerical error and accelerating the convergence. In the work by Overholt and Pope (1998), the factor of amplification was determined from a damper-like system of numerical equations, in which the large scale spectrum obtained was approaching a target spectrum. Such a scheme of forcing can be considered as a modification of the method prescribing the large scale energy spectrum, achieving a relatively better convergence efficiency. There were also works proposed an amplification factor being adjusted each numerical step to ensure a constant input power (Schumacher et al., 2007; Ghosal et al., 1995). For the existing velocity field in Fourier

space $\hat{\mathbf{u}}(\mathbf{k},t)$, the forcing $\hat{\mathbf{f}}(\mathbf{k},t)$ is

$$\hat{\mathbf{f}}(\mathbf{k},t) = \epsilon_{in} \frac{\hat{\mathbf{u}}(\mathbf{k},t)}{\sum_{\mathbf{k}\in\mathbf{K_f}} |\hat{\mathbf{u}}(\mathbf{k},t)|^2} \delta_{\mathbf{k},\mathbf{k_f}}, \tag{3.38}$$

where $\mathbf{K_f}$ is a set of small amplitude wave number vectors, i.e. the forced modes, for example $\mathbf{K_f} = \{\mathbf{k} : |\mathbf{k}|^2 \leqslant 8\}$; $\mathbf{k_f}$ is any wave number vector in $\mathbf{K_f}$; ϵ_{in} is the prescribed input power. The forcing of constant power is more physically meaningful. The simulation can generally evolve stably because the dissipation rate must be equal to the prescribed input power after the simulation is converged.

However, the forcing adding in a deterministic way means that the information of past steps always remains in the forcing. It is then hard to fully lost the effect of the initial condition. Thus there were studies that considered the stochastic forcing, which is weakly dependent on the existing fields because the random process is included. The commonly used stochastic forcings are of constant amplitude (Alvelius, 1999; Gotoh and Watanabe, 2015) and random phase. For example

$$\hat{\mathbf{f}}(\mathbf{k},t) = \sum_{\mathbf{k}\in\mathbf{K_f}} \mathbf{A_k} e^{i\phi(\mathbf{k},t)}, \tag{3.39}$$

where $\mathbf{A_k}$ is the prescribed amplitude at the mode of $\mathbf{k}$ and $\phi(\mathbf{k},t)$ is the random phase, independent for each wave number and time step. In the work of Watanabe and Gotoh (2004) and Gotoh and Watanabe (2015), the forcings for both velocity and passive scalar were added in Fourier space. The real and complex parts of the forcings were first obtained as wave number independent and time-delta Gaussian random numbers, and then normalized to ensure the constant amplitude. By adopting forcing of random phase, the convergence of simulation is accelerated since the effect of initial condition is limited. The drawback is the undeserved discontinuity in temporal evolution. Thus a compromise can be made by adopting the forcing as linear amplification of the existing fields while adjusting the phase with a random process to a certain degree (Perlekar et al., 2012). The random number for adjusting the phase can be Gaussian distributed, equally distributed, or generated from the Uhlenbeck-Ornstein process (Wax, 1954; Eswaran and Pope, 1988b).

3.4 Direct numerical simulations of reactive turbulent flows

DNS has been widely used for the numerical simulation of chemical reactions in turbulent flow, but most of the studies focused on the compressible case, such as turbulent combustion (Vervisch and Poinsot, 1998). Relatively fewer works focused on the DNS of the reactive scalar in incompressible turbulence (De Bortoli et al., 2005).

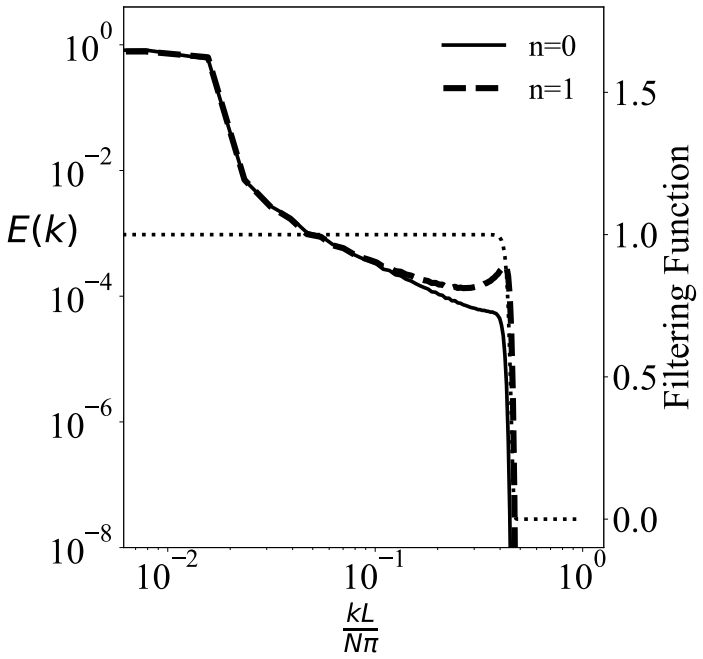

Figure 3.3: The DNS results of the energy spectra of the reaction rates ($\gamma_1 R_1 R_2^n - \gamma_2 P$) of the first order (solid line) and second order (dashed line) reactions in the form of (3.40). $k = |\mathbf{k}|$ is the amplitude of wave number vector. The dealiasing is implemented as smooth dealiasing, with a filtering function (Eq. (3.6)) shown as the dotted curve.

Since no change in density or heat release is considered in incompressible turbulence, the most noticeable difference between the reactive scalar and the passive scalar is the reaction term in the governing equation. The reaction terms are in the form of product of reactants and thus nonlinear for high order reaction (Hill, 1976; Heeb and Brodkey, 1990). These nonlinear reaction terms can introduce extra convolutions in the high wave number modes of reactive scalars, which can be physically meaningful especially with large reaction rates. When the DNS is implemented with a pseudo-spectral method, the maximum resolved wave number is needed to be large enough to resolve the non-linear reaction terms. For example, consider the reversible reaction of

$$R_1 + nR_2 \underset{\gamma_2}{\overset{\gamma_1}{\rightleftharpoons}} P \tag{3.40}$$

in homogeneous isotropic turbulence (Wu et al., 2020) with $n = 0$ or 1, corresponding to first and second order reaction respectively. The net reaction rate is $\gamma_1 R_1 R_2^n - \gamma_2 P$, whose energy spectra obtained from DNS are shown in figure 3.3. It is clearly seen that for the second order reaction, there is a peak of the spectrum at the range of high wave number modes. However, the further development of this peak to smaller scales can not be reflected in DNS due to the dealiasing, i.e. insufficient resolved wave number.

In the DNS of turbulent velocity and passive scalar fields, the spatial resolution is required to be fine enough

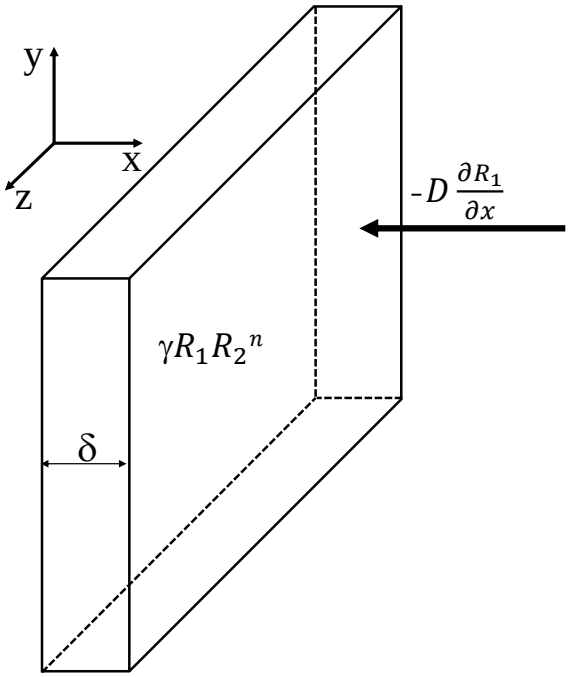

Figure 3.4: An illustration for the balance between reaction and diffusion in the reaction zone.

for resolving the Kolmogorov scale and Batchelor scale (Eq. (1.14) and (1.42)). When the reactive scalars are involved, especially with fast reaction, the thickness of reaction zone δ must also be taken into consideration. The reaction zone is like a flame front (Domingo and Vervisch, 1996; Wang et al., 2011), through which the concentration of reactants and the reaction rate can sharply change. To capture the information in the reaction zone, finite difference method with schemes of high accuracy order (Craske and van Reeuwijk, 2015; Zhao et al., 2018a) can be used. It generally also requires significantly more than 1 grids in the length of δ. For a canonical reaction $R_1 + nR_2 \xrightarrow{\gamma} \emptyset$ in turbulence, an estimation about the thickness of the reaction zone δ can be done by considering the balance between reaction and diffusion (convection is less important in the small scale). Imagine the reaction zone as a flat cuboid of the lateral area of A and the thickness of δ (figure 3.4). In an infinitesimally small time period of τ, the R_1 consumed in the cuboid by reaction is equal to $\gamma R_1 R_2^n \tau \delta A$. In addition, according to the Fick's law of diffusion (Bergman et al., 2011), there is a flux of R_1 entering the cuboid due to the gradient: $-D\frac{\partial R_1}{\partial x} A\tau$. A balance is then built as

$$-D\frac{\partial R_1}{\partial x} A\tau - \gamma R_1 R_2^n \delta A\tau = 0. \tag{3.41}$$

Since the reaction zone is supposed to contain the local maximums of the reactant concentrations, which are close to zero outside, the R_1 and R_2 in Eq. (3.41) can be considered as local maximums and the $\frac{\partial R_1}{\partial x}$ can be

estimated as $-R_1/\delta$. Thus δ can be estimated as $\sqrt{\frac{D}{\gamma}}R_2^{-n/2}$. The factor of $R_2^{-n/2}$ is for the special case, but generally, δ roughly satisfies

$$\delta \propto \sqrt{\frac{D}{\gamma}}. \tag{3.42}$$

Such a relation is similar to that derived for the thickness of flame front (Law, 2006). Eq. (3.42) suggests a finer spatial resolution for faster reaction, with the grid size inversely proportional to the square root of the reaction rate.

Chapter 4

Reactions in homogeneous isotropic turbulence

In this chapter, we focus on the fundamental properties of reactive scalar mixing in homogeneous isotropic incompressible turbulence. The flow statistics, from global to scale-dependent features are studied in details and theoretically modelled. This chapter is organized as follows: In section 4.1, we introduce the model system, its governing equations together with the set of dimensionless control parameters. Section 4.2 briefly specifies the numerical methods adopted for the numerical simulation. Then the DNS results and their analyses are presented in sections 4.3-4.7. Finally, a brief summary about this chapter is given in section 4.8.*

4.1 Problem definition

In this chapter we consider reactions of the form:

$$\mathrm{R}_1 + n\mathrm{R}_2 \underset{\gamma_2}{\overset{\gamma_1}{\rightleftharpoons}} \mathrm{P}, \tag{4.1}$$

where R_1, R_2 and P denote three generic reactive scalars and n is an integer coefficient. The process is reversible with independent non-zero forward/backward reaction rates γ_1 and γ_2. The order of the chemical reaction, which is defined as the sum of the powers of the reactants' concentration in the rate equation is $n+1$ for the forward reaction, because the rate equation reads $\gamma_1 R_1 R_2^n$, while is of the first order for the backward reaction with

*The content of this chapter is based on our published paper "Wu, W., E. Calzavarini, F. G. Schmitt, and L. Wang (2020). Fluctuations and correlations of reactive scalars near chemical equilibrium in incompressible turbulence. *Physical Review Fluids* 5, 084608."

reaction rate $\gamma_2 P$. The reactants are assumed to be subject to molecular diffusion and to fluid advection. The evolution equations for the velocity and the concentration fields $R_1(\mathbf{x},t)$, $R_2(\mathbf{x},t)$ and $P(\mathbf{x},t)$ read:

$$\frac{\partial \mathbf{u}}{\partial t} + (\mathbf{u}\cdot\nabla)\mathbf{u} = \nu\triangle\mathbf{u} - \nabla p/\rho + \mathbf{f}, \tag{4.2}$$

$$\nabla\cdot\mathbf{u} = 0, \tag{4.3}$$

and

$$\frac{\partial R_1}{\partial t} + (\mathbf{u}\cdot\nabla)R_1 = D\triangle R_1 - \gamma_1 R_1 R_2^n + \gamma_2 P + \dot{q}_{R_1}, \tag{4.4a}$$

$$\frac{\partial R_2}{\partial t} + (\mathbf{u}\cdot\nabla)R_2 = D\triangle R_2 - n(\gamma_1 R_1 R_2^n - \gamma_2 P) + \dot{q}_{R_2}, \tag{4.4b}$$

$$\frac{\partial P}{\partial t} + (\mathbf{u}\cdot\nabla)P = D\triangle P + \gamma_1 R_1 R_2^n - \gamma_2 P + \dot{q}_P. \tag{4.4c}$$

Here $\mathbf{u}(\mathbf{x},t)$ is the three-dimensional flow velocity, p is the pressure, ρ is the fluid density set as constant, ν is the kinematic viscosity and D is the species diffusivity (assumed as being the same for all species). To sustain the turbulent fluctuations, large-scale forcing terms $\mathbf{f}$ and $\dot{q}$ are introduced for the velocity and scalars, respectively. More details about the expression of these forcing terms will be provided in section 4.2.

For comparison, a non-reactive species T undergoing both advection and diffusion is also considered. Its local concentration evolves according to the following equation,

$$\frac{\partial T}{\partial t} + (\mathbf{u}\cdot\nabla)T = D\triangle T + \dot{q}_T. \tag{4.5}$$

The equations for the above model system can be made dimensionless by choosing reference scales appropriate for the present system. Since the turbulent flow is unbounded, we take the Taylor microscale (λ) and the single component velocity fluctuation (u') as the reference scales for space and velocity, respectively, which are defined as: $\lambda = \sqrt{\frac{15\nu}{\varepsilon}}u'$, $u' = \frac{1}{3}\sum_i\sqrt{\langle u_i^2\rangle}$, $\varepsilon = \frac{\nu}{2}\langle\sum_i\sum_j(\partial_i u_j + \partial_j u_i)^2\rangle$. Here ε is the mean dissipation rate; $\langle\cdot\rangle$ is the ensemble average, but numerically represented by space and time average in this chapter without special notation. The scalar quantities can be non-dimensionalized by means of their equilibrium values in no-flow conditions $R_{1,eq}, R_{2,eq}, P_{eq}$, while for the passive scalar the global mean $\langle T\rangle$ is used as the reference value. Note that at the equilibrium, the algebraic relation $\gamma_1 R_{1,eq}R_{2,eq}^n = \gamma_2 P_{eq}$ holds. Furthermore, in this chapter for simplicity we assume that $R_{1,eq} = R_{2,eq}$. This leads to the following dimensionless equations:

$$\frac{\partial \mathbf{u}}{\partial t} + (\mathbf{u}\cdot\nabla)\mathbf{u} = Re_\lambda^{-1}\triangle\mathbf{u} - \nabla p + \mathbf{f}, \tag{4.6}$$

$$\nabla \cdot \mathbf{u} = 0, \tag{4.7}$$

$$\frac{\partial R_1}{\partial t} + (\mathbf{u} \cdot \nabla) R_1 = (Sc\ Re_\lambda)^{-1} \triangle R_1 - Da(R_1 R_2^n - P) + \dot{q}_{R_1}, \tag{4.8a}$$

$$\frac{\partial R_2}{\partial t} + (\mathbf{u} \cdot \nabla) R_2 = (Sc\ Re_\lambda)^{-1} \triangle R_2 - nDa(R_1 R_2^n - P) + \dot{q}_{R_2}, \tag{4.8b}$$

$$\frac{\partial P}{\partial t} + (\mathbf{u} \cdot \nabla) P = (Sc\ Re_\lambda)^{-1} \triangle P + Da(R_1 R_2^n - P) + \dot{q}_P, \tag{4.8c}$$

$$\frac{\partial T}{\partial t} + (\mathbf{u} \cdot \nabla) T = (Sc\ Re_\lambda)^{-1} \triangle T + \dot{q}_T, \tag{4.8d}$$

where $Re_\lambda = \lambda \cdot u'/\nu$ is the Taylor based Reynolds number, the Schmidt number $Sc = \nu/D$ is the ratio of viscous diffusion to molecular diffusion, the Damköhler number $Da = \lambda\gamma_1 R_{2,eq}^n/u' = \lambda\gamma_2/u'$ represents the ratio of flow timescale to the chemical timescale of forward or backward reaction. Note that the particular choice $R_{1,eq} = R_{2,eq}$ is crucial in obtaining a single Damköhler number, instead of two distinct ones that would be present in general cases.

In conclusion the control parameters of the model system are Re_λ, Sc, n and Da.

4.2 Numerical methods

The model system presented in Sec. 4.1 is numerically simulated in a cubic tri-periodic domain. The flow is sustained by a large-scale forcing capable to generate a statistically steady homogeneous and isotropic turbulent flow. The expression of the forcing field in Fourier space, $\hat{\mathbf{f}}(\mathbf{k}, t)$ reads,

$$\hat{\mathbf{f}}(\mathbf{k}, t) = \frac{1}{\tau_f} \sum_{1 \leqslant |\mathbf{k}| \leqslant 2\sqrt{2}} \hat{\mathbf{u}}(\mathbf{k}, t), \tag{4.9}$$

with τ_f a time-scale being adjusted at each time step in order to provide a constant power input, i.e. $\int_V \mathbf{f} \cdot \mathbf{u} dx^3 = const.$. This type of forcing, called linear, has been adopted e.g. in (Schumacher et al., 2007). Note also that the zero mode $|\mathbf{k}| = 0$ is not forced in order to prevent the development of a global mean flow, i.e., in our simulations $\langle \mathbf{u} \rangle = 0$. Similarly, the external source term on scalars ($\dot{q}_\theta$ with $\theta = R_1, R_2, P$ or T in Eq. (4.8)) is also isotropic and acting at the largest scales; however it is constant in amplitude (Alvelius, 1999; Gotoh et al.,

Table 4.1: Parameters for the simulations: Re_λ is the Taylor scale based Reynolds number; Sc is the Schmidt number; $Da = \lambda\gamma_1 R_{2,eq}^n/u' = \lambda\gamma_2/u'$ is the Damköhler number based on Taylor scale; n is the order of R_2 in the reaction; N^3 is the total number of grid points; η is the Kolmogorov length or dissipative length; $|\mathbf{k}|_{max}$ is the maximum wave number amplitude kept by the dealiasing procedure; $|\mathbf{k}|_{max} \cdot \eta$ is the spatial resolution condition; dt/τ_η is the time step normalized by the Kolmogorov time scale τ_η.

No.	1	2	3	4
Re_λ	20	40	80	150
Sc	0.1-4	0.1-4	0.1-1/2-4	1
Da	0.0005 - 50	0.0003 - 30	0.0005 - 20	0.001 - 10
n	1	1 - 3	1 - 3	1 - 3
N^3	64^3	64^3 */128^3 †	128^3 */256^3 †	256^3
$\|\mathbf{k}\|_{max}\eta$	3.12	1.48 */2.95 †	1.26 */2.52 †	1.05
dt/τ_η	0.044	0.06 * - 0.03 †	0.044 * - 0.022 †	0.034

2011; Gotoh and Watanabe, 2015). In Fourier space this reads,

$$\hat{\dot{q}}_\theta(\vec{k},t) = \sum_{1\leqslant|\vec{k}|\leqslant 2\sqrt{2}} \frac{Q}{|\vec{k}|} e^{i\phi_\theta(\vec{k},t)}, \tag{4.10}$$

where Q is the constant prescribing the overall source amplitude, $|k|^{-1}$ is a normalization factor to guarantee that the forcing amplitude is larger at small wave numbers. In particular, the random phase function $\phi_\theta(\mathbf{k},t)$ is generated independently for each scalar field and delta-correlated both in time and in wave-vector (Gotoh et al., 2011; Gotoh and Watanabe, 2015). As a result, $\dot{q}_{R_1}$, $\dot{q}_{R_2}$, $\dot{q}_P$ and $\dot{q}_T$ have amplitudes of the same order, but they are statistically independent from each other both in time and in space.

The set of dynamical equations (4.6) and (4.8) are solved numerically by means of a pseudo-spectral code (Gauding et al., 2017, 2018), using a smooth dealiasing technique (Hou and Li, 2007) for the treatment of non-linear terms in the equations (Section 3.1.1).

We explore the parameter space of the problem by means of a series of simulations: the Reynolds number Re_λ varies in the range $Re_\lambda \in [20, 150]$, the Schmidt number spans the interval $[0.1, 4]$ and the Damköhler number changes from $\mathcal{O}(10^{-4})$ to $\mathcal{O}(10)$, while the reaction order n is increased from one up to $n = 3$ (i.e. from second to fourth order reaction). The values of the key parameters for the simulations are reported in table 4.1.

*corresponding to Sc of 0.1-1.

†corresponding to Sc of 2-4, better resolution condition is required to resolve the Batchelor micro scale ($\frac{\eta}{Sc^{1/2}}$) (Batchelor, 1959).

4.3 Temporal evolution the mean and fluctuation component of scalar fields

We begin by looking at the temporal evolution of the two first statistical moments of reactive fields, i.e., their mean values and root-mean-square fluctuations.

Figure 4.1 shows the typical temporal evolution of the fluctuating and the mean (volumetric average) parts of scalars for a simulation with $n = 2$, $Da = 0.1$, $Sc = 1$ and $Re_\lambda = 150$. After a sufficiently long simulation time, a statistically steady state is established where the global mean value for the reactive scalar fields is close to the respective equilibrium quantities, *i.e.*, $\langle R_1 \rangle \approx \langle R_2 \rangle \approx \langle P \rangle \approx 1$. Furthermore, in spite of the presence of a vigorous external mechanical forcing and random scalar source terms, the reactive scalar dynamics is characterised by relatively small global fluctuations from the equilibrium state. We observe that the scalar fluctuations are proportional to the amplitude of the mechanical forcing, which poses a limitation for the numerical implementation of the model system, i.e. the positiveness of the scalar concentration fields ($\theta \geq 0$). In order to fulfill this constraint, in the simulations for this chapter the r.m.s. of scalars reaches at maximum 10% of the mean value. The statistical convergence is reached by means of simulations extending in time $\sim 45T_I$, where $T_I = k/\varepsilon$ with $k = 3u'^2/2$ is the integral time scale. The temporal averages are performed after at least $8T_I$ from the beginning of the simulation (see figure 4.1).

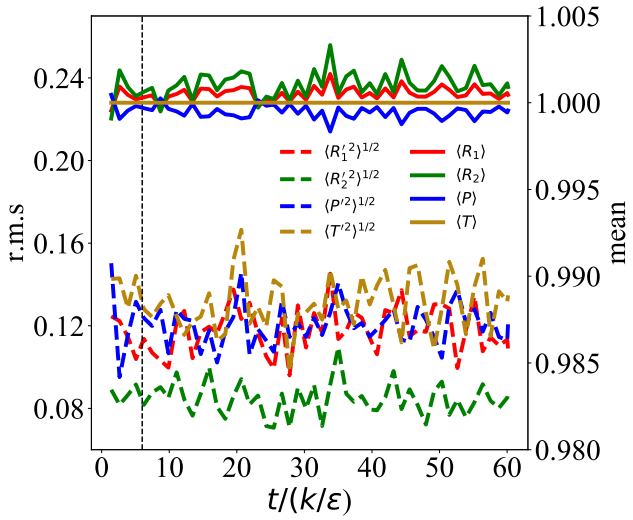

Figure 4.1: Evolution of the root mean square of scalar fluctuations and mean values for the case of $n = 2$, $Da = 0.1$, $Sc = 1$ and $Re_\lambda = 150$. Time is normalized by the integral time k/ε with $k = 3u'^2/2$. The mean quantities were represented with three-dimensional volumetric average here. The dash vertical line marks the initial time for the computation of statistical quantities.

4.4 Spectra and coherency spectra of scalars

In this section we focus on the scale-dependent behavior of reactive scalar fluctuations and their mutual correlations.

4.4.1 Energy spectra

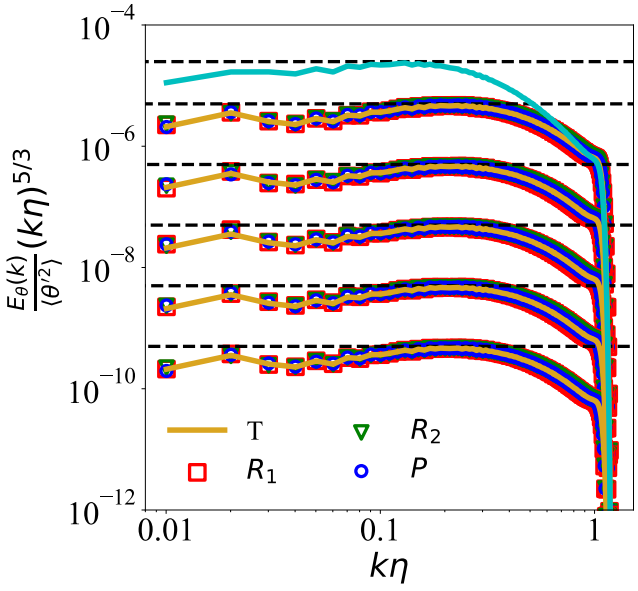

Figure 4.2: Energy spectra of reactive and passive scalar fields, i.e. $E_\theta(k)$ with $\theta = R_1, R_2, P, T$, and velocity field $E_u(k)$ (solid light-blue line) in the condition $Re_\lambda = 150$, $Sc = 1$, $n = 1$ and $Da = 10, 1, 0.1, 0.01, 0.001$ (from high to bottom). Each spectra is compensated with the KOC scaling, $(k\eta)^{5/3}$ and normalized by the global energy $\langle\theta'^2\rangle$. For clarity, the energy spectra of scalars are shifted vertically by a multiplicative factor 0.1

The energy spectra of the velocity and scalars are defined as

$$E(k) = 4\pi k^2 \langle \frac{1}{2} \hat{u}_i(\mathbf{k}) \hat{u}_i^*(\mathbf{k}) \rangle_k, \tag{4.11a}$$

$$E_\theta(k) = 4\pi k^2 \langle \hat{\theta}(\mathbf{k}) \hat{\theta}^*(\mathbf{k}) \rangle_k, \quad \theta = R_1, R_2, P \text{ and } T, \tag{4.11b}$$

where $\langle\cdot\rangle_k$ denotes the average in time and over all the modes in the shell of thickness Δk centred at $k = |\mathbf{k}|$, $\hat{u}_i(\mathbf{k})$ and $\hat{\theta}(\mathbf{k})$ are the Fourier coefficients of the mode of $\mathbf{k}$, $\hat{u}_i^*(\mathbf{k})$ and $\hat{\theta}^*(\mathbf{k})$ are the corresponding complex conjugates.

Figure 4.2 depicts the log-log plots of the three-dimensional energy spectra of scalars of a typical case at $Re_\lambda = 150$, $Sc = 1$, $n = 1$, compensated with $k^{-5/3}$, which is the scaling expected in the inertial regime both

for the velocity and for a passive scalar field, i.e., the KOC scaling Kolmogorov (1941b,a). The spectra are also normalized by the total energy for each scalar. The figure shows that the spectra are indistinguishable from the ones of a passive scalar, and display the same scaling in the inertial range. This proves that in the present condition the reaction terms have a negligible effect on the scalar energy transfer. Remarkably, this behaviour is also Damköhler number independent. The latter observation is qualitatively confirmed also by visualisations of the instantaneous scalar fields for different Da values. Despite perceptible larger fluctuations for the small Da case (the one where the chemistry is slower) it appears that the spatial structure of the fields is not affected by the magnitude of Da.

4.4.2 Coherency spectra

The coherency spectrum between two scalar fields θ_1 and θ_2 is defined as

$$Co_{\theta_1,\theta_2}(k) = \frac{\langle |\widehat{\theta_1}(\mathbf{k})\widehat{\theta_2}^*(\mathbf{k})| \rangle_k}{\sqrt{\langle \widehat{\theta_1}(\mathbf{k})\widehat{\theta_1}^*(\mathbf{k}) \rangle_k \langle \widehat{\theta_2}(\mathbf{k})\widehat{\theta_2}^*(\mathbf{k}) \rangle_k}}. \tag{4.12}$$

This function describes the scale dependence, in spectral space, of the correlation coefficient between two scalar fields.

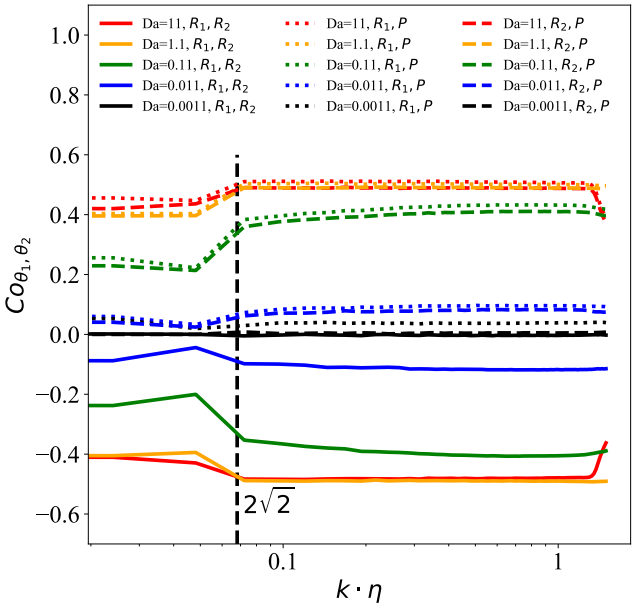

Figure 4.3: Coherency spectra of the reactive scalars, under the condition of $Re_\lambda = 80$, $Sc = 1$, $n = 1$. The horizontal axis is normalized in terms of the Kolmogorov scale η. The dash vertical line marks the maximum wave number at which the scalar source terms acts.

Figure 4.3 shows the results for the generic case at fixed $Re_\lambda = 80$, $Sc = 1$, $n = 1$ and varying Da. It is interesting to note that for all the cases the coherency spectra are nearly k independent; in particular, they are constant in the inertial range. A non constant behavior is observed at small wave-numbers $|\mathbf{k}| \geq 2\sqrt{2}$, which correspond to the largest physical scales. This is due to the action of the random scalar source that strongly reduces the intensity of correlations. Moreover, the absolute value of Co_{θ_1,θ_2} increases as Da increases, which agrees with the picture that fast chemical reactions build up correlations.

4.5 Global correlation coefficients of reactive scalars

In this section the global correlation coefficients for the scalar fields is investigated. We begin with a theoretical argument for the prediction of its functional dependence on varying the dimensionless *a priori* control parameters Re_λ, Sc, Da and n. We will later compare the prediction with the numerical results.

The global correlation coefficients between reactive scalars are defined as

$$r(\theta_1, \theta_2) = \frac{\langle \theta_1' \theta_2' \rangle}{\langle \theta_1'^2 \rangle^{1/2} \langle \theta_2'^2 \rangle^{1/2}}. \tag{4.13}$$

Here θ_1 and θ_2 are the scalars under consideration.

The global value of the cross product of scalar gradients $\langle \nabla\theta_1 \nabla\theta_2 \rangle$ can be estimated in terms of the global value of cross product of scalars $\langle \theta_1 \theta_2 \rangle$ normalized by the square of a characteristic length-scale λ_θ. For a scalar quantity θ, define λ_θ as in (Ristorcelli, 2006):

$$\lambda_\theta^2 = \frac{\langle \theta'^2 \rangle}{\langle (\partial_x \theta)^2 \rangle}. \tag{4.14}$$

Such a length scalar can be interpreted as the Taylor microscale of θ. Consequently, this allows to introduce an *a posteriori* control parameter, the Damköhler number based on scalar Taylor micro-scale and diffusivity, denoted here Da_θ, which is defined as

$$Da_\theta = Re_\lambda Sc Da \lambda_\theta^2 = \frac{\lambda_\theta^2}{D} \gamma_1 R_{2,eq}^n. \tag{4.15}$$

It has to be noted that such a number includes a combination of the three a priori control parameters (Re_λ,Sc,Da) for the model system, with the addition of the λ_θ scale, which therefore plays a key role in the analysis.

The theoretical prediction is based on the following two hypotheses. First, given the fact that the reactive

scalar fluctuations are small with respect to the equilibrium global value, the chemical sources can then be linearized in the following way.

$$R_1 R_2^n - P \approx (\langle R_1\rangle + R_1')(\langle R_2\rangle + n\langle R_2\rangle^{n-1} R_2') - (\langle P\rangle + P') \approx R_1' + nR_2' - P', \tag{4.16}$$

where we have used also the fact that $\langle R_1\rangle \approx \langle R_2\rangle \approx \langle P\rangle \approx 1$ (see again figure 4.1)). Second, we assume that there are no correlations between the source term for a given scalar and other reactive scalars, which is here reasonably guaranteed from the fact that the source terms are delta-correlated in time with a fixed amplitude. Such an assumption, however, is not a general feature of reactive turbulence, and needs to be considered specifically.

In the following sections, theoretical prediction is presentation step be step in section 4.5.1, 4.5.2, and 4.5.3. And the comparison with number results is in section 4.5.4.

4.5.1 Relation between correlation coefficients and coherency spectra

First, we prove that in current configuration, the global correlation coefficient between two scalars is the same as their correlation coefficient at each length scale.

In a two reactive scalar system where fluctuations are introduced by external perturbations, e.g., randomly introduced in the phase space, in the simulations for this chapter. It is reasonable to assume that:

1. the energy distribution of R_1 is the same as that of R_2 on different length scales;

2. the correlation coefficient between R_1 and R_2 conditional on different length scales is invariant.

Consider the one-dimensional case and analysis in three-dimensional space can be implemented similarly. The fluctuating parts of R_1 and R_2 are expressed in the form of Fourier modes as

$$R_1' = \sum_k A_k(t)\sin(kx) + a_k(t)\cos(kx), \quad R_2' = \sum_k B_k(t)\sin(kx) + b_k(t)\cos(kx). \tag{4.17}$$

The global correlation coefficient is

$$\begin{aligned} r(R_1, R_2) =& \frac{\langle[\sum_k A_k(t)\sin(kx) + a_k(t)\cos(kx)][\sum_k B_k(t)\sin(kx) + b_k(t)\cos(kx)]\rangle}{\langle[\sum_k A_k(t)\sin(kx) + a_k(t)\cos(kx)]^2\rangle^{1/2}\langle[\sum_k B_k(t)\sin(kx) + b_k(t)\cos(kx)]^2\rangle^{1/2}} \\ =& \frac{\sum_k \overline{A_k B_k} + \overline{a_k b_k}}{[\sum_k(\overline{A_k^2} + \overline{a_k^2})]^{1/2}[\sum_k(\overline{B_k^2} + \overline{b_k^2})]^{1/2}}, \end{aligned} \tag{4.18}$$

where $\bar{\cdot}$ denotes time average.

Since the energy distributions of R_1 and R_2 on different length scales are the same (assumption 1), we define α as

$$\frac{\overline{A_1^2}+\overline{a_1^2}}{\overline{B_1^2}+\overline{b_1^2}} = \frac{\overline{A_2^2}+\overline{a_2^2}}{\overline{B_2^2}+\overline{b_2^2}} = \cdots = \frac{\sum_k(\overline{A_k^2}+\overline{a_k^2})}{\sum_k(\overline{B_k^2}+\overline{b_k^2})} = \alpha^2.$$

Then the denominator of Eq. (4.18) can be further written as

$$[\sum_k(\overline{A_k^2}+\overline{a_k^2})]^{1/2}[\sum_k(\overline{B_k^2}+\overline{b_k^2})]^{1/2} = (\sum_k \overline{B_k^2}+\overline{b_k^2})\cdot\alpha = \sum_k \alpha(\overline{B_k^2}+\overline{b_k^2}) = \sum_k(\overline{A_k^2}+\overline{a_k^2})^{1/2}(\overline{B_k^2}+\overline{b_k^2})^{1/2}.$$

Thus it yields

$$r(R_1,R_2) = \frac{\sum_k \overline{A_kB_k}+\overline{a_kb_k}}{\sum_k(\overline{A_k^2}+\overline{a_k^2})^{1/2}(\overline{B_k^2}+\overline{b_k^2})^{1/2}}. \tag{4.19}$$

The coherency spectrum between R_1' and R_2', Co_{R_1,R_2}, describes the correlation coefficients between two scalars corresponding to each length scale. At the mode k,

$$\begin{aligned} Co_{R_1,R_2}(k) =& \frac{\langle[A_k(t)\sin(kx)+a_k(t)\cos(kx)][B_k(t)\sin(kx)+b_k(t)\cos(kx)]\rangle}{\langle[A_k(t)\sin(kx)+a_k(t)\cos(kx)]^2\rangle^{1/2}\langle[B_k(t)\sin(kx)+b_k(t)\cos(kx)]^2\rangle^{1/2}} \\ =& \frac{\overline{A_kB_k}+\overline{a_kb_k}}{(\overline{A_k^2}+\overline{a_k^2})^{1/2}(\overline{B_k^2}+\overline{b_k^2})^{1/2}}. \end{aligned} \tag{4.20}$$

From the second assumption that the correlation coefficients of R_1 and R_2 are the same at each length scales, for any k, we obtain

$$\begin{aligned} Co_{R_1,R_2}(k) =& \frac{\overline{A_1B_1}+\overline{a_1b_1}}{(\overline{A_1^2}+\overline{a_1^2})^{1/2}(\overline{B_1^2}+\overline{b_1^2})^{1/2}} = \frac{\overline{A_2B_2}+\overline{a_2b_2}}{(\overline{A_2^2}+\overline{a_2^2})^{1/2}(\overline{B_2^2}+\overline{b_2^2})^{1/2}} \\ =& \dots \\ =& \frac{\sum_k \overline{A_kB_k}+\overline{a_kb_k}}{\sum_k(\overline{A_k^2}+\overline{a_k^2})^{1/2}(\overline{B_k^2}+\overline{b_k^2})^{1/2}} = r(R_1,R_2). \end{aligned} \tag{4.21}$$

Therefore, the global correlation coefficient between R_1 and R_2 is the same as the correlation coefficient at each wave number or length scale.

4.5.2 Correlation coefficients of reactive scalar gradients

As shown in figure 4.2 and figure 4.3, the energy distribution and the correlation coefficients of the reactive scalars remain almost independent of the length scale. Under these two conditions, it is ready to derive that the global correlation coefficient between two reactive scalars is the same as their coherency spectrum at each length scale (section 4.5.1).

Another quantity of primary importance is the global correlation coefficients of the gradients of scalars, which can be defined along one direction (e.g. x) only because of isotropy:

$$r(\theta_{1,x},\theta_{2,x}) = \frac{\langle \frac{\partial\theta_1}{\partial x}\frac{\partial\theta_2}{\partial x}\rangle}{\langle(\frac{\partial\theta_1}{\partial x})^2\rangle^{1/2}\langle(\frac{\partial\theta_2}{\partial x})^2\rangle^{1/2}}. \tag{4.22}$$

For various scalars, the (almost) identical spectra of the scalar energy (figure 4.2) implies the (almost) identical spectra of the energy of scalar gradient quantities. In addition, since Eq. (4.12) is the definition of the coherency spectrum between not only θ_1 and θ_2 but also their gradients, the coherency spectra between the gradients of two reactive scalars are also almost k independent. Therefore, the correlation coefficient of the gradients of two reactive scalars is also identical at each length scale, and supposed to be the same as the correlation coefficient of these two reactive scalars. Figure 4.4 presents the global correlation coefficients of the reactive scalars and their gradients against Da with $Re_\lambda = 150$, $Sc = 1$, $n = 1$. The speculation that the correlation coefficients between the reactive scalars are the same as that of their gradients is well testified, except for the cases of $Da = 0.01$ and 0.1, in which the condition that the coherency spectra is k independent is not satisfied at the largest scales (figure 4.3).

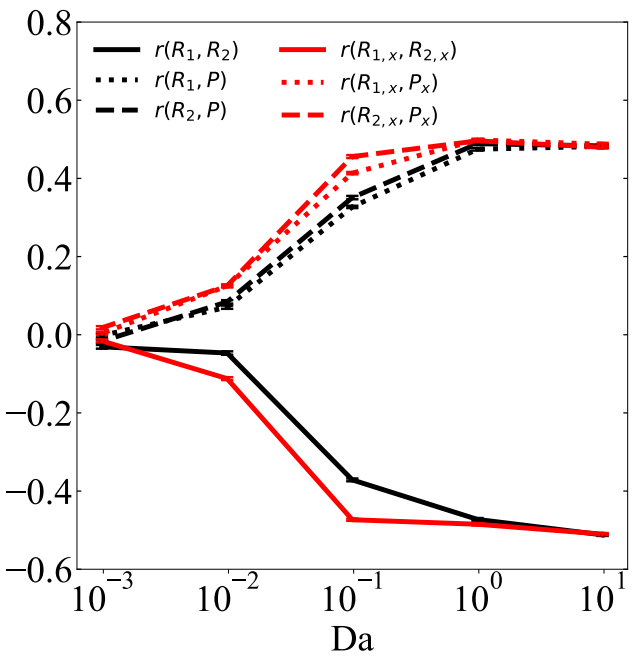

Figure 4.4: The global correlation coefficients of the reactive scalars and their gradients along x direction, under the condition of $Re_\lambda = 150$, $Sc = 1$, $n = 1$.

4.5.3 Analytical prediction for reactant correlations

Under the conditions of $R_1' \ll \langle R_1 \rangle$, $R_2' \ll \langle R_2 \rangle$, $P' \ll \langle P \rangle$ and $\langle R_1 \rangle \approx \langle R_2 \rangle \approx \langle P \rangle \approx 1$ (figure 4.1), the net reaction rate can be estimated as

$$R_1 R_2^n - P \approx (\langle R_1 \rangle + R_1')(\langle R_2 \rangle + n\langle R_2 \rangle^{n-1} R_2') - (\langle P \rangle + P') \approx R_1' + nR_2' - P'. \tag{4.23}$$

Correspondingly, the equations for fluctuating scalars become

$$\frac{DR_1'}{Dt} \approx \frac{1}{Re_\lambda Sc} \triangle R_1' - Da(R_1' + nR_2' + M') + \dot{q}_{R_1}, \tag{4.24a}$$

$$\frac{DR_2'}{Dt} \approx \frac{1}{Re_\lambda Sc} \triangle R_2' - nDa(R_1' + nR_2' + M') + \dot{q}_{R_2}, \tag{4.24b}$$

$$\frac{DM'}{Dt} \approx \frac{1}{Re_\lambda Sc} \triangle M' - Da(R_1' + nR_2' + M') + \dot{q}_M, \tag{4.24c}$$

where $M' = -P'$ and $\dot{q}_M = -\dot{q}_P$. The same form of Eq. (4.24c) as Eq. (4.24c) implies that R_1' and M' behave statistically the same.

By multiplying Eq. (4.24a), (4.24b) and (4.24c) with R_2', M' and R_1' respectively and averaging ($\langle \cdot \rangle$) on time and space, it yields:

$$\langle \frac{DR_1'}{Dt} R_2' \rangle + \frac{1}{Re_\lambda Sc} \langle \nabla R_2' \nabla R_1' \rangle \approx -Da(\langle R_2' R_1' \rangle + n\langle R_2'^2 \rangle + \langle R_2' M' \rangle) + \langle R_2' \dot{q}_{R_1} \rangle, \tag{4.25a}$$

$$\langle \frac{DR_2'}{Dt} M' \rangle + \frac{1}{Re_\lambda Sc} \langle \nabla M' \nabla R_2' \rangle \approx -nDa(\langle M' R_1' \rangle + n\langle M' R_2' \rangle + \langle M'^2 \rangle) + \langle M' \dot{q}_{R_2} \rangle, \tag{4.25b}$$

$$\langle \frac{DM'}{Dt} R_1' \rangle + \frac{1}{Re_\lambda Sc} \langle \nabla R_1' \nabla M' \rangle \approx -Da(\langle R_1'^2 \rangle + n\langle R_1' R_2' \rangle + \langle R_1' M' \rangle) + \langle R_1' \dot{q}_M \rangle. \tag{4.25c}$$

In Eq. (4.25a), the term $\langle R_2' \dot{q}_{R_1} \rangle$ is estimated as 0, because the time-delta forcing to one scalar (R_1) can not be strongly correlated with another scalar (R_2). Moreover, the small net reaction rate implies that the instantaneous reactive scalar is weakly influenced by other scalar(s). Thus at the statistical stationary state, $\langle \frac{DR_1'}{Dt} R_2' \rangle$ can be assumed negligibly small, i.e. $\langle \frac{DR_1'}{Dt} R_2' \rangle \sim 0$.

As discussed in section 4.5.2, the correlation coefficients of the reactive scalars is roughly the same as the

correlation coefficients of their gradients, which in isotropic turbulence can be estimated as

$$\begin{aligned}\langle \partial_x R_2' \partial_x R_1' \rangle &\approx \langle \partial_y R_2' \partial_y R_1' \rangle \approx \langle \partial_z R_2' \partial_z R_1' \rangle \\ &\approx \langle (\partial_x R_2')^2 \rangle^{1/2} \langle (\partial_x R_1')^2 \rangle^{1/2} \cdot \frac{\langle R_2' R_1' \rangle}{\langle R_2'^2 \rangle^{1/2} \langle R_1'^2 \rangle^{1/2}} \\ &\approx \frac{\langle R_2'^2 \rangle^{1/2} \langle R_1'^2 \rangle^{1/2}}{\lambda_\theta^2} \cdot \frac{\langle R_2' R_1' \rangle}{\langle R_2'^2 \rangle^{1/2} \langle R_1'^2 \rangle^{1/2}} \approx \frac{\langle R_2' R_1' \rangle}{\lambda_\theta^2},\end{aligned} \tag{4.26}$$

where λ_θ is the Taylor microscale for scalars (Eq. (4.14)).

Consequently,

$$\frac{1}{Re_\lambda Sc} \langle \nabla R_2' \nabla R_1' \rangle = \frac{1}{Re_\lambda Sc} (\langle \partial_x R_2' \partial_x R_1' \rangle + \langle \partial_y R_2' \partial_y R_1' \rangle + \langle \partial_z R_2' \partial_z R_1' \rangle) \approx \frac{3}{Re_\lambda Sc \lambda_\theta^2} \langle R_2' R_1' \rangle. \tag{4.27}$$

From Eq. (4.25a) it yields

$$3\langle R_2' R_1' \rangle \approx -Da_\theta (\langle R_2' R_1' \rangle + n \langle R_2'^2 \rangle + \langle R_2' M' \rangle), \tag{4.28}$$

where $Da_\theta = Re_\lambda Sc \lambda_\theta^2 Da = \frac{\lambda_\theta^2 \gamma_1 R_{2,eq}^n}{D}$ is the Damköhler number based on scalar Taylor micro-scale and diffusivity (Eq. (4.15)).

Similarly, from Eq. (4.25b) and (4.25c),

$$3\langle M' R_2' \rangle \approx -nDa_\theta (\langle M' R_1' \rangle + n \langle M' R_2' \rangle + \langle M'^2 \rangle), \tag{4.29}$$

$$3\langle R_1' M' \rangle \approx -Da_\theta (\langle R_1'^2 \rangle + n \langle R_1' R_2' \rangle + \langle R_1' M' \rangle). \tag{4.30}$$

Because R_1' and M' are statistically the same (see Eq. (4.24a) and (4.24c)), we can define

$$C = \langle R_1' M' \rangle, \quad c = \langle R_2' R_1' \rangle = \langle R_2' M' \rangle, \quad V = \langle R_1'^2 \rangle = \langle M'^2 \rangle, \quad v = \langle R_2'^2 \rangle, \tag{4.31}$$

i.e.

$$\frac{C}{V} = r(R_1, M) = -r(R_1, P), \qquad \frac{c}{\sqrt{Vv}} = r(R_1, R_2) = r(R_2, M) = -r(R_2, P).$$

Then Eq. (4.28), (4.29) and (4.30) can be rewritten as

$$3c \approx -Da_\theta (2c + nv), \tag{4.32a}$$

$$3c \approx -nDa_\theta (C + nc + V), \tag{4.32b}$$

$$3C \approx -Da_\theta(C + nc + V), \tag{4.32c}$$

which then leads to the solutions as

$$r(R_1, P) \approx \frac{Da_\theta}{3 + n^2 Da_\theta + Da_\theta}, \tag{4.33a}$$

$$r(R_1, R_2) = -r(R_2, P) \approx \frac{-nDa_\theta}{\sqrt{3 + n^2 Da_\theta + Da_\theta}\sqrt{3 + 2Da_\theta}}. \tag{4.33b}$$

4.5.4 Comparison with numerical results

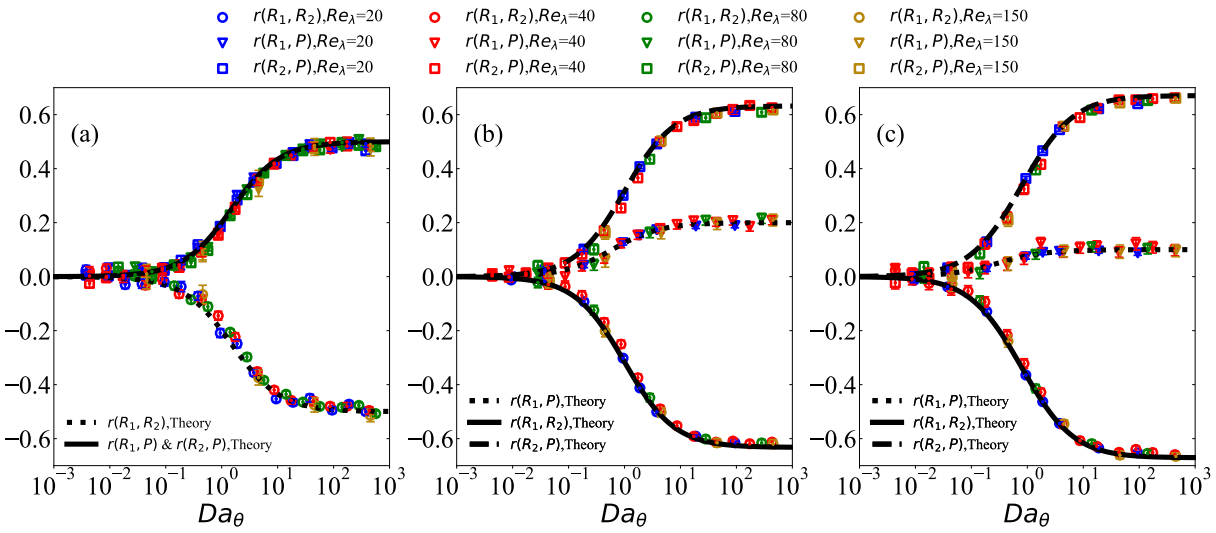

Figure 4.5: Correlation coefficients between R_1 and R_2 ($r(R_1, R_2)$), R_1 and P ($r(R_1, P)$), R_2 and P ($r(R_2, P)$) as functions of Da_θ, under the condition of (a): $n = 1$ (b): $n = 2$ and (c): $n = 3$ and the Schmidt number $Sc = 1$. Theoretical predictions are shown in black lines.

We provide here the central result of the derivation based on the above steps. The above expressions of Eq. (4.33a) and (4.33b) show that the concentration field for R_1 is positively correlated to P, while is negatively correlated to R_2. Furthermore, the correlations $r(R_1, R_2)$ and $r(R_2, P)$ are opposite in sign. They also show that for large Da_θ the correlations reach a saturation plateau, whose value depends on the reaction order n. For $n = 1$ the correlations coefficients have all the same intensity and only differs in sign. The asymptotically large Da_θ limit in this case leads to the values $r = \pm 1/2$. At asymptotically large n and Da_θ, it yields $r(R_1, P) \simeq 0$ and $r(R_1, R_2) = -r(R_2, P) \simeq 1$. On the opposite, in the condition of vanishing values of Da_θ, corresponding to a negligible role of chemical processes and predominance of mixing, all the correlations coefficients tend to zero.

In figure 4.5 we report the numerical measurements of the correlation coefficients between the reactive scalars

as functions of Da_θ, for a set of simulations characterized by different reaction order n and different Re_λ, ranging over more than a decade. It can be seen that for low Da_θ values, corresponding to slow reaction rates, R_1, R_2 and P behave as almost independent passive scalars, as expected. Thus the correlation coefficients are about zero when Da_θ is small. As Da_θ increases, the scalars become more and more correlated and the correlation coefficients gradually approach plateaus, which are n dependent. All these tendencies are in excellent agreement with the theoretical predictions, which are also reported on the same figure.

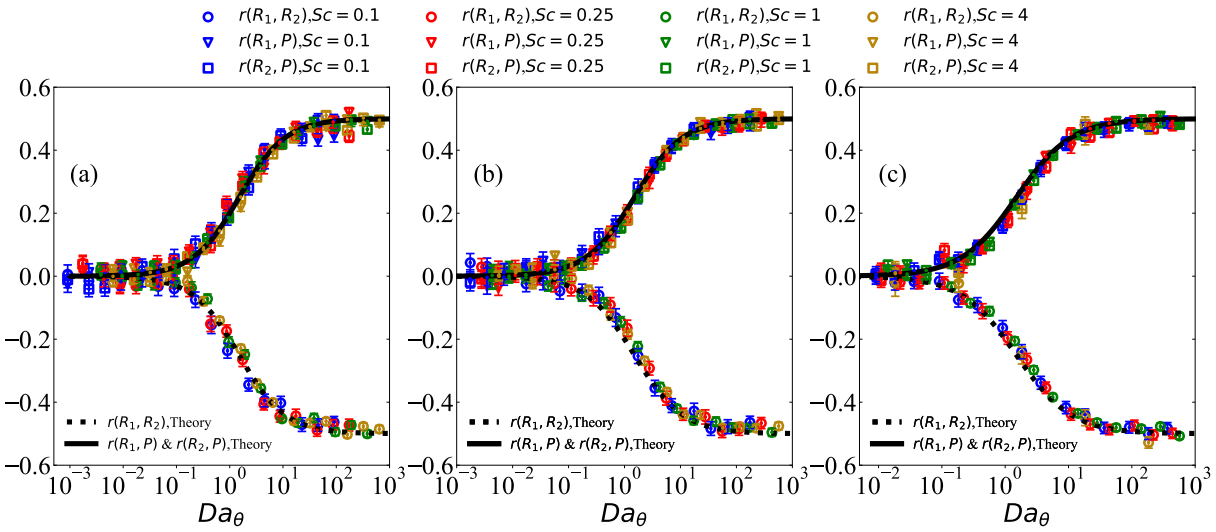

Figure 4.6: Correlation coefficients between R_1 and R_2 ($r(R_1, R_2)$), R_1 and P ($r(R_1, P)$), R_2 and P ($r(R_2, P)$) as functions of Da_θ, under the condition of (a): $Re_\lambda = 20$ (b): $Re_\lambda = 40$ and (c) $Re_\lambda = 80$. The order of R_2 (n) is 1. Theoretical predictions are shown in black lines.

Figure 4.6 further confirms the range of validity of the prediction, by displaying the same correlations now for the case of different Schmidt numbers in the range from 0.1 to 4 and for $n = 1$. Again the trends are well captured by the theoretical predictions.

4.6 Reactant variances

4.6.1 Chemical equilibrium and the effect of reaction on it

The probability density functions (PDF) of the scalar fields are reported in figure 4.7. It can be seen that despite the different amplitudes of the standard deviations, their normalised shapes do not deviate significantly from Gaussian. No noticeable difference is observed in the comparison of reactive scalars with the passive one. Furthermore, side-by-side visualisations of instantaneous snapshots of reactive and passive scalars do not allow to perceive clear difference in their spatial structure (figure 4.8).

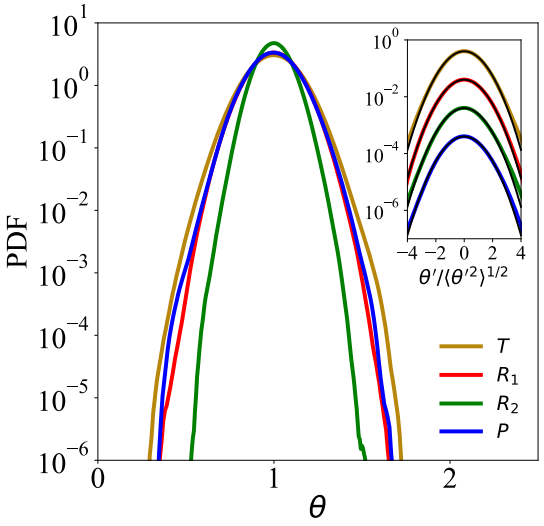

Figure 4.7: PDF of the scalar quantities (main panel) and normalized with respect to their standard deviations (inset, the black lines are Gaussian curves) under the condition of $Re_\lambda = 150$, $Sc = 1$, $n = 2$ and $Da = 0.1$.

In our system the global chemical equilibrium condition $\langle R_1 R_2^n \rangle = \langle P \rangle$ is toughly satisfied by construction due to the irreversible reactive scalar source term. We also note that in the above described statistically steady condition the advecting flow is the main responsible for local departures in time and space from the chemical equilibrium condition. The magnitude of such deviations depends on the turbulent intensity and it grows with Re_λ. We observe that the root-mean-square intensity of the local reaction rate $Da(R_1 R_2^n - P)$ scales approximately as $\sim Re_\lambda^{3/2}$ in the range of Reynolds number explored in this chapter (figure 4.9). Moreover, as shown in the bottom panels of figure 4.9, it is interesting to see that the reaction rate normalized by its standard deviation is of a PDF independent of Re_λ.

4.6.2 Analytical prediction for reactant variances and comparison with DNS

As we have already mentioned the turbulent advection and the scalar forcing are the sources of scalar spatial-temporal fluctuations. In the case of passive scalars such fluctuations are smoothed out by diffusion. For the reactive case, the chemical sources function as an additional dumping mechanism. In other words, it is expected that the chemical reaction term acts as a global sink to suppress the scalar energy in addition to dissipation via molecular diffusion.

In the present model system this scenario can be understood by means of the following argument. We multiply the linearized transport equations for the reactive scalars (Eq. (4.24)) with the corresponding fluctuation field R_1', R_2' and P' and perform volume and time average $\langle \cdot \rangle$. At statistical stationary state, summing the

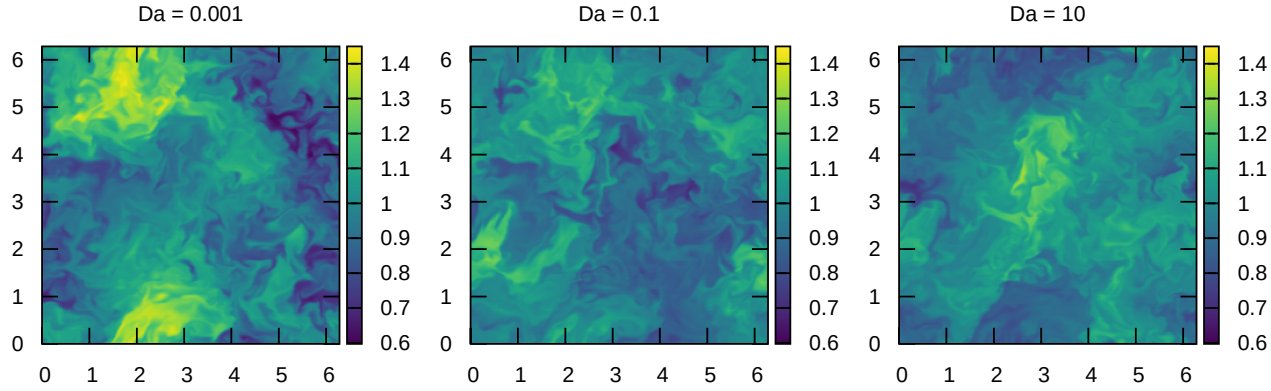

Figure 4.8: Visualisation of two-dimensional instantaneous sections of the R_1 field at $Re_\lambda = 150$, $Sc = 1$ and for three different Da values.

obtained equations of scalar dissipation rates (ε_{R_1}, ε_{R_2} and ε_P) for the considered reactive fields reads:

$$\begin{aligned}\varepsilon_{R_1} + \varepsilon_{R_2} + \varepsilon_P &= \frac{\langle(\nabla R_1')^2\rangle}{Re_\lambda Sc} + \frac{\langle(\nabla R_2')^2\rangle}{Re_\lambda Sc} + \frac{\langle(\nabla P')^2\rangle}{Re_\lambda Sc} \\ &\approx -Da\langle R_1' + nR_2' - P'\rangle^2 + \langle R_1'\dot{q}_{R_1}\rangle + \langle R_2'\dot{q}_{R_2}\rangle + \langle P'\dot{q}_P\rangle. \end{aligned} \tag{4.34}$$

The above equation shows that the reaction is always responsible of removing the scalar energy. A consequence of this is that one expects smaller scalar fluctuations for the reactive fields as compared to a passive scalar. In particular, we expect that the scalar variance will be a monotonically decreasing function in Da_θ.

To have a quantitative understanding for such scenario we compare the fluctuations of the reactive scalars with the ones of a passive scalar in the same dynamical conditions, i.e., subject to the same advective flow, and having the same diffusion and under the effect of an independent statistical realization of the source term $\dot{q}_\theta$.

In order to develop also in this case a quantitative prediction for the phenomenon we need to introduce the key assumption that the scalar energy input due to the source term on the field R_1 is approximately same as the one provided on a passive scalar field T in the same conditions, i.e.

$$\langle R_1'\dot{q}_{R_1}\rangle \simeq \langle T\dot{q}_T\rangle. \tag{4.35}$$

The soundness of this hypothesis lies on the fact that in the present conditions the reactant R_1 has fluctuation of similar intensity as the passive scalar case.

Now we derive the theoretical expressions of the variance of reactant scalars normalized by that of the passive scalar (T).

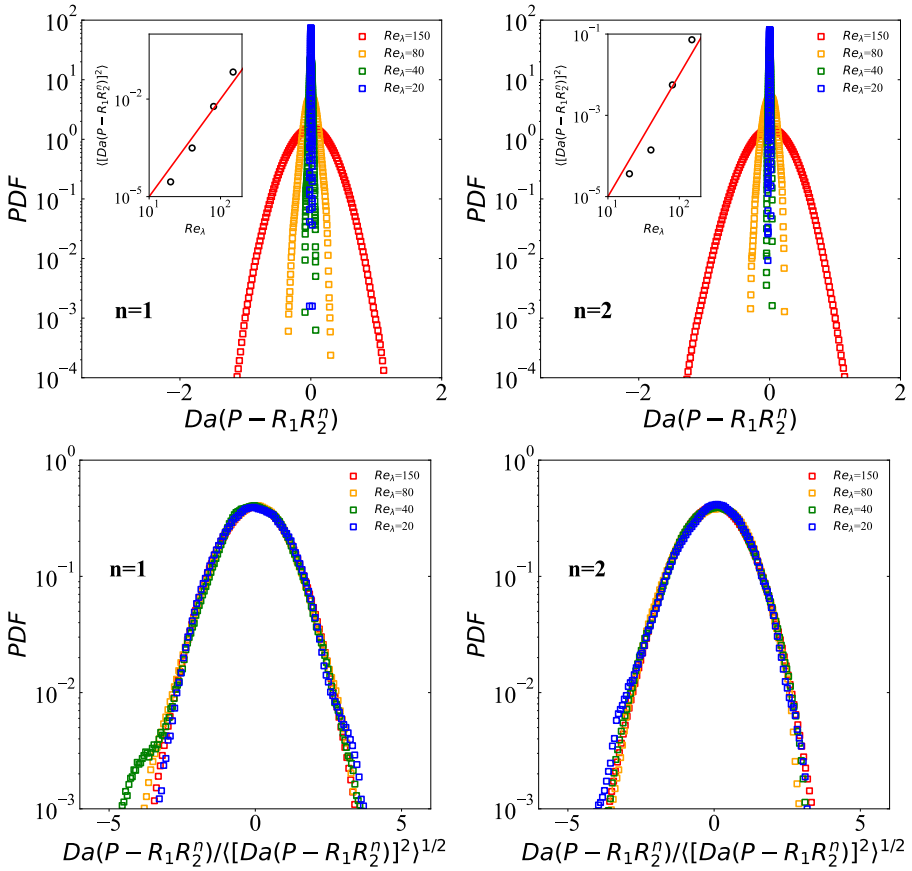

Figure 4.9: PDF of reaction rate $Da(R_1R_2^n - P)$ at $Da = 0.1$ and $Sc = 1$ for $n = 1$ (left) and $n = 2$ (right) for different Reynolds numbers $Re_\lambda = 20, \ldots, 150$. The top panels shows the raw PDF while the bottom ones show the PDF of the normalised variable with respect to its standard deviation. The two insets display the trend of the variance of the reaction rate as a function of the Reynolds number in log-log scale, the red line has a slope 3.

By multiplying Eq. (4.24a), (4.24b) and (4.24c) with R_1', R_2' and M', respectively and averaging ($\langle\cdot\rangle$) in space and time, we obtain

$$\frac{1}{2}\frac{D\langle R_1'^2\rangle}{Dt} + \frac{1}{Re_\lambda Sc}\langle|\nabla R_1'|^2\rangle \approx -Da(\langle R_1'^2\rangle + n\langle R_1'R_2'\rangle + \langle R_1'M'\rangle) + \langle R_1'\dot{q}_{R_1}\rangle, \tag{4.36a}$$

$$\frac{1}{2}\frac{D\langle R_2'^2\rangle}{Dt} + \frac{1}{Re_\lambda Sc}\langle|\nabla R_2'|^2\rangle \approx -nDa(\langle R_1'R_2'\rangle + n\langle R_2'^2\rangle + \langle R_2'M'\rangle) + \langle R_2'\dot{q}_{R_2}\rangle, \tag{4.36b}$$

$$\frac{1}{2}\frac{D\langle M'^2\rangle}{Dt} + \frac{1}{Re_\lambda Sc}\langle|\nabla M'|^2\rangle \approx -Da(\langle R_1'M'\rangle + n\langle R_2'M'\rangle + \langle M'^2\rangle) + \langle M'\dot{q}_M\rangle. \tag{4.36c}$$

The dissipation terms above, e.g. $\frac{1}{Re_\lambda Sc}\langle|\nabla R_1'|^2\rangle$, can be estimated similarly as Eq. (4.26). Under the isotropic

and statistical stationary conditions, the turbulent energy of R_1', R_2' and P' are approximately determined as

$$3\langle R_1'^2\rangle \approx -Da_\theta(\langle R_1'^2\rangle + n\langle R_1'R_2'\rangle + \langle R_1'M'\rangle) + Re_\lambda Sc\lambda_\theta^2\langle R_1'\dot{q}_{R_1}\rangle, \tag{4.37a}$$

$$3\langle R_2'^2\rangle \approx -nDa_\theta(\langle R_1'R_2'\rangle + n\langle R_2'^2\rangle + \langle R_2'M'\rangle) + Re_\lambda Sc\lambda_\theta^2\langle R_2'\dot{q}_{R_2}\rangle, \tag{4.37b}$$

$$3\langle M'^2\rangle \approx -Da_\theta(\langle R_1'M'\rangle + n\langle R_2'M'\rangle + \langle M'^2\rangle) + Re_\lambda Sc\lambda_\theta^2\langle M'\dot{q}_M\rangle. \tag{4.37c}$$

Similarly, based on Eq. (4.8d), the turbulent energy of T' is

$$3\langle T'^2\rangle \approx Re_\lambda Sc\lambda_\theta^2\langle T'\dot{q}_T\rangle. \tag{4.38}$$

Define

$$\begin{aligned} w = Re_\lambda Sc\lambda_\theta^2\langle R_2'\dot{q}_{R_2}\rangle, \qquad & W = Re_\lambda Sc\lambda_\theta^2\langle R_1'\dot{q}_{R_1}\rangle = Re_\lambda Sc\lambda_\theta^2\langle M'\dot{q}_M\rangle, \\ V_T = \langle T'^2\rangle, \qquad & W_T = Re_\lambda Sc\lambda_\theta^2\langle T'\dot{q}_T\rangle. \end{aligned} \tag{4.39}$$

Together with Eq. (4.31), (4.37a), (4.37b) and (4.38) we obtain

$$3V \approx -Da_\theta(V + nc + C) + W, \tag{4.40a}$$

$$3v \approx -nDa_\theta(2c + v) + w, \tag{4.40b}$$

$$3V_T \approx W_T. \tag{4.40c}$$

It is worthy noting that for all the scalar quantities the delta-correlated external forcing is exerted in the same way with constant amplitude. When $\langle R_1'^2\rangle$ is close to $\langle T'^2\rangle$ ($\frac{V}{V_T}$ close to 1), it is reasonable to assume $W \approx W_T$. Together with Eq. (4.33a), (4.33b), (4.40a) and (4.40c) we obtain

$$\frac{\langle R_1'^2\rangle}{\langle T'^2\rangle} = \frac{\langle P'^2\rangle}{\langle T'^2\rangle} = \frac{V}{V_T} \approx \frac{3 + n^2Da_\theta + Da_\theta}{3 + n^2Da_\theta + 2Da_\theta}. \tag{4.41}$$

From Eq. (4.32), the ratio between the fluctuation magnitudes of R_2 and R_1 is determined as

$$\frac{\langle R_2'^2\rangle}{\langle R_1'^2\rangle} = \frac{v}{V} \approx \frac{3 + 2Da_\theta}{3 + n^2Da_\theta + Da_\theta}, \tag{4.42}$$

which leads to

$$\frac{\langle R_2'^2\rangle}{\langle T'^2\rangle} = \frac{\langle R_1'^2\rangle}{\langle T'^2\rangle}\frac{\langle R_2'^2\rangle}{\langle R_1'^2\rangle} = \frac{V}{V_T}\frac{v}{V} \approx \frac{3+2Da_\theta}{3+n^2Da_\theta+2Da_\theta}. \tag{4.43}$$

It is found that the fluctuations of the reactive scalars (R_1, R_2 and P) are close to that of passive scalar (T) when Da_θ is small, but gradually decrease as Da_θ increases. The figure 4.10 shows the normalized fluctuations

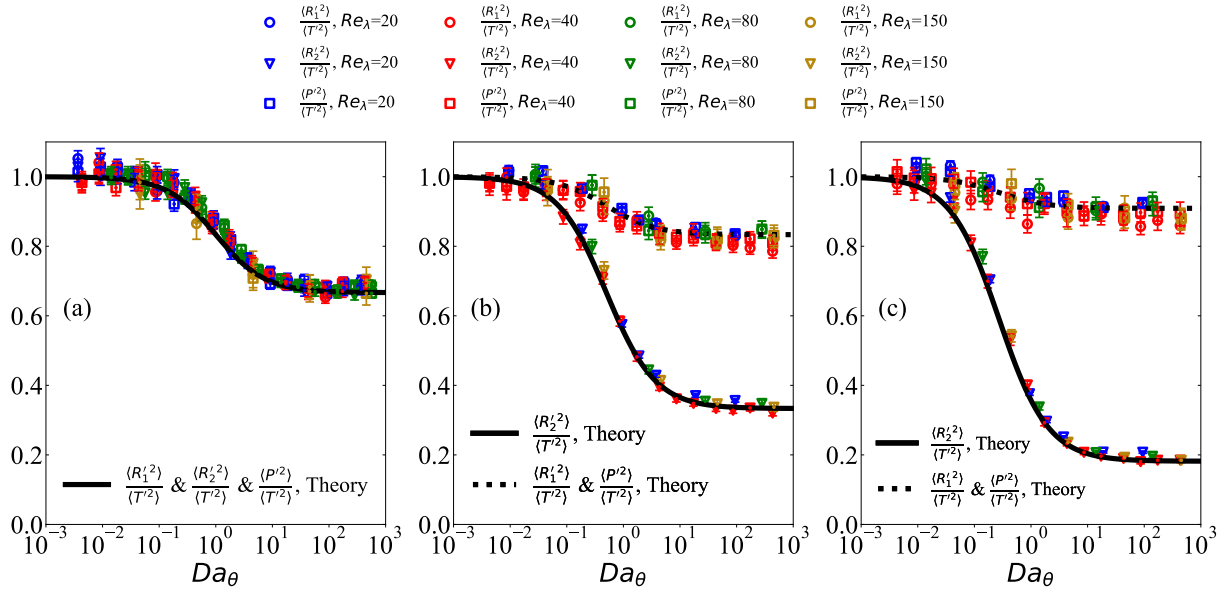

Figure 4.10: The fluctuations of the reactive scalars normalized by the fluctuation of passive scalar (T) as functions of Da_θ, under the condition of (a): $n = 1$ (b): $n = 2$ and (c): $n = 3$ and the Schmidt number $Sc = 1$. Theoretical predictions are shown in black lines.

of the reactive scalars (R_1, R_2 and P) as measured from the DNS, in agreement with the above theoretical prediction.

4.7 Taylor micro scale of scalar concentration fields

As we have discussed in the above sections the correlations and fluctuations of the concentration of reactive scalars are well described by means of the control parameter Da_θ, which contains the scalar Taylor micro scale of λ_θ. In this section we aim at gaining more insight into this key spatial scale.

The scalar Taylor microscale was notably first studied by Stanly Corrsin (Corrsin, 1957), in the context of scalar mixing in turbulent flows. He hypothesized that such a scale is proportional to the intensity of turbulence and inversely to the Schmidt number of the problem, i.e.

$$\frac{\lambda_\theta^2}{\lambda^2} \propto \frac{1}{Sc}.$$

However, further experimental and numerical studies (Bahri et al., 2015; Corrsin, 1964b) have reported that such a dependence is not straightforward, as it shows finite Re_λ effects and different trends for asymptotically small and large Sc values (see (Ristorcelli, 2006) for a recent discussion).

We show the results of our simulations in figure 4.11(a). The figure reports the dimensionless λ_θ^2 (actually $\lambda_\theta^2/\lambda^2$, because the length is non-dimensionalized by λ) as functions of Sc under the conditions of Re_λ from 20 to 150. Figure 4.11(a) indicates that a clear -1 scaling law exists between λ_θ^2 and Sc for the largest Re_λ case, with a prefactor $\simeq 0.3$, implying that in the limit of intense turbulence the Da_θ number can be approximated as

$$Da_\theta \simeq 0.3 Re_\lambda Da = 3T_I/\tau_r. \tag{4.44}$$

Here $\tau_r = (\gamma_1 R_{2,eq})^{-1}$ is the typical time of the reaction. Remarkably, this result reveals that the unique *a posteriori* control parameter that we have identified with Da_θ can be considered as the ratio of the largest time scale of the turbulent flow to the typical time scale associated to the chemical process.

Finally, we remark that λ_θ does not vary significantly over the different scalar fields R_1, R_2, P and the reference passive scalar field T. This is exemplified in Figure 4.11(b) for all the simulations at $Re_\lambda = 150$ and $Sc = 1$. The figure shows that any λ_θ evaluated on a reactive field is at best 15% different from the reference λ_T case. Such difference vanishes for very small (the mixing dominated limit) or very large Da and shows a weak increase trend with the order of the reaction. We can conclude that λ_T can here be taken as a convenient approximation of λ_θ. The estimations of Da_θ in the this chapter are based on such an assumption.

4.7.1 Taylor micro scale of scalars advected by a coarse-grained turbulent flow field

In order to understand better the role of λ_θ, we perform a series of simulations where the scalar fields are advected by a coarse-grained, *i.e.* spatially filtered turbulent flow, denoted as $\tilde{\mathbf{u}}$. The filter functions as a spectral low pass, defined as

$$\hat{\tilde{\mathbf{u}}} = \sum_{|\mathbf{k}| \leqslant K} \hat{\mathbf{u}}(\mathbf{k}), \tag{4.45}$$

where K specifies the maximum wave number kept in the modified field. Such a filter retains only the large eddies of the turbulent flow, down to a wavelength $2\pi/K$. The Taylor scale for scalars convected by the filtered flow is denoted as $\tilde{\lambda}_\theta$. It is noteworthy that the length quantities are always non-dimensionalized by the Taylor scale of unfiltered flow λ, instead of the Taylor scale of the filtered flow. Interestingly, it is worth exploring what is the impact of the hierarchy of flow scales, extending from the domain size down to the dissipative

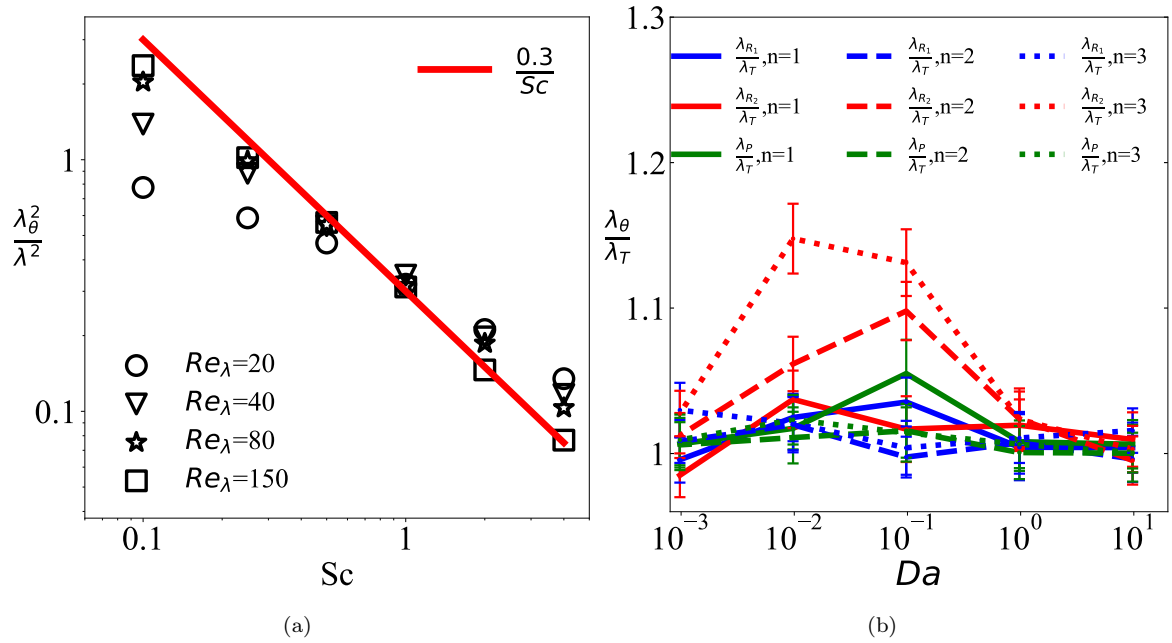

Figure 4.11: a) Taylor micro scales of scalars (computed on T) as functions of Sc. The red line draw is $0.3/St$. A power law fit of the form aSc^b on the $Re_\lambda = 150$ data set gives $a = 0.29 \pm 0.1$ and $b = -0.93 \pm 0.02$. b) Taylor micro scales of the reactive scalars with respect to the passive scalar one with different order of reaction, as functions of Da for all the simulations at $Re_\lambda = 150$ and $Sc = 1$.

scales, on the reactive scalar dynamics. In particular, we aim to understand the dependence of the scalar correlation coefficients and the scalar Taylor microscale on the maximum wavenumber K. According to the above discussion, it is reasonably expected that the small scales of the fluid have a negligible influence, because the scaling mixing process and relevant quantities are controlled by the large eddy turnover time T_I.

Results are presented for a typical case, i.e. $Sc = 1$, $Re_\lambda = 80$ and $Da = 0.05$ corresponding to $Da_\theta = 1.42$. Figure 4.12(a) shows that the correlation coefficients vary quite weakly with the filter parameter K. The deviation becomes noticeable only for $K \leq 3$, which corresponds to scales larger than the large eddy turnover scale of the flow, in the sense that the forcing is active up to $|\mathbf{k}| = 2\sqrt{2}$. Such behavior is also well captured by the theoretical predictions of (4.33a) and (4.33b) if the Damköhler number $Da_{\tilde{\theta}}$ adopted is built on the measured scalar Taylor scale $\tilde{\lambda}_\theta$, instead of the original Da_θ. This confirms again the relevance of the scalar Taylor microscale in characterizing the present reactive scalar system. It is worth noting that, differently from the correlation coefficients, the scale $\tilde{\lambda}_\theta$ varies sensibly with the filter wavenumber K, as reported in figure 4.12(b).

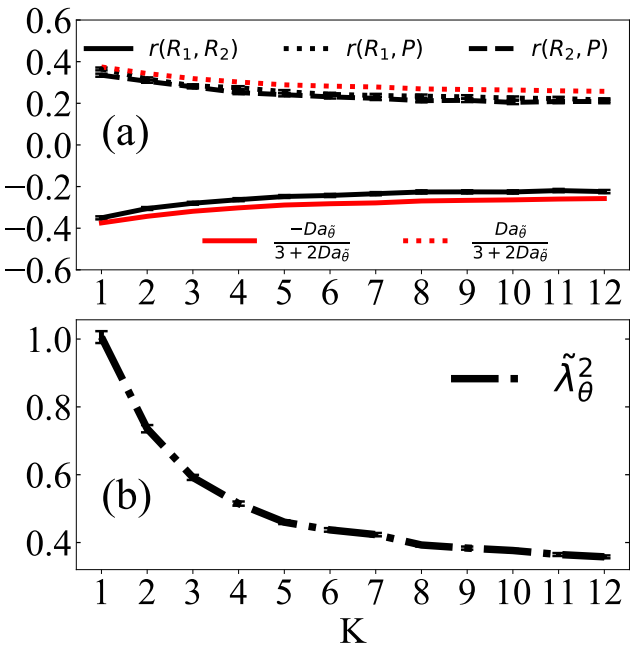

Figure 4.12: (a) Correlation coefficients of scalar evolving in a coarse-grained turbulent flow filed, compared with theoretical predictions and (b) Taylor micro scales of the scalars convected by filtered velocity ($\tilde{\lambda}_\theta$) as functions of the maximum wave number of filtered velocity (K), at $Sc = 1$, $Re_\lambda = 80$ and $Da = 0.05$ ($Da_\theta = 1.42$).

4.8 Summary

In summary, the statistical properties of species undergoing reversible chemical reactions in a turbulent environment have been studied. We have addressed this by means of a model system in which the flow is statistically steady turbulence and the chemical species are retained in a dynamical equilibrium state due to the action of random large-scale source terms. It is observed that the reactive scalar fluctuations have a Gaussian distribution and energy spectra are essentially identical to the one of a passive scalar field transported by the same flow. This can be explained by the overall small amplitude of the reaction terms in the present close-to-equilibrium conditions. However, in such a state a competition still exists between the chemical processes, which tend to dump reactant concentration fluctuations and enhance their correlation intensity, and the turbulent mixing, which on the contrary increases fluctuations and remove relative correlations.

We quantitatively describe this phenomenon by considering the linearised equations for the reactive scalar fluctuations. A unique control parameter, the Damköhler number (Da_θ), can be constructed as the ratio between the time scale of scalar diffusion across a domain of the size of the scalar Taylor micro-scale (λ_θ^2/D) and the chemical reaction time scale τ_r. Importantly, Da_θ characterises the functional dependence of fluctuations and correlations of the scalar quantities in the full range of explored conditions with variable reaction order, the

Reynolds number and the Schmidt number. The larger is such a Damköhler number the more depleted are the scalar fluctuations as compared to the fluctuation of a passive scalar field in the same conditions, and the more intense are the correlations. A saturation in this behaviour is observed beyond $Da_\theta \simeq \mathcal{O}(10)$. These results reveal the significance of the scalar Taylor micro-scale for problems involving the mixing of chemical species. We have shown that in the limit of intense turbulence the relation proposed by Corrsin (1957) $\lambda_\theta \sim \lambda Sc^{-1/2}$ holds approximately, meaning that Da_θ can also be viewed as the ratio of the large-eddy-turnover time of the flow over the typical chemical reaction time.

Chapter 5

Turbulent Kolmogorov flows and chemical reactions

In Chapter 4, the statistical behaviors of the reactive scalars in homogeneous isotropic turbulence were investigated. However, realistic turbulent flows are rarely homogeneous or isotropic, because of the presence of boundaries or spatial dependent forces, such as the channel flow and the wall bounded flow. The Kolmogorov flow (Meshalkin and Sinai, 1961; Green, 1974; She, 1987; Borue and Orszag, 1996; Lucas and Kerswell, 2014) is an example of open turbulent flow, i.e. a flow without boundaries, which is statistically non-homogeneous along one direction and anisotropic. In the late 1950s, A. N. Kolmogorov has proposed to few of his students to study the stability properties of such flow, and an answer was proposed soon after Meshalkin and Sinai (1961), with a Reynolds number threshold of $\sqrt{2}$ confirmed also later by Green (1974). The KF system hence corresponds to the Navier-Stokes equations studied in a periodic domain, with a constant pressure, and forced by a sinusoidal forcing. Above the critical Reynolds number, the flow becomes turbulent and we denote this as turbulent Kolmogorov flow (TKF), a flow which is statistically stationary and anisotropic in one direction.

In this chapter, the TKF and the reactive scalars convected in it are discussed based on direct numerical simulations and theoretical analyses. This chapter is divided into two parts. First the classical turbulence closure based on eddy-viscosity Boussinesq's approach and a nonlinear quadratic closure about the velocity fields in the TKF are numerical examined. Then numerical studies about reactive scalars were carried out for extending the theoretical models about the reactive scalars in chemically quasi-equilibrium state discussed in Chapter 4 to reactions in the TKF.

5.1 Numerical examinations about closure models

The TKF is now considered a classical flow model system to study non-homogenous, anisotropic, sheared turbulence (Borue and Orszag, 1996; Shebalin and Woodruff, 1997; Biferale and Toschi, 2001; Balmforth and Young, 2002; Boffetta et al., 2005; Musacchio and Boffetta, 2014). As discussed by Musacchio and Boffetta (2014), TKF can be considered, to some respect, as a turbulent channel flow without boundaries. Many of the numerical studies devoted to TKF have focused on two-dimensional configurations (She, 1987; Berti and Boffetta, 2010; Lucas and Kerswell, 2014, 2015). In this section we consider a three-dimensional Navier-Stokes incompressible turbulence forced in the x direction by a sinusoidal force depending on the z coordinate.*

5.1.1 The Kolmogorov flow model system

Equations of motion and numerical implementations

To generate the TKF, the forcing in the governing equations for the incompressible Navier-Stokes equations (Eq. (4.2)) is a sinusoidal function in the form:

$$\mathbf{f} = A \sin\left(2\pi \frac{z}{H}\right) \mathbf{e}_x, \tag{5.1}$$

where A is a constant, H is the length of the side of the cubic domain chosen here as the characteristic length scale. Such force, in the x direction and depending on the z variable, makes the flow anisotropic in the z direction. It is convenient to introduce the following reference scales for velocity and time for this section:

$$U_0 = (AH)^{1/2}, \tag{5.2}$$

$$T_0 = \frac{H}{U_0} = \left(\frac{H}{A}\right)^{1/2}. \tag{5.3}$$

From this one can construct the Reynolds number as

$$Re_0 = \frac{U_0 H}{\nu}, \tag{5.4}$$

which thus becomes the only dimensionless control parameter in the system.

In the following discussion in this section, the quantities are in dimensionless units. As in section 4.2, the model system is numerically simulated in a cubic tri-periodic domain, using the means of a pseudo-spectral code

*The content of this chapter is based on our paper "Wu, W., F. G. Schmitt, E. Calzavarini, and L. Wang. A quadratic constitutive equation for the turbulent Kolmogorov flow." to be submitted to *Physical Review E*.

Table 5.1: The dimensionless key global parameters after reaching a statistically stationary state. $A = 1$ is the amplitude of forcing to velocity; $H = 1$ is the length of the domain, also reference scales for length; $U_0 = 1$ and $T_0 = 1$ are the reference scales for velocity and time respectively as indicated in Eq. (5.2). The first column is the Run number; $Re_0 = \frac{HU_0}{\nu}$ is the Reynolds number based on domain length; $Re_{\lambda_0} = \frac{\lambda_0 u_0'}{\nu}$ is the Reynolds number based on global Taylor microscale, where $\lambda_0 = \sqrt{15\nu/\epsilon_0}u_0'$, ν is the kinematic viscosity, $u_0' = \sqrt{\frac{1}{3}\sum_i \langle u_i'^2 \rangle}$ is the global root-mean square of single component velocity, $\epsilon_0 = \frac{\nu}{2}\langle \sum_i \sum_j (\partial_i u_j + \partial_j u_i)^2 \rangle$ is the global energy dissipation rate, $\langle \cdot \rangle$ denotes the average in time and all over the domain. N^3 is the grid size; $\eta_0 = (\nu^3/\epsilon_0)^{1/4}$ is the global Kolmogorov scale; $|\mathbf{k}|_{max} \cdot \eta_0$ is the resolution condition; T_{total} is the total simulation time and T_l is the large eddy turnover time, i.e. T_{total}/T_l denotes the number of large eddy turnover time spanned by the simulation.

No.	Re_0	Re_{λ_0}	ν	ϵ_0	η_0	N^3	$\lvert\mathbf{k}\rvert_{max} \cdot \eta_0$	T_{total}/T_l
1	787.5	38.7	0.0013	0.51	0.008	128^3	2.64	462.5
2	984.4	43.5	0.001	0.52	0.0067	128^3	2.22	445.0
3	1211.5	49.3	0.00083	0.52	0.0058	128^3	1.90	427.1
4	1575.0	57.4	0.00063	0.52	0.0047	128^3	1.56	403.5
5	2099.9	66.9	0.00048	0.54	0.0038	128^3	1.25	761.2
6	3149.9	83.9	0.00032	0.57	0.0028	256^3	1.82	259.4
7	6299.8	123.4	0.00016	0.56	0.0016	256^3	1.08	386.0
8	15749.6	198.3	6.3e-05	0.56	0.00083	512^3	1.09	70.2

with a smooth dealiasing technique. The time-marching scheme adopts a third order Runge-Kutta method.

The global non-dimensional values of the key parameters for the simulations are reported in table 5.1. The total integration time is long enough, as shown in Table 5.1, not only to ensure that the statistics have converged, but also to have a sample space large enough for the statistical estimations, especially for the runs with small number of grids. It is noteworthy that the adimensionalization implemented in this section is different from Chapter 4. Because of anisotropy along z direction, the quantities such as the Taylor micro scale λ and Kolmogorov length η are functions of position z in the TKF. The quantities listed in table 5.1 with the subscript of 0 means they are the global values obtained from the average also over z, i.e. $\langle \cdot \rangle$.

Reynolds decomposition and velocity moments

Let us consider a Reynolds decomposition of the velocity into mean and fluctuating quantities $\mathbf{u} = \langle \mathbf{u} \rangle_z + \mathbf{u}'$ ($\langle \cdot \rangle_z$ denotes the average over time and spatially in x and y directions) and note the three components of the velocity $\mathbf{u} = (u, v, w)$. Because of the periodicity in x and y directions, the derivatives with respect to x and y of mean quantities are 0. By taking the average in time and spatially in x and y direction of the Navier-Stokes equations, one obtains the following relations:

$$\begin{aligned} -\partial_z \tau &= \frac{1}{Re_0}\partial_z^2 U(z) + \sin(2\pi z), \\ \partial_z \langle w'^2 \rangle_z &= -\partial_z \langle p \rangle_z, \end{aligned} \tag{5.5}$$

where $U = \langle u \rangle_z$ and the shear stress is $\tau = -\langle u'w' \rangle_z$. Using the first line of this relation, it is found that for laminar flows when $\tau = 0$, the mean velocity profile is also sinusoidal while the pressure field is constant (Meshalkin and Sinai, 1961).

For turbulent flows, it is well-known that the mean velocity profile is also sinusoidal (Borue and Orszag, 1996), but this is a numerical result which has, to our knowledge, no direct analytical explanation. We obtain the following z-dependence for U:

$$U(z) = \kappa \sin(2\pi z). \tag{5.6}$$

The numerical estimations of κ are plotted in figure 5.1. The maximum value of the mean turbulent velocity is of the order of the characteristic velocity built using the forcing values, since we obtain values of κ between 1.01 and 1.12, increasing with the Reynolds number (figure 5.1 and Table 5.2). The values of κ found here are compatible with the value of $\kappa = 1.1$ found by Borue and Orszag (1996) (the value of the Reynolds number in the latter work is not provided).

For large Reynolds number, using equations (5.5) and (5.6) we find that $\partial_z \tau$ is proportional to $\sin(2\pi z)$, obtaining finally:

$$\tau = \frac{1}{2\pi} \left(1 - (2\pi)^2 \frac{\kappa}{Re_0} \right) \cos(2\pi z). \tag{5.7}$$

The different first and second moments of the velocity obtained after averaging Navier-Stokes equations are shown in figures 5.2 and 5.3. As proposed by Sarris et al. (2007), one criterion for the convergence of Kolmogorov flow simulations is that the left-hand-side and right-hand-side of equation (5.7) must be comparable. As shown in figure 5.2(b), this criterion is satisfied in our simulation (when the Re_0 is large enough for the diffusion term to be neglected). Moveover, only one component of the mean velocity is non-zero; concerning second moments, only one shear stress term is non-zero, involving the product $u'w'$. The turbulence is anisotropic since all normal stress components of the stress tensor are different: $\langle u'^2 \rangle_z > \langle w'^2 \rangle_z > \langle v'^2 \rangle_z$. The diagonal terms have twice the spatial frequency of the forcing. Since $\cos(2\theta) = 2\cos^2\theta - 1$, they can be written as:

$$\begin{aligned} \langle u'^2 \rangle_z &= \alpha_1 + \beta_1 \cos^2(2\pi z), \\ \langle v'^2 \rangle_z &= \alpha_2 + \beta_2 \cos^2(2\pi z), \\ \langle w'^2 \rangle_z &= \alpha_3 + \beta_3 \cos^2(2\pi z), \end{aligned} \tag{5.8}$$

where numerically the couple of values (α_i, β_i) of each component of the velocity, for each run, are listed in table 5.2. This will be an important information for the quadratic closure done in the next section. Consequently,

No.	α_1	β_1	α_2	β_2	α_3	β_3	κ
1	0.2247	0.1121	0.1483	0.0837	0.2279	0.0498	1.0084
2	0.2291	0.1155	0.1545	0.0885	0.2271	0.0504	1.0253
3	0.2282	0.1152	0.1622	0.0886	0.2378	0.0553	1.0273
4	0.2327	0.1141	0.1665	0.0920	0.2483	0.0587	1.0438
5	0.2385	0.1223	0.1704	0.0951	0.2489	0.0643	1.0734
6	0.2422	0.1291	0.1749	0.1034	0.2674	0.0772	1.1288
7	0.2605	0.1394	0.1749	0.1092	0.2678	0.0744	1.1325
8	0.2766	0.1364	0.1811	0.1092	0.2590	0.0714	1.1242

Table 5.2: The numerical values of the coefficients in Eq. 5.8 for each run.

we can write also the evolution of the mean kinetic energy:

$$K(z) = \alpha + \beta \cos^2(2\pi z), \tag{5.9}$$

where the coefficients α and β are plotted in figure 5.1. The values found for the latter are in good agreement with the values reported in (Borue and Orszag, 1996) ($\alpha = 0.34$ and $\beta = 0.14$). We address again here that these values are Reynolds-number dependent. Since the Reynolds number of the simulation in Borue and Orszag (1996) is not known, quantitative results cannot be precisely compared here.

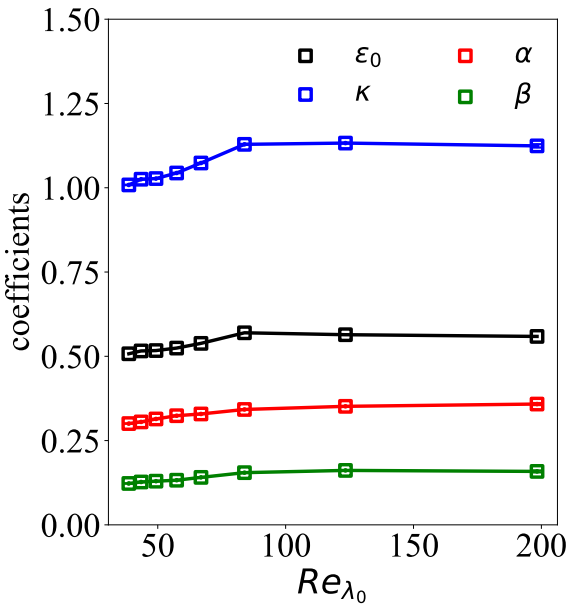

Figure 5.1: The coefficients obtained by fitting the profiles of mean velocity and kinetic energy, κ in Eq. 5.6 and α and β in Eq. 5.9, as function of Re_{λ_0}.

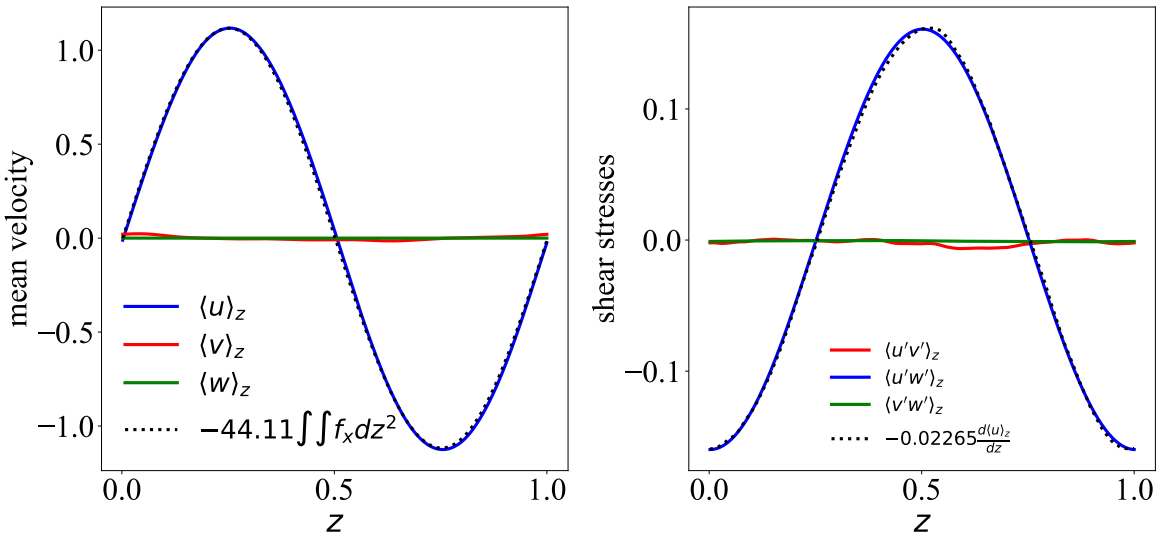

(a) (b)

Figure 5.2: (a) The adimensional mean quantities of each component of the velocity of Run 8. The only non-zero term is $\langle u \rangle_z$, having a maximum value of κ, where $\kappa = 2.82$. (b) The different adimensional shear stress terms of Run 8. The only non-zero term is $\langle u'w' \rangle_z$. Its z dependence is given by relation (5.7).

5.1.2 Closures for the turbulent Kolmogorov flow

Introduce the Reynolds stress tensor defined as $\mathbf{T} = -\langle u_i' u_j' \rangle_z$. The anisotropic stress tensor is $\mathbf{R} = -\mathbf{T} + \frac{2}{3} K \mathbf{I}$, where K is the kinematic energy and $\mathbf{I}$ is the unitary tensor. The mean velocity gradient tensor $\mathbf{A} = \partial U_i / \partial x_j$, and the mean strain-rate $\mathbf{S}$ and rotation-rate $\mathbf{W}$ tensors are also introduced as:

$$\mathbf{S} = \frac{1}{2}\left(\frac{\partial U_i}{\partial x_j} + \frac{\partial U_j}{\partial x_i}\right), \tag{5.10}$$

$$\mathbf{W} = \mathbf{A} - \mathbf{S}. \tag{5.11}$$

Closure of the turbulence equations corresponds to express the Reynolds stress tensor using mean quantities, e.g. when the closure is local, using the tensors $\mathbf{S}$ and $\mathbf{W}$. Below we first consider the simplest linear closure and estimate the eddy-viscosity, and then we address a nonlinear closure using a quadratic constitutive equation.

Boussinesq's eddy-viscosity hypothesis and its assessment

It is seen from equations (5.6) and (5.7) that, concerning the only non-zero non-diagonal term in the stress tensor, its z-behaviour is the same as the mean gradient term, giving an eddy-viscosity of the form:

$$\nu_T = \frac{\tau}{U'(z)} = \left(\frac{1}{(2\pi)^2 \kappa} - \frac{1}{Re_0}\right). \tag{5.12}$$

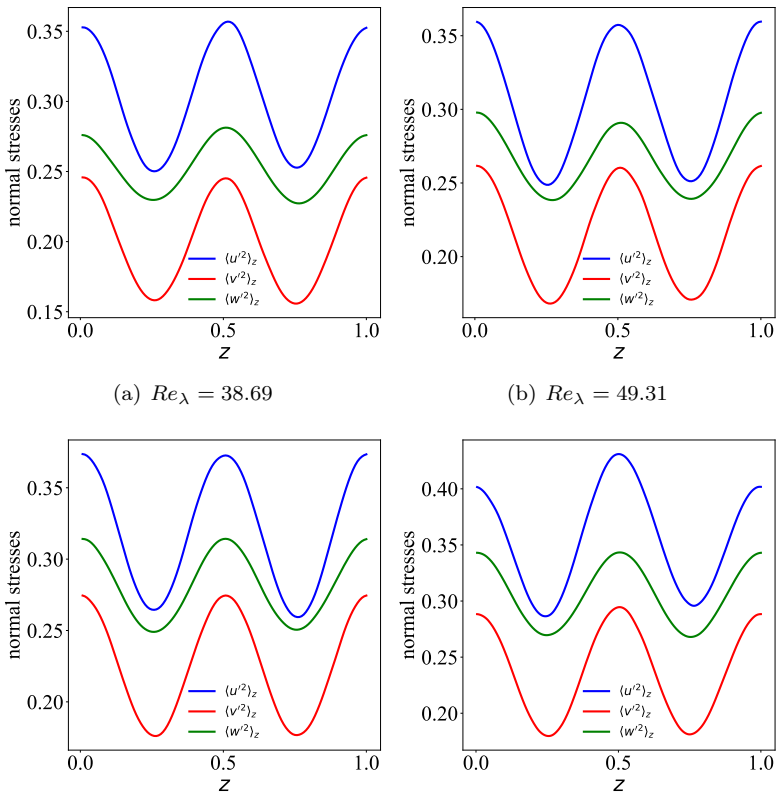

(a) $Re_\lambda = 38.69$ (b) $Re_\lambda = 49.31$

(c) $Re_\lambda = 66.9$ (d) $Re_\lambda = 122.85$

Figure 5.3: The different normal stresses: one finds $\langle u'^2\rangle_z > \langle w'^2\rangle_z > \langle v'^2\rangle_z$. The z-dependence is given by the fits of equation (5.8).

The eddy-viscosity does not depend on z, but depend on the Reynolds number and the coefficient κ. For Run 7 we find a value of $\nu_T = 0.0224$, as an overall estimation of the eddy-viscosity with a constant value which does not depend on z. However, the estimation of an eddy-viscosity does not validate the linear closure. The Boussinesq's hypothesis, which is at the basis of all eddy-viscosity turbulence models, corresponding to a linear proportionality between tensors (Boussinesq, 1877) :

$$\mathbf{R} = 2\nu_T \mathbf{S}. \tag{5.13}$$

For the flow considered here, there are some symmetries so that the strain as well as the stress have a simplified form:

$$\mathbf{S} = \frac{a}{2}\begin{pmatrix} 0 & 0 & 1 \\ 0 & 0 & 0 \\ 1 & 0 & 0 \end{pmatrix} \tag{5.14}$$

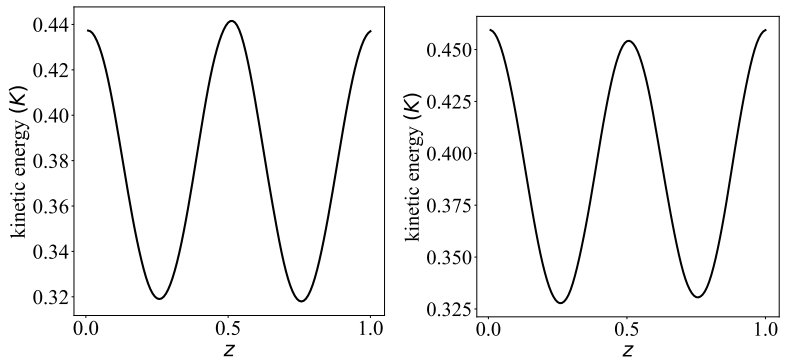

(a) $Re_\lambda = 38.69$ (b) $Re_\lambda = 49.31$

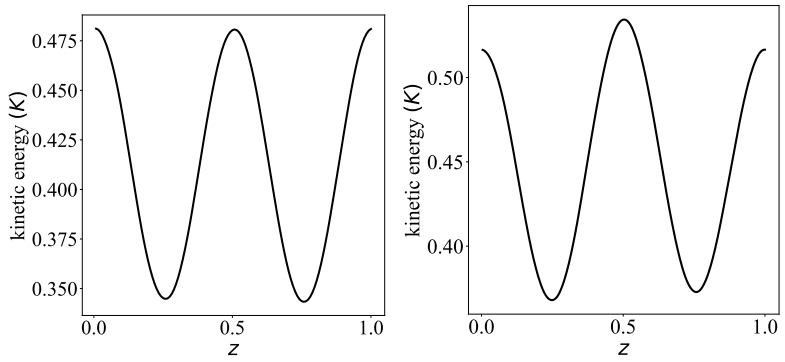

(c) $Re_\lambda = 66.9$ (d) $Re_\lambda = 122.85$

Figure 5.4: The mean kinetic energy $K(z) = \frac{1}{2}\langle u_i u_i \rangle_z$.

and

$$\mathbf{R} = \begin{pmatrix} \frac{2}{3}K - \sigma_u^2 & 0 & \tau \\ 0 & \frac{2}{3}K - \sigma_v^2 & 0 \\ \tau & 0 & \frac{2}{3}K - \sigma_w^2 \end{pmatrix}, \tag{5.15}$$

where $a = U'(z)$, $\sigma_u^2 = \langle u'^2 \rangle_z$ and the same for σ_v^2 and σ_w^2.

It is then clear, as is also the case for turbulent channel flows (Speziale, 1987; Nisizima and Yoshizawa, 1987; Pope, 2000), that such linear relation between tensors can be realized only when diagonal terms are zero, i.e. in an isotropic situation. However, the TKF is anisotropic and as seen in figure 5.3, the three normal stresses are all different, which means that a precise proportionality cannot be found.

In order to quantify this alignment, we consider the inner product between tensors: $\mathbf{A} : \mathbf{B} = \{\mathbf{A}^t\mathbf{B}\} = A_{ij}B_{ij}$, where $\{\mathbf{X}\}$ is a notation for the trace of $\mathbf{X}$. The norm is then $||\mathbf{A}||^2 = \mathbf{A} : \mathbf{A}$. As a direct test of Boussinesq's hypothesis, we first represent here the normalized inner product of $\mathbf{R}$ and $\mathbf{S}$ tensors (which is

similar to the cosine of an "angle" between vectors, see (Schmitt and Hirsch, 2000; Schmitt, 2007a)):

$$\rho_{RS} = \frac{\mathbf{R} : \mathbf{S}}{||\mathbf{R}||\ ||\mathbf{S}||}. \tag{5.16}$$

The ratio ρ_{RS} is thus a number between -1 and 1, which characterizes the validity of Boussinesq's hypothesis: it is 1 when this hypothesis is valid, and when close to 0 it corresponds to "perpendicular" tensors.

This is shown in figure 5.5. It is seen that a plateau is obtained, and that this hypothesis is approximately valid when the velocity gradient is not small, whereas it completely fails for some range of values around the positions where the mean velocity gradient vanishes.

More precisely, from Run 7, we find $\rho_{RS} = 0.93$ for $z = 1/2$. And by putting a threshold at $\rho_{RS} = 0.9$, we find that $0.9 \leq \rho_{RS} \leq 1$ for $z \in [0, 0.13] \cup [0.39, 0.59] \cup [0.87, 1]$. Hence it is larger than 0.9 for approximately 46% of the volume considered: for about half the volume, the linear relation between strain and stress tensors is approximately valid.

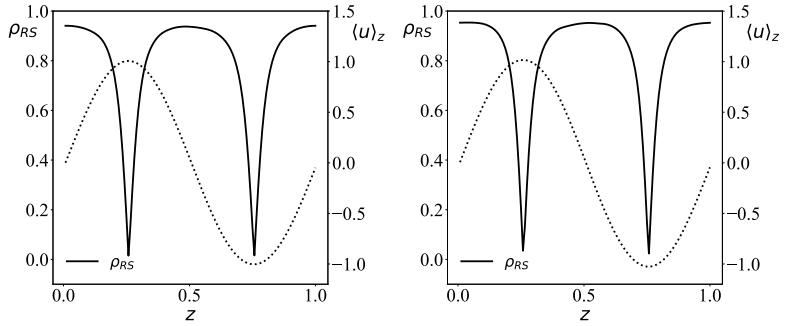

(a) $Re_\lambda = 38.69$ (b) $Re_\lambda = 49.31$

(c) $Re_\lambda = 66.9$ (d) $Re_\lambda = 122.85$

Figure 5.5: Simulation results for the test of the validity of Boussinesq's hypothesis, representing the alignment ρ_{RS} between $\mathbf{R}$ and $\mathbf{S}$. The mean velocity profile is superposed in dotted line for reference.

Test of a quadratic constitutive equation

We have seen above that the linear model cannot produce an anisotropic Reynolds stress tensor for anisotropic flow such as the TKF. Pope (1975) has proposed to use invariant theory in turbulence modeling, representing the stress tensor as a development into a tensor basis. Originally it was on the form $\mathbf{R} = \sum_{i=1}^{10} a_i \mathbf{T}_i$ with 10 basis tensors. By considering a quadratic development, only three tensors are used. This is complete for two dimensional flows (Pope, 1975), and is also a good approximation for fully 3-dimensional flows (Jongen and Gatski, 1998). It can be used for channel flows (Schmitt, 2007b; Modesti, 2020) and we propose to use it also here for the TKF.

In this framework, the anisotropic stress tensor writes as a three-terms development $\mathbf{R} = a_1\mathbf{T}_1 + a_2\mathbf{T}_2 + a_3\mathbf{T}_3$, where the three tensors of the basis are all symmetric and traceless (Pope, 1975):

$$\begin{aligned} &\mathbf{T}_1 = \mathbf{S}, && \mathbf{T}_2 = \mathbf{SW} - \mathbf{WS}, \\ &\mathbf{T}_3 = \mathbf{S}^2 - \tfrac{1}{3}\eta_1\mathbf{I}. \end{aligned} \tag{5.17}$$

The coefficients a_i can be written using scalar invariants of the flow, which correspond to scalar fields whose values are independent of the system of reference. Invariants can be defined as the traces of different tensor products (Spencer, 1971). Some of the first invariants are the following: $\eta_1 = \{\mathbf{S}^2\}$, $\eta_2 = \{\mathbf{W}^2\}$, $\eta_3 = \{\mathbf{S}^3\}$, $\eta_4 = \{\mathbf{SW}^2\}$, $\eta_5 = \{\mathbf{S}^2\mathbf{W}^2\}$, $\mu_1 = \{\mathbf{R}^2\}$, $\mu_2 = \{\mathbf{RS}\}$, $\mu_3 = \{\mathbf{RSW}\}$ and $\mu_4 = \{\mathbf{RS}^2\}$. All these invariants can be here estimated numerically. Furthermore, the coefficients a_1, a_2 and a_3 can be expressed using the invariants. This is done by projecting the constitutive equation onto the tensor basis: successive inner product of this equation with tensors $\mathbf{T}_i$ provides a system of scalar equations involving the invariants (Jongen and Gatski, 1998). For 2D flows such as TKF, we have $\eta_3 = 0$ and $\eta_5 = \eta_1\eta_2/2$, and the system of scalar equations is inverted to provide finally the quadratic constitutive equation using invariants:

$$\mathbf{R} = \frac{\mu_2}{\eta_1}\mathbf{S} - \frac{\mu_3}{\eta_1\eta_2}\mathbf{T}_2 + 6\frac{\mu_4}{\eta_1^2}\mathbf{T}_3. \tag{5.18}$$

For the TKF the invariants write:

$$\eta_1 = \frac{a^2}{2}, \quad \eta_2 = -\frac{a^2}{2}, \quad \mu_2 = a\tau, \tag{5.19}$$

$$\mu_3 = \frac{a^2}{4}\left(\sigma_u^2 - \sigma_w^2\right), \tag{5.20}$$

$$\mu_4 = \frac{a^2}{4}\left(\sigma_v^2 - \frac{2}{3}K\right). \tag{5.21}$$

The two remaining tensors of the tensor basis are:

$$\mathbf{T}_2 = \frac{a^2}{2}\begin{pmatrix} -1 & 0 & 0 \\ 0 & 0 & 0 \\ 0 & 0 & 1 \end{pmatrix} \tag{5.22}$$

and

$$\mathbf{T}_3 = \frac{a^2}{12}\begin{pmatrix} 1 & 0 & 0 \\ 0 & -2 & 0 \\ 0 & 0 & 1 \end{pmatrix}. \tag{5.23}$$

The quadratic constitutive equation finally writes, replacing invariants in equation (5.18):

$$\mathbf{R} = \frac{2\tau}{a}\mathbf{S} + \left(\sigma_u^2 - \sigma_w^2\right)\frac{1}{a^2}\mathbf{T}_2 + \left(6\sigma_v^2 - 4K\right)\frac{1}{a^2}\mathbf{T}_3. \tag{5.24}$$

Equation (5.24) is a quadratic constitutive equation which is expressing a nonlinear closure of the turbulent Kolmogorov flow. The first coefficient is twice the eddy-viscosity and therefore a constant, as discussed above. Whereas the other coefficients involve ratio of [constant + $\cos^2$] divided by $\cos^2$ terms.

When $a = U'(z) \simeq 0$, for $z \simeq 1/4$ and $z \simeq 3/4$, $\cos(2\pi z) = 0$ and all $\mathbf{S}$, $\mathbf{T}_2$ and $\mathbf{T}_3$ vanish, but in the three-terms development of $\mathbf{R}$, the second term and the third are non-zero constants, since the coefficients diverge (the a^2 terms cancel). In those positions, we see that $\mathbf{R}$ is a diagonal tensor which is not vanishing (see figure 5.6); we see numerically that the second term is also very small and that the third term is dominant. This means that in those positions, Boussinesq's linear eddy-viscosity development is no more valid and the anisotropic stress tensor is a constant perpendicular to the linear term and approximately proportional to $\mathbf{T}_3 = \mathbf{S}^2 - \frac{1}{3}\eta_1\mathbf{I}$.

5.1.3 Summary

In this section, the classical turbulence closure based on eddy-viscosity Boussinesq's approach and a nonlinear quadratic closure about the velocity fields in the turbulent Kolmogorov flow (TKF) are numerical examined. It was found that the mean velocity profile has the same form, with a damping of a factor κ, with respect to the mean velocity value calculated from the forcing term. The value of this parameter was found to weakly increase with the Reynolds number with indications of a possible asymptotic saturation at very large Re. The only non-zero shear stress term is proportional to the cosine function, and the normal stress components all involve a square cosine expression. The normal stresses are never equal, showing that as expected the turbulence is

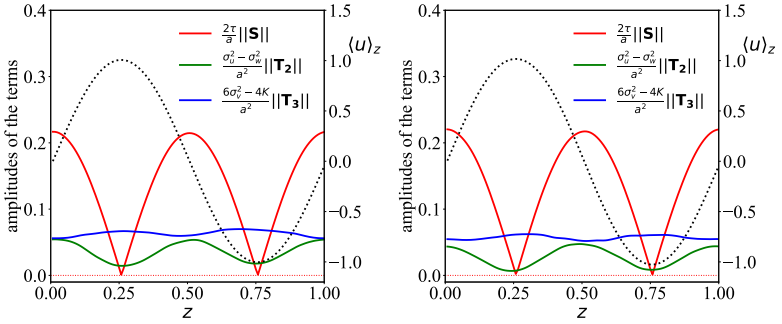

(a) $Re_\lambda = 38.69$ (b) $Re_\lambda = 49.31$

(c) $Re_\lambda = 66.9$ (d) $Re_\lambda = 122.85$

Figure 5.6: The amplitudes of the terms at the right hand side of Eq. (5.24) as function of z. The mean velocity profile is also represented as a dotted line, for reference. The horizontal red dotted lines mark the 0 value for the amplitudes. The simulation results of Run 1, 3, 5, 7 are shown here.

anisotropic. It was also shown that a quadratic nonlinear constitutive equation can be proposed for this flow, involving a linear term and two nonlinear terms in the form of traceless and symmetric tensors. For about half of the flow domain, the linear term is dominating. Whereas for the vanishing mean velocity gradient regions, only one non-linear term remains non-zero and becomes constant. Hence an effective viscosity coefficient can indeed be estimated for TKF, but contrary to what has been stated previously (Rollin et al., 2011), globally all linear and nonlinear terms are needed for the complete closure. Some of the values obtained here are in agreement with a previous work (Borue and Orszag, 1996), even if the Reynolds number was not provided in their work. We have checked the Reynolds-number dependence of the different parameters considered here, with 8 different runs with different grid sizes from 128^3 to 512^3, and with Reynolds numbers from $Re_\lambda = 38.7$ to 198. The parameters are found to converge for the largest Reynolds numbers considered.

Table 5.3: Key global parameters after reaching statistically stationary state. $Re_{\lambda_0} = u'\lambda_0/\nu$ is the global Taylor microscale, where u' is the global root mean square of single component velocity, ν is kinematic viscosity, λ_0 is the global Taylor micro scale; Sc is the Schmidt number; n is the reaction order of R_2 in the reaction; N^3 is total number of grids; $\eta_0 = (\nu^3/\epsilon_0)^{1/4}$ is the global Kolmogorov length scale; $|\mathbf{k}|_{max}$ is the maximum wave number amplitude kept by the dealiasing procedure, $|\mathbf{k}|_{max} \cdot \eta$ is the resolution condition; $Da = \lambda_0\gamma_1 R_{2,eq}^n/u' = \lambda_0\gamma_2/u'$ is the Damköhler number based on Taylor scale.

Re_{λ_0}	Sc	n	λ_0	u'	N^3	η_0	$\|\mathbf{k}\|_{max} \cdot \eta_0$	Da
54.7	1	1	1	1	128^3	0.052	1.55	0.0085-8.5

5.2 Reactions in turbulent Kolmogorov flow

In Chapter 4, the reactive scalar mixing in homogeneous isotropic incompressible turbulence was studied by direct numerical simulation and theoretical analysis. The fluctuations and correlations of the reactive scalars were the main focus, and found to be uniquely dependant on the control parameter of Da_θ. However, according to the definition of Da_θ (Eq. (4.15)), this number is based on scalar Taylor micro-scale, diffusivity and reaction rate, no the velocity fields. In addition, in the modeling analysis, the fundamental condition is that the reacting system is constrained to a quasi-equilibrium state, weakly relevant to the turbulent flow environment. Therefore, this lead us to consider extending our theoretical analysis about the statistical properties of turbulent reactive scalars in Chapter 4 to non-homogeneous and anisotropic turbulence, for example the TKF discussed above.

In this section we consider the same reactions and passive scalar as that discussed in section 4.1, sustained by the same isotropic constant amplitude forcing (Eq. (4.10)). Specifically, only the second order reaction (n=1) is discussed here. The global non-dimensional values of the key parameters for the simulations are reported in table 5.3. It is noteworthy that the adimensionalization implemented in this section is in the same way as Chapter 4, instead of section 5.1. Similarly with table 5.1, the quantities of the Taylor micro scale λ, Kolmogorov length η and dissipation rate ϵ are functions of position z in TKF. The subscript of 0 means λ_0, η_0 and ϵ_0 are the global values obtained from the average also over z, i.e. $\langle\cdot\rangle$.

5.2.1 Scalar Taylor micro-scale

As the Taylor microscale of θ, λ_θ is a key quantity in the definition of Da_θ (Eq. (4.15)). In this chapter, because the flow is supposed to be homogeneous in y direction, λ_θ is quantified as

$$\lambda_\theta^2 = \frac{\langle\theta'^2\rangle_z}{\langle(\partial_y\theta)^2\rangle_z}. \tag{5.25}$$

Figure 5.7 shows the numerical estimations of the square of Taylor microscale of the reactive scalars under the condition of Da=8.5, in comparison with the profile of λ^2. Although it can be found that λ_θ^2 is of the same

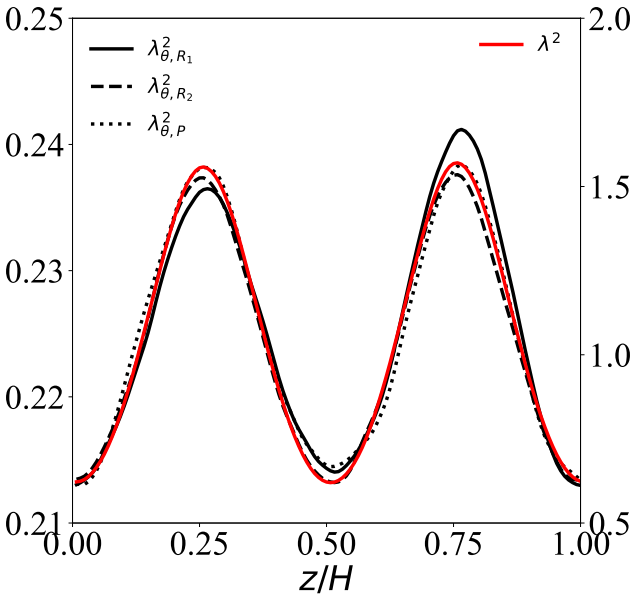

Figure 5.7: The square of the Taylor microscale of θ under the condition of Da=8.5 compared with that of the velocity, as functions of z.

shape with λ^2, their fluctuations are hugely different. The value of λ is proportional to the mean gradient of velocity $\frac{\partial\langle u\rangle_z}{\partial z}$, and therefore of great variety. However, λ^2_θ is not of large fluctuation, within 10% of the mean value. Thus Da_θ can be reasonably considered as independent on z and scalar. According to Eq. (4.15), the Da_θ can be roughly considered as independent of z.

5.2.2 Correlation coefficient

The correlation coefficients between reactive scalars are defined based on the fluctuating parts of scalars as

$$r(\theta_1,\theta_2)(z)=\frac{\langle\theta_1'\theta_2'\rangle_z}{\langle\theta_1'^2\rangle_z^{1/2}\langle\theta_2'^2\rangle_z^{1/2}}. \tag{5.26}$$

Here θ_1 and θ_2 are the scalars under consideration. The statistics of the correlation coefficients are implemented for each specific z position. Thus they are functions of z.

According to the theoretical prediction about the correlation coefficients between scalars based on Da_θ given in Chapter 4, under the condition of $n=1$, we have

$$r(R_1,P)=r(R_2,P)=-r(R_1,R_2)\approx\frac{Da_\theta}{3+2Da_\theta}. \tag{5.27}$$

In figure 5.8(a), the correlation coefficients between reactive scalars at an example position are shown, and

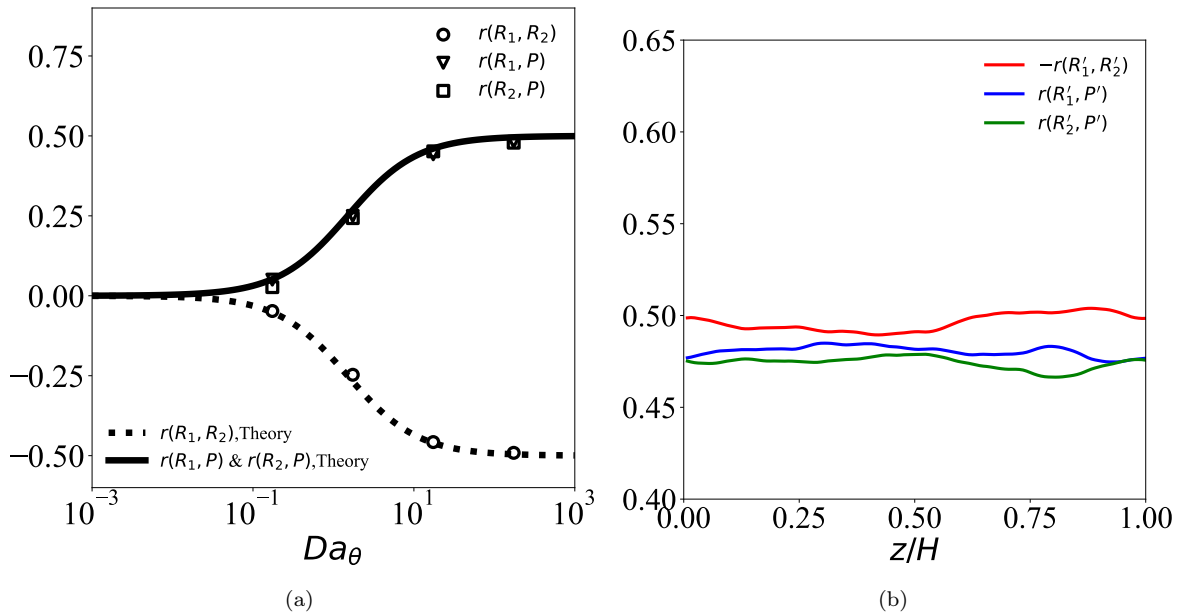

Figure 5.8: Correlation coefficients between reactive scalars (a) as function of Da_θ at the position of $z = H/2$; (b) as function of z under the condition of Da=8.5.

found to be in excellent agreement with the theoretical predictions by Eq. (5.27). Moreover, as shown in figure 5.8(b), the correlation coefficients between scalars are independent of z. This result further confirms that the theoretical model about the correlations between reactive scalars proposed in Chapter 4 relies weakly on the specific flow environment.

5.2.3 Variances of scalars

Similar with the correlation coefficients, the scalar fluctuations are also functions of z in the TKF. Figure 5.9(a) illustrates such a dependence. The fluctuations of reactive scalars are evidently smaller than that of the passive scalar. It indicates that, like in the homogenous isotropic turbulence, the reaction here also tends to dump the fluctuations of scalars. In addition, the profile of the scalar fluctuations are toughly of sinusoidal shapes, although the amplitude is small compared with the mean. A theoretical prediction about the fluctuations of reactive scalars normalized by that of the passive scalar was proposed in the modeling analysis in Chapter 4. These quantities in TKF are shown in figure 5.9(b) as functions of z. Roughly, they can be considered as independent of z. Following the procedure described in section 4.6.2, under the condition of $n = 1$, the analytical predictions about the dependence of the normalized fluctuations of reactive scalars, at any z in the

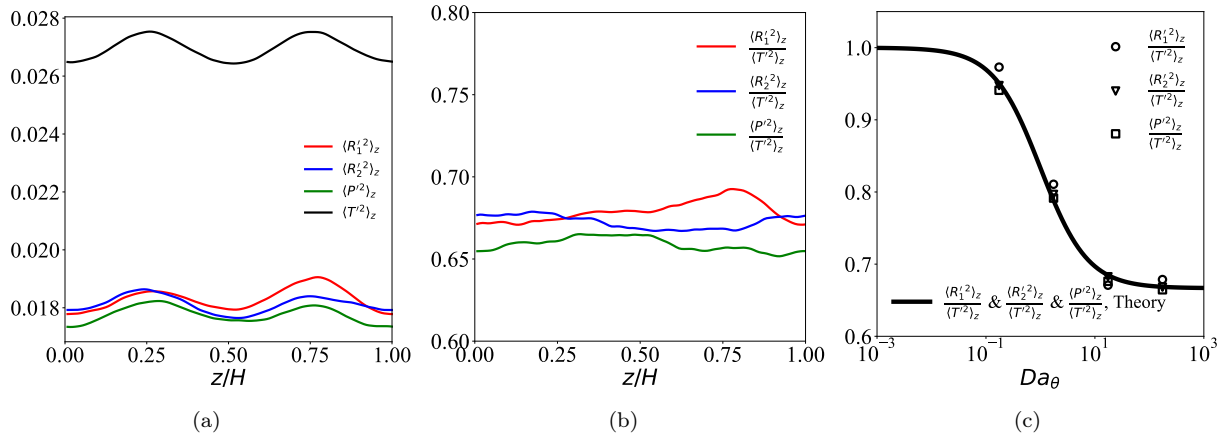

(a) (b) (c)

Figure 5.9: (a) Variances of reactive scalars, under the condition of Da=8.5, and passive scalar as function of z. (b) Variances of reactive scalars normalized by the variance of passive scalar as function of Da_θ at the position of $z = H/2$. (b) Variances of reactive scalars normalized by the variance of passive scalar as function of z under the condition of Da=8.5.

TKF, on the Da_θ can be determined as

$$\frac{\langle R_1'^2\rangle_z}{\langle T'^2\rangle_z} \approx \frac{\langle R_1'^2\rangle_z}{\langle T'^2\rangle_z} \approx \frac{\langle R_1'^2\rangle_z}{\langle T'^2\rangle_z} \approx \frac{3+2Da_\theta}{3+3Da_\theta}. \tag{5.28}$$

As shown in figure 5.9(c), the normalized fluctuations of the reactive scalars measured from the DNS are in agreement with the theoretical predictions by Eq. (5.28).

5.2.4 Summary

In this section, the reversible reaction discussed in Chapter 4 was introduced into the TKF. The Taylor microscales of reactive scalars as functions of the position were found to fluctuate only slightly. Thus parameter of Da_θ (the ratio of scalar diffusion time scale to the reaction time scale) is weakly influenced by the anisotropy of the velocity fields. The statistical properties including the fluctuations and correlations of the reactive scalars are numerical examined, whose dependence on Da_θ were found to be in good agreement with the theoretical predictions proposed by the modeling analysis discussed in Chapter 4. This indicates that, in the quasi-equilibrium state, the relations between the statistical properties of reactive scalars and the Da_θ is weakly influenced by the background velocity field.

Chapter 6

Chemical reactions sustained by Dirichlet boundary conditions

In Chapter 4, the theoretical model was based on the linearization of reaction term, which is valid only when the fluctuations of the scalars are not comparable to the mean quantities. The chemical source was not strong enough to change the scaling behavior of scalars. The main reason is that the reacting system is not strongly deviated from the global equilibrium state in the homogeneous isotropic configuration. In this chapter, a combustor-like configuration of reactive scalars, in which the scalar fields are of Dirichlet boundary conditions in one direction, is explored. The fluctuations of the scalars are maintained by an intrinsic mean gradient instead of isotropic forcing. Accordingly, the reacting system is supposed to be strongly deviated from the chemical equilibrium state and of rich physical interest. The statistical and scaling properties of reactive scalars are investigated, in comparison with a passive scalar. The rest of this chapter is organized as follows. In section 6.1, the definitions of the configuration and problem studied are provided. Section 6.2 elaborates the details of the numerical methods; then in section 6.3, the modeling analysis and numerical results are presented and discussed. Finally the conclusions of this chapter are summarized in section 6.4.*

*The content of this chapter is based on our paper "Wu, W., L. Wang, E. Calzavarini, F. G. Schmitt. Reactive scalars in incompressible turbulence with strongly non-equilibrium chemistry." to be submitted to *Journal of Fluid Mechanics*.

6.1 Introduction of the model system

In this chapter, The velocity fields are exactly the same as that described in section 4.1. While the scalars are different. The reactions considered here are second order reversible reaction, in the following form

$$\mathrm{R}_1 + \mathrm{R}_2 \underset{\gamma_2}{\overset{\gamma_1}{\rightleftharpoons}} \mathrm{P}, \tag{6.1}$$

where R_1, R_2 and P denote the three involved reactive scalars. The process is reversible with the respective forward and backward reaction rate coefficients γ_1 and γ_2. The reactants are assumed to undergo diffusion and to be transported in a passive manner by an incompressible velocity flow field upon which they do not exert any effect. The evolution equations scalar concentrations ($R_1(\mathbf{x},t)$, $R_2(\mathbf{x},t)$ and $P(\mathbf{x},t)$) read

$$\frac{\partial R_1}{\partial t} + (\mathbf{u}\cdot\nabla)R_1 = D\triangle R_1 - \gamma_1 R_1 R_2 + \gamma_2 P + \dot{s}_{R_1}, \tag{6.2a}$$

$$\frac{\partial R_2}{\partial t} + (\mathbf{u}\cdot\nabla)R_2 = D\triangle R_2 - \gamma_1 R_1 R_2 + \gamma_2 P + \dot{s}_{R_2}, \tag{6.2b}$$

$$\frac{\partial P}{\partial t} + (\mathbf{u}\cdot\nabla)P = D\triangle P + \gamma_1 R_1 R_2 - \gamma_2 P + \dot{s}_{P}. \tag{6.2c}$$

Here $\mathbf{u}(\mathbf{x},t)$ is the flow velocity and D is the species diffusivity (assumed identical for all species). The source terms $\dot{s}$ are precised later below.

In the following analyses, to gain primary insights of the flow physics, a non-reactive species T is also considered for comparison with the following governing equation

$$\frac{\partial T}{\partial t} + (\mathbf{u}\cdot\nabla)T = D\triangle T + \dot{s}_T. \tag{6.3}$$

In Chapter 4, it was shown that large-scale statistically homogeneous and isotropic reactive scalar sources/sinks are not able to sustain strong deviation from the chemical equilibrium, which instead needs to be realized by imposing non-zero mean gradients profiles for the reactants. The canonical homogeneous shear flow, although with adjustable mean scalar gradients, can not be adopted because the scalar concentrations defining the reaction rates in Eqs. (6.2) are undetermined. Moreover, other flow cases such as the shear layer (Mellado et al., 2009) are not suitable either because of the unstationary evolution or inherent spatial non-homogeneity. Thus we propose here a new flow configuration, which is schematically illustrated in figure 6.1. In a cubic domain a large-scale forcing term $\mathbf{f}$ (Eq. (4.9)) is exerted into the momentum equation (4.2) to sustain an homogeneous and isotropic velocity field with periodic boundary conditions along the three directions. Differently, the scalar

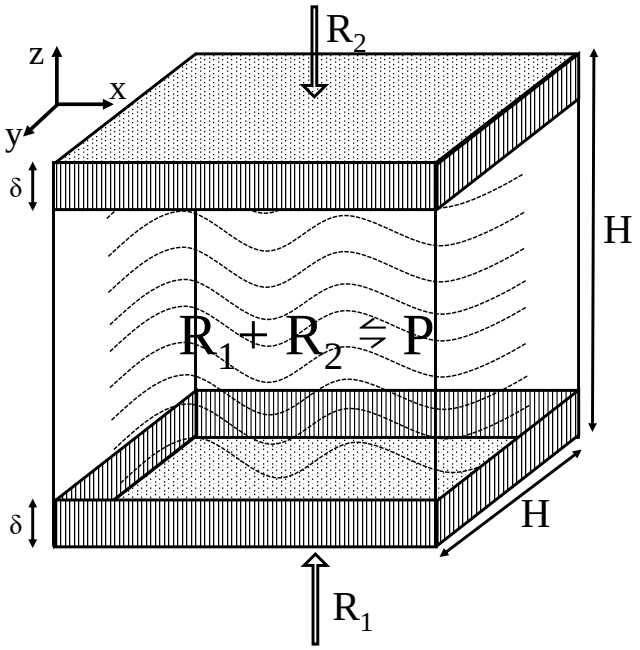

Figure 6.1: Schematic diagram of the flow configuration and computational domain. For the scalars quantities, the periodic boundary conditions are set along x and y directions, while a Dirichlet boundary condition is used along the z direction. The shadowed layers near the boundaries are the "buffer layers" generated artificially, in which the quantities of scalars are close to the preset boundary values, as defined in Eq. (6.5). The part between buffer layers is denote as the bulk region. Such setup is statistically stationary and ensures the local positiveness of scalar concentrations.

fields are periodic only in x and y directions. Along the z direction, the following Dirichlet boundary conditions are implemented:

$$\begin{cases} R_1 = R_0, R_2 = 0, P = 0, T = R_0 & \text{when } z = 0, \\ R_1 = 0, R_2 = R_0, P = 0, T = 0 & \text{when } z = H, \end{cases} \tag{6.4}$$

where H is the length of domain in z direction and R_0 is the constant boundary condition.

Numerically it is found that to realize a reasonably large fluctuation for the scalar fields, buffer layers in the vicinity of the Dirichlet boundaries are needed, as shown in figure 6.1 by the shadowed parts with the bulk region in between. Inside both the upper and bottom buffer layers, the artificial sources $\dot{s}_\theta$ with $\theta = R_1, R_2, P$ or T are added in the scalar equations Eq. (6.2) and Eq. (6.3). Specifically, $\dot{s}_\theta$ is designed here as

$$\dot{s}_\theta = \begin{cases} \frac{1}{\tau}(\theta_0 - \theta), \text{ in the buffer with } z > H - \delta \text{ or } z < \delta, \\ 0, \text{ in the bulk.} \end{cases} \tag{6.5}$$

Here θ_0 is the boundary value of θ, as defined in Eq. (6.4); τ is a characteristic time scale to control the strength

of the source terms. Obviously, small values of τ imply a large source to reduce the defect of the scalar quantities from the boundary values. In our present simulation cases, τ is set at the order of 100 times of the numerical time step. Another parameter δ is the buffer layer thickness, which can be tailored to adjust the scalar source (i.e. lager thickness corresponds to larger species source) and the scalar mean gradient.

6.2 Numerical implementation

First of all, it is convenient to non-dimensionalize the above set of equations by choosing reference scales appropriate for the present system. The domain size H, the overall scalar difference R_0 in Eq. (6.4) and the overall fluctuating velocity u' are used as the reference quantities for the length scale, scalar and velocity, respectively. For simplicity, in the following, symbols by default denote the corresponding nondimensionalized ones. It then yields

$$\frac{\partial R_1}{\partial t} + (\mathbf{u}\cdot\nabla)R_1 = (Sc\ Re)^{-1}\triangle R_1 - Da_1 R_1 R_2 + Da_2 P + \dot{s}_{R_1}, \tag{6.6a}$$

$$\frac{\partial R_2}{\partial t} + (\mathbf{u}\cdot\nabla)R_2 = (Sc\ Re)^{-1}\triangle R_2 - Da_1 R_1 R_2 + Da_2 P + \dot{s}_{R_2}, \tag{6.6b}$$

$$\frac{\partial P}{\partial t} + (\mathbf{u}\cdot\nabla)P = (Sc\ Re)^{-1}\triangle P + Da_1 R_1 R_2 - Da_2 P + \dot{s}_P, \tag{6.6c}$$

$$\frac{\partial T}{\partial t} + (\mathbf{u}\cdot\nabla)T = (Sc\ Re)^{-1}\triangle T + \dot{s}_T, \tag{6.6d}$$

where $Re = H\cdot u'/\nu$ is the Reynolds number; the Schmidt number $Sc = \nu/D$ is the ratio of viscous diffusion to molecular diffusion; the ratio of flow timescale to the chemical timescale of forward and backward reaction are characterized by the Damköhler number $Da_1 = H\gamma_1 R_0/u'$ and $Da_2 = H\gamma_2/u'$, respectively, and $\Gamma = Da_1/Da_2$. In this chapter, Da_2 is set as constant and Da_1 is changeable. For the near equilibrium case in Chapter 4, the forward and backward reactions almost balance each other and thus only one Damköhler number was needed to describe the reaction intensity of reaction. However, for the present configuration at strongly non-equilibrium state, the global forward and backward reactions deviate. As shown in Fig 6.2 with the increase of Γ, the global forward rate defined by the mean scalar concentrations, i.e. $Da_1\langle R_1 R_2\rangle_z$, can be much larger than the global backward rate $Da_2\langle P\rangle_z$, where $\langle\cdot\rangle_z$ means the ensemble average with respect to z. The dimensionless boundary conditions (for scalars) are

$$\begin{cases} R_1 = 1, R_2 = 0, P = 0, T = 1 & \text{when } z = 0, \\ R_1 = 0, R_2 = 1, P = 0, T = 0 & \text{when } z = 1. \end{cases} \tag{6.7}$$

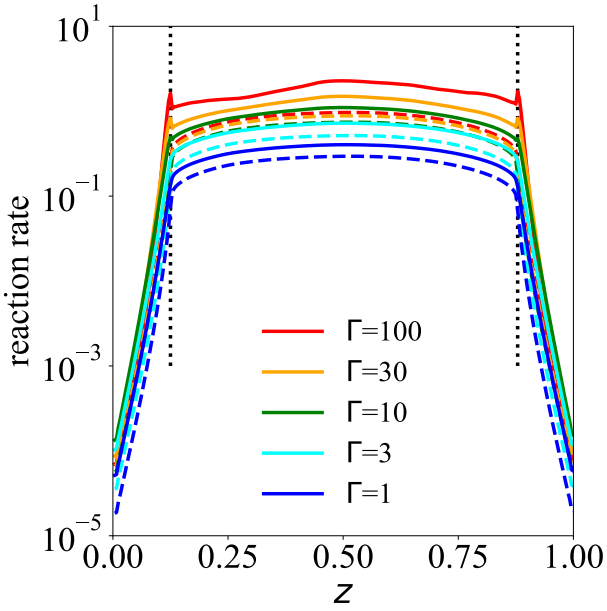

Figure 6.2: The reaction rates computed with the mean quantities as functions of z. The solid lines are for the forward reaction rates $Da_1\langle R_1 R_2\rangle_z$ and the dashed lines are for the backward reaction rates $Da_2\langle P\rangle_z$. The clear difference can be observed. Vertical dotted lines mark the interfaces between the buffer layers and the bulk region.

Re	Re_λ	Sc	u'	λ	N^3	$\lvert\mathbf{k}\rvert_{max}\cdot\eta$	τ_η	Da_2	Γ	L_I	T_I	Δt
1180	82.3	1	1	0.067	256^3	2.53	0.017	1.34	100-1	0.24	0.52	7.6×10^{-5}

Table 6.1: Non-dimensionalized parameters for the simulations: $Re = u'H/\nu$ is the Reynolds number based on large scale, where u' is the single-component root-mean-square velocity, H is the length of the domain, ν is the viscosity; $Re_\lambda = u'\lambda/\nu$ is the Taylor scale λ based Reynolds number; Sc is the Schmidt number (ν/D); N^3 is the number of total grid points; $\lvert\mathbf{k}\rvert_{max}\cdot\eta$ is the resolution condition, where $\lvert\mathbf{k}\rvert_{max}$ is the maximum amplitude of wave number kept by the dealiasing procedure, η if the Kolmogorov lenght scale; τ_η is the Kolmogorov time scale; $\Gamma = Da_1/Da_2$, with Da_1 and Da_2 as the Damkholer numbers for forward and backward reactions respectively; L_I is the integral length scale; T_I is the integral time scale; Δt is the numerical time step.

The key involved parameters in the present simulations are listed in table 6.1.

The same as described in section 4.2, the turbulent flow is statistically stationary homogeneous and isotropic, sustained by a large-scale forcing term of (4.9). The isotropic velocity field is obtained by numerically solved by using a pseudo-spectral code (Gauding et al., 2017, 2018) with a smooth dealiasing technique (Hou and Li, 2007) for the treatment of non-linear terms in the equations. Differently, the scalar equations Eq. (6.6) are solved by the finite difference method.

The velocity field is initialized by prescribing the spectrum of kinematic energy in the Fourier space $\hat{\mathbf{u}}(\mathbf{k};0)$ (Schumacher et al., 2007), where both the modulus and phases are randomly determined, under the constraint

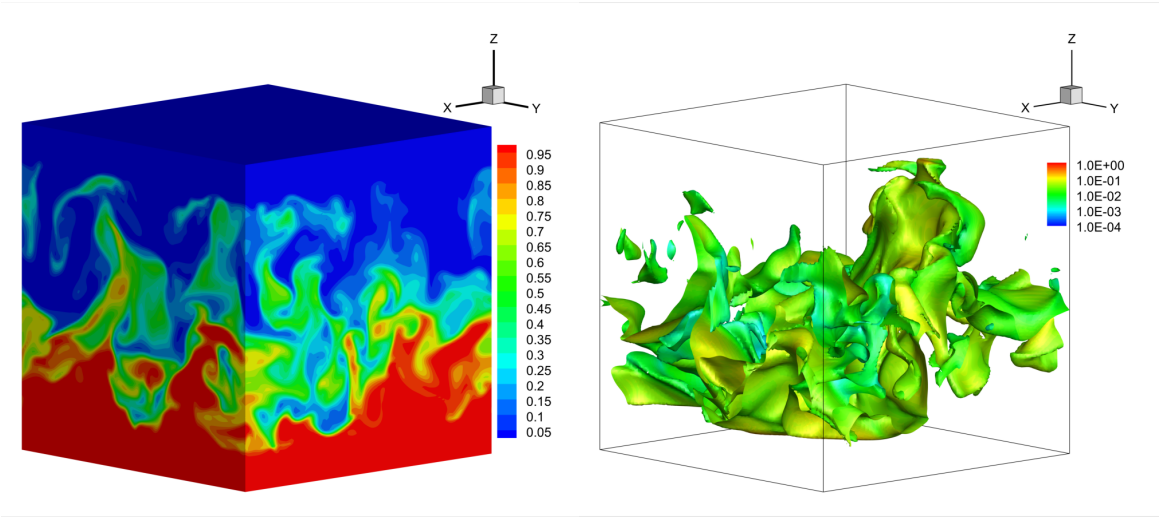

(a) (b)

Figure 6.3: The three-dimensional instantaneous snapshot of (a) R_1, and (b) reaction rate $(Da_1 R_1 R_2 - Da_2 P)$ on the isosurface of $R_1 = 0.5$, under the condition of $\Gamma = 10$.

of zero mean ($\hat{\mathbf{u}}(\mathbf{0}; 0) = 0$) and prescribed kinematic energy spectrum of

$$E(k;0) = \sum_{k=|\mathbf{k}|} |\hat{\mathbf{u}}(\mathbf{k};0)|^2 \propto |\mathbf{k}|^4 e^{-2(|\mathbf{k}|/2)^2}.$$

Meanwhile, the scalars are linearly initialized as:

$$\begin{cases} R_1(x,y,z;0) &= 1-z, \\ R_2(x,y,z;0) &= z, \\ P(x,y,z;0) &= 0, \\ T(x,y,z;0) &= 1-z. \end{cases} \tag{6.8}$$

Figure 6.3 shows the typical visualization of R_1 and the reaction rate $(Da_1 R_1 R_2 - Da_2 P)$ on the isosurface of $R_1 = 0.5$ under the condition of $\Gamma = 10$. It can be seen that with the properly defined buffer layer, the spatial fluctuation of scalar can be self sustained with the total scalar quantities confined in the prescribed $[0, 1]$ range.

The statistical stationarity of the setup can be appreciated from the temporal evolution of the scalar statistical moments. As an example, figure 6.4 shows that the evolutions of the spatial average of scalar concentrations and root mean square of scalar fluctuation in the bulk region for the case $\Gamma = 10$. This indicates that the

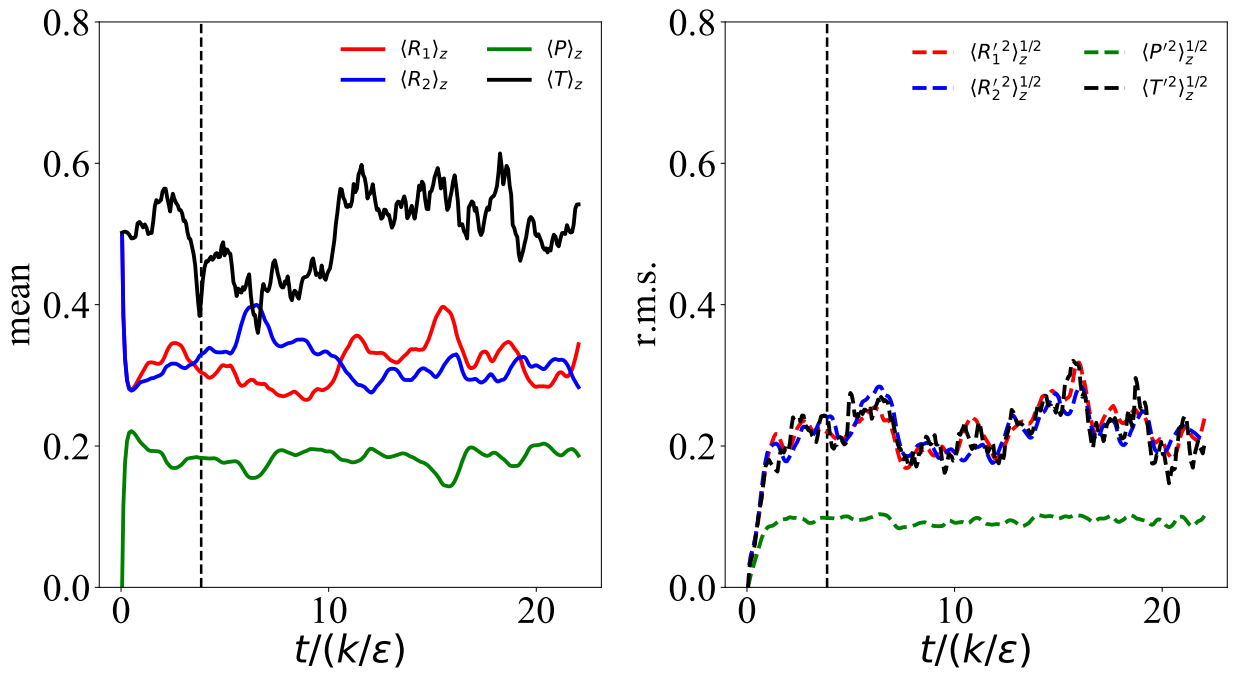

(a) mean (b) fluctuation

Figure 6.4: Evolution of the spatial average of the mean and root mean square of scalar fluctuation in the bulk region for the case of $\Gamma = 10$. Time is normalized by the integral time k/ϵ with $k = 3u'^2/2$. The dashed vertical lines marks the initial time for the computation of statistical quantities.

reacting system is strongly deviated from chemical equilibrium. The following analyses will be focused on the bulk region. Data samples are collected in a time span of about ten times of the integral time $T_I = k/\epsilon$ with $k = 3u'^2/2$, once the statistically stationary state is reached.

6.3 Result analyses

6.3.1 Properties of the buffer layer and the bulk region

In the present configuration, the two buffer layers function as a source which sustain the mean scalar gradient with positive scalar concentrations, while the bulk domain is where the turbulent mixing occurs and where the present analysis is focused on. The means and root-mean-square (r.m.s.) of the fluctuations of the passive scalars (T) in the configurations with different buffer layer thickness δ are shown in figure 6.5 (a) and (b), respectively. As can be expected, in the bulk region the mean scalar profile follows a linear relation with respect to z, i.e. constant gradient, under the action of isotropic turbulent velocity. From the prescribed geometrical and boundary conditions, the constant gradient is about $1/(1-2\delta)$.

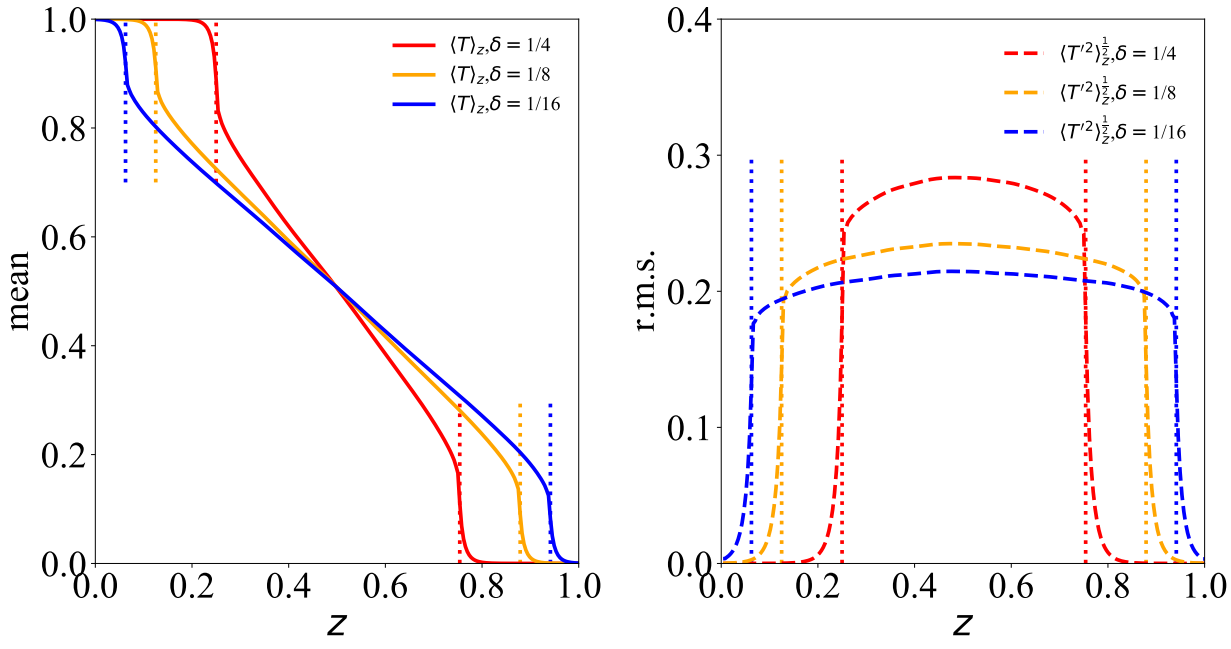

(a) (b)

Figure 6.5: Numerical profiles of: (a) the mean, and (b) the r.m.s. of T with different buffer layers thickness δ. The vertical dotted lines mark the interfaces between the buffer layers and the bulk region.

For the scalar fluctuation, figure 6.5(b) demonstrates that in the bulk region the scalar r.m.s. is almost constant, similar to the homogeneous shear turbulence (Mellado et al., 2009). In most of the buffer layer, the scalar r.m.s. is negligibly small, because the strong modulation effect from the source term $\dot{s}_T$ makes the scalar T roughly constant. Specifically, the strength of such modulation is determined by the control parameter τ. In this sense, the present flow can be effectively tailored by the control parameters τ and δ.

Further insights of the relation between the buffer and bulk regions can be gained by the following analytical approach. By taking the ensemble average ($\langle\cdot\rangle_z$) of Eq. (6.6d), it yields

$$\partial_t \langle T\rangle_z = (D_T + D)\triangle\langle T\rangle_z + \langle \dot{s}_T\rangle_z, \tag{6.9}$$

where the Reynolds stress term has been absorbed into the turbulent diffusivity D_T according to the following relation

$$\langle \mathbf{u}T\rangle_z = -D_T \frac{\partial\langle T\rangle_z}{\partial z}. \tag{6.10}$$

Because of symmetry, only a half of the domain, in the range of $z \in [0, 1/2]$ needs to be studied. Under the statistical stationary condition, the temporal derivative term in Eq. (6.9) vanishes. Let us denote D_T in the bulk region and buffer layer as $D_{T,1}$ and $D_{T,2}$, respectively. Combining the specific form of $\dot{s}_T$ (Eq. (6.5)) and

neglecting the laminar diffusivity D in Eq. (6.9), an ordinary differential equation about $\langle T\rangle_z$ is then found:

$$\begin{cases} D_{T,2}\frac{d^2\langle T\rangle_z}{dz^2} = \frac{1}{\tau}(\langle T\rangle_z - 1) & \text{when } 0 \le z \le \delta, \\ D_{T,1}\frac{d^2\langle T\rangle_z}{dz^2} = 0 & \text{when } \delta \le z \le 1/2. \end{cases} \tag{6.11}$$

The numerical evolution of D_T, calculated according to Eq. (6.10), is shown in figure 6.6 (a). Similar to the r.m.s. profile of T, D_T is also negligibly small in most of the buffer layer, following the same modulation mechanism as found for the source $\dot{s}_T$. From the analytical point of view, we approximate $D_{T,1}$ and $D_{T,2}$ as z-independent constants. As discussed before, the strong modulation effect from $\dot{s}_T$, or more specifically from the controlling parameter τ, leads to a small value of $D_{T,2}$, while physically $D_{T,1}$ is determined by the flow integral time T_I. Thus we further assume that $\frac{D_{T,2}}{D_{T,1}} \sim \frac{\tau}{T_I}$, or quantitatively $\frac{D_{T,2}}{D_{T,1}} = K\frac{\tau}{T_I}$, where the proportionality coefficient K ($K = O(1)$) needs to be determined numerically.

To solve this set of ODE, four boundary conditions are needed, including $\langle T\rangle_z(0) = 1$, $\langle T\rangle_z(1/2) = 1/2$, the continuity of $\langle T\rangle_z$ at $z = \delta$, and the continuity of the flux of $\langle T\rangle_z$ at $z = \delta$. Because of the different diffusivity in the buffer layer' and the bulk region, the continuity of the flux of $\langle T\rangle_z$ at $z = \delta$ can be expressed as

$$D_{T,2}\frac{d\langle T\rangle_z}{dz}(z \to \delta^-) = D_{T,1}\frac{d\langle T\rangle_z}{dz}(z \to \delta^+). \tag{6.12}$$

Therefore, the analytical solution of Eq. (6.11) for $\langle T\rangle_z$ is obtained as

$$\langle T\rangle_z(z) = \begin{cases} C_1 \sinh(\sqrt{\frac{1}{D_{T,2}\tau}}z) + 1 & \text{when } 0 \le z \le \delta, \\ C_2 z + C_3 & \text{when } \delta \le z \le 1/2. \end{cases} \tag{6.13}$$

where

$$\begin{aligned} C_1 &= \frac{-1}{2(A - \frac{B(\delta-0.5)}{D_{T,1}})}, \\ C_2 &= \frac{BC_1}{D_{T,1}}, \\ C_3 &= \frac{1}{2} - \frac{C_2}{2}, \end{aligned}$$

with $A = \sinh(\sqrt{\frac{1}{\tau D_{T,2}}}\delta)$ and $B = \cosh(\sqrt{\frac{1}{\tau D_{T,2}}}\delta)\sqrt{\frac{D_{T,2}}{\tau}}$. Numerically, it is found that the model solution with $\frac{D_{T,2}}{D_{T,1}} = 4\frac{\tau}{T_I}$ matches DNS results well, as shown in figure 6.6 (b). In summary, the difference between the buffer layer and the bulk region is mainly induced by the different turbulent diffusivity, because of the strong

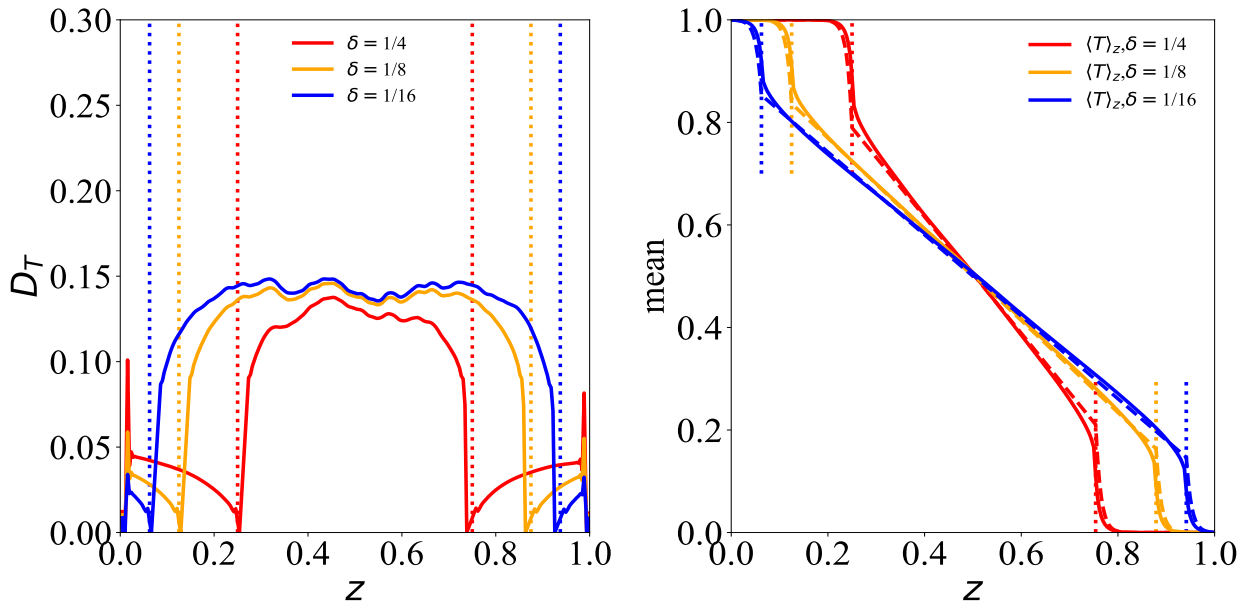

(a) (b)

Figure 6.6: (a) Turbulent diffusivity calculated from Eq. (6.10). (b) Theoretical prediction of the mean of T (dashed lines) compared with the DNS results (solid lines with same color). The vertical dotted lines mark the interfaces between the buffer layers and the bulk region.

modulation effect from the source term $\dot{s}_T$ (and other $\dot{s}$ terms as well) in the buffer.

6.3.2 Statistical properties of the reactive scalars

In this section, we focus on the difference between the z-dependent statistical properties of the reactive and passive scalars, or the effects of the chemical reaction. It can be seen from Eq. (6.6) and the corresponding boundary conditions (6.7) that $R_1(z) = R_2(1-z)$ statistically, i.e. R_1 and R_2 are symmetric with respect to the middle of the domain with $z = 1/2$. Therefore, for the sake of brevity the results for R_2 will be omitted in the rest analyses.

Figure 6.7 shows on the middle plane with $z = 1/2$ the PDFs of the scalar quantities R_1 and P, together with that of the passive scalar T. Overall, the PDF of T, denoted as p_T, is symmetric and has a central maximum at $T = 0.5$. Moreover, since the effect of the buffer layers can be compared to the mixing process in the shear layer, two other local peaks appear at the tails of p_T at $T = 0$ and $T = 1$ (same for other PDFs) (Mellado et al., 2009). Larger Γ lead to stronger skew of p_{R_1} toward the $R_1 = 0$ side. Such skewness property is the consequence of chemical reactions, because faster forward chemical reactions tend to deplete the reactants R_1 and R_2 but enrich the product P, enhancing p_{R_1} at the $R_1 = 0$ end and extending the p_P toward the larger P side.

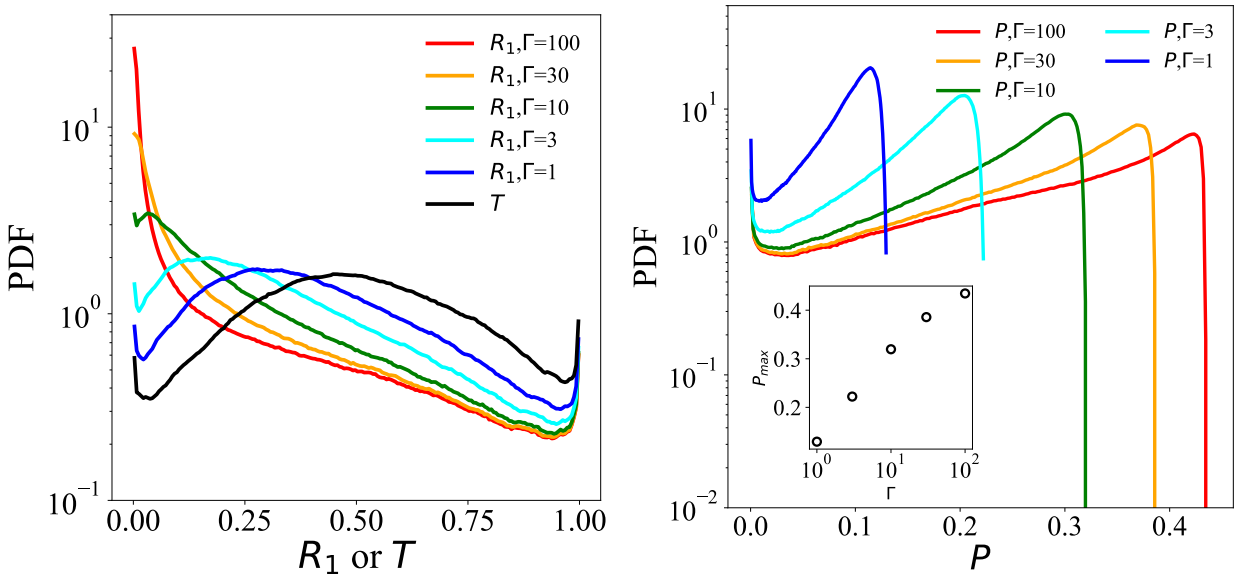

Figure 6.7: Dependence of PDFs at $z = 1/2$ on Γ for: (a) R_1 and T, and (b) P. The insert panel in (b) plots the peak of p_P as function of Γ.

At different z values the scalar concentration PDFs are shown in figure 6.8 (a) for R_1 and figure 6.8 (b) for T. We can see clearly the mirror symmetry between $p_T(z)$ and $p_T(1-z)$, which, however, breaks down for the R_1 case, because of the strong influence from the chemical sources. In addition, the PDF of T is of particular importance. In the modelling analysis discussed in the following section, the moments of the reactive scalars can be theoretically predicted based on p_T undergoing the same turbulent environment.

The dependence of the PDF of the net reaction rate $R_{net} = Da_1 R_1 R_2 - Da_2 P = Da_1(R_1 R_2 - P/\Gamma)$ on Γ is presented in figure 6.9 (at $z = 1/2$). Toward the fast chemical limit with large Γ, the PDF peaks higher at the $R_{net} = 0$ end and meanwhile becomes more extended toward the higher R_{net} side. When Da_1 and Da_2 are comparable, the PDF peaks at some moderate value of R_{net}. Since all the cases are under the control of the identical turbulence velocity, such difference must be caused by the chemical mechanism, which can be more clearly viewed from the spatial distribution of the reaction rates. From the comparison between figure 6.10 (a) and (d), there is a clear difference between the distribution of R_{net} for $\Gamma = 100$ and $\Gamma = 1$. For large Γ (and large Da_1 as well), the large R_{net} regions are highly concentrated in thin stripes, while for small Γ, regions with high R_{net} are much broader distributed, which explains the local bump in the PDF profile in figure 6.9. More detailed understanding of such property can be clarified from the separated results of the forward and backward reaction rates. It can be seen that a similar difference appears between figure 6.10 (b) and (e), while, figure 6.10 (c) and (f) are weakly influenced or even uninfluenced by Γ. Because the forward reaction rate is determined

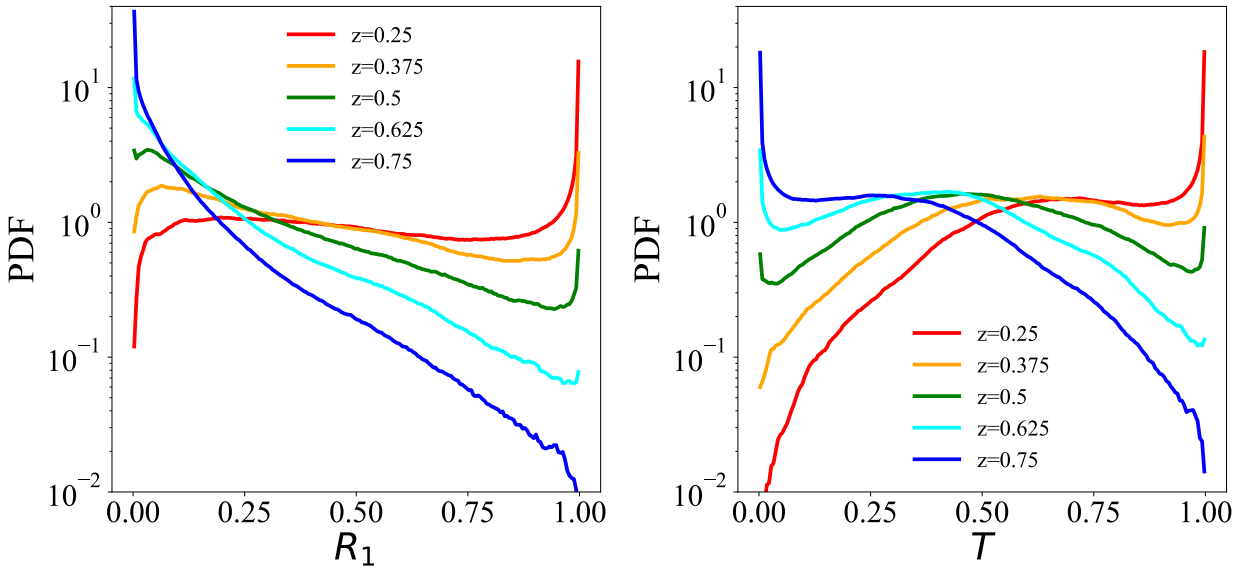

(a) (b)

Figure 6.8: PDF of (a) R_1 under the condition of $\Gamma = 10$ and (b) T at different positions.

by the correlation between R_1 and R_2, larger Γ will reduce in most of the flow field their coexistence, which explains the stripe like distribution in figure 6.10 (a). Since for the present chemical kinetics the backward reaction rate is solely determined by P, the effect of Γ on the scalar correlation is not relevant in determining the backward reaction rate. Therefore figure 6.10 (c) and (f) are almost identical. In summary, under different Γ the PDF and spatial distribution of the net reaction rate will be mainly determined by the forward part.

6.3.3 Moments of the reactive scalars

The reactive scalar θ (e.g. R_1, R_2 or P) can be decomposed into the z-dependent mean part and the fluctuating part as $\theta(\mathbf{x}, t) = \langle\theta\rangle_z(z, t) + \theta'(\mathbf{x}, t)$, whose numerical results are shown in figure 6.11.

Different from the linear profile of the passive scalar T, the profiles of $\langle R_1\rangle_z$ are concave in the bulk region, because of chemical consumption of R_1 with R_2. With increasing Γ, $\langle R_1\rangle_z$ decreases while $\langle P\rangle_z$ increases, because stronger forward reaction depletes more R_1 and produce more P. The scalar means tend to saturate at the infinite large Γ. Figure 6.11 (c) shows interestingly that the normalized $\langle P\rangle_z$ by the corresponding maximum overlaps for different Γ, which suggests a kind of universality of $\langle P\rangle_z$.

Concerning the fluctuation of R_1, in the upper half of domain, i.e. $z > 1/2$, larger Γ leads to smaller fluctuation, while in the lower half with $z < 1/2$, larger Γ leads to larger fluctuation. From the gradient hypothesis, in isotropic turbulence the r.m.s. of R_1 is reasonably determined by its mean gradient, i.e. the larger means gradient leads to larger fluctuation, as shown in in figure 6.11 (a). Close to the middle plane where

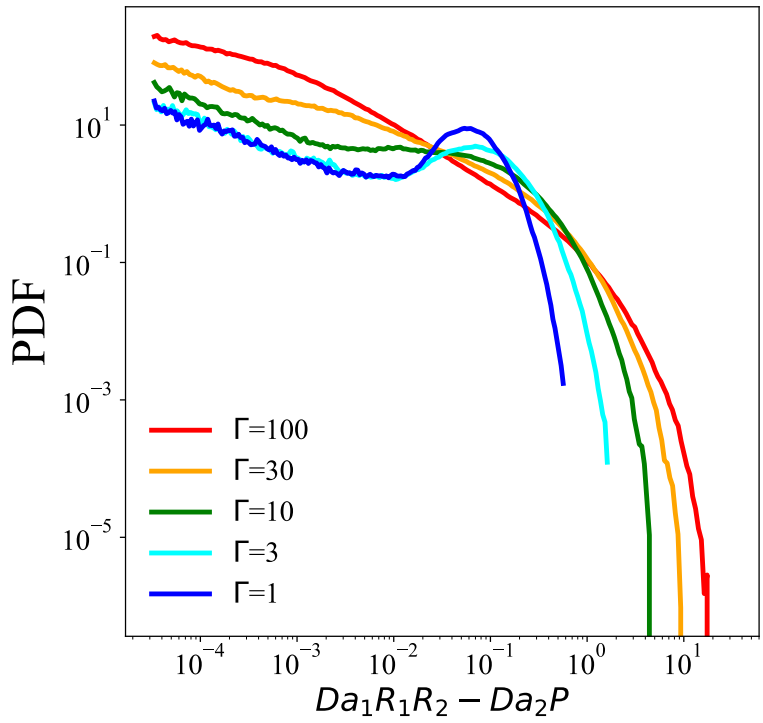

Figure 6.9: PDF of the reaction rate ($Da_1R_1R_2 - Da_2P$) under the conditions of different Γ, at the position of $z = 1/2$.

z is slightly greater than $1/2$, the gradient of $\langle R_1 \rangle_z$ is equal to that of $\langle T \rangle_z$, resulting in equality of r.m.s. of R_1 and r.m.s of T. For the product P, its r.m.s reaches a maximum at the edge of the bulk region and a minimum in the middle ($z = 1/2$). A tentative explanation is that the fluctuation of P is determined by the fluctuation of R_1 and R_2 because of the chemical kinetics and flow dynamics, i.e. turbulent transport. At the edge of the bulk, the r.m.s. of R_1 is large, but R_2 fluctuates weakly, which can not lead to high peak of the r.m.s. of P. Therefore, such maximum must come from the contribution from turbulent transport, or specifically, the large gradient of $\langle P \rangle_z$ close to the bulk edge (see the $\langle P \rangle_z$ results), due to the gradient hypothesis. In parallel, at $z = 1/2$ the gradient of $\langle P \rangle_z$ and the turbulent transport part vanish, leading to the minimum of the r.m.s. of P at $z = 1/2$.

To have further understanding of the effects of chemical reaction on the scalar statistics, the present reactive turbulent system needs to be analyzed theoretically. Let us define $X = R_1 - R_2$. Subtracting Eq. (6.6a) by Eq. (6.6b), it yields

$$\partial_t X + (\mathbf{u} \cdot \nabla) X = (Sc\ Re)^{-1} \triangle X + \dot{s}_{R_1} - \dot{s}_{R_2}, \tag{6.14}$$

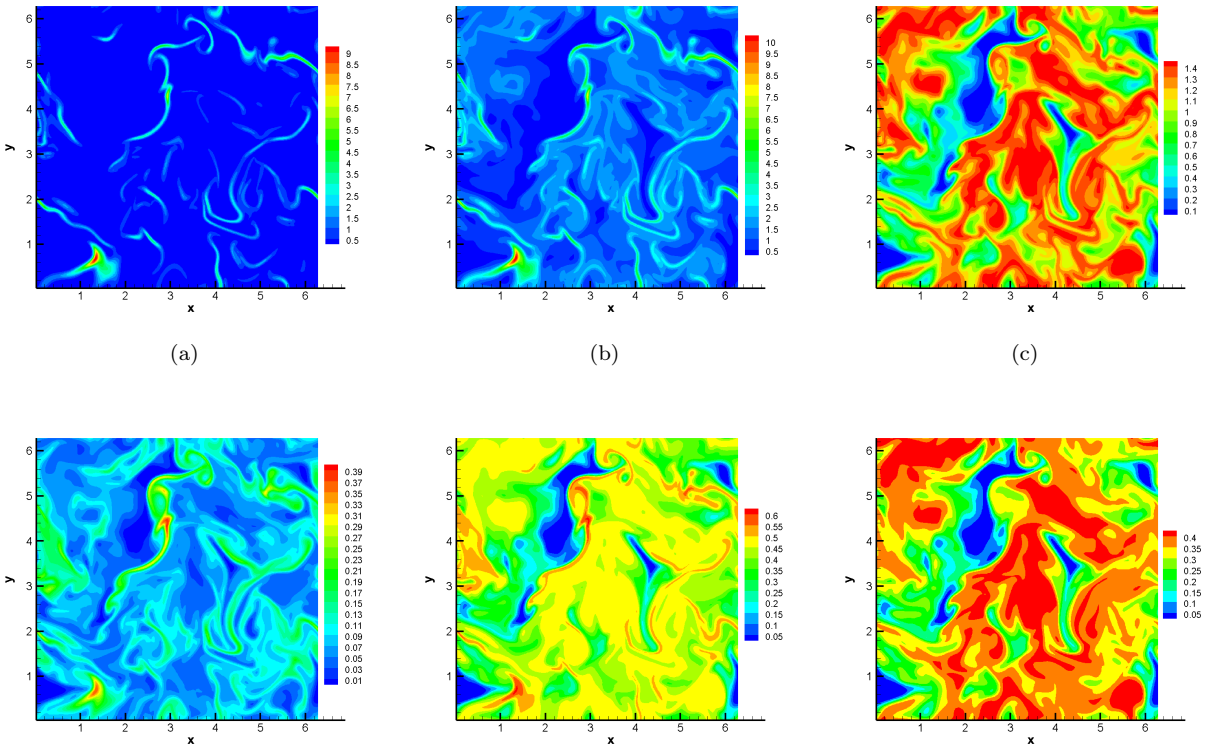

Figure 6.10: The instantaneous two-dimensional snapshot of reaction rate at the position of $z = 1/2$. The upper row (a,b,c) correspond to $\Gamma = 100$; the lower row (d,e,f) correspond to $\Gamma = 1$. The first column (a,d) show the net reaction rate ($Da_1 R_1 R_2 - Da_2 P$); the second column (b,e) show the forward reaction rate ($Da_1 R_1 R_2$); the third column (c,f) show the backward reaction rate ($Da_2 P$).

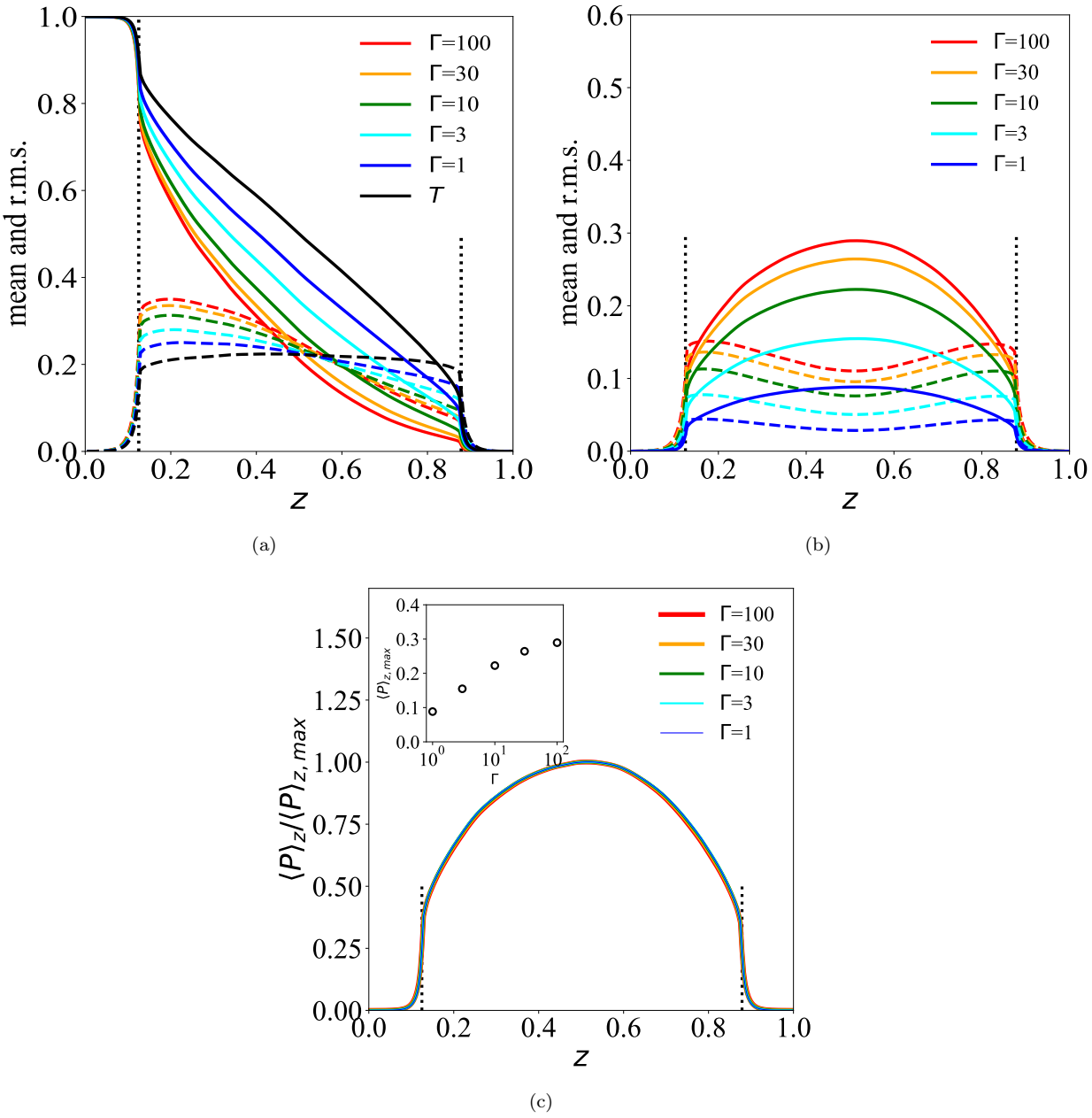

Figure 6.11: The mean (solid lines) and r.m.s. (dashed lines) of (a) R_1 compared with T; (b) P under the conditions of different Γ as functions of position (z). The main panel of (c) shows the mean profile of P normalized by its maximum, whose function as Γ is plotted in the inset plot. There is a prefect superposition for all Γ values. In all the plots, the vertical dotted lines mark the interfaces between the buffer layers and the bulk region.

with boundary conditions of

$$\begin{cases} X = 1 & \text{when } z = 0, \\ X = -1 & \text{when } z = 1. \end{cases} \tag{6.15}$$

Comparing the governing equation and boundary conditions of X with that of the passive scalar T (Eq. (6.6d) and (6.7)), it yields

$$X = R_1 - R_2 = 2T - 1. \tag{6.16}$$

Let us define $p_X(x; z)$ as the pdf of X at the position of z (similar definition for other random quantities). Relation (6.16) gives:

$$p_X(x; z) = \frac{1}{2} p_T(\frac{x+1}{2}; z). \tag{6.17}$$

First consider the case of infinitely large Da_1. This implies that R_1 and R_2 cannot coexist because of the finite chemical source $Da_1 R_1(\mathbf{x}, t) R_2(\mathbf{x}, t)$, leading to $R_1(\mathbf{x}, t) R_2(\mathbf{x}, t) = 0$. Therefore, a positive $X(\mathbf{x}, t)$ is equivalent to $R_1(\mathbf{x}, t) = X(\mathbf{x}, t)$ and $R_2(\mathbf{x}, t) = 0$, while $X(\mathbf{x}, t) < 0$ implies $R_1(\mathbf{x}, t) = 0$ and $R_2(\mathbf{x}, t) = -X(\mathbf{x}, t)$. For the quantity P, subtracting Eq. (6.6d) to Eq. (6.6a), together with the boundary conditions, we conclude that

$$P(\mathbf{x}, t) = T(\mathbf{x}, t) - R_1(\mathbf{x}, t). \tag{6.18}$$

Therefore, a relation between $P(\mathbf{x}, t)$ and $X(\mathbf{x}, t)$ can be obtained directly. Here, the infinitely large Da_1 leads to the following relations:

$$\begin{cases} R_1(\mathbf{x}, t) = 2T(\mathbf{x}, t) - 1, R_2(\mathbf{x}, t) = 0, P(\mathbf{x}, t) = 1 - T(\mathbf{x}, t), \text{ when } T(\mathbf{x}, t) \geqslant 1/2, \\ R_1(\mathbf{x}, t) = 0, R_2(\mathbf{x}, t) = 1 - 2T(\mathbf{x}, t), P(\mathbf{x}, t) = T(\mathbf{x}, t), \text{ when } T(\mathbf{x}, t) < 1/2. \end{cases} \tag{6.19}$$

Consequently, given that the passive scalar field T is known, the mean and r.m.s. of R_1 (at infinite Γ) can be respectively determined as

$$\begin{aligned} \langle R_1 \rangle_z(z) = &\int_0^1 x p_X(x; z) dx = \int_0^1 \frac{1}{2} x p_T(\frac{x+1}{2}; z) dx \\ = &2\langle T | T > \frac{1}{2} \rangle_z(z) - \int_{\frac{1}{2}}^1 p_T(t; z) dt, \end{aligned} \tag{6.20}$$

and

$$\begin{aligned}\langle R_1'^2\rangle_z(z) &= \langle R_1^2\rangle_z(z) - \langle R_1\rangle_z^2(z) \\ &= \int_0^1 \frac{1}{2}x^2 p_T(\frac{x+1}{2};z)dx - [\int_0^1 \frac{1}{2}x p_T(\frac{x+1}{2};z)dx]^2. \end{aligned} \tag{6.21}$$

The similar derivation can be done for P. The predictions are shown in figure 6.12 and 6.13.

For the finite but large Γ, $R_1(\mathbf{x},t)$ and $R_2(\mathbf{x},t)$ can locally coexist, i.e. $R_1R_2 > 0$. Since the overall forward reaction is still strong (if Γ is sufficiently larger than unity), we assume here that there exits a upper limit for $R_1(\mathbf{x},t)R_2(\mathbf{x},t)$, i.e.

$$R_1(\mathbf{x},t)R_2(\mathbf{x},t) \leq \frac{C}{\Gamma}, \tag{6.22}$$

where C is a constant to be determined. Moreover, for any given $X(\mathbf{x},t) \in [-1,1]$, another constraint is $R_1(\mathbf{x},t)R_2(\mathbf{x},t) \leq 1-|X(\mathbf{x},t)|$. The reason can be explained by the fact that the species concentrations $R_1(\mathbf{x},t)$ and $R_2(\mathbf{x},t)$ need to be confined in the range of $[0,1]$. Thus for a given value of $X(\mathbf{x},t) = R_1(\mathbf{x},t) - R_2(\mathbf{x},t)$, if $R_1(\mathbf{x},t) \geq R_2(\mathbf{x},t)$ i.e. $X(\mathbf{x},t) \geq 0$, we have

$$R_1(\mathbf{x},t)R_2(\mathbf{x},t) \leq R_2(\mathbf{x},t) = R_1(\mathbf{x},t) - X(\mathbf{x},t) \leq 1 - X(\mathbf{x},t). \tag{6.23}$$

Similarly,

$$R_1(\mathbf{x},t)R_2(\mathbf{x},t) \leq R_1(\mathbf{x},t) = R_2(\mathbf{x},t) + X(\mathbf{x},t) \leq 1 + X(\mathbf{x},t), \tag{6.24}$$

in the case of $X(\mathbf{x},t) < 0$. In summary, $R_1(\mathbf{x},t)R_2(\mathbf{x},t) \leq 1 - |X(\mathbf{x},t)|$. Putting these together, it gives $R_1R_2 \in [0, \min(\frac{C}{\Gamma}, 1-|X(\mathbf{x},t)|)] = [0, \beta_{max}]$. For a given $X(\mathbf{x},t) = \alpha$ and $R_1(\mathbf{x},t)R_2(\mathbf{x},t) = \beta$, $R_1 = \frac{\alpha+\sqrt{\alpha^2+4\beta}}{2}$. If the conditional PDF of R_1R_2 on X, i.e. $p_{R_1R_2|X}(\beta|\alpha;z)$, is known, $\langle R_1\rangle_z$ as function of z can be determined as

$$\langle R_1\rangle_z(z) = \int_{-1}^1 p_X(\alpha;z) \int_0^{\beta_{max}} \frac{\alpha+\sqrt{\alpha^2+4\beta}}{2} p_{R_1R_2|X}(\beta|\alpha;z)d\beta d\alpha. \tag{6.25}$$

A hypothesis assumed here is that with given $X(\mathbf{x},t)$, $R_1(\mathbf{x},t)R_2(\mathbf{x},t)$ is equally distributed in $[0, \beta_{max}(\alpha)]$. Together with the numerical results of the PDF of the passive scalar T, the mean $\langle R_1\rangle_z(z)$ and variance $\langle R_1'^2\rangle_z(z) = \langle R_1^2\rangle_z(z) - \langle R_1\rangle_z^2(z)$ can then be calculated (similar analyses for R_2 and P). As shown in figure 6.12 and 6.13, when $\Gamma \geqslant 10$, the modeling and numerical results can satisfactorily match if the constant C in

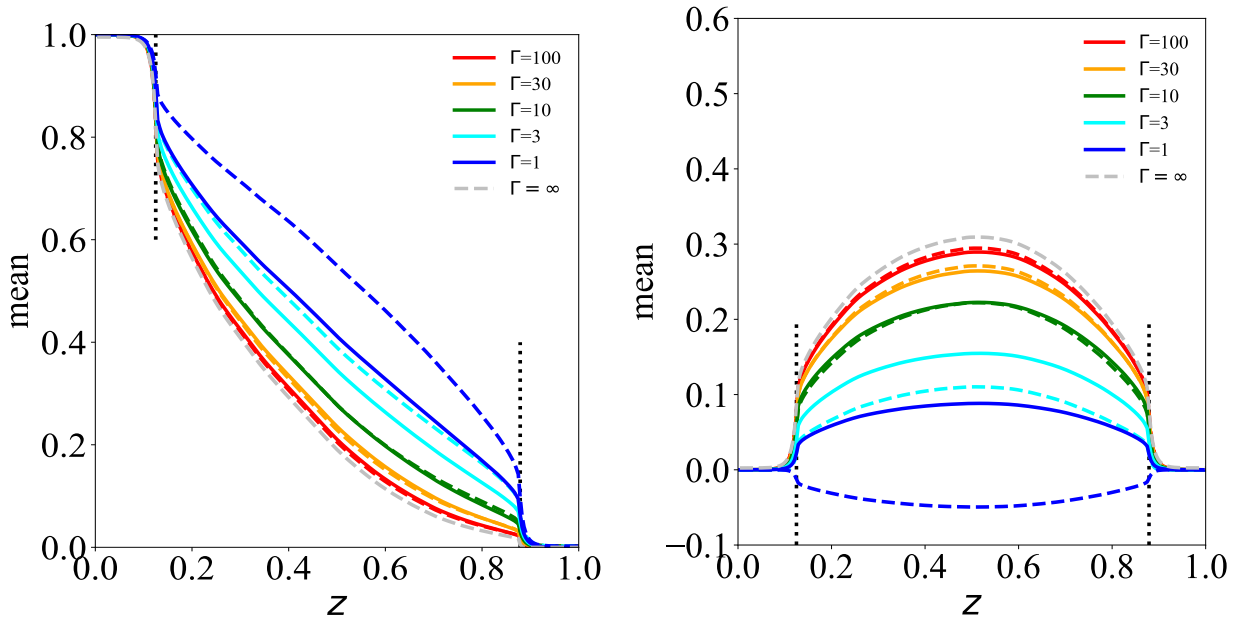

(a) R_1 (b) P

Figure 6.12: The scalar mean: (a) $\langle R_1 \rangle_z$ and (b) $\langle P \rangle_z$, as a function of z obtained from theoretical analysis (dashed lines) based on Eq. (6.25) and DNS (solid lines with the same colors). The grey dashed lines are from the theoretical prediction at infinitely large Da_1 according to Eq. (6.20). We see that the prediction for $\Gamma = \infty$ is close to the curves for $\Gamma = 100$ and also the predictions for large Γ are close to the DNS results when Γ=10, 30, 100. The vertical dotted lines mark the interfaces between the buffer layers and the bulk region.

Eq. (6.22) is set as 0.7. When $\Gamma < 10$, these predictions do not hold.

6.3.4 Correlation Coefficients

For scalars θ_1 and θ_2 under consideration, the correlation coefficients are defined (based on the fluctuating parts) as

$$r(\theta_1, \theta_2)(z) = \frac{\langle \theta_1' \theta_2' \rangle_z}{\langle \theta_1'^2 \rangle_z^{1/2} \langle \theta_2'^2 \rangle_z^{1/2}}. \tag{6.26}$$

The scalar correlation is jointly determined by the chemical reaction and the turbulent mixing. In the present flow configuration, the numerical simulations of the z-dependent correlation coefficients are shown in figure 6.14.

In Chapter 4, it was found that a competition exists between the chemical reaction and turbulent mixing. Specifically, the chemical reaction tends to dump reactant concentration fluctuations and enhance their correlation intensity, while turbulent mixing increases fluctuations and removes relative correlations. For the present non-equilibrium configuration, the reactants R_1 and R_2 consume each other, especially when the forward reaction is strong, which explains the negative $r(R_1, R_2)$ in figure 6.14(a). In the bulk region, R_1 and R_2 are less

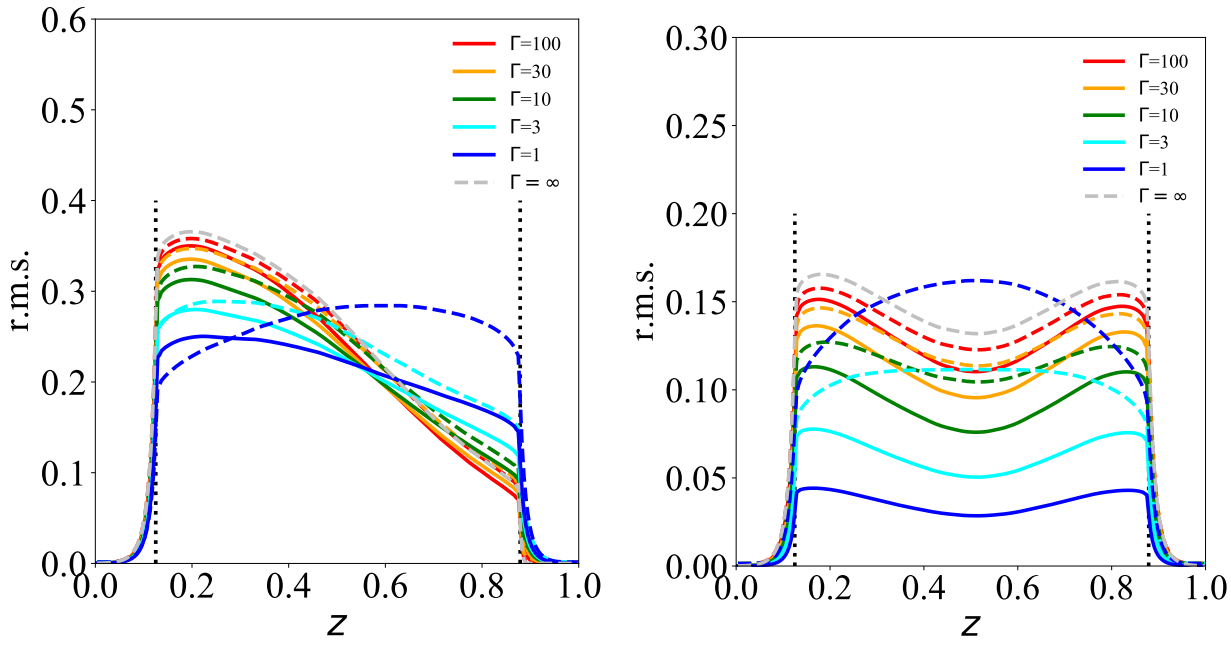

(a) (b)

Figure 6.13: The scalar fluctuations: (a) $\langle R_1'^2 \rangle_z^{1/2}$ and (b) $\langle P'^2 \rangle_z^{1/2}$ as function of z obtained from theoretical analysis (dashed lines) and DNS (solid lines with the same colors). The grey dashed lines are from the theoretical prediction at infinitely large Da_1 according to Eq. (6.21). We see that the prediction for $\Gamma = \infty$ is close to the curves for $\Gamma = 100$ and also the predictions for large Γ are close to the DNS results when Γ=10, 30, 100. The vertical dotted lines mark the interfaces between the buffer layers and the bulk region.

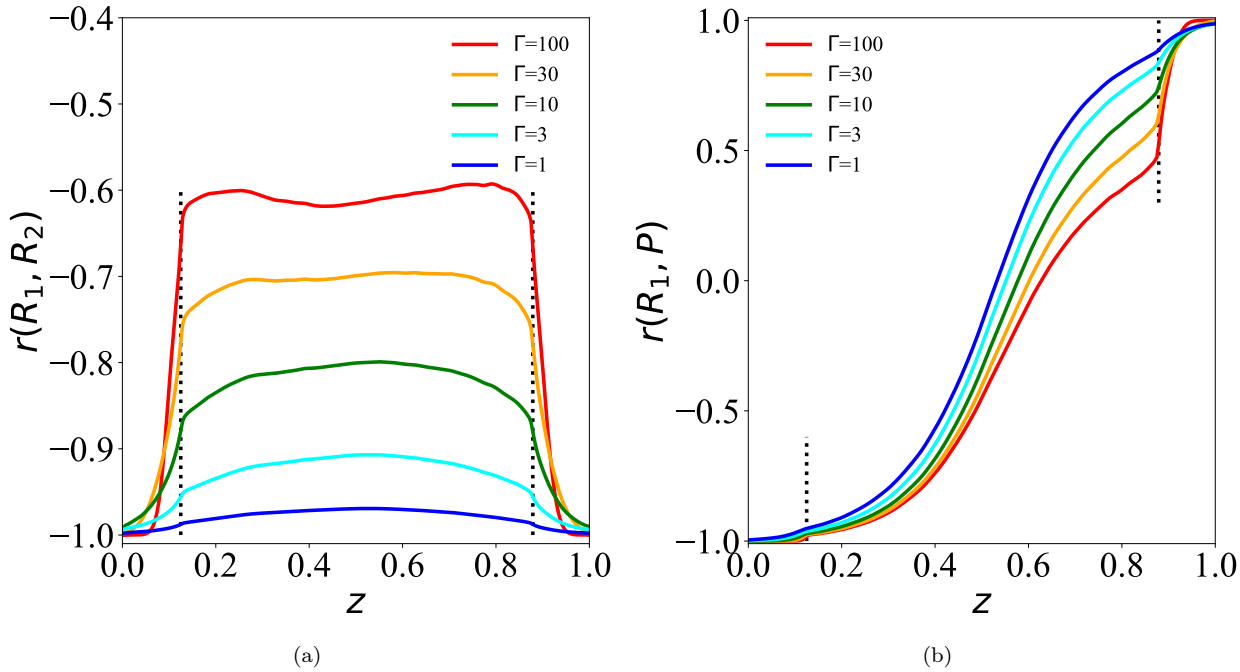

Figure 6.14: DNS simulations of the correlation coefficients between (a) R_1 and R_2; (b) R_1 and P as function of z, for different Γ cases. The vertical dotted lines mark the interfaces between the buffer layers and the bulk region.

correlated (with less negative $r(R_1, R_2)$) at larger Γ, but more correlated (with more negative $r(R_1, R_2)$) at smaller Γ. The reason can be given as follows. For the non-reactive case with $Da_{1,2} = 0$, the influence from the chemical reaction on the correlation coefficient vanishes. In the present flow configuration, the fluctuations of R_1 and R_2 are forced exclusively by their respective mean gradients, which are opposite with each other. Thus R_1 and R_2 are perfectly negatively correlated. In the bulk region with a stronger chemical source $Da_1 R_1 R_2$, as Γ increases, the chemical reaction depletes more the reactants, resulting in the skewness of the PDFs of of R_1 and R_2 toward the $R_{1,2} = 0$ side, as shown in figure 6.7. Therefore, the product $R_1' R_2'$ tends to be more positive. As a result, according to the definition in Eq. (6.26), $r(R_1, R_2)$ increases, i.e. R_1 and R_2 become less negatively correlated. Interestingly, in the buffer layer when Γ is sufficiently large (e.g. $\Gamma = 100$) $r(R_1, R_2)$ becomes abnormally more negative. This abnormal property can be explained by the fact that at sufficiently large Γ the chemical source $Da_1 R_1 R_2$ in the buffer layer is much weaker, because either R_1 or R_2 is negligibly small. Therefore, $r(R_1, R_2)$ is close to be that of the non-reactive case.

For $r(R_1, P)$, since R_1 and P function as the mutual sources rather than sink, the result is different from $r(R_1, R_2)$. Overall, $r(R_1, P)$ increases from -1.0 at $z = 0.0$ to 1.0 at $z = 1.0$. At $z = 0$ the reaction rate of P is mainly determined by R_2 since R_1 remains close to constant as 1.0. Because of the stoichiometric relation, the defect of R_1 from 1.0 is determined by either R_2 or P. Therefore, $r(R_1, P) \sim -1.0$. In a similar manner, at

$z = 1$ the reaction rate or the generation rate of P is mainly determined by R_1 and thus $r(R_1, P) \sim 1.0$. For the nonreactive case, at the middle plane with $z = 0.5$, $\langle R_1 \rangle_z$ and $\langle R_2 \rangle_z$ are exactly equal. Thus, the concentration of P is not influencing either R_1 or R_2, yielding $r(R_1, P) \sim 0$. With increasing Γ, R_1 will be more consumed and P will be more produced. As shown in figure 6.7, larger Γ leads to the PDF of R_1 more skewed toward the $R_1 = 0$ side, while the PDF of P skews differently toward the large P side. Therefore, $r(R_1, P)$ will unanimously decrease and shift downwards with increasing Γ, as demonstrated in figure 6.14(b).

6.3.5 Scalar Energy Spectra

The z-dependent scalar energy spectra is also investigated. At a specific z, the energy spectra corresponding to a two-dimensional scalar field is defined as

$$E_\theta(k, z) = 2\pi k^2 \langle \hat{\theta}(\mathbf{k}) \hat{\theta}^*(\mathbf{k}) \rangle_k, \quad \theta = R_1, R_2, P \text{ or } T, \tag{6.27}$$

where $\mathbf{k}$ is the 2D wave number and $k = |\mathbf{k}|$, $\langle \cdot \rangle_k$ denotes the average in time, $\hat{\theta}(\mathbf{k})$ is the Fourier coefficients of the mode of $\mathbf{k}$, $\hat{\theta}^*(\mathbf{k})$ is the corresponding complex conjugate.

In Chapter 4, it was shown that the scalar energy spectra at the quasi-equilibrium state with different chemical sources are almost identical, because of the negligibly small reaction rates. For the present non-equilibrium reactive turbulence cases, the chemical source plays important roles in determining the structure and statistics of the scalar quantities. It is interesting to consider if such chemical source will largely influence or change the energy spectra. Consider the R_1 case for instance in figure 6.15 (a)-(c), higher Γ makes more scalar energy to shift from small wave number range to the large wave number range, indicating that stronger chemical reactions tend to lump the local scalar quantity and strengthen the scalar intermittency. A similar tendency appears for the scalar P, as shown in figure 6.15 (d)-(f). Such Γ effect becomes stronger at $z = 1/2$ (more difference between the curves in figure 6.15 (e)), since $\langle P \rangle_z$ reaches maximum at $z = 1/2$.

In addition, the coherency spectrum between two scalars θ_1 and θ_2 is defined as:

$$Co_{\theta_1,\theta_2}(k) = \frac{\langle |\widehat{\theta_1}(\mathbf{k}) \widehat{\theta_2}^*(\mathbf{k})| \rangle_k}{\sqrt{\langle \widehat{\theta_1}(\mathbf{k}) \widehat{\theta_1}^*(\mathbf{k}) \rangle_k \langle \widehat{\theta_2}(\mathbf{k}) \widehat{\theta_2}^*(\mathbf{k}) \rangle_k}}, \tag{6.28}$$

which describes the dependence of the correlation on the scale. The plots of $Co_{R_1,R_2}(k)$ with different Γ are shown in figure 6.16. In the previous work for the near equilibrium case studied in Chapter 4, it was reported that the reactive scalar coherency spectra are almost wave number independent, in particular, constant in the inertial range, since the chemical source is negligibly small and the random scalar source strongly reduces the

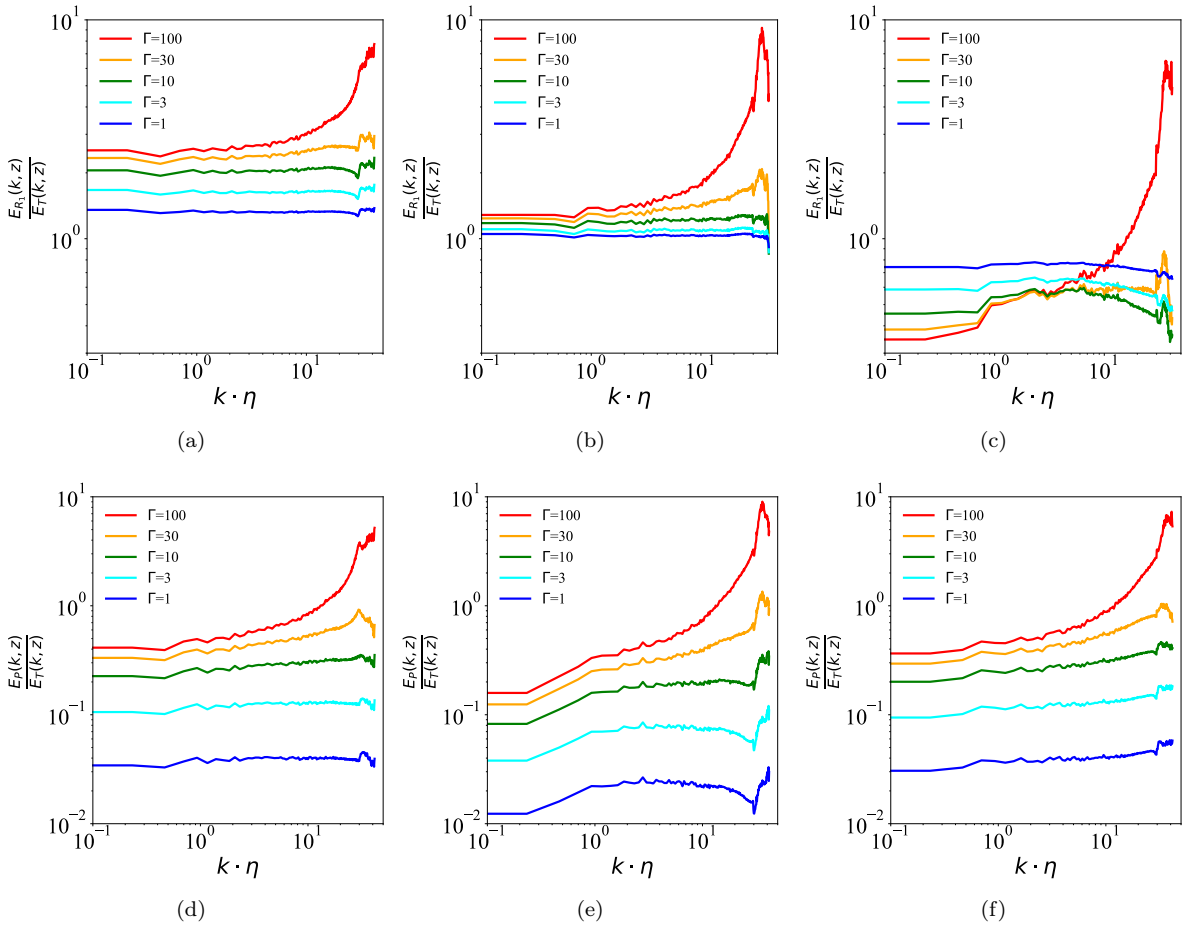

Figure 6.15: The ratio of the energy spectra of (a) R_1 at $z = \frac{1}{4}$; (b) R_1 at $z = \frac{1}{2}$; (c) R_1 at $z = \frac{3}{4}$; (d) P at $z = \frac{1}{4}$; (e) P at $z = \frac{1}{2}$; (f) P at $z = \frac{3}{4}$ to the energy spectrum of T at the same z.

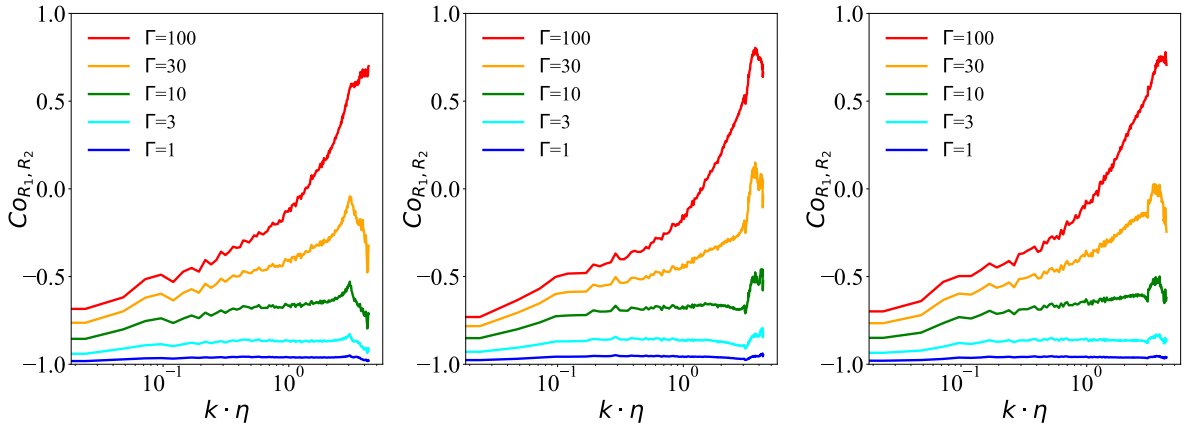

Figure 6.16: 2D coherency spectra between R_1 and R_2 at the positions of (a) $z = 1/4$, (b) $z = 1/2$ and (c) $z = 3/4$.

intensity of correlations. Both for the near equilibrium and the non-equilibrium cases, on average the absolute value of $Co_{R_1,R_2}(k)$ increases as Da increases, because fast chemical reactions build up correlations. However, in the present non-equilibrium state, the coherency spectra of reactive scalars are strongly wave number dependent, especially when the reaction is strong. In figure 6.16, the spectrum peaks toward the high wave number end, indicating that the correlation between R_1 and R_2 is mainly from the small scale contribution, in consistence with the stripe like structures visible in figure 6.10.

6.4 Summary

To maintain the definite positiveness of the species concentration, an original flow configuration has been proposed, where the species are supplied from the buffer boundaries with adjustable thickness to drive chemical reactions at the strongly out of equilibrium state. This allows to go beyond our previous exploration of reactive scalar fields in homogeneous turbulence, where only a moderate out of equilibrium state could be attained, and their results could be explained in term of a linearization approach of the reaction rates (Chapter 4).

Here, a theoretical modelization that take as an input the PDF of a passive scalar field can satisfactorily predict the local mean and fluctuation of reactants for $\Gamma \geqslant 10$. The correlation coefficient between the scalar quantities are determined by two counteracting effects, the turbulent mixing and the chemical kinetics. For larger Γ, the spatial distribution of the forward reaction and net reaction takes a stripe like structure, making the scalar field more intermittent.

In comparison with the existing results of the isotropic turbulence case as discussed in Chapter 4, we

conclude that the scalar correlation is jointly determined by the chemical source and physical conditions, e.g., flow configuration and boundary setup. Under the non-equilibrium condition with strong chemical sources, the chemical reaction also plays important roles in determining the scalar energy spectra. Consistently, large Γ will shift both the scalar energy and coherency spectra from the small wave number range to the large wave number range, which is in a sharp contrast with the near equilibrium case.

Chapter 7

Conclusion and future works

7.1 Summary of the thesis

In this thesis, the statistical properties of reactive scalars undergoing reversible chemical reactions in incompressible turbulence were studied by the means of direct numerical simulations and theoretical analyses. The cases studied include the reactions close to and strongly deviated from the chemical equilibrium states, in homogeneous isotropic and non-homogeneous anisotropic turbulent flow. Theoretical analysis on the statistical properties of scalars at different order of moments were carried out based on appropriately proposed approximations and models. The theoretically derived results were then compared with numerical results obtained by direct numerical simulation.

In the direct numerical simulations, for solving the PDEs of the quantities with periodic boundary conditions, the spatial derivatives were approximated by using a pseudo-spectral method with smooth dealiasing. Otherwise, for the special configurations in which the boundary conditions are not periodic, a finite difference method with high-order schemes was used. The statistical analysis of the quantities of interest was implemented in a statistical stationary state, which was maintained by numerical forcing for the velocity and scalars. In the anisotropic configuration, the forcing is the inherent mean gradient. While in the isotropic configuration, the velocity and scalar fluctuations are sustained with constant input power and amplitude respectively.

In the case of reversible chemical reactions in homogeneous isotropic turbulence, the reacting system is found to be in a chemical quasi-equilibrium state. Such a state is maintained by the competition between the reversibility of reaction, which enforces a global chemical equilibrium in the statistically stationary state, and the variability of the scalar forcing, which introduces stochasticity into the scalar fields. The overall reaction

rate is small in such a dynamical equilibrium state, and thus too weak to change the scaling behavior and statistical distribution of the scalars. Moreover, the fluctuations of the scalars are found to be small compared with the mean quantities. Thus a linearization of the reaction terms in the scalar equations is a viable analysis approach. Based on the linearization of the reaction terms and other appropriately proposed hypotheses, modeling analysis about the correlations and variances of fluctuations of reactive scalars were carried out. A theoretical analysis showed that the correlation coefficients and the fluctuations of reactive scalars are functions of a unique control parameter: the Damköhler number (Da_θ), which is constructed as the ratio between the time scale of scalar diffusion across a domain of the size of the scalar Taylor micro-scale (λ_θ^2/D) and the chemical reaction time scale τ_r. The larger is such a Damköhler number, the more depleted are the scalar fluctuations as compared to the fluctuation of a passive scalar field in the same conditions, and the more intense are the correlations. A saturation in this behaviour is observed beyond $Da_\theta \simeq \mathcal{O}(10)$. It indicates that the chemical processes tend to reduce reactant concentration fluctuations and enhance their correlation intensity. While on the contrary, the turbulent mixing increases fluctuations and removes relative correlations. Importantly, the functional dependence of the fluctuations and the correlations of the scalar quantities characterized by Da_θ are well confirmed by the DNS results in the full range of explored conditions with variable reaction order, the Reynolds number and the Schmidt number. The key role of Da_θ also implies the significance of the scalar Taylor micro-scale λ_θ in the mixing of chemical species. A deeper insight into λ_θ reveals that Da_θ can also be viewed as the ratio of the large-eddy-turnover time of the flow over the chemical reaction time.

In the homogeneous isotropic case, the theoretical analysis about the statistical properties of the reactive scalars are weakly affected by the small scale properties of the turbulent flow. This inspired us to consider the non-homogeneous anisotropic turbulence, such as the turbulent Kolmogorov flow (TKF). First, we gained a deeper insight into the TKF with a forcing of the sinusoidal form. It was found that the mean velocity profile has the same form, with a damping of a factor κ, with respect to the mean velocity value calculated from the forcing term. The value of this factor was found to weakly increase with the Reynolds number with indications of a possible asymptotic saturation at very large Re. The only non-zero shear stress term is proportional to the cosine function, and the normal stress components all involve a square cosine expression. The normal stresses are never equal, showing that as expected the turbulence is anisotropic. It was also shown that a quadratic nonlinear constitutive equation can be proposed for this flow, involving a linear term and two nonlinear terms in the form of traceless and symmetric tensors. For about half of the flow domain, the linear term is dominating. Whereas for the vanishing mean velocity gradient regions, only one non-linear term remains non-zero and becomes constant. Hence an effective viscosity coefficient can indeed be estimated for TKF, but contrary to

what has been stated previously (Rollin et al., 2011), globally all linear and nonlinear terms are needed for the complete closure. Then, the reversible reactions discussed for the homogeneous isotropic case was also studied with the background flow as the TKF. The theoretical predictions about the dependence of the fluctuations and the correlations of the reactive scalars on the Da_θ in homogeneous isotropic flow are found to work also for the TKF case. It indicates that, in the quasi-equilibrium state, the dependence of the statistical properties of reactive scalars on the scalar diffusion and reaction rate is weakly influenced by the background velocity field.

For the irreversible reactions in homogeneous isotropic turbulence, the linearization of the reaction term is valid because the fluctuations of the reactive scalars are small when compared to the mean quantities in the quasi-equilibrium state. However, a reacting system strongly deviated from the global equilibrium state and with relatively larger fluctuations of reactive scalars can be more practically meaningful and physically interesting. This is because the reaction flow possesses stronger non-linearities, which is a symbolic feature of turbulence problems. Thus, a combustor-like configuration of reactive scalars, in which the scalar fields are of Dirichlet boundary conditions in one direction, was explored. In such a configuration, the entire flow consists of two buffer layers and a bulk region. The fluctuations of the scalars are maintained by intrinsic mean gradient instead of isotropic forcing. Accordingly, the reacting system is supposed to be far from the chemical equilibrium state. The statistical and scaling properties of reactive scalars are investigated, in comparison with a passive scalar. A theoretical model based on the PDF of the passive scalar can satisfactorily predict the mean and fluctuation of reactants, if the associated Damköhler number (Da_1) is sufficiently large. For large Da_1, the spatial distributions of the forward reaction and net reaction assume stripe like structures, which makes the scalar field more intermittent as compared to the reference passive scalar case. The correlation coefficient between the scalar quantities are determined by two counteracting effects, the turbulent mixing and the chemical kinetics. Under the non-equilibrium condition with strong chemical sources, the chemical kinetics also plays important roles in determining the scalar energy spectra. Consistently, large Da_1 will shift the scalar energy from the small wave number range to the large wave number range, which is different from the near equilibrium case. In addition, the coherency spectra of the reactive scalars are strongly wave number dependent, in sharp distinction with the near equilibrium case.

In summary, reactions in incompressible turbulence of both homogeneous isotropic and non-homogeneous anisotropic cases were explored in this thesis. Theoretical analyses about the statistical properties of the reactive scalars, in comparison with a passive scalar, were implemented and examined with direct numerical simulations for different configurations.

7.2 Scientific contributions

The scientific contributions of this thesis can be summarized as following:

- The topic of this thesis, which is a combination of reaction and passive scalar in turbulence, is novel;
- We developed a configuration for the numerical simulation of turbulent reaction, in which the positiveness and strong fluctuation of reactive scalars are ensured;
- In the study about reactions in homogeneous isotropic turbulence, we introduced a key parameter (Da_θ) characterizing the competition between scalar diffusion and reaction, and showed its important role in determining the fluctuations and correlations of reactive scalar;
- In study about Chemical reactions sustained by Dirichlet boundary conditions, we proposed modeling analysis building a link between the moments of reactive scalar and the PDF of non-reactive scalar.

7.3 Future works

Compared with studies about turbulent combustion and passive scalars in turbulence, relatively few works have been devoted to the reaction in incompressible turbulence, especially reversible reactions. One unavoidable issue concerning reversible reactions is the chemical equilibrium. The statistical properties of reactive scalars can be hugely different in a reacting system close to and strongly deviated from the chemical equilibrium state. For the case with quasi-equilibrium state discussed in this thesis, the fluctuations of scalars have to be constrained as about 10% of the mean quantities for ensuring the positiveness of the concentrations. However, such a phenomenon does not make good practical sense for typical turbulence problems. In the real ocean, the fluctuations displayed by planktonic populations can attain values that are comparable to the ones of the mean population density, because there exist regions where nearly no individual or where huge accumulation can be observed. Simple solutions can be to enforce the numerical negative concentrations as zero or to express the concentration quantities in the form of power functions. However, these operations introduce too much arbitrary interference into the problem. It is thus important to propose configurations ensuring chemical quasi-equilibrium, the positiveness of reactive scalars and not small scalar fluctuations, preferably without too much artificial interference or at least only with physically reasonable corrections to the concentration quantities.

A straightforward way to amplify the fluctuations is by deriving the system into a non-equilibrium state. Another reason that the non-equilibrium state is of interest is that the reaction term can be more important. One operation offered in this thesis is by introducing Dirichlet boundary conditions for the reactive scalars (as

in Chapter 6). However, such a configuration breaks the isotropy of the scalars. Further consideration about a configuration retaining the isotropy of the scalar fields and meanwhile possessing a reaction source non-negligible compared with the convection or diffusion can be interesting. Moreover, it is also interesting to investigate the irreversible reactions, in which the reaction term can be non-negligible because the chemical equilibrium is not involved.

Based on the homogeneous isotropic cubic domain investigated in Chapter 4, an anisotropic configuration with Dirichlet boundary conditions and buffer layers for scalars was developed and discussed in Chapter 6. The reactive scalar fields in the latter configuration are much more complex, because the non-linearity induced by the reaction source is well reserved. Thus, the modeling analyses about the statistical properties of reactive scalars is much more challenging. Such a configuration is of great potential for deeper and broader exploration beyond the theoretical analysis carried out so far in this thesis. In the present works, the theoretical predictions about the mean profiles and fluctuations of the reactive scalars could match the numerical tests only for the cases with forward reaction infinitely large or much larger than the backward reaction. In addition, the current theoretical predictions about the mean profiles and fluctuations of the reactive scalars requires the prerequisite that the PDF of the passive scalar undergoing the same convection and diffusion is known. In future works on such a configuration, an important focus can be the improvement of the modeling analysis for a wider application range and proposing more compact expressions about the moments of the reactive scalars. Another direction can be the modification of the current hypotheses, which work poorly for the weak forward reaction case. Or any new theoretical frameworks based directly on the governing equations of the reactive scalars can also be considered. Furthermore, more in-depth and comprehensive analysis about other statistical properties of reactive scalars, for example the correlation coefficients, can also be a interesting subject for future works.

Concerning the Kolmogorov flow case studied in this thesis, in future works we suggest also to explore different shapes of forcing, to better understand the expressions of the different moments of the velocity field. It remains also to be understood from analytical arguments why the eddy-viscosity does not depend on z for such flow, contrary to what is found in similar but different flow such as channel flow (Schmitt, 2007b) or boundary-layer flows. Moreover, the closure models for passive scalar in the Kolmogorov flow can also be examined, and the extension to the reactive scalars will be more interesting.

The scaling behavior of turbulent scalars has always been of high interest since the Kolmogorov-Obukhov-Corrsin theoretical framework. The reaction, especially fast reaction, is supposed to introduce cliff structure into the scalar fields, and thus to promote the intermittency. For examining this idea and further exploring, comparison of the relevant statistics, such as the structure functions and the energy spectra, between passive

and reactive scalars can be useful. Since the reaction term are commonly non-linear, the convolution of the existing scalar fields can be reflected in high wave number motions. Thus, for a convincing direct numerical simulation about the turbulent problems concerning reaction, the demand in the computational resource is higher, since the numerical spatial resolution needs be finer than that required for passive scalar.

In one word, this thesis carried out basic and preliminary studies about the reactive scalars in incompressible turbulence by direct numerical simulations and theoretical analyses. The new discoveries always accompany with new problems. As the complement or development of the works done in this thesis, a lot of interesting questions are still waiting for further investigations in future works.

Acknowledgments

This thesis is under the joint support by Shanghai Jiao Tong University and French Region "Hauts-de-France" in the framework of a cotutella PhD programme. I will be eternally grateful of such a wonderful opportunity for improving my academic ability and broadening my horizons.

It can never be enough for me to express my gratitude to my advisors: Mr. Lipo Wang, Mr. François G. Schmitt and Mr. Enrico Calzavarini. Thank you for every comment you have given on my works. Thank you for every knowledge you have taught me. Thank you for every major or minor correction you have made to my writing. Thank you for every help you have given to my study and life. Thank you for every criticism on me. In my mind, you are most respectful because of your profound knowledge and meticulous attitude in science. It is absolutely my great honor to study under your supervision. This experience is the unforgettable memory and priceless fortune in my whole life.

I would like to thank Dr. Michael Gauding (CORIA (CNRS UMR 6614), Rouen, France) for providing the original code and patience in the further instruction; thank Dr. Yongxiang Huang (Xiamen University) for the kind academic suggestions or friendly help in life; thank all the staffs in UM-JI, especially Fiona Li, for your sweet help in my daily affairs.

I acknowledge the computing resources for the numerical simulations in this thesis including the cluster in UM-SJTU Joint Institute, the CALCULCO computing platform supported by SCoSI/ULCO (Service COmmun du Système d' Information de l' Université du Littoral Côte d' Opale), the National Supercomputer Center in Guangzhou, the High Performance Computing Center (HPCC) at Université de Lille and the Center for High Performance Computing at Shanghai Jiao Tong University.

I would like to also thank all my friends who made me feel not lonely during my PhD: Himani Garg, Ali Amar Katia, Hoan, Xiaodan Cao, Yang Gao, Peipei Zhao, Shibo Gu, Qianhui Li, Xiang Li, Hui Cao, Yuqing Guo, Kun Wang, Yu Cang, Guiwen Tan, Qun Hu, Chenlin Guo, Kunlin Li, Chun Gong ... Thank goodness for letting me acquaint all of you.

Last, I would like to give my most sincere gratitude to my family. Thank you for raising me up. Thank you for your unconditional support. Thank you for being an inseparable part of my life. Thank you for your love.

Bibliography

Alvelius, K. (1999). Random forcing of three-dimensional homogeneous turbulence. *Physics of Fluids 11*(7), 1880–1889.

Ardeshiri, H. (2016, October). *Dynamics of Copepods in Turbulent Flows*. Ph. D. thesis, University of Lille.

Bahri, C., G. Arwatz, W. K. George, M. E. Mueller, and M. Hultmark (2015). Self-similarity of passive scalar flow in grid turbulence with a mean cross-stream gradient. *Journal of Fluid Mechanics 780*, 215–225.

Balmforth, N. J. and Y. N. Young (2002). Stratified kolmogorov flow. *Journal of Fluid Mechanics 450*, 131.

Batchelor, G. K. (1949). Diffusion in a field of homogeneous turbulence. i. eulerian analysis. *Australian Journal of Scientific Research 2*, 437–450.

Batchelor, G. K. (1959). Small-scale variation of convected quantities like temperature in turbulent fluid. part 1. general discussion and the case of small conductivity. *Journal of Fluid Mechanics 5*(1), 113–133.

Batchelor, G. K., I. D. Howells, and A. A. Townsend (1959). Small-scale variation of convected quantities like temperature in turbulent fluid. part 2. the case of large conductivity. *Journal of Fluid Mechanics 5*(1), 134–139.

Batchelor, G. K. and A. A. Townsend (1949). The nature of turbulent motion at large wave-numbers. *Proceedings of the Royal Society of London A 199*, 238–255.

Bergman, T. L., A. S. Lavine, F. P. Incropera, and D. P. Dewitt (2011). *Fundamentals of Heat and Mass Transfer* (7 ed.). Hoboken: John Wiley & Sons.

Berti, S. and G. Boffetta (2010). Elastic waves and transition to elastic turbulence in a two-dimensional viscoelastic kolmogorov flow. *Physical Review E 82*(3), 036314.

Biferale, L. and I. Procaccia (2005). Anisotropy in turbulent flows and in turbulent transport. *Physics Reports 414*(2), 43 – 164.

Biferale, L. and F. Toschi (2001). Anisotropic homogeneous turbulence: hierarchy and intermittency of scaling exponents in the anisotropic sectors. *Physical Review Letters 86*(21), 4831.

Blazek, J. (2005). *Computational Fluid Dynamics: Principles and Applications* (2 ed.). Oxford: Elsevier Science.

Boffetta, G., A. Celani, A. Mazzino, A. Puliafito, and M. Vergassola (2005). The viscoelastic kolmogorov flow: eddy viscosity and linear stability. *Journal of Fluid Mechanics 523*, 161.

Borgas, M. S., B. L. Sawford, S. Xu, D. A. Donzis, and P. K. Yeung (2004). High schmidt number scalars in turbulence: Structure functions and lagrangian theory. *Physics of Fluids 16*(11), 3888–3899.

Borue, V. and S. A. Orszag (1996). Numerical study of three-dimensional kolmogorov flow at high reynolds numbers. *Journal of Fluid Mechanics 306*, 293–323.

Boussinesq, J. (1877). *Essai sur la théorie des eaux courantes.* Mémoires présentés par divers savants à l'Académie des Sciences vol. XXIII, Imprimerie Nationale.

Briard, A. and T. Gomez (2015). Passive scalar convective-diffusive subrange for low prandtl numbers in isotropic turbulence. *Physical Review E 91*(1), 011001.

Canuto, C., M. Y. Hussaini, and A. Quarteroni (1987). *Spectral Methods in Fluid Dynamics.* New York: Springer.

Chakrabarti, M., R. M. Kerr, and J. C. Hill (1995). Direct numerical simulation of chemical selectivity in homogenous turbulence. *Aiche Journal 41*(11), 2356–2370.

Chasnov, J. R. (1991). Simulation of the kolmogorov inertial subrange using an improved subgrid model. *Physics of Fluids A: Fluid Dynamics 3*, 188–200.

Chen, S. and R. H. Kraichnan (1998). Simulations of a randomly advected passive scalar field. *Physics of Fluids 68*, 2867–2884.

Corrsin, S. (1951). On the spectrum of isotropic temperature fluctuations in an isotropic turbulence. *Journal of Applied Physics 22*, 469.

Corrsin, S. (1957). Simple theory of an idealized turbulent mixer. *Aiche Journal 3*(3), 329–330.

Corrsin, S. (1958). Statistical behavior of a reacting mixture in isotropic turbulence. *Physics of Fluids 1*, 42–47.

Corrsin, S. (1961). The reactant concentration spectrum in turbulent mixing with a first-order reaction. *Journal of Fluid Mechanics 11*, 407–416.

Corrsin, S. (1962). Some statistical properties of the product of a turbulent first-order reaction. In J. B. Diaz and S. I. Pai (Eds.), *Fluid Dynamics and Applied Mathematics*, pp. 105–124. Gordon and Breach.

Corrsin, S. (1964a). Further generalization of onsager's cascade model for turbulent spectra. *The Physics of Fluids 7*, 1156–1159.

Corrsin, S. (1964b). The isotropic turbulent mixer: Part ii. arbitrary schmidt number. *Aiche Journal 10*(6), 870–877.

Courant, R., K. O. Friedrichs, and H. Lewy (1928). Uber die partiellen differenzengleichungender mathematisches physik. *Mathematische Annalen 100*, 32–74.

Courant, R., K. O. Friedrichs, and H. Lewy (1967). On the partial differenence equations of mathematical physics. *IBM Journal 11*, 215–234.

Craske, J. and M. van Reeuwijk (2015). Energy dispersion in turbulent jets. part 1. direct simulation of steady and unsteady jets. *Journal of Fluid Mechanics 763*, 500–537.

Currie, I. G. (2002). *Fundamental Mechanics of Fluids* (3 ed.). New York: Marcel Dekker.

Davidson, P. A. (2004). *Turbulence: An Introduction for Scientists and Engineers*. Oxford: Oxford Univeristy Press.

De Bortoli, A. L., G. S. L. Andreis, and F. N. Pereira (2005). *Modeling and Simulation of Reactive Flows*. Amsterdam: Elsevier.

Demosthenous, E., G. Borghesi, E. Mastorakos, and R. S. Cant (2016). Direct numerical simulations of premixed methane flame initiation by pilot n-heptane spray autoignition. *Combustion and Flame 163*, 122–137.

Derot, J., F. G. Schmitt, V. Gentilhomme, and S. B. Zongo (2015). Long-term high frequency phytoplankton dynamics, recorded from a coastal water autonomous measurement system in the eastern english channel. *Continental Shelf Research 109*, 210–221.

Desjardins, O., G. Blanquart, G. Balarac, and H. Pitsch (2008). High order conservative finite difference scheme for variable density low mach number turbulent flows. *Journal of Computational Physics 227*(15), 7125–7159.

Dewar, W. K. (2009). A fishy mix. *Nature 460*, 581–582.

Domingo, P. and L. Vervisch (1996). Triple flames and partially premixed combustion in autoignition of non-premixed turbulent mixtures. *Symposium (International) on Combustion 26*(1), 233 – 240.

Donzis, D. A., K. R. Sreenivasan, and P. K. Yeung (2010). The batchelor spectrum for mixing of passive scalars in isotropic turbulence. *Flow Turbulence and Combustion 85*(3-4), 549–566.

Elperin, T., N. Kleeorin, M. Liberman, A. N. Lipatnikov, I. Rogachevskii, and R. Yu (2017). Turbulent diffusion of chemically reacting flows: Theory and numerical simulations. *Physical Review E 96*(5), 053111.

Elperin, T., N. Kleeorin, and I. Rogachevskii (1998). Effect of chemical reactions and phase transitions on turbulent transport of particles and gases. *Physical Review Letters 80*(1), 69–72.

Eswaran, V. and S. B. Pope (1988a). Direct numerical simulations of the turbulent mixing of a passive scalar. *Physics of Fluids 31*, 506–520.

Eswaran, V. and S. B. Pope (1988b). An examination of forcing in direct numerical simulations of turbulence. *Computers and Fluids 16*(3), 257–278.

Ferziger, J. H. and M. Perić (2001). *Computational Methods for Fluid Dynamics*. New York: Springer.

Frisch, U. (1995). *Turbulence*. Cambridge: Cambridge University Press.

Frisch, U., P. L. Sulem, and M. Nelkin (1978). A simple dynamical model of intermittent fully developed turbulence. *Journal of Fluid Mechanics 87*(4), 719–736.

Gauding, M., L. Danaila, and E. Varea (2017). High-order structure functions for passive scalar fed by a mean gradient. *International Journal of Heat and Fluid Flow 67*, 86–93.

Gauding, M., L. Danaila, and E. Varea (2018). One-point and two-point statistics of homogeneous isotropic decaying turbulence with variable viscosity. *International Journal of Heat and Fluid Flow 72*, 143–150.

Germano, M., U. Piomelli, P. Moin, and W. H. Cabot (1991). A dynamic subgrid-scale eddy viscosity model. *Physics of Fluids 3*, 1760–1765.

Ghosal, S., T. S. Lund, P. Moin, and K. Akselvoll (1995). A dynamic localization model for large-eddy simulation of turbulent flows. *Journal of Fluid Mechanics 286*, 229–255.

Gotoh, T. and T. Watanabe (2015). Power and nonpower laws of passive scalar moments convected by isotropic turbulence. *Physical Review Letters 115*(11), 114502.

Gotoh, T., T. Watanabe, and H. Miura (2015). Spectrum of passive scalar at very high schmidt number in turbulence. *Plasma and Fusion Research 9*, 3401019.

Gotoh, T., T. Watanabe, and Y. Suzuki (2011). Universality and anisotropy in passive scalar fluctuations in turbulence with uniform mean gradient. *Journal of Turbulence 12*(48), 1–27.

Green, J. S. A. (1974). Two-dimensional turbulence near the viscous limit. *Journal of Fluid Mechanics 62*, 273–287.

Grošelj, D., F. Jenko, and E. Frey (2015). How turbulence regulates biodiversity in systems with cyclic competition. *Physical Review E 91*(3), 033009.

Heeb, T. G. and R. S. Brodkey (1990). Turbulent mixing with multiple second-order chemical reactions. *Aiche Journal 36*(10), 1457–1470.

Hernandez-Garcia, E. and C. Lopez (2004). Sustained plankton blooms under open chaotic flows. *Ecological Complexity 1*(3), 253–259.

Hill, J. C. (1976). Homogeneous turbulent mixing with chemical reaction. *Annual Review of Fluid Mechanics 8*(1), 135–161.

Hill, R. J. (2017). Spectra of turbulently advected scalars that have small schmidt number. *Physical Review Fluids 2*, 094601.

Hou, T. Y. and R. Li (2007). Computing nearly singular solutions using pseudo-spectral methods. *Journal of Computational Physics 226*(1), 379–397.

Huang, Y. (2009, July). *Arbitrary Order Hilbert Spectral Analysis Definition and Application to Fully Developed Turbulence and Environmental Time Series*. Ph. D. thesis, University of Lille.

Iyer, K. P., J. Schumacher, K. R. Sreenivasan, and P. K. Yeung (2018). Steep cliffs and saturated exponents in three-dimensional scalar turbulence. *Physical Review Letters 121*(26), 264501.

Jayesh and Z. Warhaft (1991). Probability distribution of a passive scalar in grid-generated turbulence. *Physical Review Letters 67*(25), 3503–3506.

Jones, W. P. and B. E. Launder (1972). The prediction of laminarization with a two-equation model of turbulence. *International Journal of Heat and Mass Transfer 15*, 301–314.

Jongen, T. and T. B. Gatski (1998). General explicit algebraic stress relations and best approximation for three-dimensional flows. *International Journal of Engineering Science 36*(7-8), 739–763.

Kerr, R. M. (1981). *Theoretical investigation of a passive scalar such as temperature in isotropic turbulence*. Ph. D. thesis, Cornell University.

Kerr, R. M. (1985). Higher-order derivative correlations and the alignment of small scale structures in isotropic numerical turbulence. *Journal of Fluid Mechanics 153*, 31.

Koblitz, A. R., S. Lovett, N. Nikiforakis, and W. D. Henshaw (2017). Direct numerical simulation of particulate flows with an overset grid method. *Journal of Computational Physics 343*, 414–431.

Kolmogorov, A. N. (1941a). Dissipation of energy in locally isotropic turbulence. *Doklady Akademii Nauk SSSR 32*, 16–18.

Kolmogorov, A. N. (1941b). The local structure of turbulence in incompressible viscous fluid for very large reynolds numbers. *Doklady Akademii Nauk SSSR 30*, 301–305.

Kolmogorov, A. N. (1962). A refinement of previous hypotheses concerning the local structure of turbulence in a viscous incompressible fluid at high reynolds number. *Journal of Fluid Mechanics 13*, 82–85.

Komori, S., J. C. R. Hunt, T. Kanzaki, and Y. Murakami (1991). The effects of turbulent mixing on the correlation between two species and on concentration fluctuations in non-premixed reacting flows. *Journal of Fluid Mechanics 228*, 629–659.

Kristoffersen, R. and H. I. Andersson (1993). Direct simulations of low-reynolds-number turbulent flow in a rotating channel. *Journal of Fluid Mechanics 256*, 163–197.

Kundu, P. K., I. M. Cohen, and D. R. Dowling (2012). *Fluid Mechanics* (5 ed.). Boston: Academic Press.

Kunze, E. (2019). Biologically generated mixing in the ocean. *Annual Review of Marine Science 11*, 215–226.

Laizet, S. and E. Lamballais (2009). High-order compact schemes for incompressible flows: A simple and efficient method with quasi-spectral accuracy. *Journal of Computational Physics 228*(16), 5989–6015.

Lamb, R. G. and W. R. Shu (1978). A model of second-order chemical reactions in turbulent fluid. i. formulation and validation. *Atmospheric Environment 12*(8), 1685–1694.

Law, C. K. (2006). *Combustion Physics*. Cambridge: Cambridge University Press.

Le Veque, R. J. (1990). *Numerical Methods for Conservation Laws*. Basel: Birkhäuser.

Leonard, A. D. and J. C. Hill (1988). Direct numerical simulation of turbulent flows with chemical reaction. *Journal of Scientific Computing 3*(1), 25–43.

Libby, P. A. and F. A. Williams (1976). Turbulent flows involving chemical reactions. *Annual Review of Fluid Mechanics 8*(1), 351–376.

Lilly, D. K. (1992). A proposed modification of the germano subgrid-scale closure method. *Physics of Fluids 4*, 633–635.

Liseikin, V. D. (1999). *Grid Generation Methods*. New York: Springer-Verlag.

Lopez, C., Z. Neufeld, E. Hernandez-Garcia, and P. H. Haynes (2001). Chaotic advection of reacting substances: Plankton dynamics on a meandering jet. *Physics and Chemistry of the Earth Part B-Hydrology Oceans and Atmosphere 26*(4), 313–317.

Lovejoy, S., W. J. S. Currie, Y. Tessier, M. R. Claereboudt, E. Bourget, J. C. Roff, and D. Schertzer (2001). Universal multifractals and ocean patchiness: phytoplankton, physical fields and coastal heterogeneity. *Journal of Plankton Research 23*, 117–141.

Lucas, D. and R. Kerswell (2015). Recurrent flow analysis in spatiotemporally chaotic 2-dimensional kolmogorov flow. *Physics of Fluids 27*(4), 045106.

Lucas, D. and R. R. Kerswell (2014). Spatiotemporal dynamics in two-dimensional kolmogorov flow over large domains. *Journal of fluid mechanics 750*, 518–554.

Machiels, L. (1997). Predictability of small-scale motion in isotropic fluid turbulence. *Physical Review Letters 79*, 3411–3414.

Mackenzie, B. R. (2000). Turbulence, larval fish ecology and fisheries recruitment: a review of field studies. *Oceanologica Acta 23*(4), 357–375.

Magoulès, F. (2011). *Computational Fluid Dynamics*. Ecole Centrale Paris: CRC Press.

Mandelbrot, B. B. (1974). Intermittent turbulence in self-similar cascades: divergence of high moments and dimension of the carrier. *Journal of Fluid Mechanics 62*(2), 331–358.

Mansour, N. N. and A. A. Wray (1994). Decay of isotropic turbulence at low reynolds number. *Physics of Fluids 6*(2), 808–814.

Mao, K. W. and H. L. Toor (1971). Second-order chemical reactions with turbulent mixing. *Industrial and Engineering Chemistry Research 10*(2), 192–197.

Mellado, J. P., L. P. Wang, and N. Peters (2009). Gradient trajectory analysis of a scalar field with external intermittency. *Journal of Fluid Mechanics 626*, 333–365.

Meneveau, C., T. S. Lund, and W. H. Cabot (1996). A lagrangian dynamic subgrid-scale model of turbulence. *Journal of Fluid Mechanics 319*, 353–385.

Menter, F. (1994). Two-equation eddy-viscosity turbulence models for engineering applications. *AIAA Journal 32*, 1598–1605.

Meshalkin, L. D. and I. G. Sinai (1961). Investigation of the stability of a stationary solution of a system of equations for the plane movement of an incompressible viscous liquid. *Journal of Applied Mathematics and Mechanics 25*(6), 1700–1705.

Mitrovic, B. M. and D. V. Papavassiliou (2004). Effects of a first-order chemical reaction on turbulent mass transfer. *International Journal of Heat and Mass Transfer 47*(1), 43–61.

Modesti, D. (2020). A priori tests of eddy viscosity models in square duct flow. *Theoretical and Computational Fluid Dynamics 34*, 713–734.

Moin, P. (2010). *Fundamentals of Engineering Numerical Analysis*. Cambridge: Cambridge University Press.

Moin, P. and K. Mahesh (1998). Direct numerical simulation: A tool in turbulence research. *Annual Review of Fluid Mechanics 30*, 539–578.

Molemaker, M. J. and J. V. G. de Arellano (1998). Control of chemical reactions by convective turbulence in the boundary layer. *Journal of the Atmospheric Sciences 55*(4), 568–579.

Monin, A. S. and A. M. Yaglom (1975). *Statistical Fluid Mechanics: Mechanics of Turbulence*, Volume 2. Cambridge, Massachusetts, and London, England: The MIT Press.

Musacchio, S. and G. Boffetta (2014). Turbulent channel without boundaries: The periodic kolmogorov flow. *Physical Review E 89*(2), 023004.

Neufeld, Z., P. H. Haynes, and T. TéL (2002). Chaotic mixing induced transitions in reaction-diffusion systems. *Chaos 12*(2), 426–438.

Neufeld, Z. and E. Hernández-García (2009). *Chemical and Biological Processes in Fluid Flows: A Dynamical Systems Approach*. London: Imperial College Press.

Nisizima, S. and A. Yoshizawa (1987). Turbulent channel and couette flows using an anisotropic k-epsilon model. *AIAA journal 25*(3), 414–420.

O'Brien, E. E. (1966). Decaying second-order isothermal reaction in final period turbulence. *Physics of Fluids 9*(1), 215–216.

O'Brien, E. E. (1971). Very rapid, isothermal, two-species reactions in final period turbulence. *Physics of Fluids 14*(8), 1804–1806.

O'Brien, E. E. (1975). Turbulent diffusion of rapidly reacting chemical species. *Advances in Geophysics 18*(3), 341–348.

Obukhov, A. M. (1941). Spectral energy distribution in a turbulent flow. *Doklady Akademii Nauk SSSR 32*(1), 22–24.

Obukhov, A. M. (1949). Structure of temperature field in turbulent flow. *Academy of Sciences of the USSR. News. Geographical Series and Geophysics 13*(1), 58–69.

Obukhov, A. M. (1962). Some specific features of atmospheric turbulence. *Journal of Geophysical Research 13*, 77–81.

Orszag, S. A. (1971). Numerical simulation of incompressible flows within simple boundaries. i. galerkin (spectral) representations. *Studies in Applied Mathematics 50*(4), 293–327.

Orszag, S. A. (1972). Comparison of pseudospectral and spectral approximation. *Studies in Applied Mathematics 51*(3), 253–259.

Overholt, M. R. and S. B. Pope (1998). A deterministic forcing scheme for direct numerical simulations of turbulence. *Computers and Fluids 27*(1), 11–28.

Pao, Y. (1964). Statistical behavior of a turbulent multicomponent mixture with first-order reactions. *AIAA Journal 2*(9), 1550–1559.

Perlekar, P., L. Biferale, M. Sbragaglia, S. Srivastava, and F. Toschi (2012). Droplet size distribution in homogeneous isotropic turbulence. *Physics of Fluids 24*, 065101.

Peters, N. (2000). *Turbulent Combustion*. Cambridge: Cambridge University Press.

Poinsot, T. (2017). Prediction and control of combustion instabilities in real engines. *Proceedings of the Combustion Institute 36*(1), 1–28.

Pope, S. B. (1975). A more general effective-viscosity hypothesis. *Journal of Fluid Mechanics 72*(2), 331–340.

Pope, S. B. (2000). *Turbulent Flows*. Cambridge: Cambridge University Press.

Powell, T. M. and A. Okubo (1994). Turbulence, diffusion and patchiness in the sea. *Philosophical transactions of the Royal Society B-Biological sciences 343*(1303), 11–18.

Rao, K. J. and S. M. de Bruyn Kops (2011). A mathematical framework for forcing turbulence applied to horizontally homogeneous stratified flow. *Physics of Fluids 23*, 065110.

Richardson, L. F. (1922). *Weather Prediction by Numerical Process*. Cambridge: Cambridge University Press.

Ristorcelli, J. R. (2006). Passive scalar mixing: Analytic study of time scale ratio, variance, and mix rate. *Physics of Fluids 18*(7), 075101.

Rollin, B., Y. Dubief, and C. R. Doering (2011). Variations on kolmogorov flow: turbulent energy dissipation and mean flow profiles. *Journal of Fluid Mechanics 670*, 204.

Sarris, I. E., H. Jeanmart, D. Carati, and G. Winckelmans (2007). Box-size dependence and breaking of translational invariance in the velocity statistics computed from three-dimensional turbulent kolmogorov flows. *Physics of Fluids 19*(9), 095101.

Schmitt, F. G. (2005). Relating lagrangian passive scalar scaling exponents to eulerian scaling exponents in turbulence. *European Physical Journal B 48*(1), 129–137.

Schmitt, F. G. (2006). Linking eulerian and lagrangian structure functions' scaling exponents in turbulence. *Physica A 368*(2), 377–386.

Schmitt, F. G. (2007a). About boussinesq's turbulent viscosity hypothesis: historical remarks and a direct evaluation of its validity. *Comptes Rendus Mécanique 335*(9-10), 617–627.

Schmitt, F. G. (2007b). Direct test of a nonlinear constitutive equation for simple turbulent shear flows using dns data. *Communications in Nonlinear Science and Numerical Simulation 12*(7), 1251–1264.

Schmitt, F. G. and C. Hirsch (2000). Experimental study of the constitutive equation for an axisymmetric complex turbulent flow. *ZAMM/Zeitschrift für Angewandte Mathematik und Mechanik 80*(11-12), 815–825.

Schumacher, J., K. R. Sreenivasan, and V. Yakhot (2007). Asymptotic exponents from low-reynolds-number flows. *New Journal of Physics 9*(4), 1–19.

Seuront, L., F. Schmitt, Y. Lagadeuc, D. Schertzer, and S. Lovejoy (1999). Universal multifractal analysis as a tool to characterize multiscale intermittent patterns: Example of phytoplankton distribution in turbulent coastal waters. *Journal of Plankton Research 21*(5), 877–922.

Seuront, L., F. Schmitt, D. Schertzer, Y. Lagadeuc, and S. Lovejoy (1996). Multifractal intermittency of eulerian and lagrangian turbulence of ocean temperature and plankton fields. *Nonlinear Processes in Geophysics 3*, 236–246.

She, Z. S. (1987). Metastability and vortex pairing in the kolmogorov flow. *Physics Letters A 124*(3), 161–164.

Shebalin, J. V. and S. L. Woodruff (1997). Kolmogorov flow in three dimensions. *Physics of Fluids 9*(1), 164–170.

Shraiman, B. I. and E. D. Siggia (2000). Scalar turbulence. *Nature 405*(6787), 639–646.

Shu, C. W. and S. Osher (1988). Efficient implementation of essentially non-oscillatory shock-capturing schemes. *Journal of Computational Physics 77*, 439–471.

Siggia, E. D. (1981). Numerical study of small-scale intermittency in three-dimensional turbulence. *Journal of Fluid Mechanics 107*, 375–406.

Siggia, E. D. and G. S. Patterson (1978). Intermittency effects in a numerical simulation of stationary three-dimensional turbulence. *Journal of Fluid Mechanics 86*, 567–592.

Smagorinsky, J. (1963). General circulation experiments with the primitive equations: I. the basic equations. *Monthly Weather Review 91*, 99–164.

Spencer, A. J. M. (1971). Part iii. theory of invariants. *Continuum physics 1*, 239–353.

Speziale, C. G. (1987). On nonlinear kl and k-ε models of turbulence. *Journal of Fluid Mechanics 178*, 459–475.

Sreenivasan, K. R. (1991). On local isotropy of passive scalars in turbulent shear flows. *Proceedings of the Royal Society of London A 434*, 165–182.

Sreenivasan, K. R. and R. A. Antonia (1997). The phenomenology of small-scale turbulence. *Annual Review of Fluid Mechanics 29*(1), 435–472.

Sripakagorn, P., S. Mitarai, G. Kosály, and H. Pitsch (2004). Extinction and reignition in a diffusion flame: a direct numerical simulation study. *Journal of Fluid Mechanics 518*, 231–259.

Stolovitzky, G., P. Kailasnath, and K. R. Sreenivasan (1995). Refined similarity hypotheses for passive scalars mixed by turbulence. *Journal of Fluid Mechanics 297*, 275–291.

Sullivan, N. P., S. Mahalingam, and R. M. Kerr (1994). Deterministic forcing of homogeneous, isotropic turbulence. *Physics of Fluids 6*(4), 1612–1614.

Sykes, R. I., S. F. Parker, D. S. Henn, and W. S. Lewellen (1994). Turbulent mixing with chemical reaction in the planetary boundary layer. *Journal of Applied Meteorology 33*(7), 825–834.

Taylor, G. I. (1935). Statistical theory of turbulence: Parts i-ii. *Proceedings of the Royal Society of London A 151*, 421–464.

Tennekes, H. and J. L. Lumley (1972). *A First Course in Turbulence*. Cambridge, Massachusetts, and London, England: MIT Press.

Toor, H. L. (1969). Turbulent mixing of two species with and without chemical reactions. *Industrial and Engineering Chemistry Research 8*(4), 655–659.

Versteeg, H. and W. Malalasekra (2007). *An Introduction to Computational Fluid Dynamics: the Finite Volume Method*. Prentice Hall: Upper Saddle River, New Jersey.

Vervisch, L. and T. Poinsot (1998). Direct numerical simulation of non-premixed turbulent flames. *Annual Review of Fluid Mechanics 30*(1), 655–691.

Vincent, A. and M. Meneguzzi (1991). The spatial structure and statistical properties of homogeneous turbulence. *Journal of Fluid Mechanics 225*, 1–20.

Wang, L., E. R. Hawkes, and J. H. Chen (2011). Flame edge statistics in turbulent combustion. *Proceedings of the Combustion Institute 33*(1), 1439 – 1446.

Warhaft, Z. (2000). Passive scalars in turbulent flows. *Annual Review of Fluid Mechanics 32*, 203–240.

Watanabe, T. and T. Gotoh (2004). Statistics of a passive scalar in homogeneous turbulence. *New Journal of Physics 6*, 40.

Wax, N. (1954). *Selected Papers on Noise and Stochastic Processes*. New York: Dover.

Wu, W., E. Calzavarini, F. G. Schmitt, and L. Wang (2020). Fluctuations and correlations of reactive scalars near chemical equilibrium in incompressible turbulence. *Physical Review Fluids 5*, 084608.

Yaglom, A. M. (1966). The influence on the fluctuation in energy dissipation on the shape of turbulent characteristics in the inertial interval. *Soviet Physics-Doklady 2*, 26–30.

Yamazaki, H., J. G. Mitchell, L. Seuront, F. Wolk, and L. Hua (2006). Phytoplankton microstructure in fully developed oceanic turbulence. *Geophysical Research Letters 33*(1), L01603.

Yeung, P. K., D. A. Donzis, and K. R. Sreenivasan (2005). High-reynolds-number simulation of turbulent mixing. *Physics of Fluids 17*, 081703.

Yeung, P. K. and K. R. Sreenivasan (2014). Direct numerical simulation of turbulent mixing at very low schmidt number with a uniform mean gradient. *Physics of Fluids 26*, 015107.

Yeung, P. K., S. Xu, and K. R. Sreenivasan (2002). Schmidt number effects on turbulent transport with uniform mean scalar gradient. *Physics of Fluids 14*(12), 4178–4191.

Zhang, J., L. Wang, and Y. Guo (2020). Non-premixed turbulent combustion modeling based on the filtered turbulent flamelet equation. *Sience China: Physics, Mechanics and Astronomy 63*(4), 244711.

Zhao, P., L. Wang, and N. Chakraborty (2018a). Analysis of the flame–wall interaction in premixed turbulent combustion. *Journal of Fluid Mechanics 848*, 193–218.

Zhao, P., L. Wang, and N. Chakraborty (2018b). Strain rate and flame orientation statistics in the near-wall region for turbulent flame-wall interaction. *Combustion Theory and Modelling 22*(5), 921–938.

Zikanov, O. (2010). *Essential Computational Fluid Dynamics*. Hoboken, New Jersey: John Wiley and Sons.